2010

CANNABINOID RECEPTORS IN THE 3D RECONSTRUCTED MOUSE BRAIN: FUNCTION AND REGULATION

Peter Nguyen
Virginia Commonwealth University

CANNABINOID RECEPTORS IN THE 3D RECONSTRUCTED MOUSE BRAIN: FUNCTION AND REGULATION

A dissertation submitted in partial fulfillment of the requirements for the degree of Doctor of Philosophy at Virginia Commonwealth University

By
Peter Tiendung Nguyen

Bachelor of Science, Chemistry, University of California, Irvine, 2003
Bachelor of Science, Biological Sciences, University of California, Irvine, 2003

Director: Dr. Laura Sim-Selley, Ph.D.
Associate Professor, Department of Pharmacology & Toxicology

Virginia Commonwealth University
Medical College of Virginia Campus
Richmond, Virginia
July 2010

Acknowledgment

I would like to express gratitude to the many important people at Virginia Commonwealth University for playing an important role in the development of my academic career. To my graduate committee members, Drs. John Bigbee, Robert DeLorenzo, Aron Lichtman, Dana Selley, and Laura Sim-Selley, thank you so much for your guidance, grateful insight, and incredible input throughout this dissertation. In particular, I would like to thank my advisor, Dr. Sim-Selley, for serving as an outstanding mentor. I can't emphasize how grateful I am to walk away after this PhD training with a deeper understanding of the scientific method, as well as the confidence and preparedness to tackle the next phase of my post-doctoral training. Thank you again for allowing me to pursue my research interests in the laboratory. I also wanted to acknowledge Dr. Bigbee and the Neuroscience Graduate Program and Dr. Archer and the MD/PhD training program, for their support, mentorship, and many opportunities to enrich my graduate training.

To current and past members of the Selley (Catherine He, Dr. Tricia Smith, Jordon Cox) and Sim-Selley (Uzo Mba, Dr. Lisa Middleton, Dr. James Burston, Dr. Katie Falenski, Matt Lazenka, Aaron Tomarchio) laboratory, thank you for your assistance and all the wonderful memories working together in the laboratory. Special thanks to Dr. Katie Falenski for the initial introduction to the lab and to various laboratory techniques. Also to Patraic Lichtman and James Gillespie, thank you for your assistance in image processing and data collection. I also wanted to thank our collaborator Dr. Laura Bohn and her laboratory (Scripps Research Institute, FL) for providing βarr2 knockout mice and technical assistance.

Finally, I'd like to thank my family for believing and inspiring me to push forward through this enduring journey of becoming a physician-scientist. Thank you mom and dad for your unending support and personal sacrifices to achieve your own American dream - witness the successes of your children. Your high standards for education have been monumental. To my sisters Theresa and Julie, and brothers Peter (Tung) and Peter (Binh), thank you for your inspiration and years of encouragment. Lastly to my best friend and loving wife Sonya, for understanding and supporting me throughout my academic training. Even in the most stressful and difficult times, your comfort allowed me to overcome these challenges to propel forward. I love you all so much.

This work was supported by NIH grants R01-DA014277 (to Laura Sim-Selley) and F30-DA023758 (to Peter Nguyen), and a VCU A.D. Williams Award (to Laura Sim-Selley).

Table of Contents

Page

List of Tables

Table:

List of Figures

Figure:

Appendix

Figures

Tables

Abbreviations:

2-AG: 2-arachidonoylglycerol

AEA: Arachidonoylethanolamide (anandamide)

ANOVA: Analysis of variance

β-Arr1: Beta-arrestin type 1

β-Arr2: Beta-arrestin type 2

B_{max}: Maximal specific binding site

BSA: Bovine serum albumin

CB_1: Cannabinoid receptor type 1

CB_2: Cannabinoid receptor type 2

CP: CP55,940 ((-)-*cis*-3-[2-hydroxy-4-(1,1-dimethylheptyl)phenyl]-*trans*-4-(3-hydroxypropyl)cyclohexanol)

dH_2O: Deionized water

EC_{50}: Concentration at half maximal effect

E_{max}: Maximal effect

FAAH: Fatty acid amide hydrolase

GPCR: G-protein coupled receptor

GRK: G-protein coupled receptor kinase

GTP: Guanosine triphosphate

[^{35}S]GTPγS: Guanosine 5'-O-[gamma-thio]triphosphate

i.p.: Intraperitoneal

KO: Knockout

MAGL: Monoacylglyceride lipase

ROI: Region of interest

THC: Δ^9-tetrahydrocannabinol

SPM: Statistical Parametric Mapping

SR1: SR141716A (N-piperidino-5-(4-chlorophenyl)-1-(2,4-dichlorophenyl)-4-methyl-3-pyrazole-carboxamide), Rimonabant

SR2: SR144528 (N-[(1S)-endo-1,3,3-trimethyl bicyclo [2.2.1] heptan-2-yl]-5-(4-chloro-3-methylphenyl)-1-(4-methylbenzyl)-pyrazole-3-carboxamide)

THC: Δ^9-tetrahydrocannabinol

WIN: WIN55,212-2 (R-(+)-[2,3-Dihydro-5-methyl-3-[(morpholinyl)methyl]pyrrolo[1,2,3-de]-1,4-benzoxazinyl]-(1-naphthalenyl)methanone mesylate)

WT: Wild-type

Neuroanatomical abbreviations

AMYG: Amygdala

A/V: Auditory/Visual

CBLM: Cerebellum

CG: Cingulate

CPu: Caudate Putamen

CTX: Cortex

GP: Globus Pallidus

HIPP: Hippocampus

HYPO: Hypothalamus

LC: Locus Coeruleus

LEnt: Lateral Entorhinal

NAc: Nucleus Accumbens

PAG: Periaqueductal gray

PIR: Piriform

SN: Substantia Nigra

SS: Somatosensory

THAL: Thalamus

Abstract

CANNABINOID RECEPTORS IN THE 3D RECONSTRUCTED MOUSE BRAIN: FUNCTION AND REGULATION

By Peter Tiendung Nguyen
Bachelor of Science, Chemistry, University of California, Irvine, 2003
Bachelor of Science, Biological Sciences, University of California, Irvine, 2003

A dissertation submitted in partial fulfillment of the requirements for the degree of Doctor of Philosophy at Virginia Commonwealth University

Virginia Commonwealth University, 2010

Director: Dr. Laura Sim-Selley, Ph.D.
Associate Professor
Department of Pharmacology and Toxicology

CB_1 receptors (CB_1R) mediate the psychoactive and therapeutic effects of cannabinoids including Δ^9-tetrahydrocannabinol (THC), the main psychoactive constituent in marijuana. However, therapeutic use is limited by side effects and tolerance and dependence with chronic administration. Tolerance to cannabinoid-mediated effects is associated with CB_1R adaptations, including desensitization (receptor-G-protein uncoupling) and downregulation (receptor degradation). The objectives of this thesis are to investigate the regional-specificity in CB_1R function and regulation. Previous studies have investigated CB_1Rs in a subset of regions involved in cannabinoid effects, but an inclusive regional comparison of the relative efficacies of different classes of cannabinoids to activate G-proteins has not been conducted. A novel unbiased whole-brain analysis was developed based on Statistical Parametric Mapping (SPM)

for 3D-reconstructed mouse brain images derived from agonist-stimulated [^{35}S]GTPγS autoradiography, which has not been described before. SPM demonstrated regional differences in the relative efficacies of cannabinoid agonists methanandamide (M-AEA), CP55,940 (CP), and WIN55,212-2 (WIN) in mouse brains. To assess potential contribution of novel sites, CB_1R knockout (KO) mice were used. SPM analysis revealed that WIN, but not CP or M-AEA, stimulated [^{35}S]GTPγS binding in regions that partially overlapped with the expression of CB_1Rs. We then examined the role of the regulatory protein Beta-arrestin-2 (βarr2) in CB_1R adaptations to chronic THC treatment. Deletion of βarr2 reduced CB_1R desensitization/downregulation in the cerebellum, caudal periaqueductal gray (PAG), and spinal cord. However in hippocampus, amygdala and rostral PAG, similar desensitization was present in both genotypes. Interestingly, enhanced desensitization was found in the hypothalamus and cortex in βarr2 KO animals. Intra-regional differences in the magnitude of desensitization were noted in the caudal hippocampus, where βarr2 KO animals exhibited greater desensitization compared to WT. Regional differences in βarr2-mediated CB_1R adaptation were associated with differential effects on tolerance, where THC-mediated antinociception, but not catalepsy or hypothermia, was attenuated in βarr2 KO mice. Overall, studies using SPM revealed intra- and inter-regional specificity in the function and regulation of CB_1Rs and underscores an advantage of using a whole-brain unbiased approach. Understanding the regulation of CB_1R signaling within different anatomical contexts represents an important fundamental prerequisite in the therapeutic exploitation of the cannabinoid system.

I. Introduction

A. Cannabis use: past and present

Marijuana, also known as cannabis, is perhaps one of the oldest psychoactive plants known to civilization. Its cultivation and utility as an industrial fiber (hemp fiber) has been approximated by modern historians to have started 10,000 years ago, roughly around pottery making and before metal working (Herer, 2000). Americans began using hemp for the production of rope, sails, and clothing in the 17th century. In the 1920s, Mexican immigrants introduced the recreational use of marijuana leaves, which sparked the early anti-marijuana campaigns and initiated an era of 'Reefer Madness' or national propaganda efforts to campaign against the "dangerous weed" (Herer, 2000). This eventually led Congress to pass the Marijuana Tax Act in 1937, which essentially criminalized marijuana and restricted its possession for authorized medical and industrial uses. Despite the enactment of stricter sentencing laws in the mid 1950s, marijuana usage surged in the 1960s following a shifting political and cultural climate. In 1996, the medical use of marijuana was first legalized in the state of California under the successful passing of proposition 215, allowing for the sale and medicinal use of marijuana for patients with debilitating conditions such as AIDS and cancer (Herer, 2000). Presently, 14 states have legalized the medical use of marijuana and two states have passed laws that, although favorable towards medicinal usage of marijuana, does not legalize its use (www.ProCon.org, 2010).

Currently marijuana, including various other tetrahydrocannabinol constituents of the plant (i.e. Δ^9-tetrahydrocannabinol (THC), Δ^8-tetrahydrocannabinol, etc.), is classified as a

Schedule I drug, along with other drugs of abuse such as heroin, lysergic acid diethylamide (LSD), and psilocybin (constituent of "Magic Mushrooms") (www.justice.gov, 2010). THC is also the primary psychoactive constituent in marijuana. Under the Controlled Substances Act for the United States, Schedule I drugs or substances are classified by the DEA to have a high potential for abuse, have no currently accepted medical indication, and lack safe standards of use under medical supervision. However, the FDA has approved two cannabinoids for use as medical therapies. For example, Dronabinol (Marinol) or synthetic THC is currently used to treat nausea and vomiting associated with cancer chemotherapy and to treat anorexia associated with AIDS-related weight loss. In addition, Nabilone, a synthetic cannabinoid that mimics the effects of THC, is used as a last resort to treat nausea related to cancer chemotherapy for patients not responsive to other existing anti-emetics. More recently in March 2010, encouraging results from a large scale U.S. phase IIb trial reported better pain scores (indicitive of pain management) comparing Sativex (an oromucusol spray containing THC and cannabidiol) versus placebo in patients with advanced stages of cancer. Plans are now underway to commence Phase III trials for Sativex in managing cancer pain.

B. The Endocannabinoid System

Pharmacological evidence of a cannabinoid receptor in brain was first suggested by Howlett and Fleming in their work demonstrating the inhibition of adenylate cyclase by cannabimimetic drugs (Howlett and Fleming, 1984). This work eventually led to the elucidation and characterization of a cannabinoid agonist binding site (Devane et al., 1988), and shortly thereafter, the CB_1 receptor was cloned from rat cerebral cortex cDNA library (Matsuda et al., 1990). A second cannabinoid receptor (CB_2) with 44% structural homology to CB_1, has also

been cloned from cDNA prepared from the human promyelocytic leukaemic line HL60 (Munro et al., 1993). Molecular characterization and identification of these receptors stimulated a search for their endogenous ligands. Several lipid-based compounds have since been isolated from brain and identified as endogenous ligands to the cannabinoid receptor. Of these, arachidonoylethanolamide (also known as anandamide; AEA) (Devane et al., 1992) and 2-arachidonoylglycerol (2-AG) (Mechoulam et al., 1995; Sugiura et al., 1995) are best characterized. Unlike classical neurotransmitters, endocannabinoids are not stored in vesicles, but are synthesized on demand via membrane phospholipid precursors. Synthesis of AEA was previously thought to occur from the enzymatic hydrolysis of *N*-acyl-phosphatidylethanolamines (NAPE) by a NAPE selective phospholipase D (Schmid et al., 1990). However, studies using NAPE-PLD knockout mice demonstrated equivalent levels of AEA as in wild-type animals (Leung et al., 2006), suggesting existence of other biosynethic pathways. Alternative NAPE-PLD independent pathways thought to contribute to the synthesis of AEA include for example the double-deacylation of NAPE by α/β-hydrolase 4 (ABH4) followed by posphodiesterase-mediated cleavage by GDE1 (Simon and Cravatt, 2006). In addition, phospholipase C-catalyzed cleavage of NAPE and its subsequent dephosphorylation (Liu et al., 2006) represents another potential biosnythetic pathway. Interestingly, a recent report found unaltered levels of AEA in GDE1 knockout mice, as well as only partial disruption of N-acyl ethanolamine biosynthesis in GDE1/NAPE double knockout mice (Simon and Cravatt, 2010). Collectively, these reports suggest multiple biosynthetic pathways for AEA, which may be brain region-dependent. As for 2-AG, the biosynthetic substrates are the *sn*-1-acyl-2-arachidonoylglycerols (DAGs) and requires DAG lipase (DAGL) (Bisogno et al., 2003). Recent studies using mice lacking either DAGL isotype (DAGLα or DAGLβ) suggest that DAGLα is the primary biosynethic enzyme for 2-AG

in the CNS as well as an important mediator of retrograde signaling (Gao et al., 2010; Tanimura et al., 2010).

The actions of endocannabinoids are relatively short lived and endocannabinoid tone is regulated by metabolic enzymes that are codistributed in most cannabinoid containing brain regions. Fatty acid amide hydrolase (FAAH) is primarily responsible for the metabolism of AEA (Cravatt et al., 1996) and other fatty acid amides, whereas monoacylglyceride lipase (MAGL) is the major metabolic enzyme of 2-AG (Dinh et al., 2002). The regional differences in the distribution of these two enzymes and their intricate cellular compartmentalization within the CNS (Dinh et al., 2002; Gulyas et al., 2004; Thomas et al., 1997), creates an elaborate metabolic machinery to modulate endocannabinoid signaling. Together, the cannabinoid receptors, endogenous ligands that bind these receptors, and degradative and synthetic enzymes, comprise the endogenous cannabinoid system.

A

CB_1 receptor antagonist
SR141716A (Rimonabant)

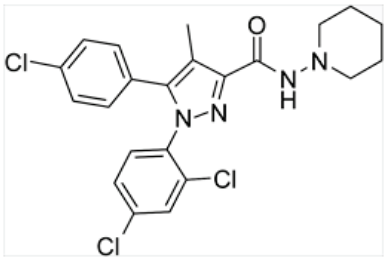

CB_2 receptor antagonist
SR144528

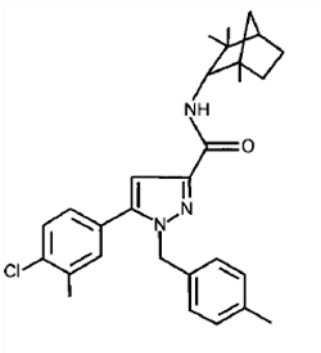

B

Phytocannabinoid
Δ^9-tetrahydrocannabinol

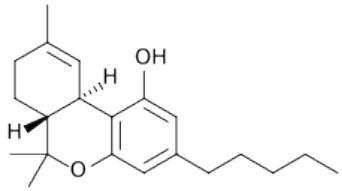

Non-classical
CP 55,940

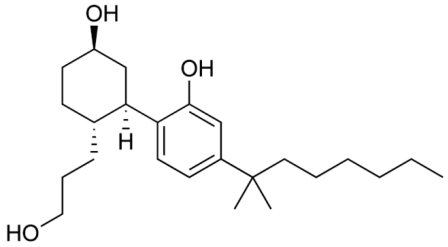

Aminoalkylindole
WIN 55,212-2

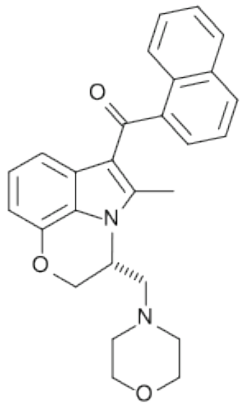

Eicosanoid
(R)-(+) Methanandamide

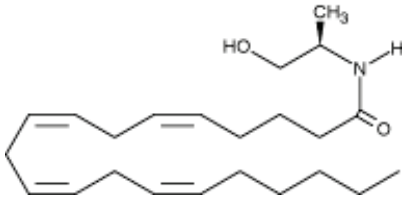

Arachidonoylethanolamide (Anandamide)

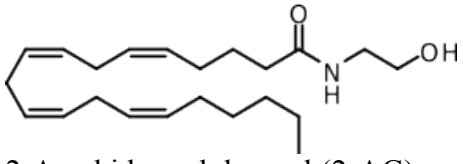

2-Arachidonoylglycerol (2-AG)

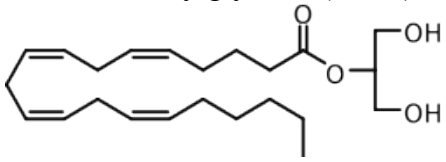

Figure 0.1. Chemical structures of CB_1 and CB_2 receptor selective antagonists (A) and different classes of cannabinoid receptor agonists (B).

C. Cannabinoid Pharmacology

The cannabis plant, *Cannabis sativa*, contains a mixture of cannabinoids (Elsohly and Slade, 2005) including Δ^9-tetrahydrocannabinol (THC), the primary psychoactive constituent of marijuana. The structural elucidation of THC by Gaoni and Mechoulam in 1964 (Gaoni and Mechoulam, 1964) led to the development of more potent synthetic cannabinoid agonists, such as CP55,940 and WIN55,212-2 (Fig. 0.1), which has advanced our understanding of the cannabinoid system (Melvin and Johnson, 1987). CP55,940 ((-)-*cis*-3-[2-hydroxy-4-(1,1-dimethylheptyl)phenyl]-*trans*-4-(3-hydroxypropyl)cyclohexanol), a bicyclic analog of THC, belongs to the class of nonclassical cannabinoids. It is a high efficacy partial agonist at the CB_1 receptor and is a full agonist at the CB_2 receptor, with similar binding affinities to both CB_1 and CB_2 receptors (Howlett et al., 2002). CP55,940 is one of the most widely used radiolabeled cannabinoid ligands and has historical significance, as it was first used to demonstrate a specific cannabinoid binding site (Devane et al., 1988) and to anatomically map the distribution of cannabinoid receptors in rat brain tissue (Herkenham et al., 1991). WIN55,212-2 (R-(+)-[2,3-Dihydro-5-methyl-3-[(morpholinyl)methyl]pyrrolo[1,2,3-de]-1,4-benzoxazinyl]-(1-naphthalenyl)methanone mesylate) is a full agonist at CB_1 receptors, and the prototype of the aminoalkylindole family (Howlett et al., 2002). Synthesis of a CB_1 selective antagonist SR141716A (N-piperidino-5-(4-chlorophenyl)-1-(2,4-dichlorophenyl)-4-methyl-3-pyrazole-carboxamide) helped establish the specificity of CB_1 receptor-mediated effects, and demonstrate that most *in vivo* effects of cannabinoids are mediated by the CB_1 receptor (Rinaldi-Carmona et al., 1994). SR141716A is a highly potent CB_1 antagonist that effectively inhibits and reverses CB_1-mediated effects both for *in vitro* and *in vivo* assays (Howlett et al., 2002). SR141716A has also been shown to act as an inverse agonist by reducing the constitutive activity (functional

coupling to effector mechanisms in the absence of an agonist) of CB_1 receptors, although concentrations significantly greater than the normal dose range to antagonize CB_1-mediated effects may be required in brain (Bouaboula et al., 1997; Landsman et al., 1997; Pertwee, 2005a; Sim-Selley et al., 2001).

The eicosanoid class of cannabinoids include the endocannabinoids AEA and 2-AG, which are derivatives of arachidonic acid and are the prototypic and most investigated members of this group. Although AEA and 2-AG have similar binding affinities, 2-AG exhibits higher efficacy than AEA at both CB_1 and CB_2 receptors (Pertwee, 2005b). Because AEA is highly susceptible to metabolism, synthetic derivates such as (R)-(+)-Methanandamide have been developed, which exhibit greater metabolic stability, affinity, and CB_1 selectivity (Di Marzo et al., 2001; Lin et al., 1998).

D. Cannabinoid receptor neuroanatomy

Cannabinoid receptors are among the most abundant G-protein coupled receptors (GPCR) in the brain. CB_1 receptors represent the predominant subtype in the CNS, whereas CB_2 receptor expression is restricted mainly to the immune system with limited expression in the CNS (Onaivi et al., 2006; Van Sickle et al., 2005). CB_1 receptors are highly expressed in brain areas, including the cortex, basal ganglia, hippocampus, amygdala, and cerebellum (Herkenham et al., 1991; Jansen et al., 1992; Tsou et al., 1998). This neuroanatomical distribution is consistent with *in vivo* effects of cannabinoids, including antinociception, cognitive and memory disruption, catalepsy, decreased motor activity, and hypothermia (Dewey, 1986; Hollister, 1998). Studies utilizing CB_1 receptor knockout mice (Zimmer et al., 1999) and CB_1 receptor selective antagonists (Rinaldi-Carmona et al., 1994) have also indicated that most of the *in vivo* effects of

THC and other cannabinoids are primarily mediated via the CB_1 receptor. Development of agonist-stimulated [^{35}S]GTPγS autoradiography in our laboratory (Sim et al., 1995) allowed for the initial demonstration of regional differences in desensitization (see *Receptor Desensitization* below) of cannabinoid-receptor mediated G-protein activity following chronic administration of THC (Sim-Selley and Martin, 2002; Sim et al., 1996a). Agonist-stimulated [^{35}S]GTPγS autoradiography provides not only a measurement of receptor-mediated G-protein activation, but also its neuroanatomical distribution. Figure 0.2 illustrates the first 3D image reconstruction of cannabinoid-stimulated G-protein activity produced by the full CB_1 receptor agonist WIN55,212-2 and was derived from the average of multiple naive mouse brain (n = 7) images (image reconstruction is described in *Chapter 1*). CB_1 receptor-mediated G-protein activity was found highest in regions including the amygdala and basal ganglia output nuclei, such as the substantia nigra and globus pallidus. Moderate levels of agonist-stimulated [^{35}S]GTPγS binding was noted in the hippocampus, deeper layers of cortex, and the cerebellum. In medullary nuclei important for mediating respiration, CB_1 receptors are low in abundance and therefore have low probability of lethality from overdose.

Studies on the subcellular localization of CB_1 receptors revealed that they are highly expressed on axon terminals and preterminal segments (Hajos et al., 2000; Katona et al., 2001). Double-label immunostaining experiments in the forebrain have also indicated that CB_1 receptors are primarily found on GABAergic interneurons (Tsou et al., 1999). Cannabinoid receptor modulation of other neurotransmitters have also been demonstrated. Interestingly, the synthethic cannabinoid WIN inhibited glutamatergic neurotransmission in the hippocampus of both CB_1 receptor wild-type and knockout mice (Hajos et al., 2001), a brain area that has previously been reported to contain putative non-CB_1 sites and exhibiting WIN-stimulated G-

protein activity ((Breivogel et al., 2001; Nguyen et al., 2010) and see *Chapter 2*). As opposed to inhibition, systemic administration of WIN has been shown to result in the efflux of norepinephrine in the rat frontal cortex, which appears to be modulated by the presnyaptic localization of CB_1 receptors on noradrenergic axon terminals (Oropeza et al., 2007; Oropeza et al., 2005; Reyes et al., 2009). The spatial localization of CB_1 receptors thus suggests that the cannabinoid system plays an important neuromodulatory role in the CNS.

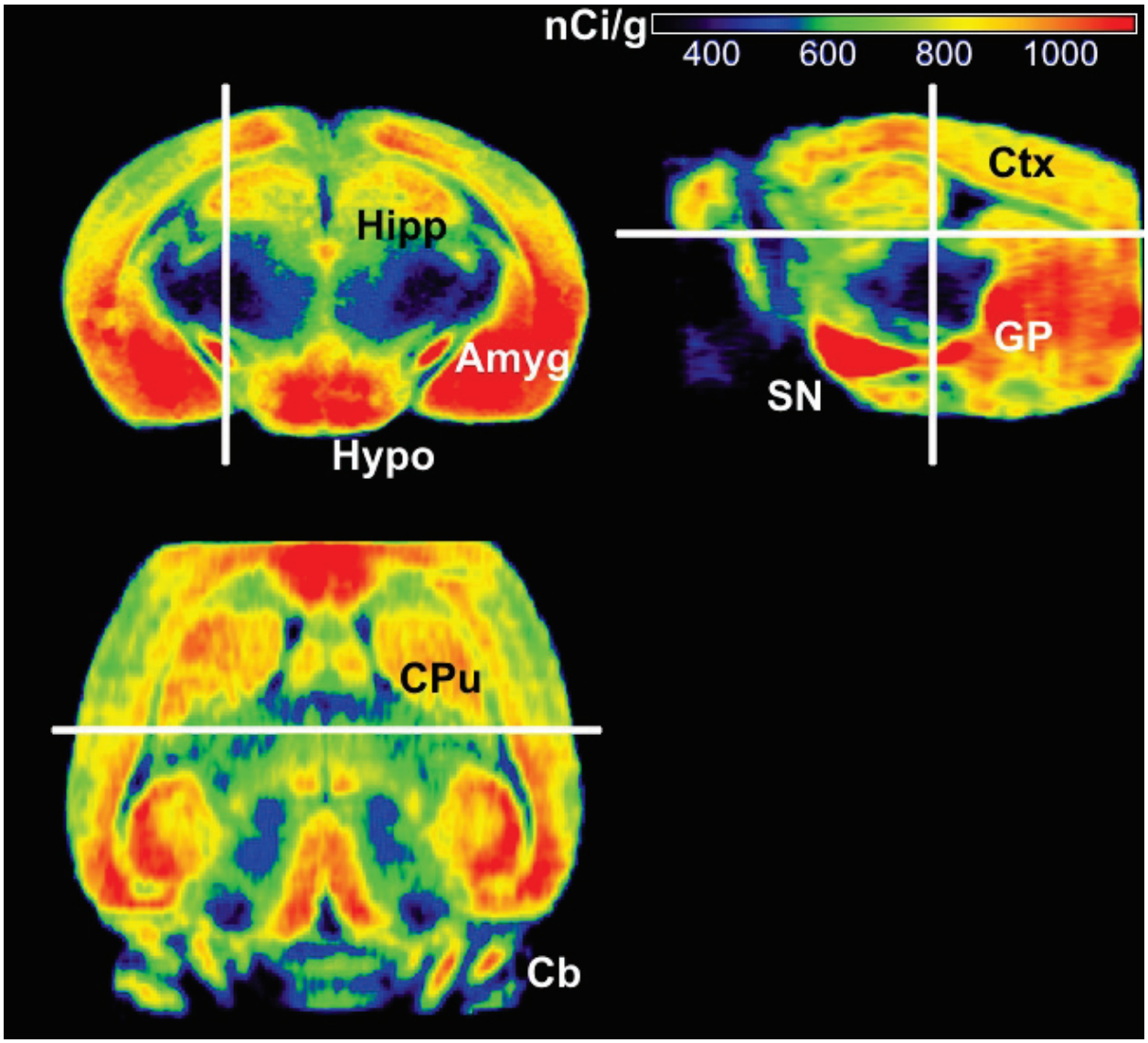

Figure 0.2. Image average (N = 7) of WIN55,212-2-stimulated [^{35}S]GTPγS binding in the 3D reconstructed mouse brain produced by a maximally effective concentration of the full CB_1 receptor agonist WIN55,212-2 (10 μM). A coronal, sagittal, and transverse section are shown in the upper left, upper right, and bottom left corners, respectively. Stimulated [^{35}S]GTPγS binding values (nCi/g) are shown in pseudocolor, demonstrating highest and lowest magnitudes of stimulated G-protein activation in red/orange and blue/black, respectively. White lines represent the level of each respective anatomical plane as shown in the figure. Highest WIN-stimulated G-protein activity are shown in the basal ganglia output nuclei (substantia nigra (SN), globus pallidus (GP)), amygdala (Amyg), cerebellum (Cb), hypothalamus (Hypo), hippocampus (Hipp), caudate-putamen (CPu), and cortex (Ctx). Details of 3D image reconstruction is described in *Chapter 1*

E. CB_1 receptor signal transduction pathways

Cannabinoid receptors belong to the superfamily of seven-transmembrane spanning G-protein coupled receptors (Fig. 0.3). CB_1 receptors are predominantly expressed presynaptically and inhibit neurotransmitter release (Ishac et al., 1996; Kathmann et al., 1999; Nakazi et al., 2000; Shen et al., 1996; Szabo et al., 1999). Agonist binding activates the receptor, which promotes interaction with its cognate heterotrimeric G-protein. This facilitates exchange of GDP for GTP, which binds and activates the α subunit. The activated α subunit then dissociates from the [$\beta\gamma$] complex, and each can activate intracellular effectors (Hall et al., 1999; Wickman and Clapham, 1995). The α subunit inactivates via an intrinsic GTPase, thus increasing the affinity of α for $\beta\gamma$, and association of the subunits. G-protein activation is catalytic because each receptor can activate multiple G-proteins (Gierschik et al., 1991; Sim et al., 1996c). CB_1 receptors primarily activate the pertussis toxin-sensitive G_i/G_o family of G-proteins that inhibit adenylyl cyclase (Howlett et al., 1986; Pacheco et al., 1991). CB_1 receptors inhibit several types of voltage gated calcium channels, such as N-type and Q-type currents, and activate G-protein-coupled inwardly rectifying potassium channels 1 and 2 (Howlett et al., 2002). In addition, CB_1 receptor activation has been shown to regulate ceramide metabolism and activate various intracellular kinases such as mitogen-activated protein (MAP) kinases, phosphatidylinosital-3-kinase, focal adhesion kinase, protein kinase B/Akt, and c-Jun N-terminal kinase (JNK1 and JNK2) (Howlett et al., 2002).

The production and release of endocannabinoids is thought to occur through a number of mechanisms and has been recently reviewed (Mackie, 2008). Wilson, Nicoll, and colleagues were the first to report feedback mechanisms involving endogenous cannabinoids by which a depolarized post-synaptic neuron can modulate the pre-synaptic release of an inhibitory or

excitatory neurotransmitter (Wilson et al., 2001; Wilson and Nicoll, 2001, 2002). This retrograde modulation by endocannabinoids is also referred to as depolarization-induced suppression of inhibition (DSI) or excitation (DSE). The underlying mechanism is now understood to involve postsynaptic intracellular increases in calcium followed by retrograde inhibition of presynaptic terminals, which was first noted by Llano et al. (Llano et al., 1991). Further, a recent report found a loss of retrograde endocannabinoid signaling in mice lacking DAGLα, the biosynthetic enzyme of 2-AG, suggesting an important role for the endocannabinoid 2-AG in retrograde synaptic plasticity (Gao et al., 2010). Depolarization-induced release of endocannabinoids has also been demonstrated to occur through a $G_{q/11}$-dependent mechanism involving the activation of postsynaptic group I metabotropic glutamate receptors (Varma et al., 2001) or M1 and M3 muscarinic receptors (Ohno-Shosaku et al., 2003). The actual underlying mechanism by which cannabinoid receptors modulate neurotransmitter release is unclear, however some evidence point to involvement of various ion channels, including K^+ channels (Kreitzer et al., 2002), or N or P/Q type Ca^{2+} channels (Guo and Ikeda, 2004).

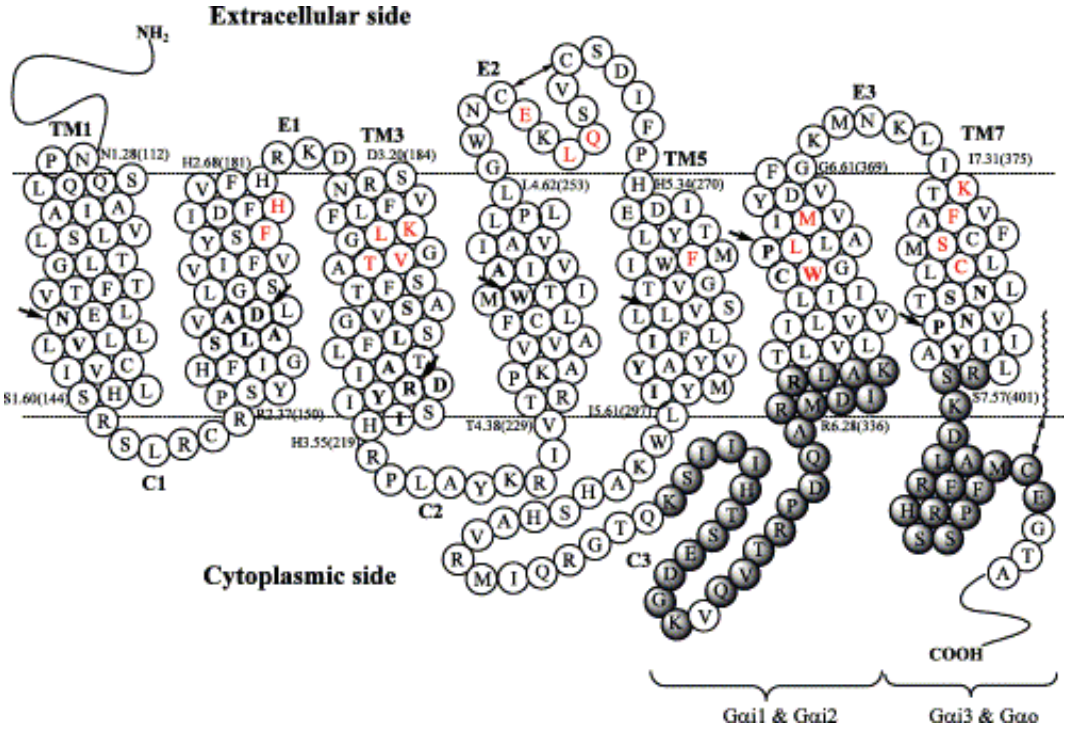

Figure 0.3. Two-dimensional structure of the human CB_1 receptor. Three extracellular (E1-3) and three intracellular (C1-3) regions are represented along with highly conserved key residues shown in bold. Sequences in the third intracellular domain (C3) important for $G_{\alpha i1}$ and $G_{\alpha i2}$ and C-terminal residues important for $G_{\alpha o}$ and $G_{\alpha i3}$ interactions are represented by shaded circles. Red colored amino acid letters illustrate proposed binding site residues within 2.5 Å of the bound non-classical cannabinoid CP55,940 (figure and caption adapted from Mukhopadhyay et al., *Chem Phys Lipids 2002*)

F. Acute effects of cannabinoids

At present, there is no evidence for structural changes in the brain following ether acute or chronic use of marijuana. Using magnetic resonance imaging (MRI), frequent marijuana users showed no evidence of cerebral atrophy or gross reductions in brain volume (Block et al., 2000). The *in vivo* effects of THC and other cannabinoids are well characterized. The most established behavioral model used to assess a wide array of cannabinoid-mediated effects in laboratory animals is the classical tetrad model, developed by Martin and colleagues (Compton et al., 1993). Acute administration of THC consistently produces hypothermia, catalepsy, antinociception, and decreased spontaneous motor activity. Porrino and colleagues (Freedland et al., 2002) have investigated the changes in cerebral metabolism using quantitative 2-[^{14}C]deoxyglucose (2-DG) autoradiography following THC administration. When assessed 15 minutes after drug administration, the acute effects of THC dose-dependently decreased regional brain metabolism, as measured by the rate of local cerebral glucose utilization. Other prominent central effects of cannabinoids include memory and cognitive impairment, which has been demonstrated in a number of memory paradigms showing the disruptive effect of cannabinoids on memory related tasks (Ferrari et al., 1999; Varvel et al., 2001). Interestingly, endocannabinoids have been implicated in the extinction of aversive memories (Marsicano et al., 2002). In this study, elevated levels of endocannabinoids were found in the basolateral amygdala following tone presentation during extinction trials. In addition, the authors found that both CB_1 knockout mice and CB_1 wild-type mice treated with the CB_1 receptor antagonist SR141716A had impaired extinction of fear-conditioned tests.

Previous reports have demonstrated the effects of cannabinoids on synaptic plasticity, particularly long-term potentiation (LTP). Nowicky and colleagues first demonstrated the effects

of THC on modulating the duration of LTP of the CA1 evoked field potential in rat hippocampal slices (Nowicky et al., 1987), thus providing insight into the role of endocannabinoids in synaptic plasticity. Inhibition of long-term depression (LTD) by cannabinoids has also been demonstrated in the hippocampal CA1 field, induced by lower frequency stimulation (Misner and Sullivan, 1999).

One other notable effect of cannabinoids include its orexogenic effect. Hyperphagia generally follows THC administration (Williams et al., 1998), whereas CB_1 receptor blockade results in a reduction in food intake (McLaughlin et al., 2003).

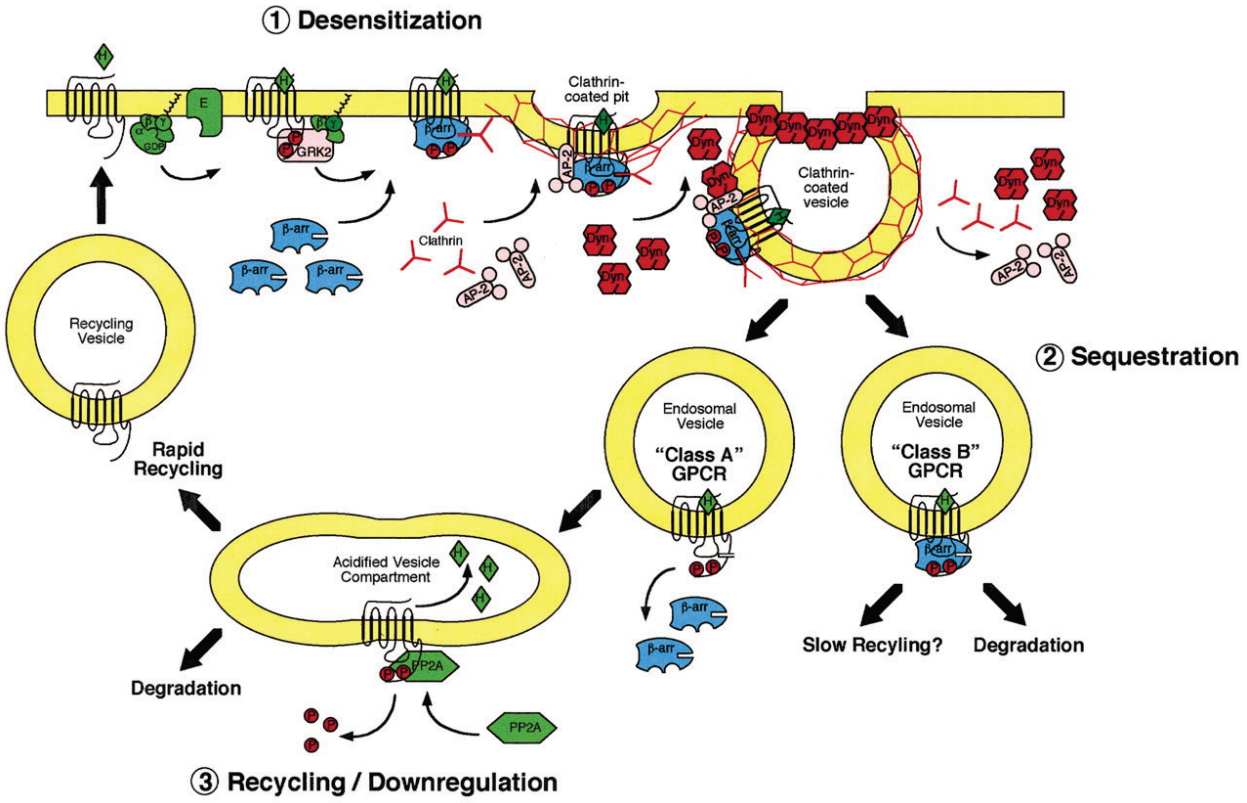

Figure 0.4. Regulatory mechanisms of G-protein coupled receptors. Following prolonged exposure to an agonist, GPCR signaling is attenuated through receptor desensitization (1), internalization (2), or downregulation where it is targeted for degradation (3). Resensitization or recycling of the receptor may also occur following internalization (from Luttrell et al, 2002).

G. Regulation of cannabinoid receptors: mechanisms of cannabinoid tolerance

Tolerance occurs when there is a reduction in the magnitude of a drug effect following chronic administration at a constant drug dose. Chronic administration of THC and other synthetic cannabinoid agonists produce tolerance to the behavioral effects of cannabinoids, which have been well characterized in laboratory animals. These include, for example, tolerance to cannabinoid-mediated antinociception, hypothermia, catalepsy, and reduction in spontaneous motor activity (Carlini, 1968; Gonzalez et al., 2005; Pertwee et al., 1993). Interestingly, tolerance to the memory impairment effects of cannabinoids does not appear to develop following prolonged administration (Barna et al., 2007; Boucher et al., 2009; Ferraro and Grilly, 1973). Studies in humans have been limited, however tolerance to the cardiovascular (Benowitz and Jones, 1975) and memory/cognitive impairment (D'Souza et al., 2008) effects of cannabinoids have been demonstrated. At the molecular level, chronic cannabinoid exposure results in the functional uncoupling of CB_1 receptors from G-proteins (desensitization) (Sim et al., 1996a) and agonist-promoted internalization (Jin et al., 1999); followed by either receptor degradation in lysosomes (downregulation) or recycling to the cell membrane (resensitization) (Sim-Selley et al., 2006; Tappe-Theodor et al., 2007). These receptor adaptations are thought to contribute to the development of cannabinoid tolerance.

Receptor downregulation

Adaptation to chronic administration of cannabinoids does not appear to be pharmacokinetic (Dewey et al., 1973; Martin et al., 1976), but rather pharmacodynamic in nature. It is also likely that these neuroadaptive changes are reversible. For example, chronically administering THC for 90 days in rats resulted in no changes in CB_1 receptor levels in the

striatum, cerebral cortex, cerebellum, hippocampus, and brainstem/spinal cord, following a 60 day recovery period (Westlake et al., 1991). However, studying CB_1 receptor properties at earlier time points after chronic treatment can resolve characteristic CNS adaptations that have been implicated to contribute towards cannabinoid tolerance.

Agonist-activated GPCRs are rapidly phosphorylated by G protein-coupled receptor kinases (GRKs) and subsequently bound by arrestin proteins, which facilitate receptor uncoupling from G-proteins (see Fig. 0.4 and next section, *Receptor Desensitization*) and receptor internalization (Claing et al., 2002; Lefkowitz et al., 1990). These molecular events have been well characterized for the β_2-adrenergic receptor (β_2AR). Like the β_2AR, CB_1 receptors are internalized through clathrin-coated pits into early endosomes and this process requires the extreme carboxy tail of the receptor (Hsieh et al., 1999). Internalization occurs rapidly, and its rate correlates well with the relative efficacy of cannabinoid agonists to activate G-proteins. Recycling of internalized CB_1 receptors back to the cell membrane also occurs rapidly following brief incubations with agonist. However, longer agonist incubation times (60 minutes) may result in irreversible internalization and receptor degradation (downregulation) via lysosomes. The targeting of CB_1 receptors toward lysosomal degradation appears to require G-protein-associated sorting protein 1 (GASP1), a protein that has been shown to interact with CB_1 receptors and was required for agonist-induced downregulation of CB_1 receptors in spinal neurons (Tappe-Theodor et al., 2007). A recent report also demonstrated that GASP1 and CB_1 receptors were colocalized in both GABAergic and glutamatergic cells of the thalamus (Martini et al., 2010). The authors of this study also found a loss in downregulation in both the spinal cord and cerebellum, as well as a lack of tolerance development to antinociception, motor incoordination, and locomotor hypoactivity, but not hypothermia, in GASP1 knockout mice treated chronically with WIN. In

other studies, prolonged agonist exposure times required new protein synthesis in order to normalize receptor levels (Hsieh et al., 1999). In fact, CB_1 receptor protein levels, but not CB_1 receptor mRNA, matched the downregulation of CB_1 receptors as well as its recovery after cessation of THC treatment, suggesting that regulation of CB_1 receptors primarily occurs at the level of the protein (Sim-Selley et al., 2006).

Downregulation of CB_1 receptors was first suggested by Oviedo et al. as one of the underlying receptor-mediated mechanisms of cannabinoid tolerance using quantitative [^{3}H]CP55,940 binding autoradiography in rat forebrain sections (Oviedo et al., 1993). In that study, animals were injected once daily with intraperitoneal (i.p.) of THC (10 mg/kg), CP55,940 (1, 3, or 10 mg/kg), or vehicle for 14 days. Behavioral assessment of a separate group of rats under the same drug paradigm demonstrated tolerance to the inhibitory effects of THC and CP55,940 on spontaneous motor activity. Tolerance to the motor effects of THC and CP55,940 was associated with a reduction in [^{3}H]CP55,940 binding (indicative of receptor levels) in THC treated compared to vehicle control rats in all brain areas examined including: olfactory tubercle, septum, caudate-putamen, and nucleus accumbens. These changes in receptor density also followed a dose-response relationship, with greatest reduction in the higher dose group (70-80% decrease) and lowest reduction in the lower dose group (40-50% decrease). Another study also found a positive association with the magnitude of CB_1 receptor downregulation and dose of THC administration (McKinney et al., 2008). Interestingly, as depicted in Figure 0.5, the magnitude of receptor downregulation in that study appeared to vary not only as a function of dose, but brain region as well.

The degree of cannabinoid tolerance appears to vary based on the specific behavior assessed. Martin and colleagues found a high degree of tolerance to the pharmacological effects

of CP55,940 when dosing mice chronically (2 mg/kg) twice a day for 6.5 days (Fan et al., 1996). The ability of CP55,940 to decrease motor activity, produce hypothermia, and induce catalepsy was reduced by 163-, 97-, and 19-fold, respectively. One implication from this study is that the magnitude of tolerance does not develop proportionally for various cannabimimetic effects. Thus, differential tolerance may reflect the relative adaptability of different regions to chronic cannabinoids. The regional specificity in CB_1 receptor downregulation has further been demonstrated by Sim-Selley and Martin (Sim-Selley and Martin, 2002) using [^{3}H]SR141716A binding autoradiography to localize changes in CB_1 receptor levels. In this study, mice were treated with escalating doses of THC, WIN-55,212-2, or vehicle subcutaneously (s.c.) twice daily for 15 days. Densitometry showed that downregulation occurred in all CB_1 receptor-containing brain regions, albeit at varying magnitudes of reduction. High levels of downregulation (55-70%) were found in prefrontal cortex, nucleus accumbens, hippocampus, amygdala, hypothalamus, thalamus, and entorhinal cortex, and intermediate levels (45-50%) in cerebral cortex, caudate-putamen, periaqueductal gray (PAG), and cerebellum. The lowest levels (10-25%) were found in basal ganglia output nuclei: globus pallidus, entopeduncular nucleus, and substantia nigra. These three regions are also highly dense in CB_1 receptor levels; however it is unclear if this is related to the relative lower magnitudes of downregulation observed in these brain areas.

Receptor desensitization

Different families of regulatory molecules are known to participate in desensitization of GPCRs: second messenger-dependent kinases (i.e. PKA, PKC, etc.), GPCR kinases (GRKs), and the arrestins (visual and non-visual) (Gainetdinov et al., 2004; Lefkowitz, 1998). GRKs

(Gainetdinov et al., 2004) selectively phosphorylate agonist-activated receptors, which leads to the recruitment and binding of an arrestin protein (Lefkowitz, 1993, 1998). The binding of arrestin sterically hinders and disrupts the ability of the receptor to initiate signal transduction by functionally uncoupling the receptor and G-protein, a process called homologous desensitization as only the activated receptor is affected (Gainetdinov et al., 2004). In the brain, the major isoforms are arrestins 2 (βar1) and 3 (βarr2), each having its unique distribution pattern in the CNS (Gurevich et al., 2002). β-arrestin is also involved in receptor internalization through its interactions with key proteins, including clathrin and adaptor protein-2 (Moore et al., 2007). There are seven known mammalian GRK isotypes. GRK2 and GRK3, also known as β-adrenergic receptor kinase 1 and 2, respectively, are the predominant CNS isotypes and are widely distributed throughout synapses in the brain (Arriza et al., 1992).

The role of GRK and β-arrestin in mediating CB_1 receptor desensitization has been demonstrated in the *Xenopus* oocyte expression system (Jin et al., 1999). Anatomically, the brain distribution of βarr2 is ubiquitous and partially overlaps with CB_1 receptors, suggesting that these two proteins may be co-distributed in similar neuronal populations (Attramadal et al., 1992). However, the regional abundance of βarr2 varies; with highest levels in cortex, hypothalamus, amygdala, and hippocampus, and lower levels in striatum and cerebellum (Attramadal et al., 1992; Gurevich et al., 2002). Chronic THC treatment also increases the expression of specific isoforms of GRKs and β-arrestins at different extents by brain region; with GRK2, GRK4, and βarr1 predominantly in striatum, GRK4 and βarr2 in cerebellum, and GRK2 and βarr2 in hippocampus (Rubino et al., 2006). This regional specificity suggests differential regulation between neuronal populations, which could account for the differences in the

regulation of CB_1 receptors in distinct brain regions (Breivogel et al., 1997; Sim-Selley, 2003; Sim et al., 1996a).

The development of functional binding assays such as cannabinoid-stimulated [^{35}S]GTPγS binding in homogenized membrane preparations (Selley et al., 1996) and brain tissue sections (Sim et al., 1995) offered the ability to quantitate CB_1 receptor-mediated G-protein activation. Sim et al. (Sim et al., 1996a) first demonstrated desensitization of CB_1 receptors in brain tissue sections from rats chronically treated with THC (10 mg/kg for 21 days). In this paradigm, almost all sampled brain regions exhibited a profound decrease in WIN-stimulated [^{35}S]GTPγS binding. Large decreases (>50%) in receptor-mediated G-protein activation were found in hippocampus, cortex, caudate-putamen, and cerebellum. However, a number of regions exhibited lesser desensitization (20-30%), such as PAG, septum, globus pallidus, and substantia nigra. Further intra-regional differences in the magnitude of desensitization occurred within brain areas. For example, greater desensitization was found in the ventral aspects (60%) compared to dorsal aspects (34%) of entorhinal cortex. Other reports have found desensitization of CB_1 receptor-mediated G-protein activation in similar brain regions chronically administering other cannabinoid agonists including THC (Breivogel et al., 1999; McKinney et al., 2008; Sim-Selley and Martin, 2002; Sim-Selley et al., 2006), CP55,940 (Rubino et al., 1997), and WIN55,212-2 (Sim-Selley and Martin, 2002; Sim-Selley et al., 2006). In most of these reports, the cortex, hypothalamus, and hippocampus, exhibited the largest magnitude in desensitization (ranging 50-70%), while others were moderate, such as cerebellum, thalamus, and PAG (ranging 40-50%). Regions dense with CB_1 receptors, such as globus pallidus, entopeduncular nucleus, and substantia nigra, tend to be least sensitive to desensitization.

Sim-Selley and Martin explored the possible ligand-specific differences in receptor adaptation in mice that were chronically treated with equally active and escalating doses of either THC or WIN55,212-2 for 15 days (Sim-Selley and Martin, 2002). In this report, desensitization had an inverse association with agonist efficacy, as the low efficacy partial agonist THC produced greater desensitization than the full CB_1 agonist WIN55,212-2 in most brain regions examined. No differences however were detected between the two agonists in the magnitude of CB_1 receptor downregulation. When comparing the regional differences in the magnitude of desensitization between the two agonists, THC produced approximately 2-fold greater desensitization than WIN55,212-2 in striatum, hippocampus, hypothalamus, PAG and amygdala. This finding is in agreement with a different study using the same treatment paradigm (Sim-Selley et al., 2006). Further, the regional desensitization profile was: hypothalamus > cortex > hippocampus > striatum > PAG > thalamus > globus pallidus > substantia nigra > entopeduncular nucleus (Sim-Selley and Martin, 2002). Interestingly, the degree of tolerance that developed in this paradigm differed by the type of behavior assessed and also by the agonist used. THC demonstrated a tolerance profile of antinociception (119 fold) > hypothermia (53 fold) > decreased spontaneous motor activity (6.3 fold). These data indicate that differential tolerance can occur during chronic THC treatment.

McKinney et al. (McKinney et al., 2008) explored the regional differences in CB_1 receptor adaptation after administration of varying doses of THC and assessed tolerance produced by this chronic paradigm. Mice were treated twice daily for 6.5 days with either vehicle, or varying doses of THC: Low = 10 mg/kg, Medium = ramping dose of 10 to 20 to 30 mg/kg, High = ramping dose of 10 to 30 to 60 mg/kg. This paradigm demonstrated differential tolerance to THC-mediated effects and regionally-specific CB_1 receptor adaptations as a function

of THC dose (Fig. 0.6). For example, desensitization of the striatum and globus pallidus occurred only after medium and high doses of THC administration, whereas CB_1 receptor downregulation occurred after the high dose, with an insignificant trend following the medium dose. This dose-dependent trend was also observed for measures of motor function that may be related to these brain regions. Here, tolerance to THC-mediated decrease in spontaneous motor activity and catalepsy was detected only in medium and high doses of THC treatment. In contrast, tolerance to THC-mediated hypothermia and antinociception (associated with desensitization in PAG) was evident beginning with the low dose group. The regional specificity in CB_1 receptor desensitization may have implications in the development of tolerance to various cannabinoid-mediated behaviors, and suggests that different mechanisms may exist in regulating CB_1 receptor function.

Recently, studies in mice lacking FAAH, the enzyme primarily responsible for the degradation of AEA, showed that repeated administration of AEA produced less adaptive changes at the CB_1 receptor than THC (Falenski et al., 2010). Conversely, sustained elevation of the endocannabinoid 2-AG produced by chronic administration of JZL184 (Long et al., 2009), an inhibitor of MAGL (the enzyme primarily responsible for the degradation of 2-AG), resulted in region-specific desensitization of CB_1 receptor-mediated G-protein activity (Appendix Fig. A1, Schlosberg et al., *in press*). Results from these studies suggest that FAAH inhibition may be a better therapeutic target versus inhibition of MAGL or chronic treatment with synthetic cannabinoids, which produce greater tolerance to their own effects.

Data on CB_1 receptor localization, interaction with various proteins, and signal transduction pathways, are providing important insight into the physiological role of the endogenous cannabinoid system. However, a growing challenge is the translation of knowledge

gained from mechanistic studies in cellular systems into native anatomical contexts. An important matter is understanding how the signaling and regulation of CB_1 receptors may vary in different neuronal populations, and how this contributes to the *in vivo* effects of cannabinoids. Studies in this dissertation will address these questions, and introduce novel approaches for the study of CB_1 receptor function and regulation in the CNS.

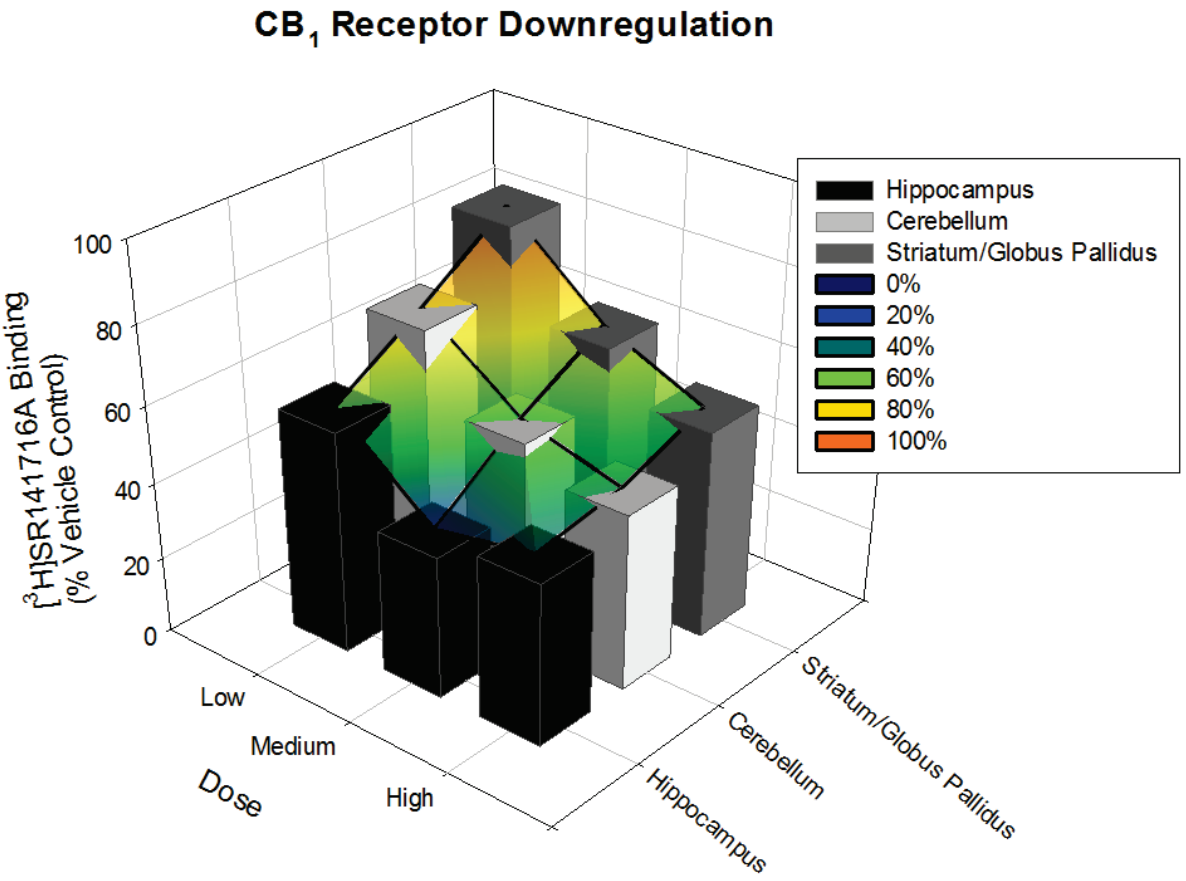

Brain Region	Dose (%Vehicle Control) Low	Medium	High
Hippocampus	58.06	37.33	42.62
Cerebellum	72.12	53.54	46.24
Striatum/Globus Pallidus	87.39	65.98	54.54

Figure 0.5. CB_1 receptor downregulation following chronic THC administration as a function of THC dose and brain region. B_{max} values were determined through [^{3}H]SR141716A saturation binding in membrane preparations from various brain regions, and is represented as %Vehicle Control. A low (10 mg/kg), medium (escalating from 10 to 20 to 30 mg/kg), or high (escalating from 10 to 30 to 60 mg/kg) dose of THC was administered twice daily for 6.5 days. A 3D pseudocolored gradient is shown to highlight differences in the magnitude of CB_1 receptor downregulation as a function of dose and region (adapted from McKinney et. al., 2008)

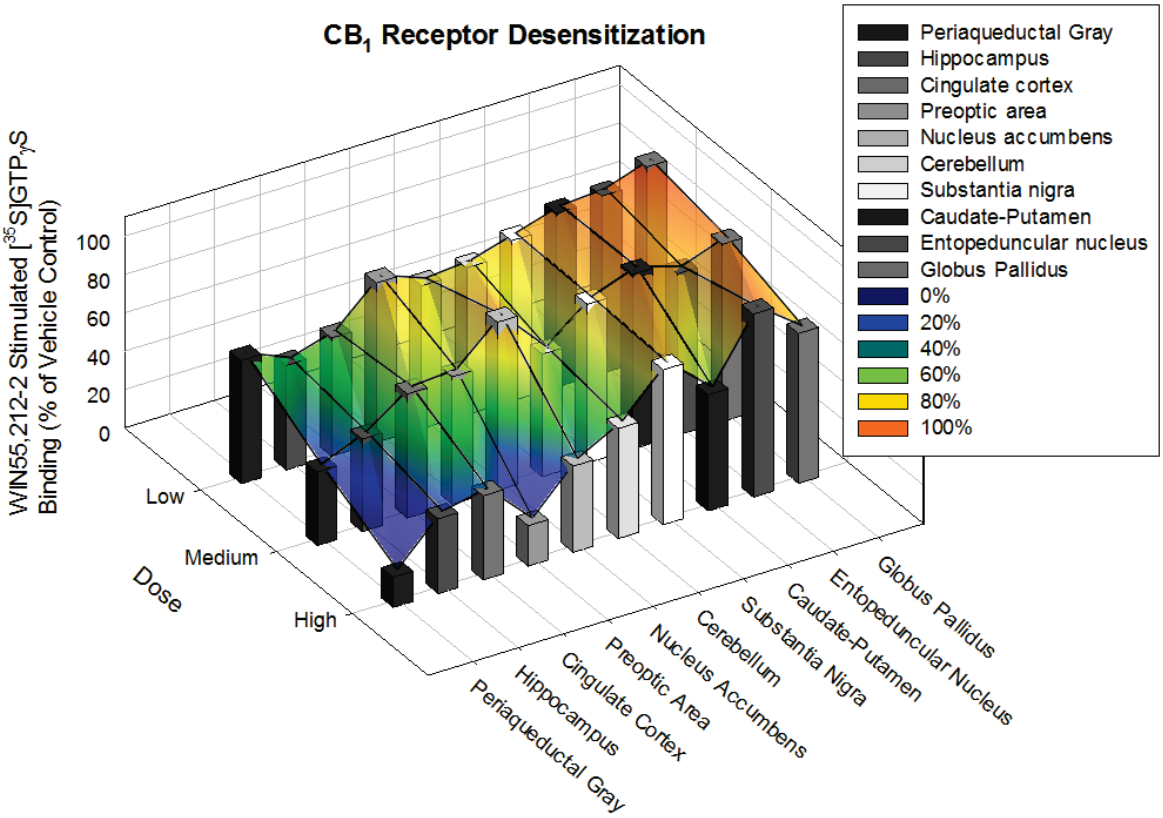

	Dose (%Vehicle Control)		
Brain Region	**Low**	**Medium**	**High**
Hippocampus	54.59	48.35	39.05
Cingulate cortex	61.64	64.82	43.79
Preoptic area	83.13	66.46	21.06
Nucleus accumbens	74.53	87.76	45.08
Cerebellum	76.66	63.84	57.40
Substantia nigra	83.64	82.75	80.85
Caudate-putamen	90.65	91.18	60.64
Entopeduncular nucleus	92.55	84.29	95.51
Globus Pallidus	100.52	92.51	78.18

Figure 0.6. CB_1 receptor desensitization following chronic THC administration as a function of THC dose and brain region. A low (10 mg/kg), medium (escalating from 10 to 20 to 30 mg/kg), or high (escalating from 10 to 30 to 60 mg/kg) dose of THC was administered twice daily for 6.5 days. WIN-stimulated [^{35}S]GTPγS binding is represented as %Vehicle Control. A 3D pseudocolored gradient is shown to highlight differences in magnitude of CB_1 receptor desensitization as a function of dose and region (adapted from McKinney et. al., 2008)

II. Rationale and Hypotheses

CB_1 cannabinoid receptors belong to the superfamily of G-protein coupled receptors (GPCR) and are widespread throughout the CNS, with greatest abundance in the basal ganglia, hippocampus, and cerebellum. CB_1 receptors also mediate the psychoactive and therapeutic effects of Δ^9-tetrahydrocannabinol (THC), the primary psychoactive constituent of marijuana. Interestingly, the acute and chronic cellular actions of CB_1 receptors vary by brain region, suggesting that specificity in CB_1 receptor signaling may contribute to differential therapeutic versus side effects of cannabinoids as well as its chronic effects, including tolerance and physical dependence. Our laboratory and others have found regional differences in the regulation of CB_1 receptors by examining a subset of CB_1 receptor containing regions that are likely to mediate various robust cannabimimetic effects, including memory disruption, antinociception, catalepsy, hypothermia, and reduction in spontaneous motor activity. However, the endocannabinoid system is implicated in diverse physiological functions, highlighting the importance of conducting an anatomically inclusive analysis. Yet, it has been difficult to conduct a comprehensive and thorough anatomical study of CB_1 receptors due to limitations in autoradiographic analytical approaches and inherent challenges in defining anatomical boundaries for sampling pre-defined regions of interest; especially when the distribution of differences are not known a priori.

In the following studies in this thesis, we propose that the acute and chronic signaling and regulation of CB_1 receptors occur in a region-specific manner. Furthermore, development of an unbiased whole-brain based approach will facilitate answering questions at the receptor level among anatomically distinct systems. This will be accomplished by using a novel voxel-based

image analysis approach, based on Statistical Parametric Mapping (SPM), to systematically investigate CB_1 receptor signaling throughout the brain, which has previously not been described. In the first chapter, we establish an approach to reconstruct mouse brain images derived from agonist-stimulated [^{35}S]GTPγS binding autoradiographic data into 3D volumetric images. In addition, various image processing techniques are implemented and assessed. This process lead to the development of a novel analytic approach for assessing autoradiographic data based on SPM that was subsequently applied in the following studies.

Ligand-dependent regulation of CB_1 receptors has been demonstrated in cellular systems examining various adaptations such as receptor desensitization, internalization, and downregulation. CB_1 receptors have also been shown to exhibit domain selectivity for coupling to various subtypes of $G\alpha_{i/o}$, and in various brain regions, activate different subtypes of G-proteins with varying efficacy and potency following agonist stimulation. Few studies however have directly compared the relative efficacy of different classes of cannabinoids in relation to receptor-mediated G-protein activation as a function of region. In the second chapter, we hypothesize that cannabinoid-receptor mediated G-protein activity will differ by cannabinoid ligand and that relative efficacy of these ligands will vary by brain region. Regional differences in the relative efficacy of cannabinoid agonists may highlight unique signaling properties of the CB_1 receptor, or suggest the existence of non-CB_1 sites. In addition, these findings may have implications regarding the regulation of CB_1 receptors following chronic administration of THC. For example, regional differences in the signaling of CB_1 receptors may invoke different downstream regulatory pathways in a region-specific manner, which may contribute to differential tolerance to various cannabinoid-mediated effects.

The regulation of cannabinoid receptors may potentially have important implications in regard to cannabinoid tolerance. Understanding the underlying mechanisms leading to cannabinoid tolerance not only is important from a therapeutic standpoint, but may also give insight into physical dependence or addiction to cannabinoids through potentially convergent regulatory pathways. This also has direct clinical relevance because THC and its synthetic derivatives are currently approved in the U.S. and indicated for treatment of adverse symptoms related to cancer chemotherapy and the anorexic effect of AIDS-related wasting syndrome. In addition, some states have permitted the medicinal use of marijuana. However, THC is the primary psychoactive constituent of marijuana, which is still the most commonly abused illicit drug in the U.S. Previously our laboratory demonstrated region-specific differences in the magnitude of CB_1 receptor desensitization and downregulation following chronic THC treatment. Other reports have demonstrated the importance of various regulatory proteins, such as β-arrestin-2 (βarr2), and kinases, such as GPCR kinase, in the regulation of CB_1 receptors in cellular systems. However, the *in vivo* physiological role of βarr2 in relation to the regulation of CB_1 receptor function is unclear. The final chapter will test the hypothesis that βarr2 plays a role in the regulation of CB_1 receptor desensitization and downregulation following chronic administration of THC. We predict that mice lacking βarr2 will exhibit a region-specific attenuation in the desensitization and downregulation of CB_1 receptors to chronic THC treatment, for example, in particular CB_1 receptor brain regions with high abundance of βarr2. Further, we propose that regional differences in βarr2-mediated regulation of CB_1 receptors will impact the development of tolerance to THC-mediated effects. Specifically, region-specific regulation of CB_1 receptor adaptation will result in a differential profile of tolerance to THC-mediated effects in associated anatomical systems.

Overall, we hypothesize that regional-differences in the acute and chronic signaling of CB_1 receptors reflect differences in its regional regulation, and that this specificity will be revealed using a novel whole-brain unbiased approach. This will be important in understanding not only the differences in the regulation of CB_1 receptors within various anatomical brain regions, but may also provide insight as to how this regional-specificity may contribute or play a role in the development of tolerance to various cannabinoid-mediated effects. As this novel approach is not restricted to predefined anatomical boundaries, we predict that it will extend our understanding of the function and regulation of the cannabinoid system with unprecedented anatomical precision.

III. Methods

Subjects

Mice were generally housed four to six per cage and maintained on a 12-hr light/dark cycle in a temperature controlled environment (20-22°C), with free access to food and water. All experiments were performed with the approval of the Institutional Animal Care and Use Committee at Virginia Commonwealth University in accordance with the *Guide for Care and Use of Laboratory Animals (National Research Council, 1996)*.

Drug treatment and Behavioral Evaluation

Specific drug treatments are described within individual chapters.

Antinociception. Antinociception is assessed using the tail warm water withdrawal assay at 52°C. The intensity of the warm water stimulus is fixed to yield control latencies of 3-4 sec, and an automatic 8 sec cutoff is used to prevent tissue damage. Tail-flick response latencies are expressed as the percentage of the maximum possible effect (%MPE) calculated by: *%MPE = [(test latency – control latency)/(cut-off time/control latency)]x100%*

Rectal Temperature. Core temperature to the nearest 1°C is measured by inserting a rectal probe connected to a Telethermometer (Yellow Springs Industries, Inc.) to a depth of 4.5 cm. Data are expressed as the difference in post- and pre-injection values from each animal expressed in units of °C.

Catalepsy. The effect of chronic cannabinoid injection on catalepsy were assessed using the ring immobility test. Each mouse was placed on a ring (5.5 cm in diameter) that is elevated 16 cm

above the tabletop for a 5 min session. The amount of time the mouse remains motionless will be recorded to the nearest second. Latencies of 100 sec or more will be considered cataleptic.

Drugs and chemicals

Guanosine 5'-O-[gamma-thio]triphosphate ([^{35}S]GTPγS, 1250 Ci/mmol) and [^{3}H]SR141716A (SA: 44.0 Ci/mmol) were purchased from PerkinElmer Life Sciences (Boston, MA). CP55,940, SR141716A, Δ^{9}-THC and [^{3}H]CP55,940 (88.3 Ci/mmol) were provided by the Drug Supply Program of the National Institute on Drug Abuse (Rockville, MD). Bovine serum albumin (BSA), GDP, GTPγS, and WIN55,212-2, WIN55,212-3 were purchased from Sigma-Aldrich (St. Louis, MO) and methanandamide (R-1) was purchased from Cayman Chemicals. All other chemicals were obtained from Sigma-Aldrich or Fisher Scientific.

Agonist-Stimulated [^{35}S]GTPγS Autoradiography

Mice were sacrificed by rapid decapitation, and brains were removed and immediately frozen in isopentane at -30°C and stored at -80°C. Autoradiographic assays were conducted as previously published from our laboratory (Sim et al., 1995). Briefly, coronal sections (20 µm) were cut on a cryostat maintained at -20°C, thaw-mounted onto gelatin-subbed slides, and stored desiccated at 4°C overnight. Slides were then stored desiccated at -80°C until use. To minimize variation in assay conditions, slides from each experimental condition within a single animal were processed concurrently. This allowed for identical assay conditions for basal and agonist incubated sections from each animal. For the [^{35}S]GTPγS autoradiography assay, slides were brought to room temperature (~22°C) for 40 min, then equilibrated in 50 mM Tris-HCl buffer (pH 7.4) with 3 mM $MgCl_2$, 0.2 mM EGTA, and 100 mM NaCl (Assay Buffer) for 10 min at

25°C. Next, slides were transferred to Assay Buffer + 0.5% BSA, with 2 mM GDP and 10 mU/ml adenosine deaminase for 20 min at 25°C. Slides were then incubated in Assay Buffer + 0.5% BSA containing 0.04 nM [^{35}S]GTPγS in the presence or absence (basal) of appropriate drug(s) and/or vehicle for 2 hrs at 25°C. After final incubation, slides were rinsed twice in 50 mM Tris buffer (pH 7.4) at 4°C, then in deionized water. Slides from each condition were then dried and loaded together in the same cassette with a [^{14}C] standard, and exposed to Kodak BioMax MR film for 24-36 hrs. Films were digitized at 8-bits per pixel with a Sony XC-77 video camera. [^{35}S]GTPγS binding data from autoradiography was generally expressed as Net Stimulation (nCi/g), which was calculated as: (agonist - basal).

[^{3}H]CP55,940 receptor binding autoradiography

[^{3}H]CP55,940 receptor binding autoradiography was conducted as previously described (Herkenham et al., 1991; Moise et al., 2008), with slight modifications. Brain tissue sections were initially thawed to room temperature for 40 mins and incubated for 3 hrs in assay buffer containing 50 mM Tris-HCl (pH 7.4), 5% BSA, and 3 nM [^{3}H]CP55,940 (88.3 Ci/mmol). Slides were then rinsed twice in wash buffer (50 mM Tris-HCl (pH 7.4), 1% BSA) maintained at 4°C for 2 hrs each. Sections were then briefly fixed in a solution containing 0.5% formalin in 50 mM Tris-HCl (pH 7.4) for 1 min and dried under a cool stream of air. Non-specific binding was assessed in the presence of 10 μM CP55,940. Slides from each subject (Total or Non-Specific) were loaded together in the same cassette with a [^{3}H] standard, and exposed to Kodak BioMax MS film for 18 weeks. Films were digitized at 8-bits per pixel with a Sony XC-77 video camera. [^{3}H]CP55,940 receptor binding data from autoradiography was generally expressed as Specific-binding (nCi/mg), which was calculated as: (Total binding - Non-specific binding).

Agonist-Stimulated [^{35}S]GTPγS binding for membrane homogenates

Membrane agonist-stimulated [^{35}S]GTPγS binding experiments were conducted as previously published (Sim-Selley et al., 2006). Briefly, mice were sacrificed by decapitation and the whole spinal cord and brain were extracted, and individual brain regions dissected. Tissue was immediately frozen on dry ice and stored at -80°C until use. On the day of assay, tissue samples were homogenized in 5 ml of cold Assay Buffer (*see Agonist-Stimulated [^{35}S]GTPγS Autoradiography section above*) and centrifuged at 50,000g at 4°C for 10 min. Supernatant was then discarded and tissue sample resuspended in 5 ml of Assay Buffer. Sample protein concentrations were determined by the Bradford method (Bradford, 1976). Tissue homogenates were then incubated with adenosine deaminase (3 mU/ml) in Assay Buffer for 15 min at 30°C. To generate concentration-effect curves, membrane protein (8 µg for whole brain, 10 µg for cerebellum or whole spinal cord) was incubated in Assay Buffer (0.5 mL total volume) containing 0.1 nM [^{35}S]GTPγS, 0.125% BSA, 30 µM GDP, and varying concentrations of drug(s) for 2 hrs at 30°C. Non-specific binding was assessed in the presence of 20 µM unlabeled GTPγS. The reaction was terminated by vacuum filtration through Whatman GF/B glass fiber filters, and rinsed three times with cold Tris Buffer (50mM Tris-HCl, pH 7.4) at 4°C. Bound radioactivity was determined by liquid scintillation spectrophotometry following 15 hr extraction in Econo-Safe scintillation fluid. [^{35}S]GTPγS binding data from membranes was generally expressed as %Net Stimulation, which was calculated as: [(agonist - basal)/basal] x 100%.

[^{3}H]SR141716A receptor binding for membrane homogenates

Membrane and protein preparations were conducted as described above. Whole spinal cord membrane protein (30 µg) was incubated in buffer (pH 7.4) containing 50 mM Tris-HCl, 0.2 mM EGTA, 3 mM $MgCl_2$, 100 mM NaCl, 0.5% BSA and varying concentrations of [^{3}H]SR141716A (0.1 - 2.5 nM) for 1.5 hrs at 30°C. Non-specific binding was assessed in the presence of 5 µM unlabeled [^{3}H]SR141716A. The reaction was terminated by vacuum filtration through Whatman GF/B glass fiber filter paper soaked in Tris buffer (50mM Tris-HCl, pH 7.4) containing 0.5% BSA, and then rinsed three times with cold Tris buffer + 0.5 BSA at 4°C. Filtered samples were then placed in scintillation vials containing Econo-Safe scintillation fluid, shaken for 1 hr, and bound radioactivity was determined by liquid scintillation spectrophotometry. [^{3}H]SR141716A receptor binding data from membranes was generally expressed as Specific-binding (pmol/mg), which was calculated as: (Total binding - Non-specific binding).

[^{3}H]CP55,940 receptor binding for membrane homogenates

Membrane and protein preparations were conducted as described above. Whole cerebellar membrane protein (8 µg) was incubated in sodium-free buffer (pH 7.4) containing 50 mM Tris-HCl, 0.2 mM EGTA, 3 mM $MgCl_2$, 0.5% BSA and varying concentrations of [^{3}H]CP55,940 (0.03 - 8.5 nM) for 1.5 hrs at 30°C. Non-specific binding was assessed in the presence of 10 µM unlabeled [^{3}H]CP55,940. The reaction was terminated by vacuum filtration through Whatman GF/B glass fiber filter paper soaked in Tris buffer (50mM Tris-HCl, pH 7.4) containing 0.5% BSA, and then rinsed three times with cold Tris buffer + 0.5 BSA at 4°C. Filtered samples were then placed in scintillation vials containing Econo-Safe scintillation fluid, shaken for 1 hr, and bound radioactivity was determined by liquid scintillation

spectrophotometry. [^{3}H]CP55,940 receptor binding data from membranes was generally expressed as Specific-binding (pmol/mg), which was calculated as: (Total binding - Non-specific binding).

Thionin (Nissl) Staining

Unfixed brain tissue sections were initially placed in a 95% ethanol solution for 15 min and then hydrated in solutions of 70% ethanol, 50% ethanol, and then dH_2O water each for 1 min. Sections were then transferred to thionin working solution containing 93% buffer (7g Na-acetate, 2 mL glacial acetic acid, 1 L dH_2O) and 7% thionin stock (1 g thionin per 100 mL hot dH_2O) for 2 min (sections requiring lighter or darker staining were left in solution shorter or longer, respectively). Sections were next dehydrated stepwise in the following solutions for 1 min each: dH_2O, 50% ethanol, 70% ethanol, 95% ethanol, 100% ethanol. Sections were finally rinsed twice in Xylene for 1 min and preserved with permount and cover slipped.

3D image reconstruction and Statistical Parametric Mapping (SPM) analysis

Please see next chapter for complete methodology and assessment

Region of Interest (ROI) analysis

To validate and compare regions found to be significant with SPM analyses, separate ROI analyses were performed. ROI measurements were conducted on the original unprocessed images, averaged bilaterally across hemispheres, and analyzed with GraphPad Prism Version 5 using appropriate statistical tests and Tukey's post-hoc analysis for ANOVA designs. ROI anatomical boundaries were defined by a mouse brain atlas (Franklin and Paxinos, 2008). The

following brain nuclei were included within each regional ROI measurement: amygdala (basomedial, basolateral, & medial, lateral, central nuclei), auditory cortex (primary, secondary), cerebellum (molecular layer), cingulate cortex (primary, secondary), hippocampus (CA1-3, dentate gyrus), hypothalamus (medial), motor cortex (primary, secondary), somatosensory cortex (primary, secondary), thalamus (central, ventral posteromedial & posterolateral, ventromedial, and ventrolateral thalamic nuclei), and visual cortex (primary, secondary). All other brain regions (i.e. caudate-putamen, globus-pallidus, periaqueductal gray, substantia nigra) were measured in entirety based on anatomical boundaries defined by a mouse atlas (Franklin and Paxinos, 2008).

IV. Chapter 1: Statistical Parametric Mapping (SPM) analysis of cannabinoid-mediated G-protein activation in the 3D reconstructed mouse brain

1.1 General overview of SPM analysis for reconstructed data sets

Previously our laboratory developed agonist-stimulated [^{35}S]GTPγS autoradiography for the examination of receptor-activated G-proteins in brain tissue sections (Sim et al., 1995). This technique allows for both anatomical- and pharmacological-specific assessment of cannabinoid-stimulated G-protein activity (Figures 1.1-1.2) in a quantitative manner. Analysis of these datasets generally involves manual measurements of pre-defined regions of interest (ROI). ROI-based approaches therefore are limited by a priori selection of regions and subject to inter-rater bias. To avoid limitations in ROI-based approaches and investigate CB_1 receptor signaling in an anatomically inclusive way, we adapted a novel whole-brain unbiased approach based on Statistical Parametric Mapping (SPM) to study CB_1 receptor signaling in the 3D reconstructed mouse brain. The volumetric reconstruction of images derived from agonist-stimulated [^{35}S]GTPγS autoradiography and procedure for SPM analysis is outlined in Figure 1.3. Briefly, coronal brain sections are collected throughout the neuroaxis, processed for agonist-stimulated [^{35}S]GTPγS autoradiography, and digitized. Digitized images are then realigned to reestablish spatial consistency and stacked into a volumetric image array. SPM software is then used for further image manipulation and processing, including spatial normalization and image smoothing, which are required before implementation of voxel-based statistical analysis of data. Application of these methods are detailed in this chapter and further demonstrated with [^{3}H]ligand autoradiographic data in Chapter 3, and Appendix Figure A3. The reference to "SPM" throughout this dissertation will refer to both the Statistical Parametric Maps generated

from SPM analysis as well as the collection of tools packaged with the SPM software, which is available in the public domain (http://www.fil.ion.ucl.ac.uk/spm/). All image processing, analyses, and display of data were done on a Windows-based 32-bit architecture PC, having 4 gigabytes of RAM, a 3.2 Ghz Intel Pentium 4 processor, and a 256 MB 3D video card.

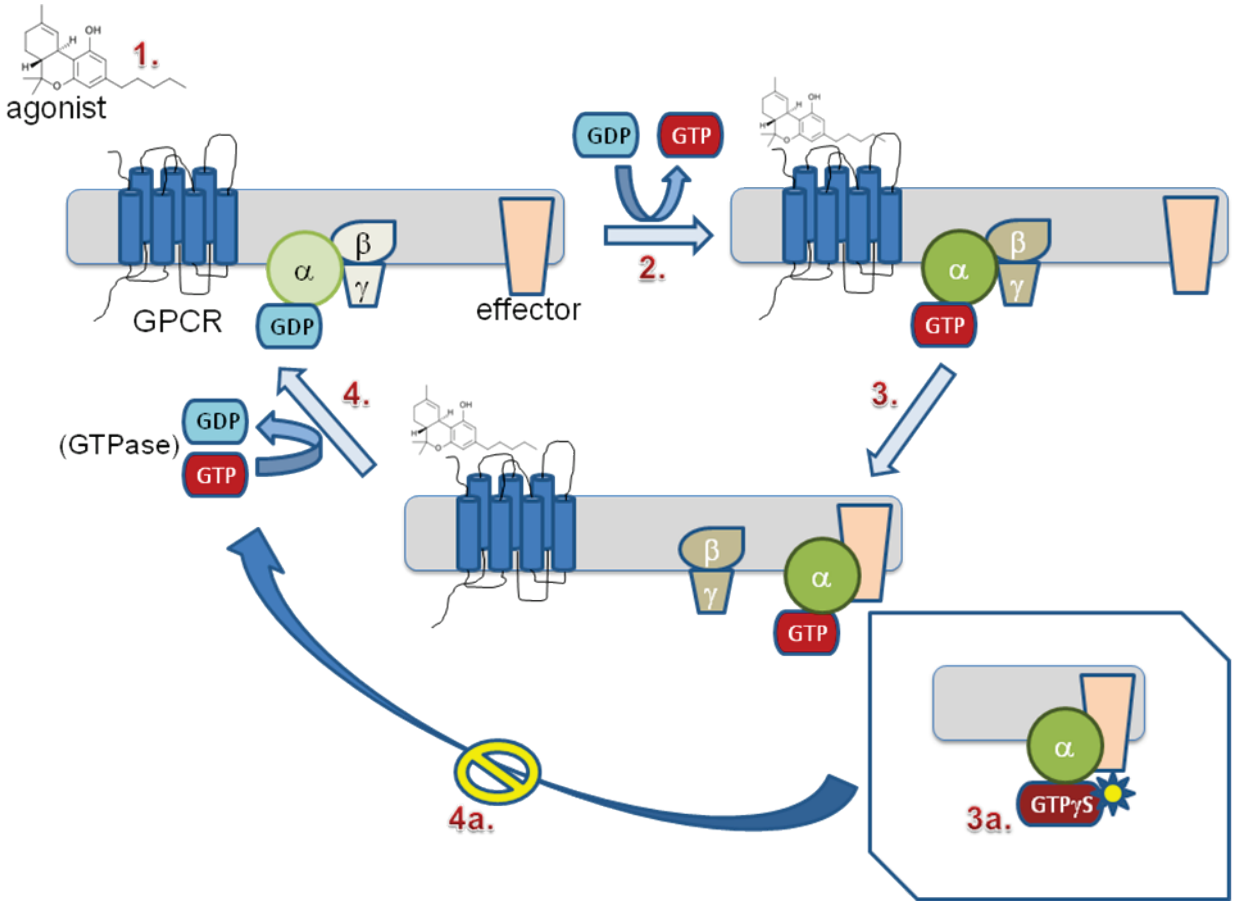

Figure 1.1. Overview of agonist-stimulated [^{35}S]GTPγS binding assay. Binding of an agonist (1) to a G-protein coupled receptor (GPCR) results in a guanine nucleotide exchange reaction of GDP to GTP (2) and subsequent activation of the G-protein. Activation leads to the dissociation of the G-protein into both βγ and α subunits, which interact with specific effectors (3). Termination of signal transduction occurs via an intrinsic GTPase (4), hydrolyzing GTP back to GDP. A non-hydrolyzable radiolabeled GTP analogue, [^{35}S]GTPγS (shown in bottom right, 3a), is used for quantification of receptor-mediated G-protein activity. This prevents the hydrolysis step and therefore leads to the accumulation of agonist-stimulated [^{35}S]GTPγS binding (4a).

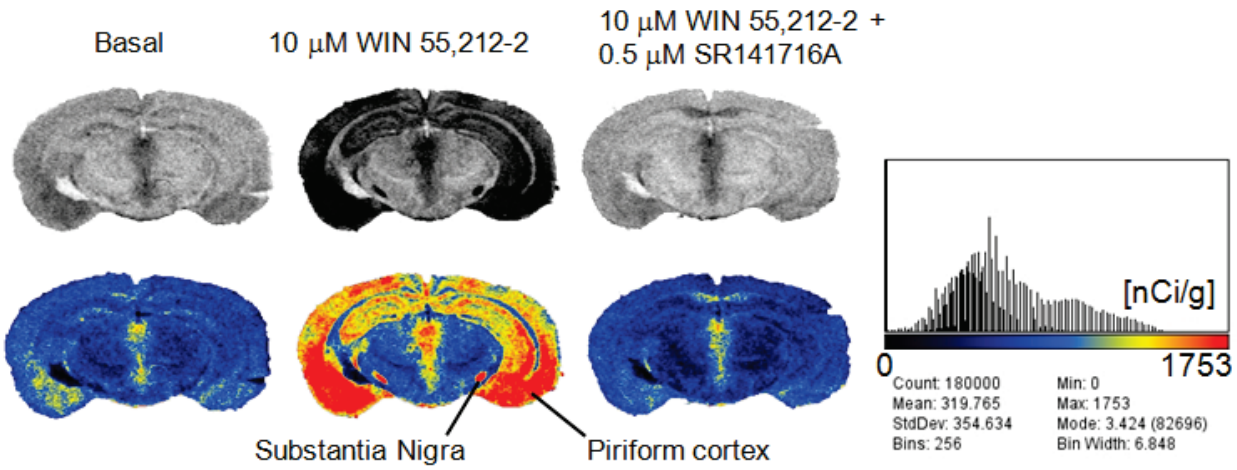

Figure 1.2. Cannabinoid-stimulated [^{35}S]GTPγS autoradiography. Agonist-stimulated [^{35}S]GTPγS autoradiography was performed as described in *Methods*. Autoradiographs are shown in grayscale (top row) and pseudocolor (bottom row), where black or red/yellow pixels represent areas with the lowest and highest levels of stimulated [^{35}S]GTPγS binding, respectively. Stimulated [^{35}S]GTPγS binding is shown for the basal (no agonist, left column) condition, and after incubation with the full CB_1 receptor agonist WIN55,212-2 alone (middle column) or in the presence of the CB_1 receptor antagonist SR141716A. A histogram shows the distribution of CB_1 receptor stimulated [^{35}S]GTPγS binding by WIN55,212-2 alone.

1.2 Preparation of brain tissue sections and image pre-processing

Brain image reconstruction of autoradiographic data was conducted based on previously published methods (Holschneider et al., 2006; Nguyen et al., 2004), with modifications. For each study in this dissertation, reconstructed brain images from each condition (i.e. agonist or basal (absence of agonist)) were created from coronal sections collected throughout the neuroaxis from bregma 2.34 mm to -6.84 mm (Franklin and Paxinos, 2008) with an inter-slice distance of 200 μm (Fig. 1.4). Volumetric reconstructions derived from coronal tissue sections produced the best results qualitatively compared to reconstructions from transverse sections (Fig. 1.5). Using an inter-slicing distance of 200 μm for transverse sections resulted in suboptimal slice realignment, likely due to rapid changes in anatomical structures as well as larger changes in overall surface area in this plane (see section *1.3 Slice registration and 3D image reconstruction*). The larger perimeter in transverse versus coronal sections also presents a greater challenge in minimizing edge distortion that results from tears and folding of tissue during collection. Larger surface areas in transverse sections in addition increase the risk for trapping debris, condensed water droplets on the surface of the blade, or pockets of air, which can create bumps or bubbles in the mounted tissue section. Furthermore, the asymmetrical surface with respect to the cutting direction in transverse (shaped like an irregular ellipsoid) versus coronal (shaped like a regular ellipsoid) sections may lead to non-uniform adhesion of biological tissue onto the glass slide, which can be further perturbed by other environmental variables such as humidity or static electricity. Significant edge distortions can lead to uneven and serrated edges, which can best be visualized in the reconstructed coronal plane (Fig. 1.5A).

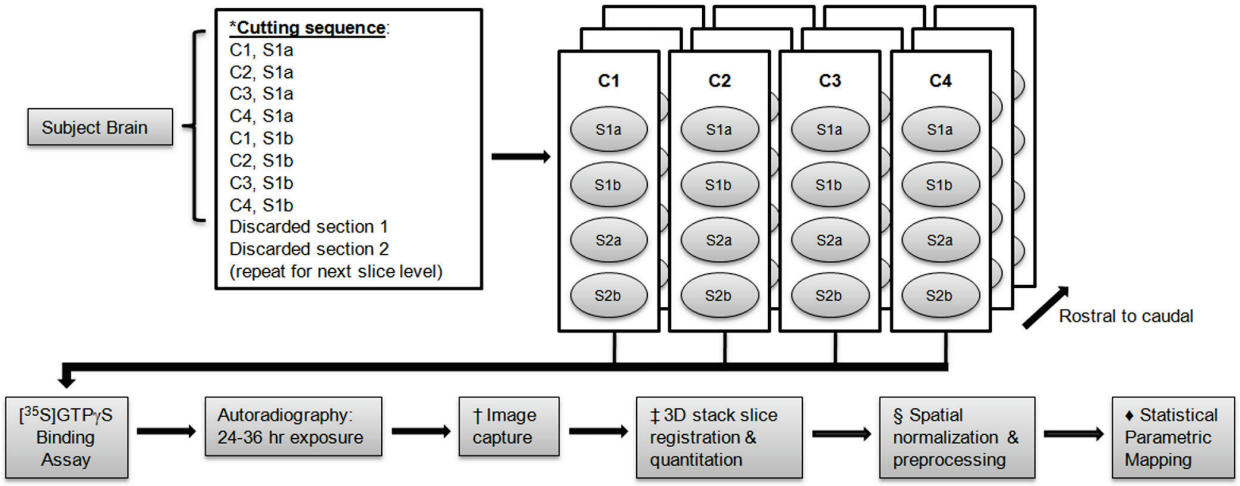

Figure 1.3. Flow chart of tissue preparation for autoradiography, 3D image reconstruction and SPM analysis (from *Nguyen et. al., NeuroImage 2010)*.

* 20 µm coronal sections are cut in a cryostat maintained at -20°C. C = condition; S = slice level; a & b = set 1 & 2 of duplicate sections

† The section free from artifact (i.e. S1a or S1b) at each slice level is digitized at 8-bits per pixel and saved in TIFF format

‡ Image reconstruction and slice registration described in *Nguyen et al., NeuroImage 2004*. Registered image stacks are quantitated and saved as 16-bit images in Analyze image format.

§ Individual image reconstructions are spatially normalized to a study-specific brain template as described in *Nguyen et al., NeuroImage 2004*. Spatially normalized images are then smoothed with a Gaussian kernel (Full Width Half-Max = 3X the voxel value)

♦ Statistical Parametric Mapping (SPM) software was used to setup experimental design and analysis of imaging data.

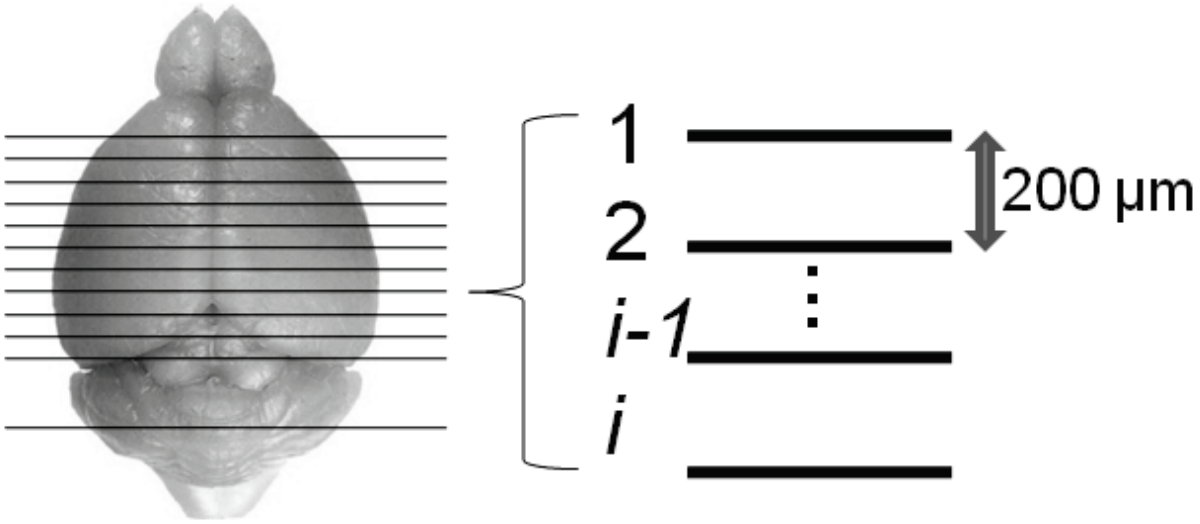

Figure 1.4. Brain sectioning strategy for 3D reconstruction. Volumetric reconstructions were derived from coronal sections (20 µm thick) collected throughout the neuroaxis from bregma 2.34 mm to -6.84 mm (Franklin and Paxinos, 2008) with an inter-slice distance of 200 µm. (i-1) = second to last slice; i = last slice

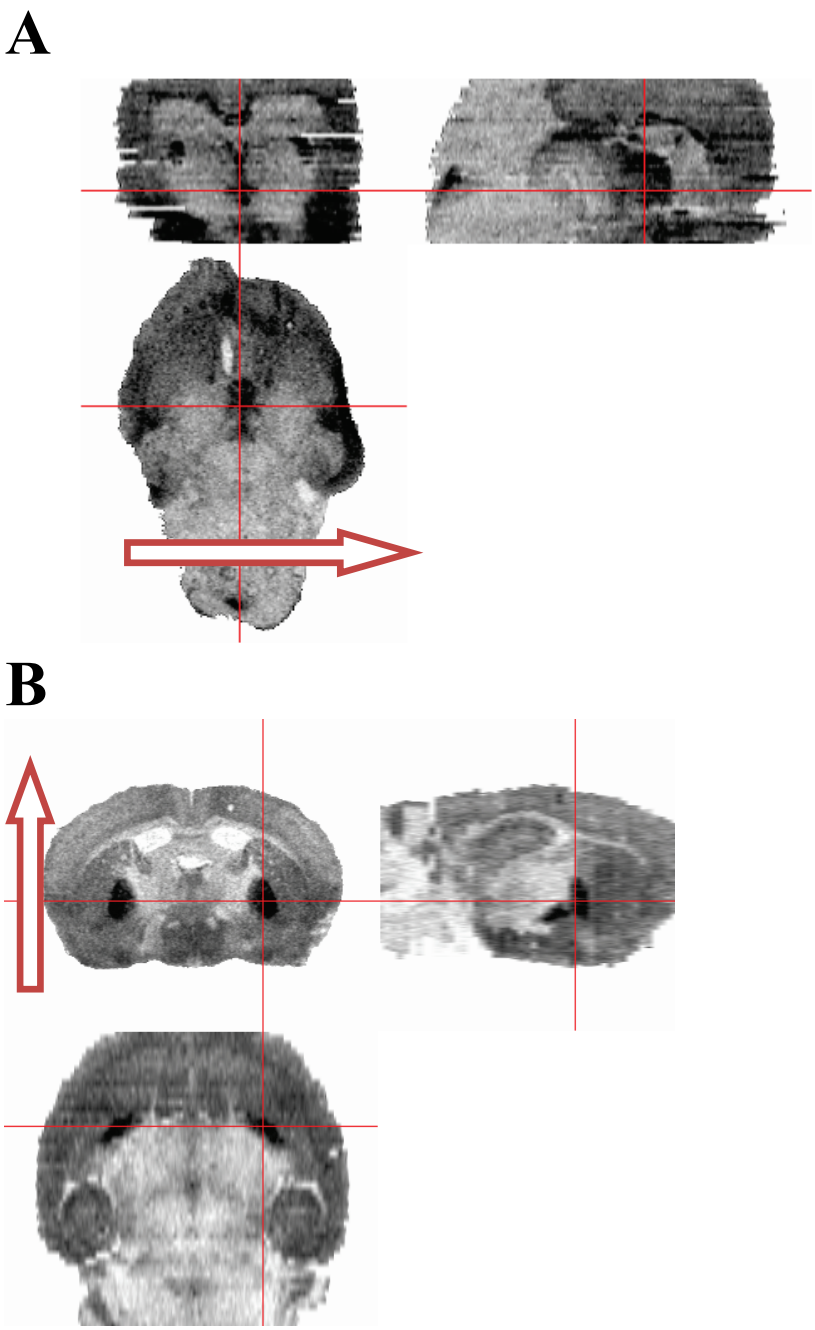

Figure 1.5. Image reconstructions derived from coronal or transverse sectioning. Volumetric reconstructions of 10 µM DAMGO- (A) and 10 µM WIN55,212-2- (B) stimulated [^{35}S]GTPγS binding autoradiographs in wild-type naive mice. Image reconstructions were derived from 200 µm spaced transverse and coronal sections for DAMGO and WIN55,212-2 images, respectively. Crosshairs highlight the medial thalamus (A) and globus pallidus (B) in three orthogonal planes. Arrows represent the direction of sectioning in the cryostat with respect to the cutting plane. Agonist-stimulated [^{35}S]GTPγS autoradiography was performed is described in *Methods*.

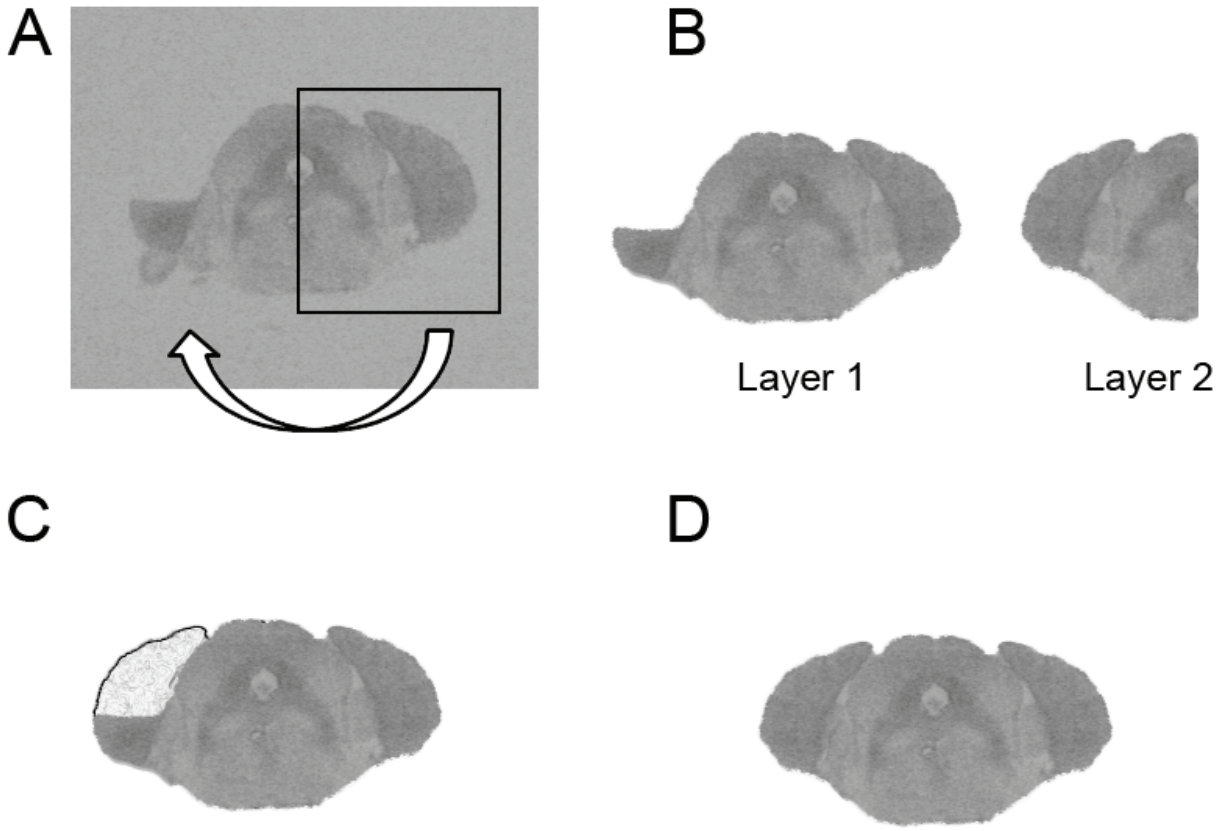

Figure 1.6. Image editing strategy for digitized autoradiographs having substantial artifact in one hemisphere. Missing tissue in one hemisphere is replaced by duplicating the missing tissue from the opposite intact hemisphere (A). The intact hemisphere is initially selected or image-masked, flipped horizontally, and duplicated as a new layer (B). The duplicated layer (layer 2 above) is placed behind the original layer (layer 1 above) and the two layers are manually aligned for spatial consistency. Replacement of the missing tissue area by the duplicated opposite hemisphere is represented as a shaded outline in the figure above (C). Both layers are then combined as a single layer or flattened image (D).

Serial adjacent sections from a single brain were collected for different assay conditions in duplicate sets. This scheme allowed for duplicate sets of at most 4 different conditions (reconstructions) from a single mouse brain as outlined in Figure 1.3. For sections with extensive artifact(s) or missing tissue in one hemisphere, the intact opposite side was duplicated and reflected (flipped horizontally) either behind or over the damaged hemisphere in order to preserve original imaging data (Fig. 1.6). For severely damaged sections that made this strategy impossible, the other duplicate section was utilized. In these special cases, the true inter-slice distance varied between 100 to 260 µm.

Tissue sections free from artifact related to extraction of the brain, tissue sectioning, etc., were selected for image reconstruction. A mask was next created for each selected digitized autoradiographic section. Most standard mask creation tools select connected pixels whose data values are within a defined tolerance of neighboring reference pixels. The Quick Selection Tool in Adobe Photoshop CS3 (Version 10) was used in these studies as it is suitable for both agonist-stimulated [^{35}S]GTPγS binding and [^{3}H]ligand binding autoradiographic data. Masked sections were then copied and pasted onto a new 8-bit grayscale image with a white background at 100 dpi and size of 300 x 250 pixels (width x height), and saved in TIFF format. Pixel size was calculated by measuring the width of a brain section on film by a ruler (units in mm) and dividing by the captured image width (units in pixels). For example from studies in this dissertation, the average width of a mouse section at bregma -1.8 mm (Franklin and Paxinos, 2008) is 10.6 mm and has an average corresponding pixel length of 266 pixels. This equates to a pixel dimension of about 40 µm/pixel. Thus for mouse brain sections captured at pixel dimensions of 40 x 40 µm^2, a white background of image size 300 x 250 pixels allowed adequate space for rigid-body transformations during slice realignment (see next section). In addition,

masked sections were centered and rotated manually so that midline was approximately parallel to the vertical reference axis of the white background image (Fig. 1.7). This initial prealignment provided a good starting estimate for slice registration.

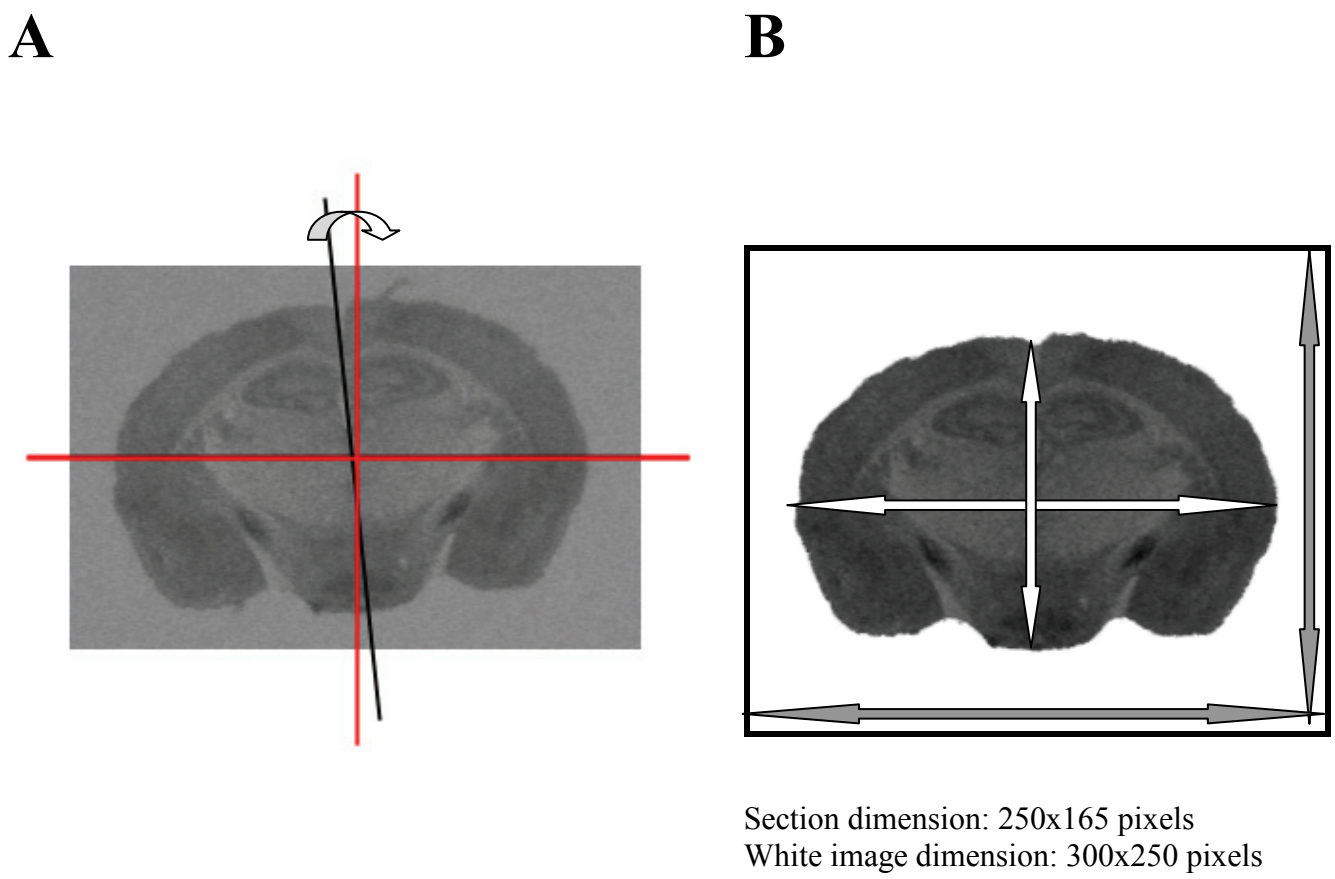

Figure 1.7. Slice image editing of digitized autoradiographs. Raw mouse brain images are initially outlined with a selection mask, pasted onto a new image with a white background and rotated manually if the midline axis of the raw image is not parallel to the vertical axis of the new image. (A) An arrow shows the manual rotation used for prealignment. The raw image is then centered vertically and horizontally to complete section prealignment. (B) Section and total image dimensions (*width x height*) in pixels are shown with white and gray arrows, respectively.

1.3 Slice registration and 3D image reconstruction

Image reconstructions were generated in ImageJ (version 1.42q, http://rsb.info.nih.gov/ij/) by importing coronal sections that were preprocessed as outlined in the previous section, and saving them as an image stack in Analyze format. The Analyze format (http://www.mayo.edu/bir/) is a common multidimensional biomedical imaging format that includes both a header (*.hdr) and data (*.img) file associated with each 3D image. The header file contains information such as voxel sizes, which must be defined prior to viewing and further processing within the SPM software. To make brain reconstructions spatially consistent in 3D, a section-to-section registration technique was used. Briefly, a section in the middle of the brain was chosen as the initial target to align adjacent sections in a stepwise fashion. Each registered section was then used as a new target to register the next adjacent section in either the anterior or posterior direction. A section in the middle of the brain was selected as the starting point to 1) allow for independent registration of slices in the anterior and posterior directions and 2) minimize the propagation of misregistration error that may occur in early slices if a section in the anterior-most pole was selected as the reference image. This registration algorithm utilizes the intensity of all image pixels for a section and searches for the transformation that maximizes a measure of intensity similarity between corresponding pixels of an adjacent section (Thévenaz et al., 1998). In other words the transformation is computed to minimize the mean-square difference between the target and source images. The registration algorithm is available as a plugin within the ImageJ environment called TurboReg (http://bigwww.epfl.ch/thevenaz/turboreg/). An auxiliary plugin, StackReg (http://bigwww.epfl.ch/thevenaz/stackreg/), was used for the recursive alignment of reconstructed image stacks in this dissertation. In order to preserve the original shape of tissue

sections, a non-warping rigid-body transformation was selected that consisted of only rotations and translations. It is important to note that the alignment algorithm performs optimally when the source and target images are comparable in size and have similar starting points (Nguyen, unpublished observations). Therefore, if the centers of two images are far apart, it is important to remove the translational offset manually (i.e. centering images) before proceeding with finer registration. StackReg offers an automatic and manual mode. In manual alignment, associated landmarks are defined on a source and target image to establish initial correspondence between them. All image registration in this dissertation used the automatic mode to minimize inter-rater variability.

Header files of registered image stacks were opened and edited using MRIcro software, which is available in the public domain (http://www.cabiatl.com/mricro/mricro/index.html) from the Center for Advanced Brain Imaging, Atlanta, GA. Voxel sizes of mouse brain images in this dissertation were scaled up 10X their true size (40 x 40 x 200 μm^3) and saved in the header files. This allowed for proper viewing within the SPM environment, which is originally designed for human brain imaging data having dimension sizes on the order of millimeters (Nguyen et al., 2004). Gray level intensities of the raw image stack were then quantitated to activity values (nCi/g of tissue) as previously described (Sim et al., 1996b). Briefly, [^{35}S] was incorporated into sections of frozen brain paste and sections were then weighed to obtain nCi/g of tissue. Radioactivity in each section was determined by liquid scintillation spectrophotometry. [^{14}C] microscale standards and [^{35}S] sections were then exposed to film and correction factors were calculated to convert [^{14}C] values to [^{35}S]. Raw optical density values (OD) are quantitated to radioactivity values (Y) using the following linear equation, where *m* is the slope and *b* is the intercept, as calculated from [^{14}C] standards:

$$Y = m \bullet OD + b$$

Reconstructed stacks were quantitated using a macro created within ImageJ and its complete code is shown in Figure 1.8. This fully automated macro script opens a registered image stack and prompts the user to enter the slope (*m*) and intercept (*b*) coefficients, as calculated from standards, in order to globally quantitate raw voxel values to radioactivity units (nCi/g) and then save the image at a bit depth of 16-bits. Saving at a dynamic range of 16-bits allowed for a potential data range from 0 to (2^{16}-1), or 65,535 nCi/g. The StackReg utility normally introduces "registration artifact" or black edges to visually show the transformations that were applied to realign sections (see registration results in Figures 1.10-1.12). The above macro also includes functionality to automatically remove registration artifact.

Although not required, volumetric images were reoriented in coordinate space to correspond to the standard viewing axis defined within the SPM software environment. In this standard coordinate space lateral, anterior-posterior, and dorsal-ventral correspond to the X, Y, and Z axes, respectively (Fig. 1.9). An automated macro script was written to reorient images using the To_AxialTP function (part of a suite of alignment plugins found at: http://www.med.harvard.edu/JPNM/ij/plugins/AlignStacks.html) within the ImageJ environment. The macro code and description is detailed in (Fig. 1.9).

Line #	ImageJ macro for quantitation of [^{35}S]GTPγS binding imaging data
1	open();
2	run("Invert", "stack");
3	run("Duplicate...", "title=mask.img duplicate");
4	run("Invert", "stack");
5	run("Max...", "stack value=1");
6	run("Calculator Plus", "i1 i2=mask.img operation=[Multiply: i2 = (i1*i2) x k1 + k2] k1=1 k2=0 create");
7	run("Invert", "stack");
8	run("32-bit");
9	run("Multiply...");
10	run("Add...");
11	run("Min...", "stack value=0");
12	run("16-bit");
13	run("Analyze 7.5...", "save");
14	close();
15	close();
16	close();

Description of macro code by line number:

1: prompts user for selecting image volume (analyze format, *.img)
2-3: inverts source image and creates a duplicate of itself
4: duplicate image is inverted
5: data values >1 are assigned a value of 1. This creates a binary (mask) image, so that areas with registration artifact have a data value of 0 and all else have a value of 1.
6: image array multiplication of source image and binary image
7: image inversion reverts source image back to original state (without registration artifact)
8: image bit depth increased to 32-bit to allow for the image quantitation
9: prompts user to enter slope coefficient calculated from ^{14}C standards using a linear fit
10: prompts user to enter the intercept (of abscissa) calculated from ^{14}C standards
11: data values < 0 (i.e. negative numbers) are assigned a data value of 0
12: quantitated images are saved at a dynamic range of 16-bit, to encompass the data range of [^{35}S]GTPγS binding imaging data, which typically ranges from 0 to 2,500 nCi/g
13: prompts user to save quantitated stack image in analyze format
14-16: closes all active windows

Note: This macro removes slice alignment artifact generated from using the StackReg plugin for ImageJ. General requirements: ImageJ ver 1.36b (or later) and calculator plus. **No other images should be open at time of use and "Scale when converting" must be disabled** (*under edit; options; conversions*).

Figure 1.8. ImageJ macro for removing slice registration artifact and quantitation of raw imaging data to radioactivity units (nCi/g).

Line #	ImageJ macro for reorienting images to correspond to SPM standard axis
1	open();
2	run("To AxialTP", "input=[Coronal (anterior-to-posterior)]");
3	run("Analyze 7.5...", "save");
4	close();
5	close();

Description of macro code by line number:

1: prompts user for selecting image volume (analyze format, *.img)
2: reorients image to correspond to the standard SPM axis (see image below)
3: prompts user to save image in analyze format
4-5: closes all active windows

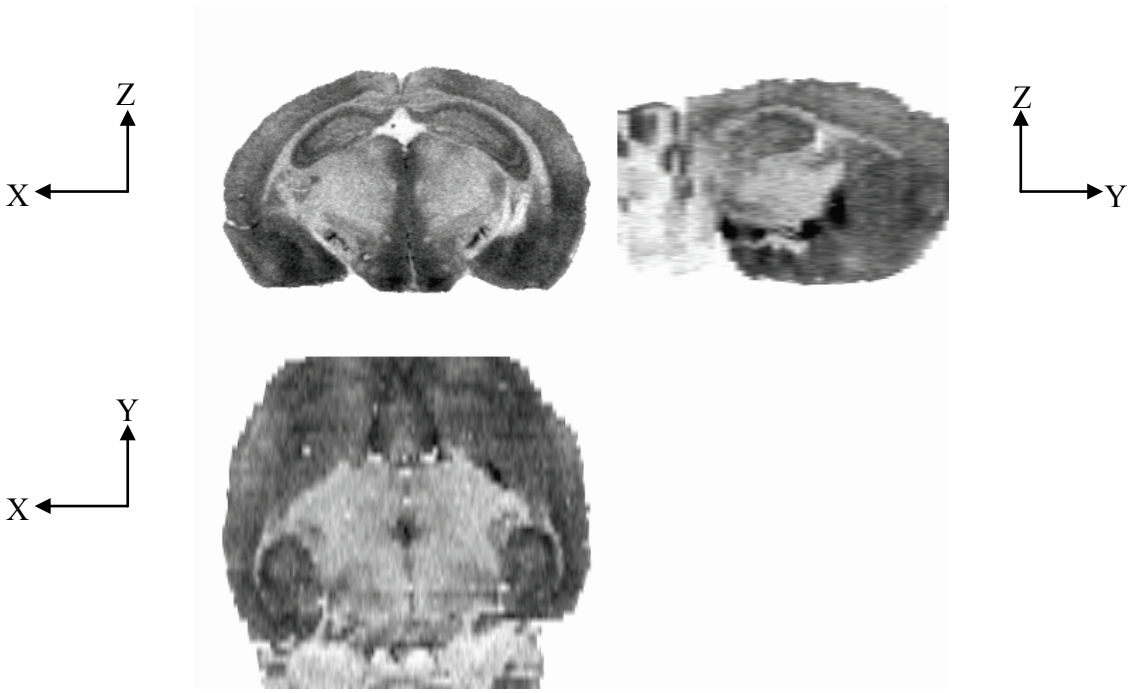

Figure 1.9. ImageJ macro for reorienting image volumes to correspond to the SPM standard axis: lateral left-right, anterior-posterior, and dorsal-ventral are the X, Y, and Z planes, respectively

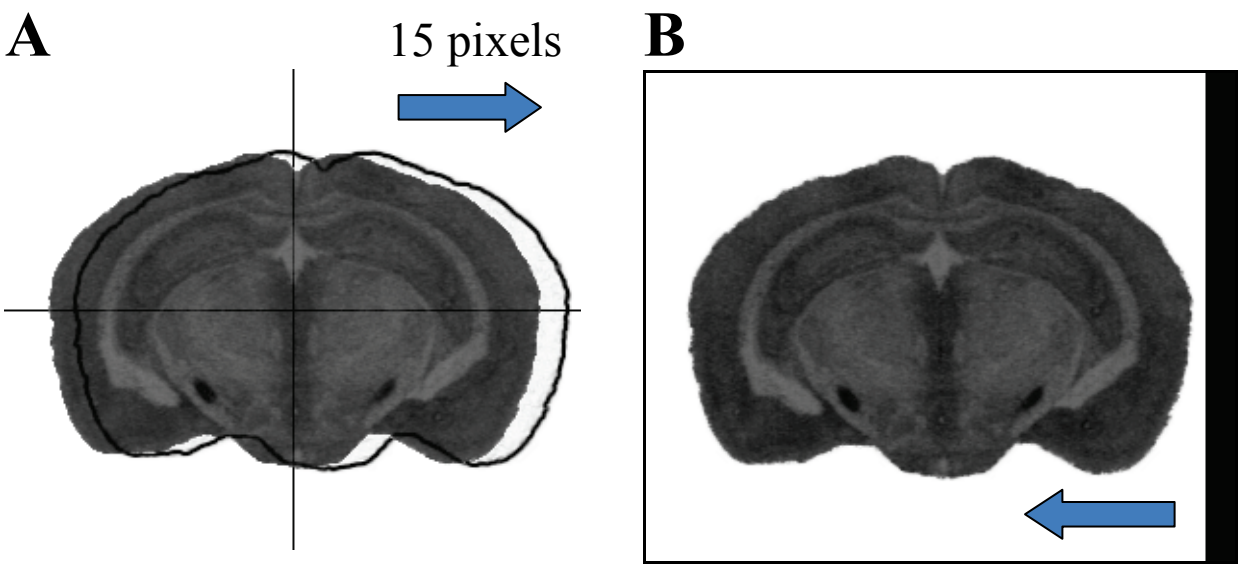

C

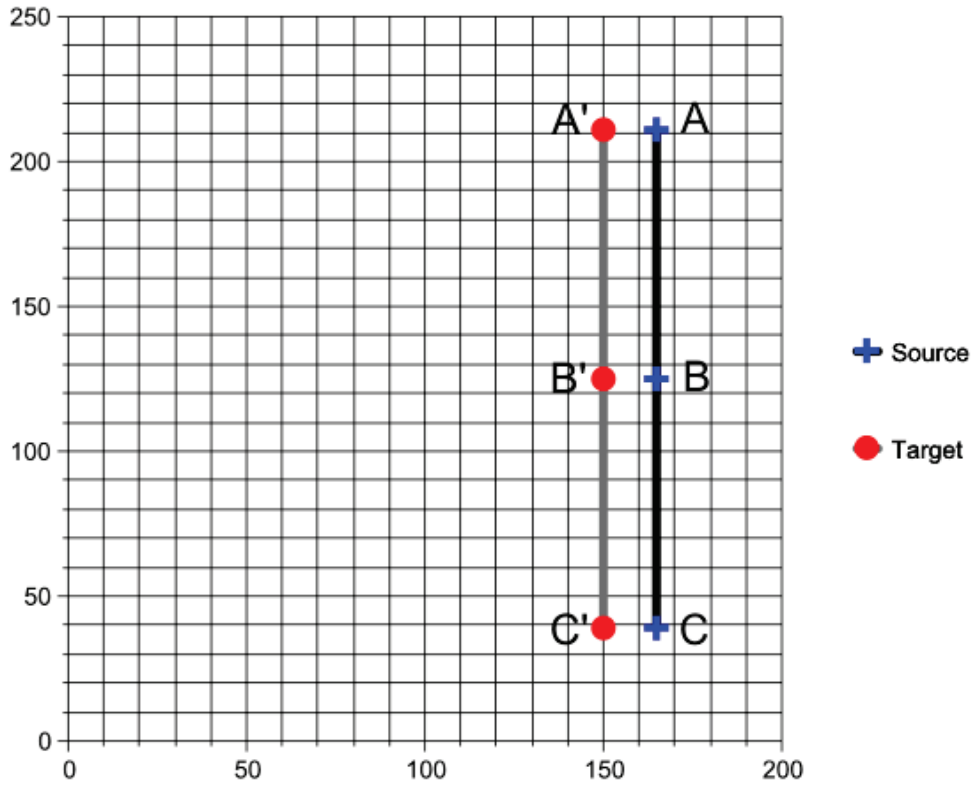

D

Refined source landmarks (x, y)	Target landmarks (x, y)
A (164.99, 210.99)	A' (150, 211)
B (164.99, 124.99)	B' (150, 125)
C (164.99, 38.99)	C' (150, 39)

Length of B' to B = B_x - B'_x = 164.99-150 = **14.99 pixels**

Figure 1.10. Image registration: translation simulation. (A) An image was duplicated and translated by 15 pixels. An outline of the translated slice is shown as an overlay on the original image. (B) An arrow and black area illustrates the applied transformation after image registration. (C) StackReg (TurboReg) utilizes landmarks on the target and source image to apply the transformation (D) Calculating the magnitude of translation can be done by vector subtraction of coordinate pairs.

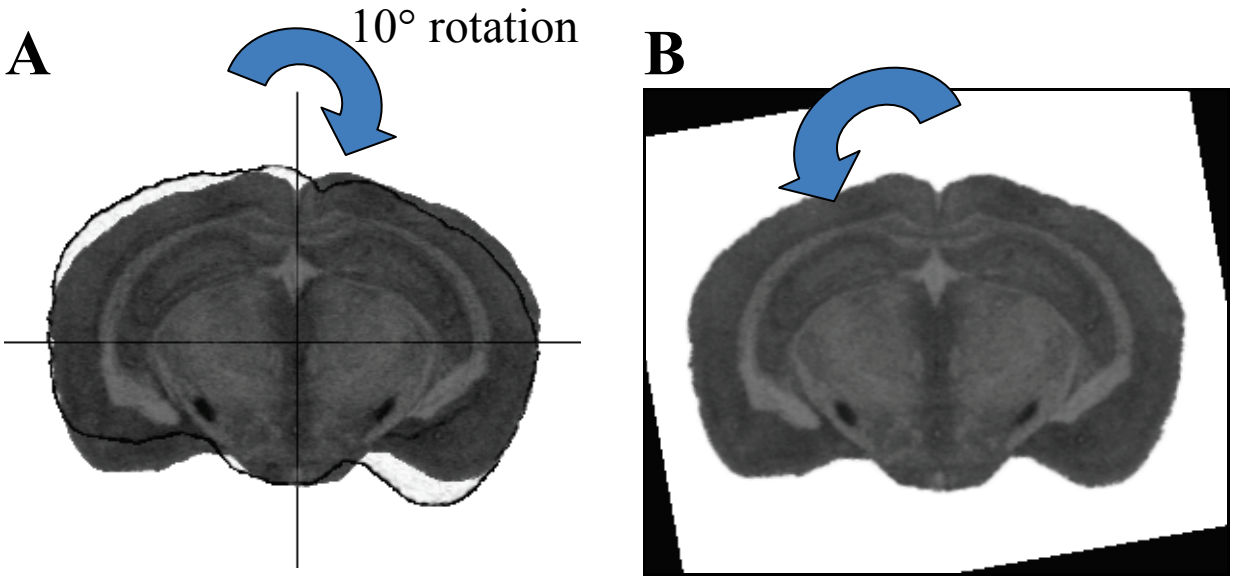

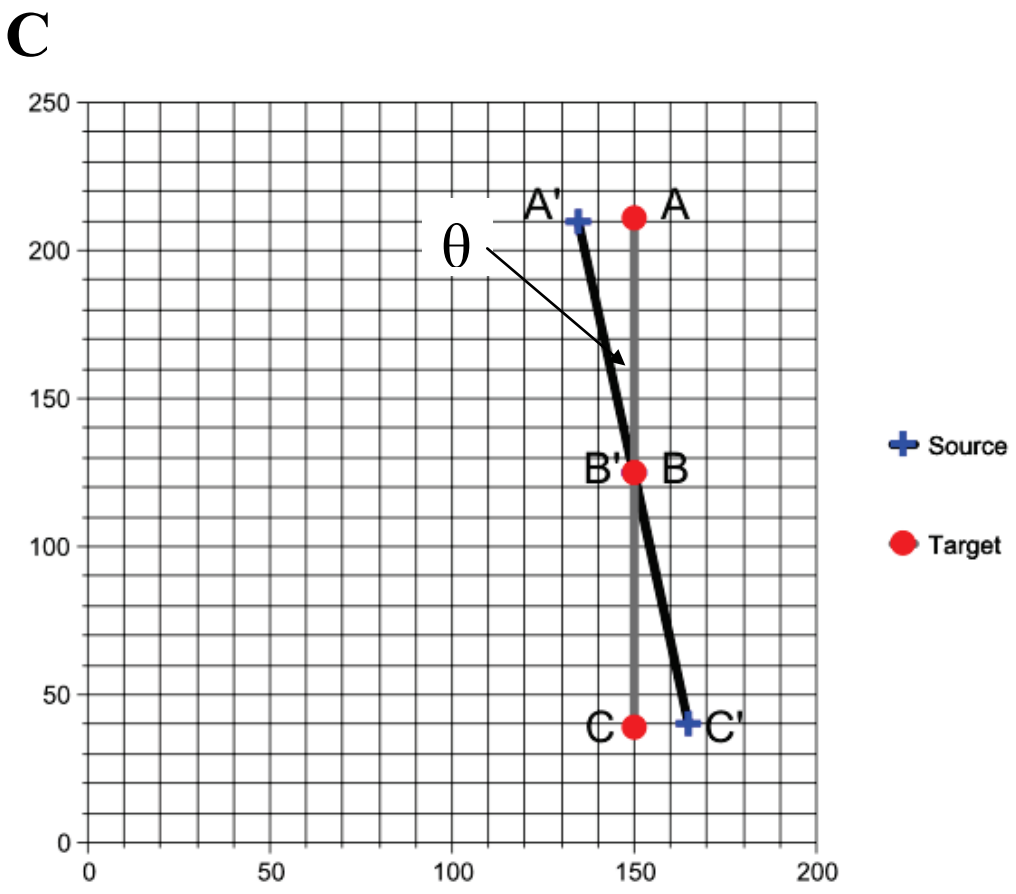

D

Refined source landmarks (x, y)	Target landmarks (x, y)
A' (134.88, 209.85)	A (150, 211)
B' (149.81, 125.16)	B (150, 125)
C' (164.75, 40.47)	C (150, 39)

$\theta = \tan^{-1}[(\text{length A' to A})/(\text{length A to B})]$

$= \tan^{-1}[(A_x - A'_x)/(A_y - B_y)] = \tan^{-1}[(150 - 134.88)/(211 - 125)] = \tan^{-1}(15.12/86) = \mathbf{9.97°}$

Figure 1.11. Image registration: rotation simulation. (A) An image was duplicated and rotated by 10 degrees. An outline of the rotated slice is shown as an overlay on the original image. (B) An arrow and black area illustrates the applied transformation after image registration. (C) StackReg (TurboReg) utilizes landmarks on the target and source image to apply the transformation. (D) Calculating the degree of rotation (θ) can be done trigonometrically.

A

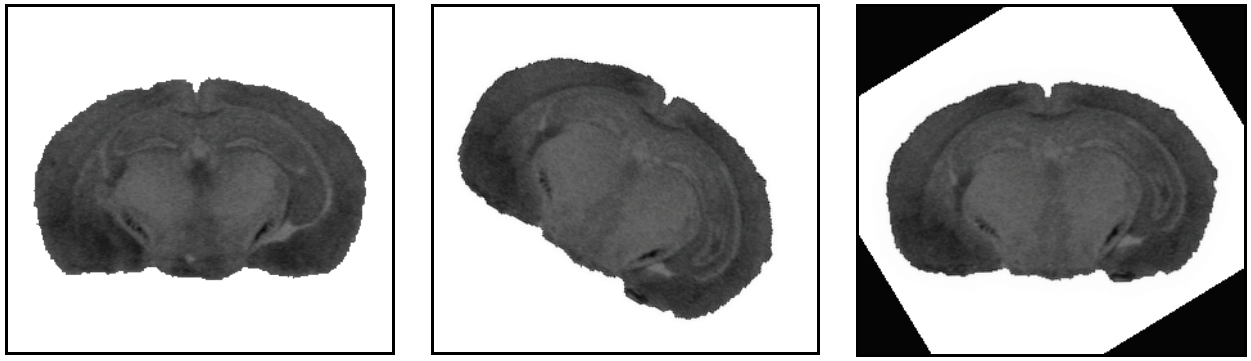

Slice A (target) Slice B (source) Slice B registered to A

B

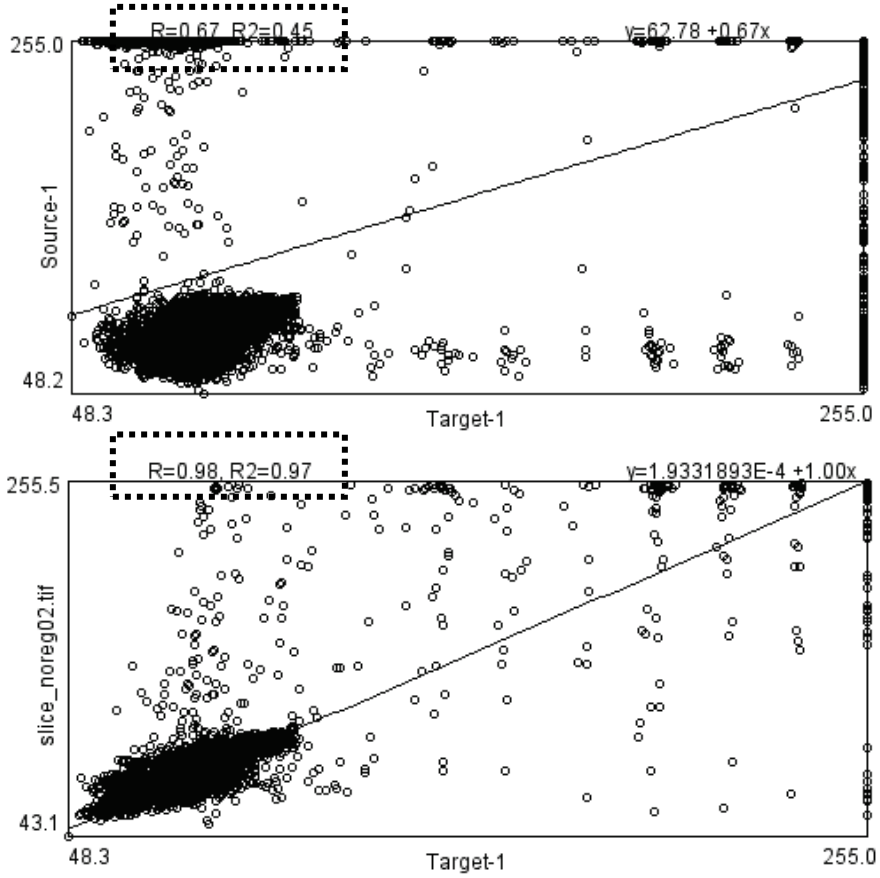

Figure 1.12. Registration of two representative coronal images (A) and image correlation plots before (B, top) and after registration (B, bottom). Slice registration increased the image correlation coefficient (R^2 value) to 0.97 (up from 0.45)

1.4 Assessment of registration algorithm: simulation studies

The quality of brain reconstructions was assessed by visual inspection of internal structures viewed in different orthogonal angles and correspondence of brain areas across reconstructions of different conditions and/or subjects. The SPM software includes a utility, called CheckReg, to load and view multiple images of the same size. Spatial correspondence between images can be assessed by a crosshair or point of reference, which updates each orthogonal frame in all loaded images. To quantitatively assess the accuracy of the registration algorithm used for agonist-stimulated [^{35}S]GTPγS autoradiographic data, simulation studies were done with representative brain tissue sections. A 2D image was registered to its duplicate that was either translated to the right by 15 pixels (Fig. 1.10) or rotated clockwise by 10° (Fig. 1.11). The calculated translation and rotation after applying image registration were 14.99 pixels and 9.97°, respectively. The differences from actual values were 0.01 pixels (misregistration error of 0.067% or about 0.4 μm) in the translation simulation and 0.03° (misregistration error of 0.3% or about 2.61 μm) in the rotation simulation.

To further assess the registration algorithm, an image correlation plot was constructed for two different adjacent sections (spaced at 200 μm) before and after applying image registration (Fig. 1.12). Corresponding pixel values from both images (source and target) at each coordinate were graphed and correlated using a linear fit. The correlation coefficient (R^2 value) was 0.45 before image registration and increased to 0.97 after application of registration, suggesting an improvement in spatial correspondence between the two adjacent sections. These simulation studies thus demonstrate the robustness and viability of using the registration algorithm implemented in StackReg for the recursive alignment of images derived from agonist-stimulated [^{35}S]GTPγS autoradiographic data.

1.5 Voxel-based Analysis using Statistical Parametric Mapping (SPM)

The SPM package exists as a collection of scripts written within the Matlab environment (http://www.mathworks.com/), which is a software program designed for numerical computation, creation of user-interfaces, implementation of algorithms, etc. SPM analyses (version SPM5, http://www.fil.ion.ucl.ac.uk/spm/) for reconstructed autoradiographs were conducted as previously published (Nguyen et al., 2004), with modifications. Prior to SPM analysis, all images from a study were spatially normalized into the same coordinate space (Ashburner J., 1999; Friston et al., 1995a) as defined by a study-specific brain template. This template was derived from brain reconstructions of the most efficacious agonist, due to its high structural information and contrast of anatomical boundaries, thus optimizing spatial normalization. Initially a subject's reconstructed brain image from the most efficacious agonist was selected based on alignment quality and freedom from artifacts. This image was then smoothed by 3X its voxel size (see below for image smoothing rationale) to serve as the preliminary template. All reconstructions of the most efficacious agonist from different subjects were then spatially normalized to the preliminary template while retaining the original voxel sizes. These spatially normalized images were then averaged, using the SPM image average tool (spm_avg.m script in SPM directory), and smoothed by 3X its voxel size to become the study-specific brain template.

Spatial normalization of reconstructions from multiple conditions (agonist(s) and basal) assayed from the same animal was performed by coregistering (using normalized mutual information option in SPM) these images to the most efficacious agonist. The coregistration technique allows within-subject registration of all reconstructions, so that they are aligned within the same coordinate space. This assumes that there are no gross differences among the shapes of

the reconstructed images, which is a reasonable assumption to make for images derived from the same animal. Intra-subject coregistration thus allows one to determine spatial normalization parameters from a single reconstruction (i.e. the most efficacious agonist) and subsequently apply them to all coregistered reconstructions from the same animal. Using this strategy has the dual advantage of reducing the number of spatial normalization routines as well as estimating the spatial normalization parameters from the set of images likely possessing the most structural information. Furthermore, this avoids spatial normalization challenges when basal images (no agonist) that have relatively low structural information/contrast are directly normalized to a template derived from an agonist (Nguyen, unpublished observations).

A total of 16 iterations were used during the SPM spatial normalization routine, where a 3D non-rigid transformation model was used to warp a source image to match the brain template. Image reconstructions of mouse brains may vary in shape and size due to intrinsic inter-subject differences in anatomical boundaries and/or from preparation of tissue. Therefore, the goal of spatial normalization is to warp, or deform, image reconstructions so that a given location in one subject (or reconstruction) corresponds to the same location in another subject's image. It is important to note that the registration approaches for spatial normalization are different from the techniques in the previous section for individual sections, which employed rigid or non-warping transformations. Correspondence of brain regions are shown in Figure 1.13 before and after performing spatial normalization. Spatial normalization of these three images for example improved the spatial correspondence of the globus pallidus as depicted by the crosshair representing the same coordinate location across all subjects. The accuracy of spatial normalization is very important as it allows signal averaging across subjects and thus the possibility to perform univariate statistical tests at each voxel for the creation of a statistical

parametric map. In addition, it allows for creation of subtraction images, such as net-stimulated images derived from subtracting basal from agonist-stimulated images (see Chapter 3). Spatial normalization lastly serves as a diagnostic point to determine whether there are underlying problems with one's dataset. Unsuccessful spatial normalization of an image may infer 1) inadequate slice registration, 2) significant artifact related to preparation of tissue, or 3) insufficient structural information/contrast related to the autoradiographic assay

Image smoothing was referenced above at various processing steps, for example after averaging of images to create a study-specific brain template. Smoothing is also applied to spatially normalized brain images prior to SPM analysis. Image smoothing essentially convolves the data using a defined kernel or function. In other words, each data point in an image is averaged with its neighbors. Specific to studies in this dissertation, data points were smoothed or replaced by a weighted average of its surrounding neighbors in 3D space, where the closest neighboring voxels were given the greatest weights (Gaussian kernel). Image smoothing is illustrated in Figure 1.14A and demonstrates one benefit of smoothing, such as increasing signal to noise. Following the addition of randomly generated noise into an image in Figure 1.14A, smoothing effectively eliminates it, however at a cost of losing spatial resolution (Fig. 1.14A rightmost column). This is noted by the general “blurring of a smoothed image” and loss of discrete borders, such as the separation of hair in the example image. The extent or magnitude of smoothing is defined by the width of the kernel, also referred as the full-width at half maximum (FWHM) of the Gaussian function. By the matched filter theorem, the optimum smoothing kernel corresponds to the size of the effect that one anticipates (Friston et al., 2007). However, this may be difficult to establish a priori especially for data sets studying receptor-mediated

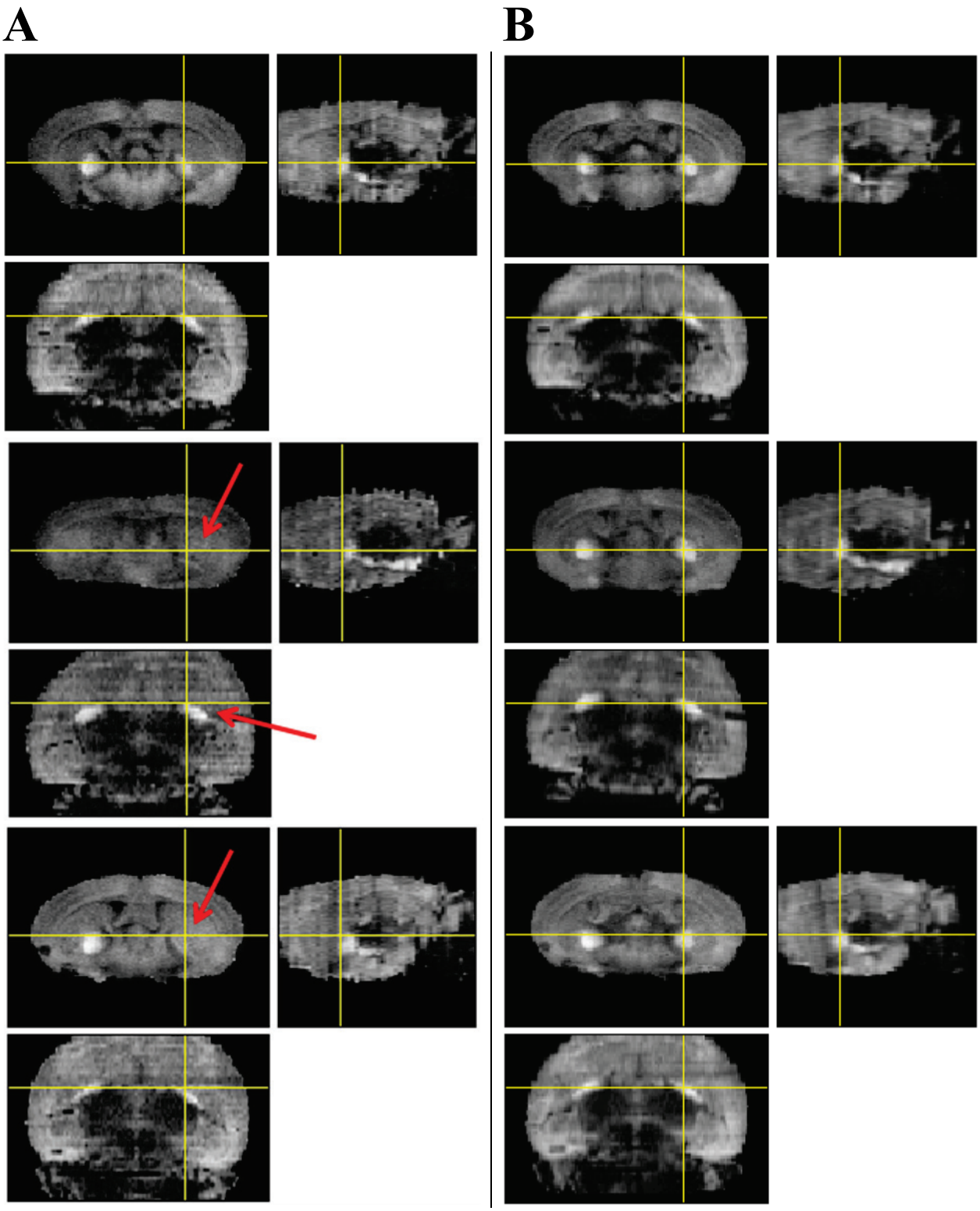

Figure 1.13. Spatial normalization of reconstructed brain images. Three representative brain reconstructions are shown before (A) and after (B) application of spatial normalization. Yellow crosshairs in each column represent identical coordinate locations within each subject. Note the poor spatial correspondence of the globus pallidus in images before spatial normalization (red arrows) and its improvement after spatial normalization.

A

Original Image | Add random noise | Smooth with Gaussian width = 2 pixels

B

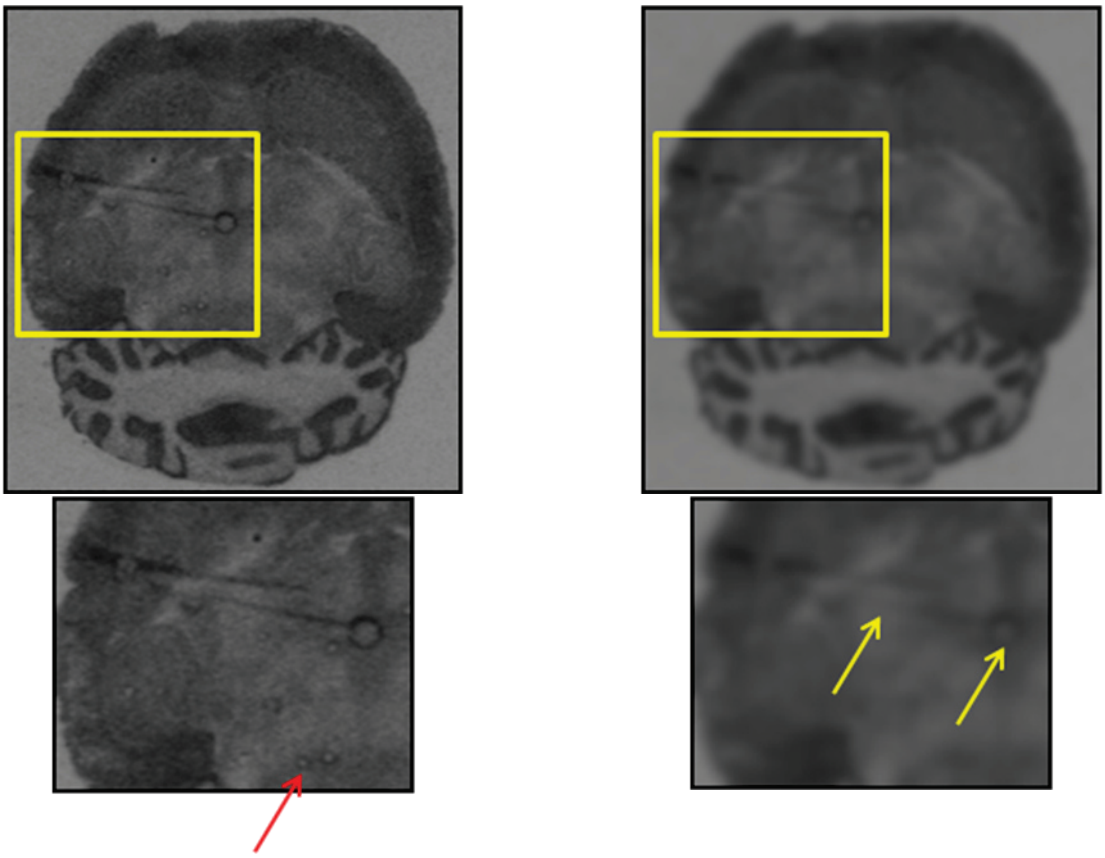

Figure 1.14. Image smoothing. (A) Smoothing with a Gaussian width equal to twice the pixel size is applied to a grayscale image after adding random noise (middle column). Note the removal of image noise after smoothing, but at the expense of spatial resolution (right column). (B) Application of image smoothing is shown for agonist-stimulated [^{35}S]GTPγS binding autoradiography. Artifacts such as the smaller air bubbles and folds are removed, but relatively larger ones fail at this given magnitude of spatial smoothing.

G-protein activity, because its magnitude may vary regionally based on the agonists intrinsic efficacy and receptor localization, or the size of the experimental effect may be unknown. Too little smoothing may result in artifactual differences, or "noisy SPMs", whereas too much smoothing may potentially exclude the detection of smaller differences when signal is "diluted" or averaged out with its neighboring voxels. Therefore, a relatively moderate FWHM equal to 3X the intrinsic voxel size (FWHM = 120 x 120 x 600 μm^3) was used whenever smoothing was required, which was generally compatible with our estimate of misregistration error and anatomical variability between our data sets. As mentioned previously, image smoothing helps to increase the signal to noise ratio, but this has its limitations. In Figure 1.14B, smoothing of autoradiographic data can account for relatively minor artifacts related to tissue preparation (i.e. bubbles, folds), but has difficulty with more extensive artifacts such as tearing. Finally, smoothing the data renders the errors more normal in their distribution and ensures the validity of inferences based on statistical parametric tests (Friston et al., 2007).

To ensure that only voxels within the brain were included for SPM analysis, an image threshold was specified to create a mask image using the SPM software. The mask was visually inspected and overlayed onto brain images, and the threshold value was calculated such that voxels less than 10% of the mean voxel value within the brain were not included for SPM analysis. This calculated threshold value of 10% ensured that only voxels in the background and within the ventricles from all brain images (basal and agonist) were excluded. Figure 1.15 shows an image histogram of voxel values from a single reconstructed mouse brain. Note that the global mean has a value of 152.32 nCi/g, which is low due to the inclusion of voxels in the background. After thresholding, the corrected mean voxel value is 496.44 nCi/g and includes about one-third of the total number of voxels in the image.

Because amounts of radiolabeled [^{35}S]GTPγS for in situ binding assays were kept constant, global normalization (Nguyen et al., 2004) in signal was omitted from SPM analysis. At each voxel, a general linear model was then used to describe the data in terms of experimental and confounding effects, and residual variability (Friston et al., 1995b). A voxel-by-voxel statistical analysis was performed to localize significant differences in receptor-mediated G-protein activation. Because of the extensive number of univariate statistical tests performed by SPM, the multiple comparisons problem was addressed using gaussian random field theory (Worsley et al., 1992). This analysis results in inference based on corrected *p*-values (Friston et al., 1991; Friston et al., 1996; Friston et al., 1994). Each study in this dissertation used an appropriate parametric statistical test at each voxel to test the effect of drug in activating G-proteins, and specific contrasts were evaluated. For all studies, significance ($p < 0.05$) was established at the voxel and/or cluster level (minimum cluster extent of 100 contiguous voxels) after correction for multiple comparisons. Statistical *p*-values were corrected using the false-discovery rate and were adjusted for small search volume for each CB_1 receptor containing region, including cortex, striatum, globus pallidus, substantia nigra, hippocampus, amygdala, hypothalamus, periaqueductal gray, and cerebellum. Small volume corrections used a sphere volume of interest to surround each CB_1 receptor containing region. Significance for novel regions not considered a priori were corrected for multiple comparisons for the whole brain search volume or used an uncorrected threshold of $p < 0.001$ and minimum cluster extent size of 100 contiguous voxels. Nissl staining of brain tissue sections from [^{35}S]GTPγS autoradiographic studies was also conducted to identify subnuclei and discrete small nuclei in the brainstem. Significant clusters of voxels representing brain regions of interest were also verified to span at least 2-3 adjacent sections. To validate and compare regions found to be significant with SPM

analysis, a separate ROI analysis was performed. ROI measurements were generally conducted on the original unprocessed images, averaged bilaterally across hemispheres, and analyzed with GraphPad Prism Version 5. ROI anatomical boundaries were defined by a mouse brain atlas (Franklin and Paxinos, 2008).

The overall assessment of image registration strategies for both 2D and 3D images derived from agonist-stimulated [^{35}S]GTPγS autoradiography can be visualized in Figure 1.16, which represents a composite brain image created from the image average (n = 8) of WIN-stimulated [^{35}S]GTPγS binding images from $CB_1^{-/-}$ mouse brains (dataset from Chapter 3). Spatial normalization resulted in correspondence between brain regions of all animals, therefore allowing successful averaging of voxel values. Success of spatial normalization can further be appreciated by the smooth cortical surface of the rendered composite brain image (Fig. 1.16A). This is further exemplified by the differentiation and contrast of anatomical boundaries of brain structures as illustrated in video sequences (download from *http://catalog.library.vcu.edu*) showing the anterior to posterior progression in the coronal plane, left to right lateral progression in the sagittal plane, and dorsal to ventral progression in the horizontal plane.

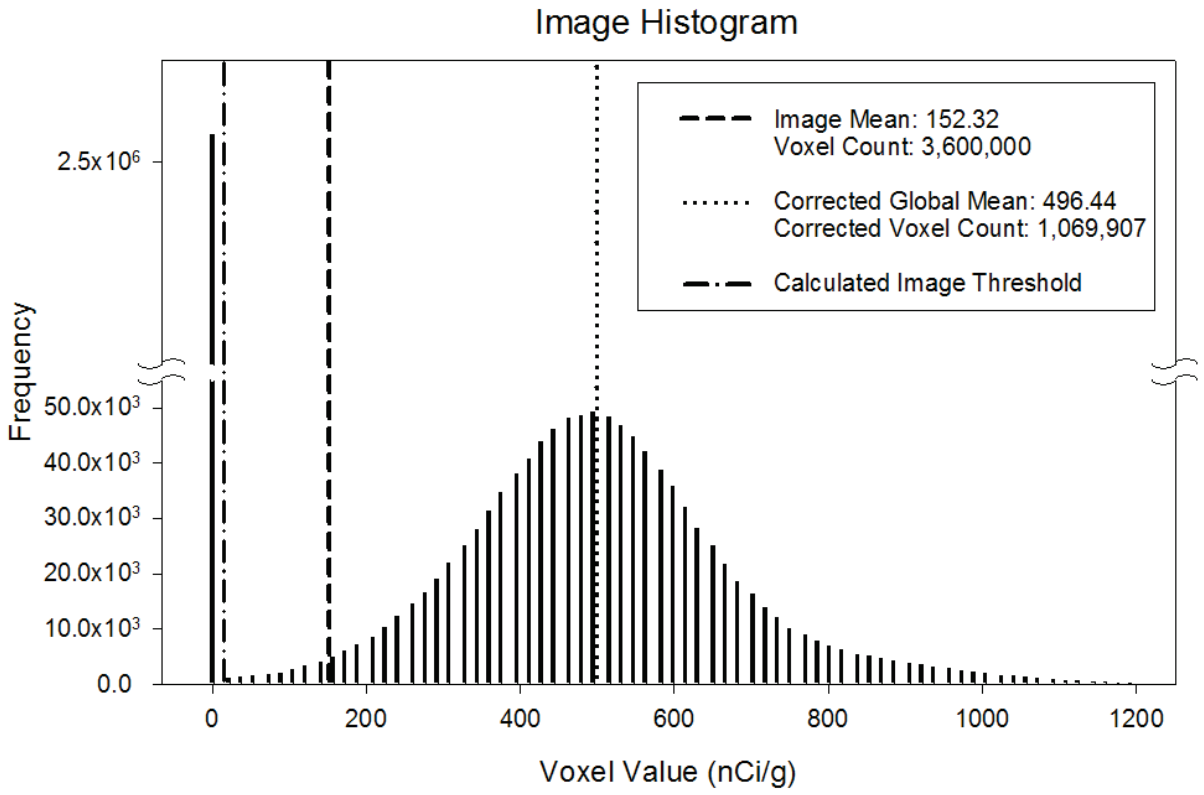

Figure 1.15. Image histogram of voxel values ([^{35}S]GTPγS) from a single reconstructed mouse brain under basal (no agonist) conditions. The global image mean (includes background outside the brain) is illustrated by a dashed line and the corrected mean (not including background outside the brain) is shown as a dotted line. Note the closer proximity of the corrected global mean to central tendency after image thresholding.

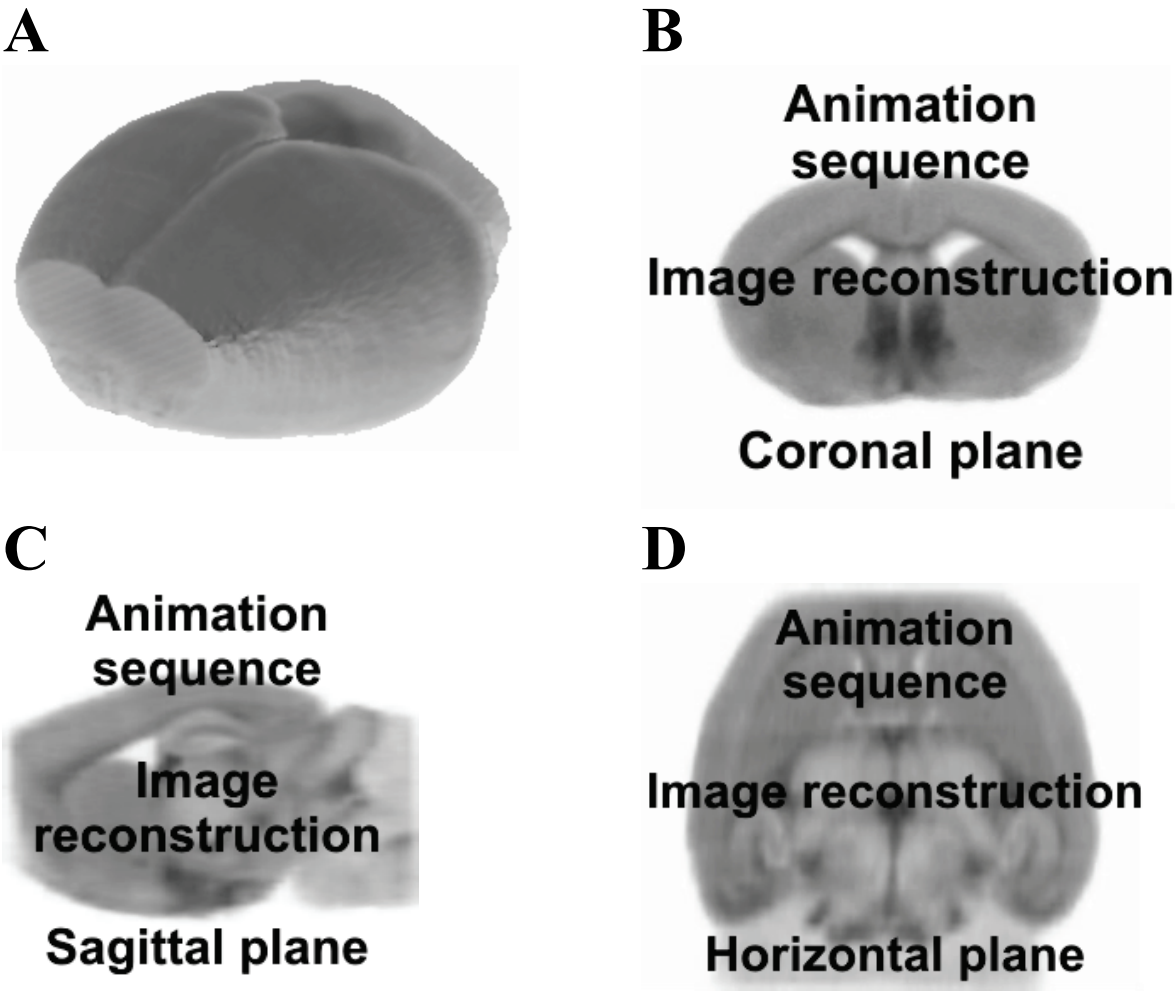

Figure 1.16. Reconstructed brain images derived from agonist-stimulated [^{35}S]GTPγS autoradiography provided 3D anatomical visualization in each orthogonal plane. A composite image created from the mean of eight reconstructed WIN-stimulated [^{35}S]GTPγS binding images from $CB_1^{-/-}$ mouse brains, was rendered in 3D (A) to demonstrate the result of slice registration and image reconstruction. Video sequences of slices are shown in the coronal (anterior to posterior) (B), sagittal (C), and transverse planes (dorsal to ventral) (D) to illustrate 3D spatial consistency of anatomical regions. The reader is referred to the web version of this dissertation to view/download video sequences in mpg format (search Peter Nguyen in http://catalog.library.vcu.edu). Video sequences can also be viewed/downloaded from the supplementary section of: Nguyen PT, Selley DE, Sim-Selley LJ. Statistical Parametric Mapping reveals ligand and region specific activation of G-proteins by CB(1) receptors and non-CB1 sites in the 3D reconstructed mouse brain. 2010. *Neuroimage* 52(4): 1243-1251.

1.6 Discussion: 3D reconstruction and analysis of cannabinoid-mediated G-protein activity

In this chapter we introduced the strategies used for reconstructing imaging data derived from agonist-stimulated [^{35}S]GTPγS autoradiography and methods to analyze these data based on Statistical Parametric Mapping (SPM). The principle behind image reconstruction is similar to creating volumetric images using confocal microscopy. In the case of autoradiography, multiple planes of data are instead collected manually, subsequently assayed and prepared for autoradiography, and digitized. Unlike confocal microscopy where a "Z-stack" contains multiple planes of data that are intrinsically aligned by virtue of the acquisition method, reconstruction of autoradiographic data requires slice realignment or registration. Several registration methods and algorithms have been developed for the alignment of serial images derived from various imaging modality, which differ mainly in the features used to establish a measure of similarity between images and also the extent of required user-input. A review of some image registration approaches for autoradiographic data has previously been published (Hess et al., 1998). We determined that an intensity-based registration algorithm developed by Thévenaz et al. (Thévenaz et al., 1998) was robust for the recursive alignment of brain tissue sections from agonist-stimulated [^{35}S]GTPγS autoradiography. The fully automated ImageJ plugin StackReg, which is based on this registration algorithm, successfully realigned 2D images with greater accuracy versus manual alignment in an unbiased fashion. 3D reconstruction offers the ability to visualize anatomical data in different orthogonal planes, as well as reslicing and visualization of data at virtually any angle. It is interesting to note that the reconstruction techniques in this chapter can possibly be adaptable and used to reconstruct data from different imaging modalities, such as immunohistochemistry or wherever multiple planes of data can be acquired. The application of these methods is extended to [^{3}H]ligand receptor-binding autoradiography in

Chapter 3 and in a study comparing differences in CB_1 receptor levels in the rat pilocarpine model of epilepsy versus controls (Appendix Fig. A3, Table A1). Important internet links for documentation related to analytical software is listed in the Appendix Table A2.

The high abundance and distribution of CB_1 receptors in brain, as well as their neuromodulatory role in synaptic transmission, make them an attractive candidate for whole brain imaging. To date, most *in vivo* based imaging approaches utilize radiotracer compounds and modalities such as positron emission tomography (PET) or single photon emission computed tomography (SPECT) to study, for example, changes in receptor occupancy after chronic drug treatment or during various neurological diseases (Gifford et al., 2002). Most radiotracer compounds are developed using structural templates derived from pre-existing cannabinoid agonists or antagonists (Horti and Van Laere, 2008). However, some of the challenges that limit usage of candidate radiotracer compounds include their affinity and specificity for binding to the receptor, as well as their lipophilicity to penetrate the blood brain barrier (Gifford et al., 2002). These challenges in radiotracer design also influence the technical limitations and resolution of PET images from both human and small animals, which ranges from 2.5 mm to 6 mm and about 1.5 mm, respectively (Cherry, 2006). Although *in vivo* studies offer the ability to study the biodistribution of radiolabeled cannabinoid compounds as a measure of receptor occupancy, it does not however give insight into the functional component of GPCR output at the receptor level.

We present the first attempt to functionally map and localize CB_1 receptor-mediated G-protein activity in 3D reconstructed mouse brains. Reconstructed brain images were analyzed by SPM, which is a well characterized approach for the analysis of human brain imaging data and has been previously adapted for autoradiographic datasets mapping cerebral blood flow (Nguyen

et al., 2004). However, the analysis of reconstructed datasets derived from agonist-stimulated [^{35}S]GTPγS autoradiography has not been described. Data from this chapter demonstrate the feasibility of using SPM to perform various imaging manipulations on reconstructed datasets including coregistration, spatial normalization, and smoothing (Supplemental data using these methods are illustrated in the Appendix Figs. A2-A3, Table A1). The SPM image registration tools were robust and accurate for the spatial normalization of brains, showing satisfactory spatial correspondence of brain areas between subjects. These novel imaging approaches will further be explored in the next two chapters to study ligand- and region-specific activation of CB_1 receptors (Chapter 2) and to determine the role of the protein beta-arrestin 2 in regulating CB_1 receptor function following chronic administration of THC (Chapter 3).

V. Chapter 2: Statistical Parametric Mapping reveals ligand and region specific activation of G-proteins by CB_1 receptors and non-CB_1 sites in the 3D reconstructed mouse brain

The development of selective CB_1 antagonists, such as SR141716A (Rinaldi-Carmona et al., 1994), and CB_1 knockout mice (Valverde et al., 2005; Zimmer et al., 1999) has shown that most effects of THC are primarily mediated by the CB_1 receptor. Our findings have demonstrated that CB_1 receptor signaling varies by brain region, for example when examined following acute activation of CB_1 receptors (Breivogel et al., 1997; Selley et al., 2001). However, the complete regional profile of CB_1 receptor activity has not been elucidated due to limitations of current strategies for design and analysis of autoradiographic studies. In this chapter, we will thest the hypothesis that CB_1 receptor-mediated G-protein activity will differ by cannabinoid ligand and that the relative efficacy of these ligands will vary by brain region.

2.1 Cannabinoid-mediated G-protein activation is ligand and region specific

Differences in the efficacy of various cannabinoid agonists to activate G-proteins have previously been studied using agonist-stimulated [^{35}S]GTPγS binding in membranes prepared from various brain regions (Breivogel and Childers, 2000). However it is unclear whether the relative efficacy of cannabinoid agonists to activate G-proteins varies by region as determined autoradiographically in brain tissue sections. SPM was used to determine regional differences in cannabinoid-mediated G-protein activity in reconstructed wild-type C57/Bl6J mouse brains (N=5) using maximally effective concentrations of cannabinoid agonists differing in efficacy and structure, including the aminoalkylindole WIN55,212-2 (WIN), bicyclic CP55,940 (CP), and the metabolically stable endocannabinoid analogue methanandamide (M-AEA). Maximally effective concentrations of agonists were determined in concentration-effect curves, using 0.003-3 μM

CP, 0.01-10 μM WIN, or 0.1-30 μM M-AEA in membrane preparations from mouse whole brain (Fig. 2.1) or cerebellum (data not shown). Membrane agonist-stimulated [^{35}S]GTPγS binding experiments were conducted as previously published (Sim-Selley et al., 2006). Results from whole brain and cerebellum membranes were similar, and thus concentrations used for agonist-stimulated autoradiographic assays in all studies ($CB_1^{+/+}$ and $CB_1^{-/-}$ animal studies) were: CP (3 μM), WIN (10 μM), M-AEA (25 μM). The calculated E_{max} had a net stimulation (agonist-stimulated minus basal [^{35}S]GTPγS binding) of 89.6 ± 4.9%, 94.2 ± 3.6%, and 110.3 ± 1.8% over basal for M-AEA, CP, and WIN, respectively. The relative rank order in potency to activate G-proteins was CP > WIN > M-AEA, with EC_{50} values of 5.7 nM, 35 nM, and 354 nM, respectively. Volumetric reconstructions of autoradiographic sections provided 3D anatomical visualization and localization of cannabinoid-mediated G-protein activity (Fig. 2.2). The spatial extent of cannabinoid-stimulated G-protein activity as illustrated in Fig. 2.2 is shown in red, and the surface of the brain is rendered in gray for the right hemisphere. All three cannabinoid agonists significantly stimulated greater [^{35}S]GTPγS binding than basal (no agonist) in all CB_1 receptor containing regions (Fig. 2.3) as determined by SPM analysis. As shown for WIN (Fig. 2.2), cannabinoid-stimulated G-protein activity was widespread in the cortex, densely distributed in the output nuclei of the basal ganglia (globus pallidus, substantia nigra) and seen in bands in the cerebellum that presumably correspond to the molecular layer. To determine the regional relative efficacy, SPM was then used to compare G-protein activity produced by the three cannabinoid agonists. WIN-stimulated G-protein activity was significantly greater than M-AEA

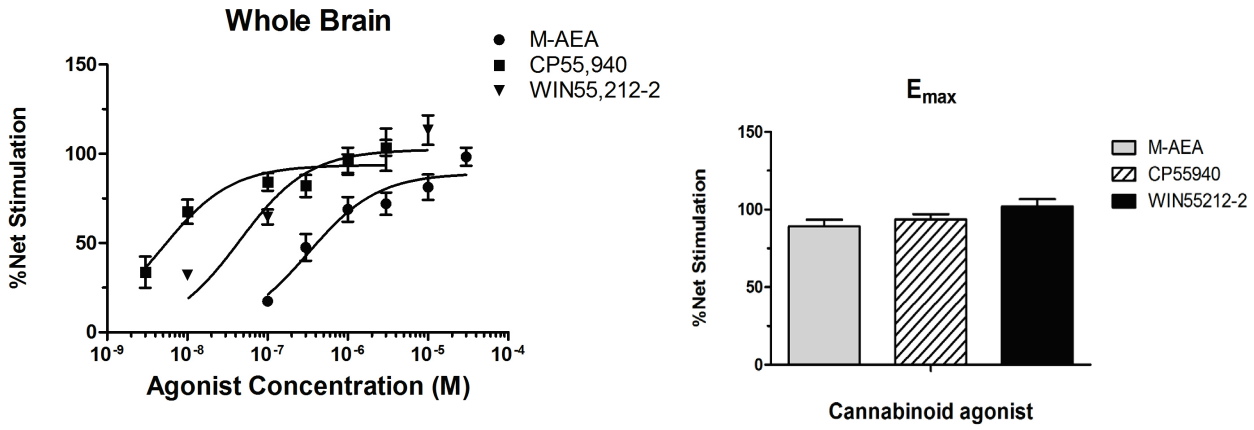

Agonist	EC_{50} (μM)	E_{max} (% Net Stim.)
M-AEA	0.32 ± 0.08	89.2 ± 4.2
CP55,940	0.005 ± 0.001	93.7 ± 3.4
WIN55,212-2	0.04 ± 0.01	102.5 ± 4.8

Figure 2.1. Concentration-effect curves for cannabinoid agonists in membranes prepared from whole mouse brain. Varying concentrations of drug were incubated in 0.1 nM [^{35}S]GTPγS, 0.125% BSA, 30 μM GDP for 2 hrs at 30°C. No significant differences were found in agonist-stimulated [^{35}S]GTPγS binding produced by M-AEA, CP, and WIN. [^{35}S]GTPγS binding experiments (N=3-4) were performed in triplicate and data are reported as the mean %Net Stimulation [(agonist-basal)/basal x 100%] + S.E.M. Data were fit using Graphpad Prism 5.

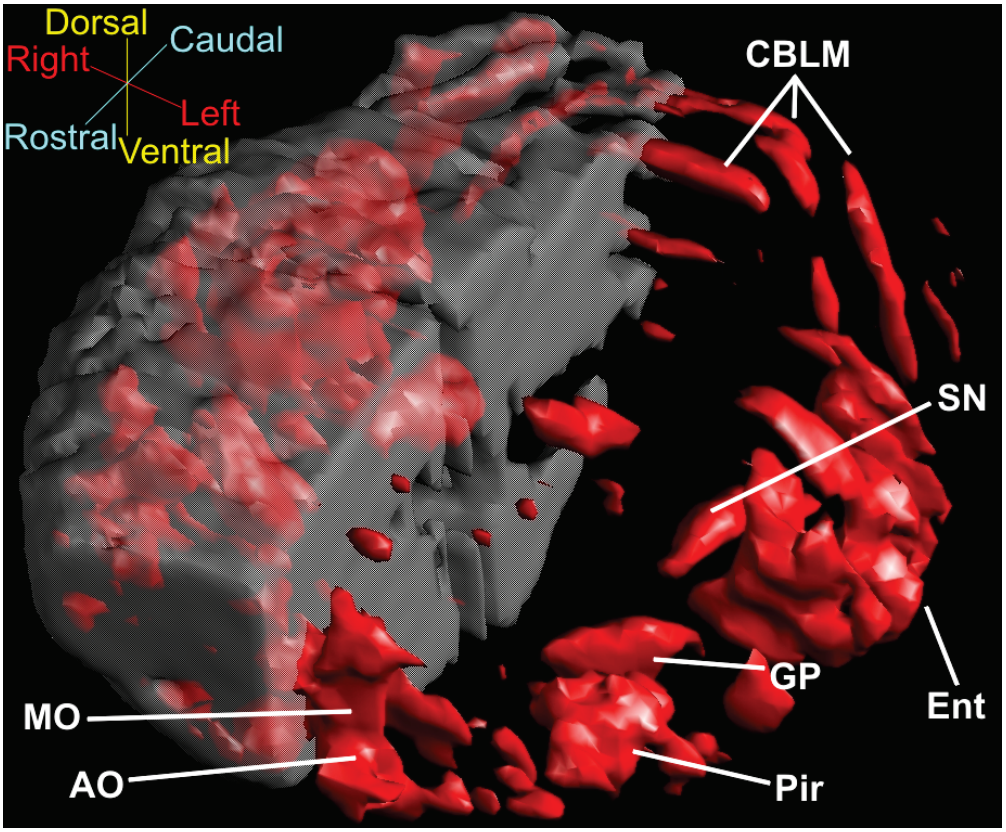

Figure 2.2. 3D image reconstruction and volumetric rendering of average (N = 3) cannabinoid-stimulated [^{35}S]GTPγS binding (red) in naïve mouse brain using a maximally effective concentration of the full CB_1 receptor agonist WIN55,212-2 (10 μM). A threshold was applied to show the spatial extent of highest WIN-stimulated G-protein activity in brain regions, including the molecular layer of the cerebellum, cortex, and basal ganglia. AO (Anterior olfactory nucleus), Ent (entorhinal cortex), GP (globus pallidus), MO (medial orbital cortex), Pir (piriform cortex), SN (substantia nigra). Agonist-stimulated [^{35}S]GTPγS binding autoradiography was performed as described in *Methods*

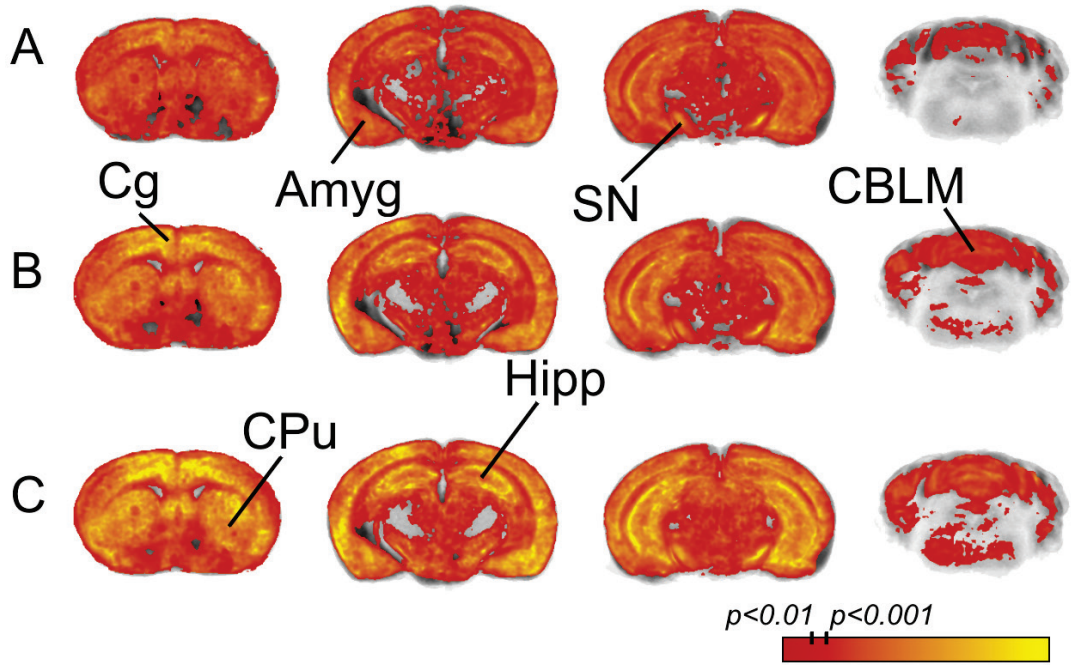

Figure 2.3. SPM analysis showing the regional distribution of significant differences between 25 µM M-AEA- (A), 3 µM CP55,940- (B), or 10 µM WIN55,212-2- (C) versus basal [^{35}S]GTPγS binding ($p < 0.01$, ANOVA, N = 5) in $CB_1^{+/+}$ reconstructed naive mouse brains. Representative coronal sections with colored overlays (red to yellow) show significant differences corresponding to a *p*-value scale. Corresponding bregma coordinates from the left- to rightmost column are: 0.26 mm, -2.46 mm, -3.16 mm, -6.12 mm (Paxinos et al., 2008). AMYG (amygdala), CBLM (cerebellum), Cg (cingulate cortex), CPu (caudate-putamen), HIPP (hippocampus), SN (substantia nigra).

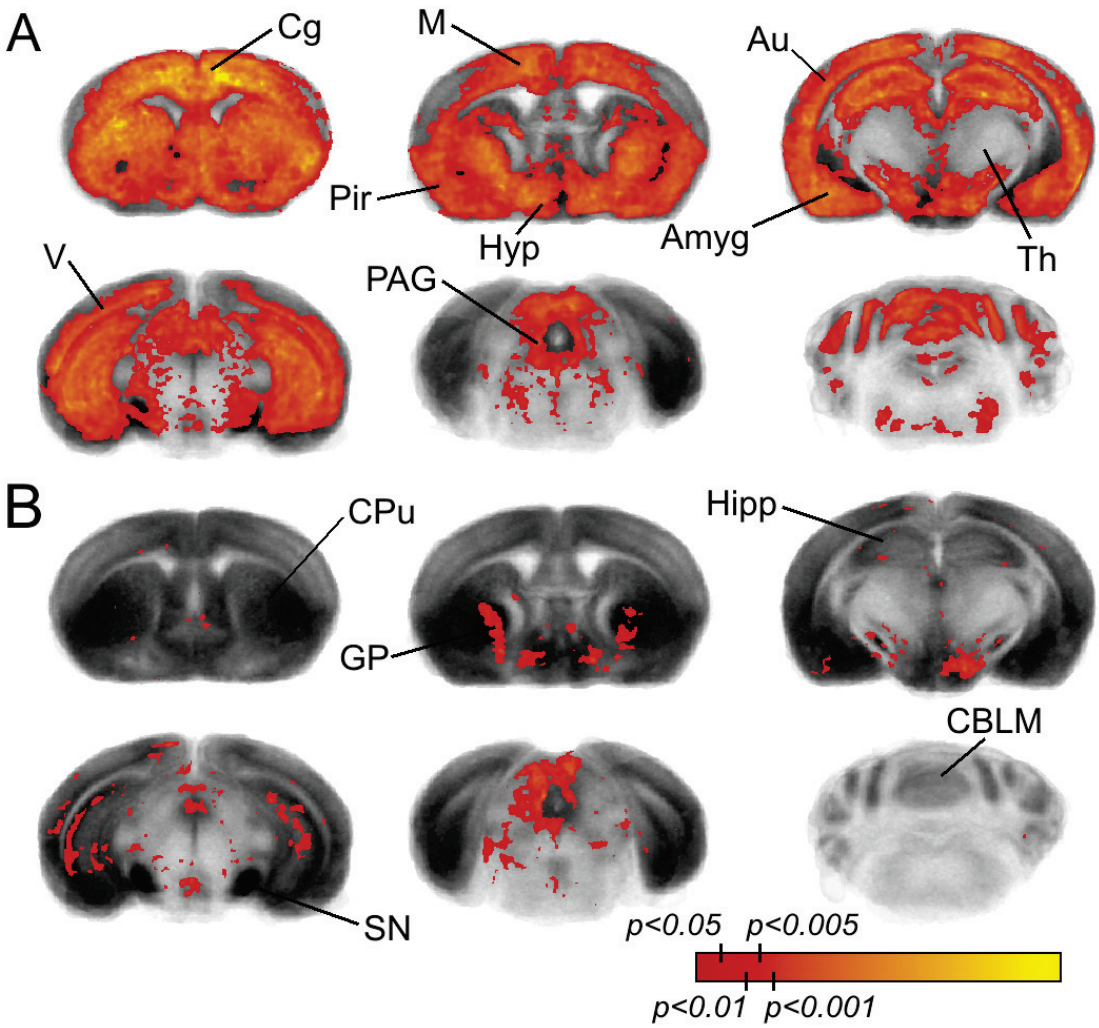

Figure 2.4. Regional comparison of agonist-stimulated [^{35}S]GTPγS binding produced by the cannabinoid agonists WIN (10 μM), CP (3 μM), and M-AEA (25 μM) in $CB_1^{+/+}$ reconstructed naive mouse brains. Representative coronal sections illustrate Statistical Parametric Maps ($p < 0.05$, ANOVA, n=5) of significant differences in receptor-mediated G-protein activation, between WIN and M-AEA **(A)**, or WIN and CP **(B)**. WIN stimulated significantly greater G-protein activity than M-AEA in most CB_1 containing regions, with the exception of the thalamus. In addition, WIN-stimulated [^{35}S]GTPγS binding was greater than CP in globus pallidus, periaqueductal gray, and hypothalamus. Colored overlays (red to orange) correspond to significance level represented by a *p*-value scale. Corresponding bregma coordinates from the top left anterior-most to bottom right posterior-most slice are: 0.02 mm, -0.7 mm, -1.7 mm, -3.4 mm, -4.16 mm, -6.12 mm (Paxinos et al., 2008). Au (auditory cortex), Hipp (hippocampus), CPu (caudate-putamen), GP (globus pallidus), Hyp (hypothalamus), M (motor cortex), PAG (periaqueductal gray), S (somatosensory cortex), SN (substantia nigra reticular), V (visual cortex), *M-AEA*, methanandamide; *WIN*, WIN55,212-2

in almost all regions examined, with exception of the thalamus (Fig. 2.4A). SPM provided a detailed anatomical comparison, as seen in the cortex (cingulate, somatosensory, and motor cortex) where WIN produced significantly greater G-protein activation than M-AEA in both superficial and deep laminae (Fig. 2.4A). A similar regional activation profile (data not shown) was seen comparing CP and M-AEA, where CP stimulated significantly greater G-protein activity than M-AEA. When comparing WIN and CP however, region-specific differences in the relative stimulation produced by these agonists were identified by SPM. For example, WIN stimulated significantly greater G-protein activity than CP in some CB_1 containing regions including globus pallidus, hypothalamus and periaqueductal gray (Fig. 2.4B). In contrast, WIN- and CP-stimulated G-protein activity were equivalent in the caudate-putamen, hippocampus, amygdala, cerebellum and cortical regions including motor, somatosensory, and cingulate cortices (Fig. 2.4B). Overall, SPM revealed that in some regions, including globus pallidus, hypothalamus, and periaqueductal gray, the activity profile was WIN > CP > M-AEA. In contrast, for most regions including caudate-putamen, hippocampus, amygdala, cerebellum and cortex (motor, somatosensory, and cingulate cortices) the relationship was WIN = CP > M-AEA. Interestingly, a different relative efficacy profile was found in the thalamus compared to all other brain regions. SPM revealed that WIN-, CP-, and M-AEA-stimulated [^{35}S]GTPγS binding did not significantly differ in thalamic nuclei, including ventral posteromedial and posterolateral, ventromedial, and ventrolateral thalamic nuclei. Subsequent ROI analyses substantiated almost all of the SPM findings, except in hypothalamus where WIN and CP did not differ in stimulating [^{35}S]GTPγS binding. In this brain region, ROI analysis revealed similar qualitative differences between WIN and CP as determined using SPM analysis, but failed to reach significance at the $p < 0.05$ level. This could be explained by differences in the analytical technique, where

significance by SPM is based at the individual voxel-level as opposed to a user-defined region of interest, which contains the average of many image pixels or subnuclei.

While the anatomical distribution of agonist-stimulated G-protein activity was similar for each of the three agonists compared to basal (no agonist), the relative magnitude of activity varied by brain region, as determined by an independent ROI analysis of cannabinoid-stimulated [^{35}S]GTPγS binding for selected brain regions (Table 2.1). The relative efficacies of the three agonists were calculated by expressing net agonist-stimulated [^{35}S]GTPγS binding produced by CP or M-AEA as percent of [^{35}S]GTPγS binding stimulated by the full agonist WIN (Table 2.1). For example, the relative efficacy of M-AEA ranged from 32% of WIN in the PAG to 76% of WIN in thalamus. In addition, the relative efficacy of CP ranged from 60% of WIN in periaqueductal gray to 105% in thalamus. Due to the potential contribution of WIN acting at non-CB_1 sites (see next section), [^{35}S]GTPγS binding data is also reported as %CP (Table 2.2). A similar relative efficacy relationship was revealed when using CP as the standard agonist. The high relative efficacy of WIN in specific brain regions did not correlate with having non-CB_1-mediated activity, indicating that CB_1 receptors contribute to the majority of the signal detected in WIN-stimualted [^{35}S]GTPγS autoradiography. When normalized to the full CB_1 agonist WIN, there was no significant correlation between the relative efficacies of M-AEA- and CP-stimulated G-protein activation (Fig. 2.5) across the sampled brain regions of interest. In addition, a significant interaction of drug x region ($p < 0.01$) was found when analyzed by a two way repeated measures ANOVA. A significant interaction between the factors drug and region and lack of correlation in the relative efficacy profile, suggests that there may be regional differences in the relative efficacies of M-AEA and CP, which cannot be explained by receptor levels or G-protein abundance. These results thus indicate that the relative G-protein activity

produced by these cannabinoid agonists was region-dependent, as revealed by both SPM and ROI analysis of 3D reconstructed agonist-stimulated [^{35}S]GTPγS autoradiographic data.

Table 2.1

Regional differences in the relative efficacies of different cannabinoid agonists (25 μM M-AEA, 3 μM CP, 10 μM WIN) were found by both SPM and ROI analysis of agonist-stimulated [^{35}S]GTPγS autoradiographic images in $CB_1^{+/+}$ naïve mice.

	Net-stimulated binding (nCi/g)			Net stimulation as %WIN		
Brain Region	**M-AEA**	**CP**	**WIN**	**M-AEA**	**CP**	**WIN**
Motor cortex	263 ± 11^{Aa}	470 ± 14^{Bb}	494 ± 13^{Bb}	53 ± 2	95 ± 3	100 ± 3
Somatosensory cortex	146 ± 29^{Aa}	272 ± 44^{Bb}	264 ± 37^{Bb}	55 ± 11	103 ± 17	100 ± 14
Cingulate cortex	273 ± 17^{Aa}	488 ± 16^{Bb}	521 ± 30^{Bb}	52 ± 3	94 ± 3	100 ± 6
Hippocampus	170 ± 34^{Aa}	313 ± 50^{Bb}	377 ± 26^{Bb}	45 ± 9	83 ± 13	100 ± 7
Amygdala	200 ± 34^{Aa}	384 ± 36^{Bb}	457 ± 28^{Bb}	44 ± 7	84 ± 8	100 ± 6
Thalamus	59 ± 20^{Aa}	81 ± 24^{Aa}	77 ± 2^{Aa}	76 ± 25	105 ± 30	100 ± 27
Hypothalamus	83 ± 23^{Aa}	203 ± 31^{Bb}	235 ± 16^{Cb}	35 ± 10	86 ± 13	100 ± 7
Periaqueductal gray	100 ± 30^{Aa}	188 ± 19^{Bb}	313 ± 23^{Cc}	32 ± 10	60 ± 6	100 ± 7
Cerebellum	210 ± 45^{Aa}	472 ± 39^{Bb}	456 ± 37^{Bb}	46 ± 10	103 ± 8	100 ± 8
Substantia Nigra	597 ± 45^{Aa}	801 ± 28^{Bb}	863 ± 42^{Bb}	69 ± 5	93 ± 3	100 ± 5
Globus Pallidus	480 ± 28^{Aa}	607 ± 16^{Bb}	788 ± 38^{Cc}	61 ± 4	77 ± 2	100 ± 5
Caudate-Putamen	189 ± 9^{Aa}	373 ± 15^{Bb}	399 ± 26^{Bb}	47 ± 2	94 ± 4	100 ± 7

$^{A, B, C}$ & $^{a, b, c}$ Net-stimulated binding values labeled with different letters within a brain region are significantly different from each other based on SPM (upper case; $p < 0.05$ corrected, ANOVA, n=5) or ROI analysis (lower case; $p < 0.05$, n=5, ANOVA, Tukey's post-hoc analysis) as described under *Methods*. Measurements in each column are mean net [^{35}S]GTPγS binding values (nCi/g) ± SEM for M-AEA-, CP-, and WIN-stimulated conditions as determined by ROI analysis. Net values were calculated by subtracting basal from agonist-stimulated [^{35}S]GTPγS binding. ROI anatomical boundaries are described in *Section III: Methods*.

Table 2.2

Relative efficacies of different cannabinoid agonists (25 μM M-AEA, 3 μM CP, 10 μM WIN) from ROI analysis of agonist-stimulated [^{35}S]GTPγS autoradiographic images in $CB_1^{+/+}$ naïve mice.

	Net stimulation as %CP		
Brain Region	**M-AEA**	**CP**	**WIN**
Motor cortex	56 ± 2	100 ± 3	105 ± 3
Somatosensory cortex	54 ± 11	100 ± 16	97 ± 14
Cingulate cortex	56 ± 3	100 ± 3	107 ± 6
Hippocampus	54 ± 11	100 ± 16	121 ± 8
Amygdala	52 ± 9	100 ± 10	119 ± 7
Thalamus	72 ± 24	100 ± 29	95 ± 26
Hypothalamus	41 ± 11	100 ± 16	116 ± 8
Periaqueductal gray	53 ± 16	100 ± 10	167 ± 13
Cerebellum	44 ± 10	100 ± 8	97 ± 8
Substantia Nigra	75 ± 6	100 ± 3	108 ± 5
Globus Pallidus	79 ± 5	100 ± 3	130 ± 6
Caudate-Putamen	51 ± 2	100 ± 4	107 ± 7

ROI measurements in each column are mean net [^{35}S]GTPγS binding values (nCi/g) ± SEM for M-AEA-, CP-, and WIN-stimulated conditions expressed as %CP. Net values were calculated by subtracting basal from agonist-stimulated [^{35}S]GTPγS binding. ROI anatomical boundaries are described in *Section III: Methods*.

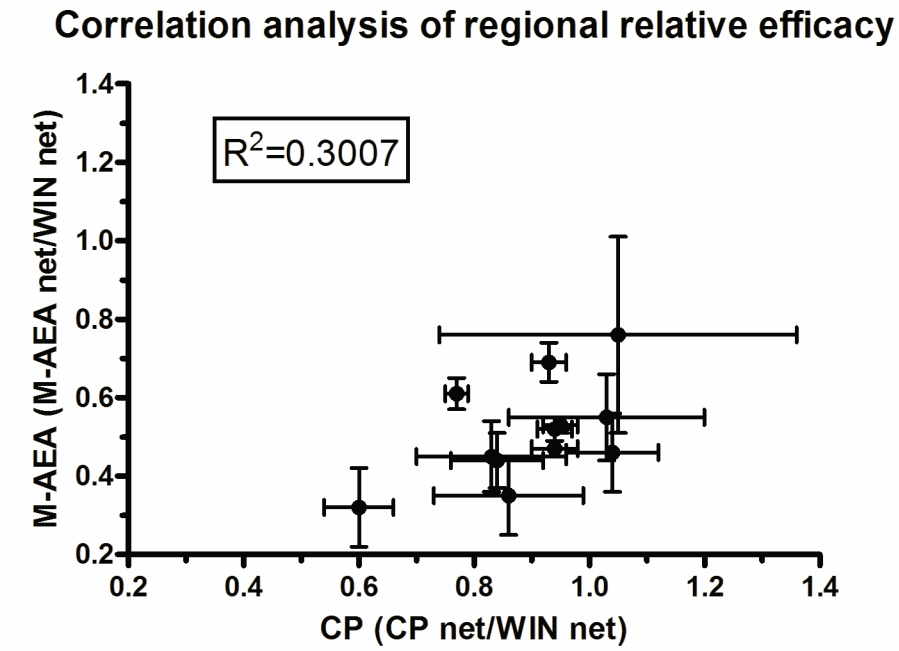

Figure 2.5. Correlation analysis of regional relative efficacy in $CB_1^{+/+}$ naive mice. No significant correlation was found between the relative efficacies of M-AEA (25 μM) and CP (3 μM) in sampled brain regions, suggesting regional differences in their relative efficacies. The axes represent the net-stimulated [^{35}S]GTPγS binding (basal activity subtracted) value of each agonist (CP or M-AEA) normalized to net-stimulation by WIN (10 μM). Error bars represent the standard error of the mean and each point represents a sampled brain region, which include: motor cortex, somatosensory cortex, cingulate cortex, hippocampus, amygdala, thalamus, hypothalamus, periaqueductal gray, cerebellum, substantia nigra, globus pallidus, and caudate-putamen. Agonist-stimulated [^{35}S]GTPγS binding autoradiography was performed as described in *Methods*.

2.2 WIN55,212-2 stimulates G-protein activity in a subset of brain regions of mice lacking CB_1 receptors

Results in wild-type mice suggested that the relative efficacy of cannabinoid agonists varies by brain region. However, the interpretation of these findings is complicated by the possible contribution of non-CB_1 binding sites to receptor-mediated G-protein activity. This question was addressed using SPM analysis of M-AEA-, CP-, and WIN-stimulated [^{35}S]GTPγS binding in reconstructed $CB_1^{-/-}$ mouse brain (N=8). SPM analysis showed that agonist-stimulated [^{35}S]GTPγS binding produced by CP or M-AEA did not significantly differ from basal activity (in the absence of agonist) in any brain region from $CB_1^{-/-}$ mice (Fig. 2.6). However, WIN-stimulated [^{35}S]GTPγS binding significantly differed from basal binding in a number of areas in $CB_1^{-/-}$ mice as determined by SPM and subsequently confirmed by ROI analyses (Table 2.3, Fig 2.6). As seen in Fig. 2.7, WIN-stimulated [^{35}S]GTPγS binding was significantly greater than basal binding in regions that partially overlapped the distribution of CB_1 receptors. SPM analysis revealed WIN-stimulated [^{35}S]GTPγS binding in visual (V) and auditory cortices (Au) that appeared to be localized to deeper laminae. In the hippocampus, WIN-stimulated [^{35}S]GTPγS binding was noted in the caudal, ventral CA1 and CA3, and to a lesser extent rostral, dorsal CA3. Although ROI analysis of the whole hippocampus showed a similar trend as in the SPM analysis, it failed to reach significance at the $p < 0.05$ criterion, possibly due to the heterogeneity of signal in this brain region as demonstrated in the SPM map (Fig. 2.7). WIN-stimulated [^{35}S]GTPγS binding was widely distributed in the amygdaloid complex, and appeared to be distributed in areas that corresponded to anterior portions of the basomedial and basolateral, and medial, lateral and central nuclei. WIN-stimulated [^{35}S]GTPγS binding was also found in the medial hypothalamus. Interestingly, the greatest magnitude of WIN-stimulated [^{35}S]GTPγS binding in

$CB_1^{-/-}$ mouse brains was found within the brain stem including tegmental nuclei that appeared to correspond to lateral and dorsal tegmentum, and areas adjacent to the fourth ventricle, which corresponds to the locus coeruleus (Table 2.3). Significant WIN-stimulated G-protein activity was also found in the cerebellum that appeared to correspond to the molecular layer. In contrast, no differences between WIN-stimulated G-protein activity and basal binding were detected in basal ganglia (globus pallidus, substantia nigra, caudate-putamen), brain areas that normally contain among the highest levels of CB_1 receptors. It is important to note that the average magnitude of net WIN-stimulated G-protein activation in significant brain areas was approximately 4-5 fold less in $CB_1^{-/-}$ mice compared to wild-type mice (Table 2.1 versus 2.3). For example, net WIN-stimulated G-protein activity (WIN stimulated – basal) in cerebellum was 83 ± 20 nCi/g in $CB_1^{-/-}$, compared to 456 ± 37 nCi/g in wild-type mice. Thus, data from reconstructed $CB_1^{-/-}$ mouse brains suggest that the aminoalkylindole WIN, but not the endocannabinoid analogue M-AEA or bicyclic CP, activates non-CB_1 sites in a subset of brain areas that only partially overlaps with CB_1 receptor containing regions.

Table 2.3

WIN (10 μM) stimulated [^{35}S]GTPγS binding in $CB_1^{-/-}$ brains in regions partially overlapping CB_1 receptors.

	[^{35}S]GTPγS binding (nCi/g)				Sig.	Sig.
Brain Region	**Basal**	**WIN**	**WIN Net**	**%Stim**	**SPM**	**ROI**
Auditory cortex	455 ± 17	533 ± 18	77 ± 21	18 ± 5	v,c	*
Visual cortex	434 ± 20	494 ± 20	60 ± 30	16 ± 7	v,c	n.s.
Amygdala	763 ± 20	911 ± 34	148 ± 27	19 ± 3	v,c	**
Hippocampus	429 ± 16	478 ± 18	49 ± 24	12 ± 6	$p < 0.01$	n.s.
Thalamus	390 ± 17	397 ± 8	7 ± 14	3 ± 3	n.s.	n.s.
Hypothalamus	735 ± 29	863 ± 35	128 ± 40	19 ± 6	v	*
Dorsal Tegmental complex	483 ± 12	687 ± 21	205 ± 19	43 ± 4	$p < 0.001$	***
Locus Coeruleus	523 ± 23	720 ± 30	197 ± 29	39 ± 6	$p < 0.001$	***
Globus Pallidus	508 ± 19	488 ± 12	-19 ± 14	-3 ± 3	n.s.	n.s.
Substantia Nigra	404 ± 17	419 ± 13	16 ± 29	6 ± 8	n.s.	n.s.
Caudate-Putamen	509 ± 24	515 ± 24	6 ± 20	2 ± 4	n.s.	n.s.
Periaqueductal gray	758 ± 27	764 ± 16	6 ± 30	2 ± 4	n.s.	n.s.
Cerebellum	223 ± 11	306 ± 20	83 ± 20	39 ± 10	v,c	**

Measurements in columns 1 and 2 are mean [^{35}S]GTPγS binding values (nCi/g) ± SEM for basal- and WIN-stimulated conditions sampled within each brain region by ROI. Net binding equals [WIN stimulated- basal binding]. Percent stimulation (%Stim) for each brain region is calculated as ([(WIN – basal)/basal]*100%). Column five shows significance ($p < 0.05$) at the voxel (v) or cluster (c) level (corrected for multiple comparisons, as described in *Section III: Methods*, ANOVA, n=8) or uncorrected *p*-value for each brain region as determined by SPM analysis. Column six shows results obtained by ROI measurement with subsequent analysis using repeated measures ANOVA, followed by Tukey's post-hoc comparison. *, $p < 0.05$, **, $p < 0.01$, ***, $p < 0.001$. ROI anatomical boundaries are described in *Methods*. *WIN*, WIN55,212-2; n.s. = not significant

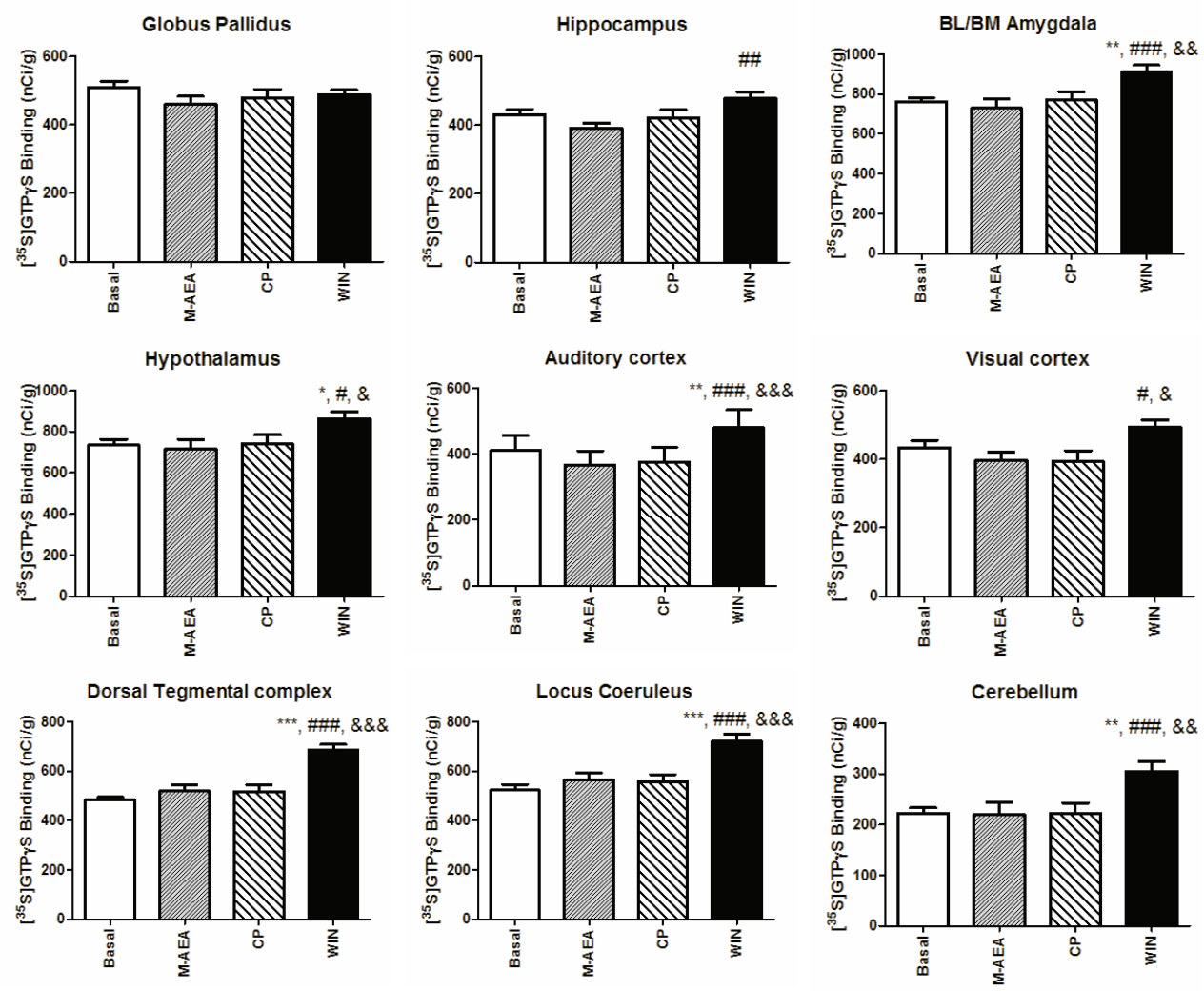

Figure 2.6. Agonist-stimulated [^{35}S]GTPγS binding values measured and analyzed using regions of interest (ROI) from a subset of brain areas from naive $CB_1^{-/-}$ mice (N = 8) using different cannabinoid agonists (25 µM M-AEA, 3 µM CP, 10 µM WIN). * $p < 0.05$, ** $p < 0.01$, *** $p < 0.001$ compared to basal; # $p < 0.05$, ## $p < 0.01$, ### $p < 0.001$ compared to M-AEA; & $p < 0.05$, && $p < 0.01$, &&& $p < 0.001$ compared to CP. All comparisons used a one-way repeated measures ANOVA followed by Tukey's Multiple Comparison Test. Agonist-stimulated [^{35}S]GTPγS binding autoradiography was performed as described in *Methods*

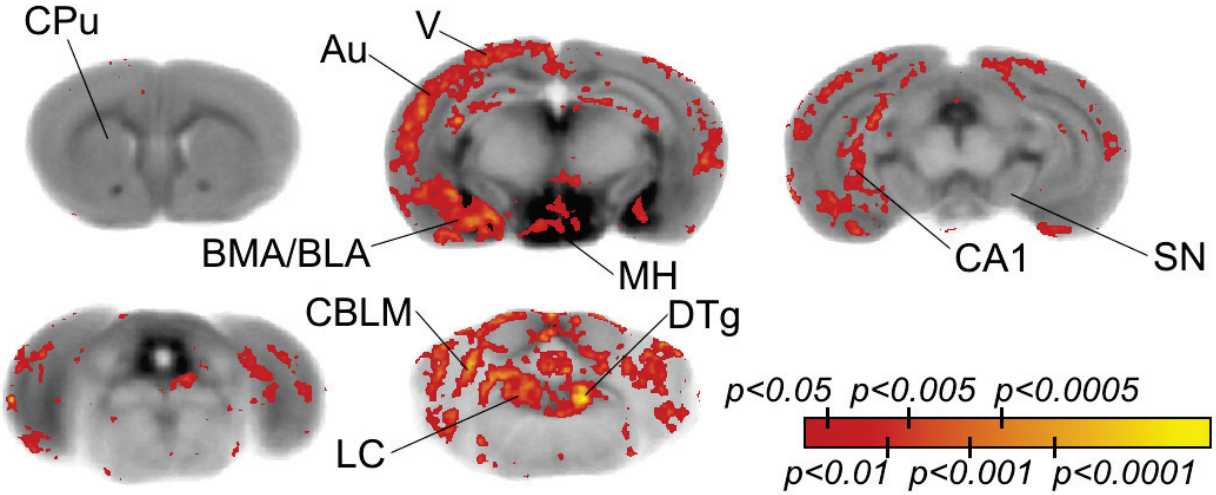

Figure 2.7. SPM analysis showing the regional distribution of significant differences between WIN-stimulated (10 μM) and basal [^{35}S]GTPγS binding ($p < 0.05$, ANOVA, n=8) in $CB_1^{-/-}$ mouse brains. Representative coronal sections with colored overlays (red to yellow) show significant differences (WIN > basal) corresponding to a *p*-value scale. Corresponding bregma coordinate from top left anterior-most slice to bottom right posterior-most slice are: 1.34 mm, -1.82 mm, -3.28 mm, -4.84 mm, -5.34 mm (Paxinos et al., 2008). Au (auditory ctx), BMA/BLA (basomedial and basolateral amygdala), CA1 (CA1 field of hippocampus), CBLM (cerebellum), CPu (caudate-putamen), DTg (tegmental nucleus, dorsal), LC (locus coeruleus), MH (medial hypothalamus), SN (substantia nigra), V (visual cortex), *WIN*, WIN55,212-2. Agonist-stimulated [^{35}S]GTPγS binding autoradiography was performed as described in *Methods*

2.3 WIN55,212-2-stimulated G-protein activity in wild-type mice is blocked by SR141716.

The aminoalkylindole WIN activated G-proteins in $CB_1^{-/-}$ mice, providing evidence for non-CB_1 sites in a genetic model. To validate this finding, a pharmacological approach was applied by incubating wild-type mouse brain sections with WIN in the presence or absence of the CB_1 antagonist SR141716A (SR1), and resulting G-protein activity was compared using SPM in the reconstructed $CB_1^{+/+}$ mouse brain (N=8). In CB_1 antagonist studies 0.5 μM SR141716A was used, which is 1,000-fold greater than its K_D value and at this concentration does not exhibit inverse agonism in [^{35}S]GTPγS autoradiographic assays, as previously determined in our laboratory (Sim-Selley et al., 2001).

SR1 (0.5 μM) alone did not significantly stimulate or inhibit [^{35}S]GTPγS binding compared to basal binding in any brain region (Fig. 2.8). WIN-stimulated G-protein activity was robust and widespread in CB_1 receptor containing regions in the absence of SR1, as discussed above (Fig. 2.8). WIN-stimulated [^{35}S]GTPγS binding in the presence of SR1 (WIN/SR1) was reduced in all brain regions and did not significantly differ from basal as determined by SPM. It is possible that WIN might exhibit lower potency and/or efficacy for putative non-CB_1 sites (Breivogel et al., 2001). Therefore, a higher concentration of WIN (50 μM) was used in the presence or absence of 0.5 μM SR1 in select brain regions that demonstrated non-CB_1 binding sites as determined in $CB_1^{-/-}$ mice (Table 2.3, Fig. 2.7). WIN alone produced greater G-protein activation compared to basal in all regions, except for dorsal tegmentum where only an insignificant trend was observed (Fig. 2.9). Variability in measured signal in this particular region was probably due to the general difficulty in collecting representative sections at the same level of dorsal tegmentum from different animals. ROI analyses of all these regions, however,

showed no significant stimulation of [^{35}S]GTPγS binding in the presence of 50 μM WIN + SR1 (Fig. 2.9). These findings suggest that SR1 might also bind to putative non-CB_1 sites.

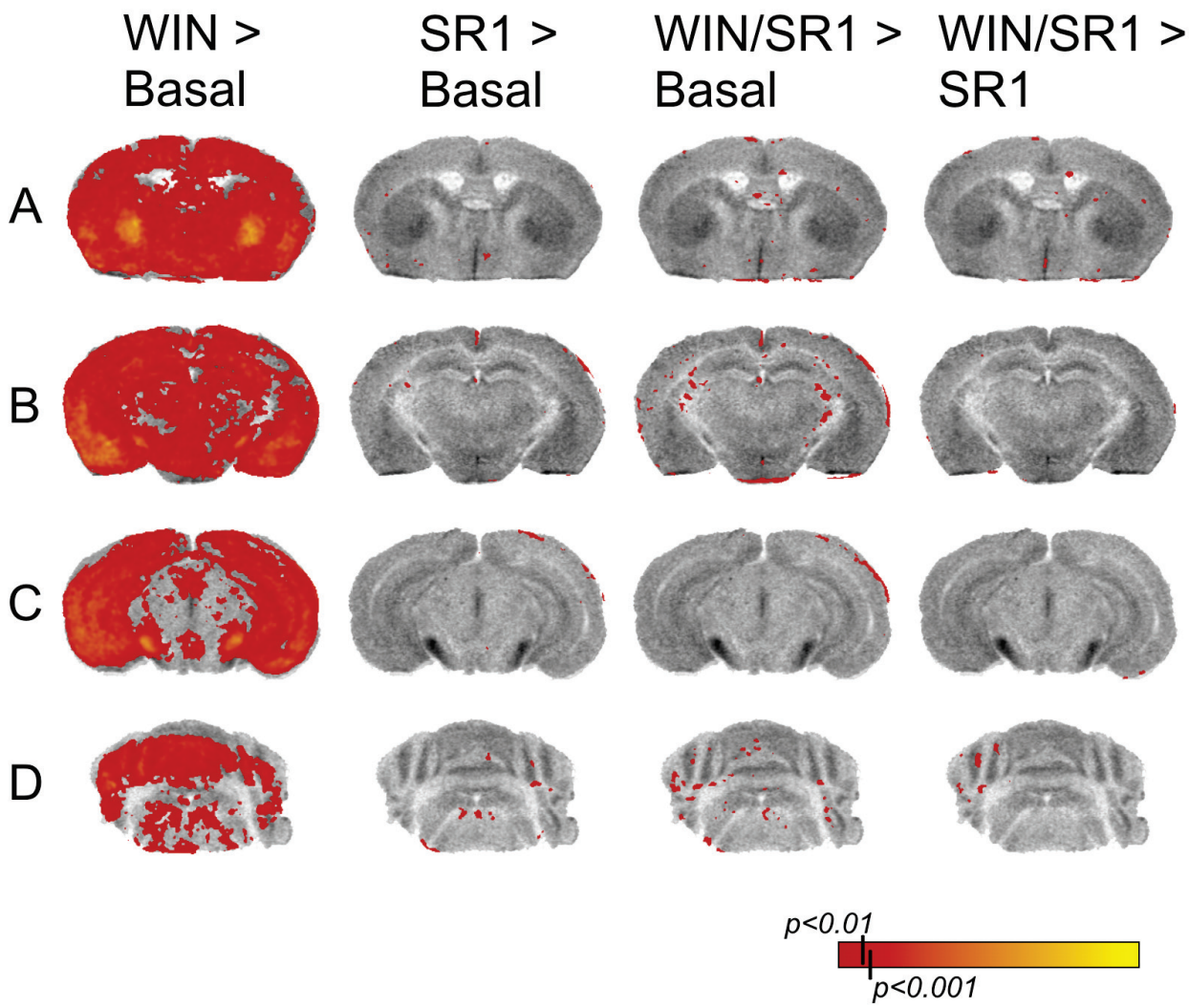

Figure 2.8. SPM analysis showing various comparisons between WIN (10 μM), WIN in the presence of the CB_1 antagonist SR1 (WIN/SR1; 0.5 μM)), SR1 alone (0.5 μM), or basal (no agonist) ($p < 0.01$, ANOVA, n=8) in $CB_1^{+/+}$ mouse brains. Representative coronal sections are shown at the level of the striatum (A), hippocampus (B), substantia nigra (C), and cerebellum (D). Colored overlays (red to yellow) show significant differences corresponding to a *p*-value scale. Corresponding bregma coordinate from top- to bottom-most row are: -0.34 mm, -1.7 mm, -3.28 mm, -5.52 mm. *WIN*, WIN55,212-2; *SR1*, SR141716A. Agonist-stimulated [^{35}S]GTPγS binding autoradiography was performed as described in *Methods*

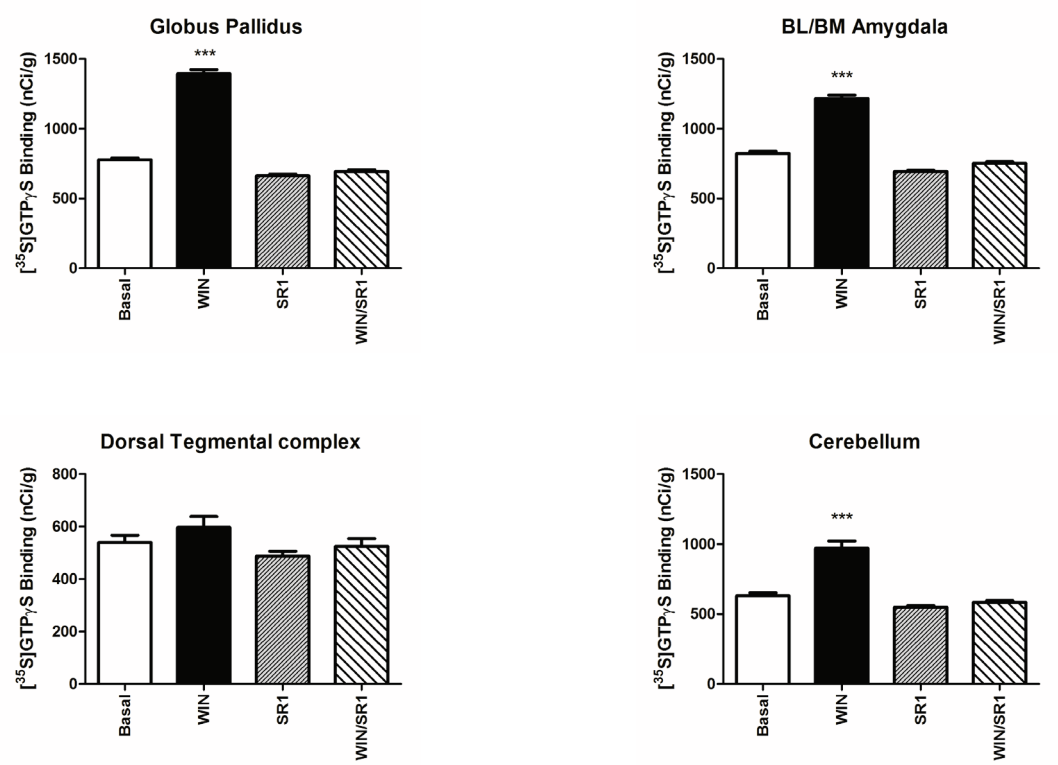

Figure 2.9. SR141716A (0.5 μM) blocked 30 μM WIN-stimulated [^{35}S]GTPγS binding (represented as the mean ± SEM) in naive CB_1 $^{+/+}$ mice (N = 7). * $p < 0.05$, ** $p < 0.01$, *** $p < 0.001$ compared to basal. All comparisons used a one-way repeated measures ANOVA followed by Tukey's Multiple Comparison Test. Agonist-stimulated [^{35}S]GTPγS binding autoradiography was performed as described in *Methods*

2.4 The inactive isomer WIN55,212-3 does not produce G-protein activation in cerebellum of $CB_1^{-/-}$ mice

To confirm the stereoselectivity of the aminoalkylindole WIN55,212-2 for putative non-CB_1 sites, we used its inactive stereoisomer WIN55,212-3 to stimulate [^{35}S]GTPγS binding in $CB_1^{-/-}$ mice. Compared to basal (354.5 ± 11.63 nCi/g), 10 μM of WIN55,212-3 produced no differences in receptor-stimulated [^{35}S]GTPγS binding (381 ± 14.1 nCi/g). The full CB_1 agonist and active isomer WIN55,212-2, however, produced significantly greater G-protein activation (443.3 ± 14.06 nCi/g) when compared to either basal or WIN55,212-3 (Fig. 2.10). As a positive control, the synthetic μ opioid receptor agonist DAMGO (10 μM) stimulated greater [^{35}S]GTPγS binding (1150 ± 9.2 nCi/g) compared to basal (686.2 ± 24.2 nCi/g) in the medial thalamus of $CB_1^{-/-}$ mice (Fig. 2.10). These results suggest that putative non-CB_1 sites in the cerebellum of $CB_1^{-/-}$ mice show stereoselectivity to the active isomer WIN55,212-2 in regard to G-protein activation. This stereoselectivity also supports the fact that G-protein activation of non-CB_1 sites is receptor-mediated.

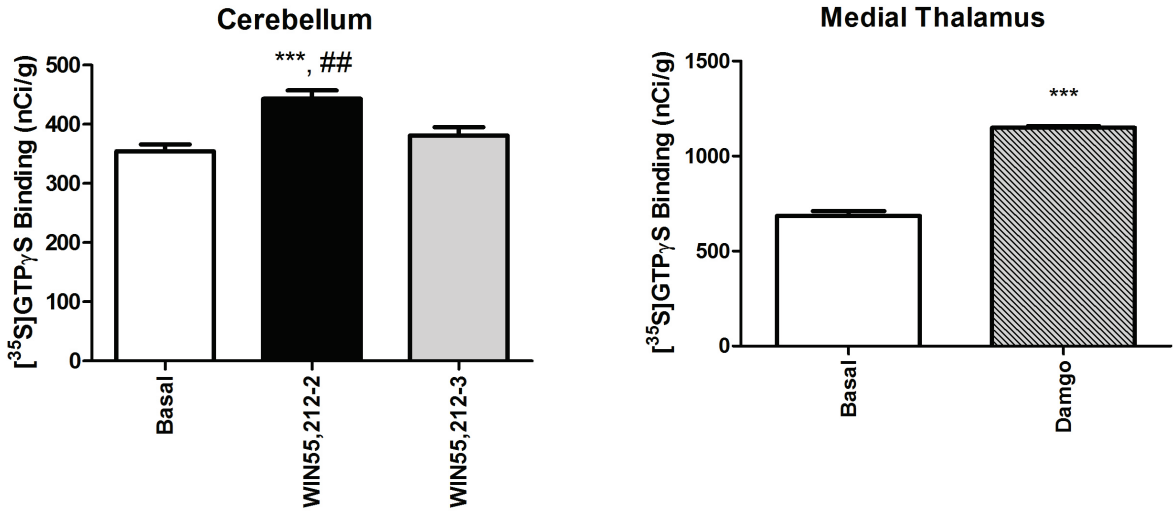

Figure 2.10. Stereoselectivity of WIN55,212-2 in stimulating [^{35}S]GTPγS binding in naive $CB_1^{-/-}$ mice. WIN55,212-2 (10 μM) produced greater [^{35}S]GTPγS binding (shown as the mean ± SEM) compared to either basal or its inactive isomer WIN55,212-3 (10 μM) in the cerebellum from naive $CB_1^{-/-}$ mice (N = 8). The synthetic μ opioid receptor agonist DAMGO (10 μM) was used as a positive control. *** $p < 0.001$ compared to basal. ## $p < 0.01$ compared to WIN55,212-3. Cerebellum analysis used a one-way repeated measures ANOVA followed by Tukey's Multiple Comparison Test and Medial Thalamus used a pair-wise t-test. Agonist-stimulated [^{35}S]GTPγS binding autoradiography was performed as described in *Methods*

2.5 Discussion

The primary goal of this study was to elucidate regional differences in the relative efficacy of receptor-mediated G-protein activity produced by cannabinoids differing in intrinsic efficacy and chemical structure. The potential contribution of non-CB_1 sites to agonist-stimulated G-protein activity was then evaluated in the $CB_1^{-/-}$ mouse model. This was accomplished using a novel approach, in which Statistical Parametric Mapping (SPM) was adapted for whole-brain analysis of 3D reconstructed agonist-stimulated [^{35}S]GTPγS autoradiographic data. SPM revealed regional differences in the efficacy of cannabinoids to activate G-proteins in brains of wild-type mice and localized novel WIN-stimulated [^{35}S]GTPγS binding sites in $CB_1^{-/-}$ mouse brains. This approach provided the dual advantages of creating a functional map of receptor-activated G-proteins in the reconstructed brain, with an unbiased statistical comparison of levels of G-protein activity, thereby providing new data on cannabinoid-mediated activity in the mouse brain.

SPM has previously been adapted for the analysis of reconstructed autoradiographic datasets mapping cerebral blood flow (Nguyen et al., 2004), and successfully applied to functionally map brain activity in small animals (Dubois et al., 2008; Holschneider et al., 2006; Soto-Montenegro et al., 2008; Yang et al., 2007). Applying SPM analysis to *in vitro* agonist-stimulated [^{35}S]GTPγS autoradiographic data offers unique advantages compared to conventional region of interest (ROI) analysis. ROI analysis is generally assessed within predefined anatomical boundaries, but effects of interest might not always conform to anatomically defined regions. For heterogenous distributions of receptor-mediated activity, the size and shape of ROIs and plane(s) of data might be difficult to define a priori in order to maximize signal detection. In addition, if regions of receptor activity are substantially smaller than the defined ROI,

significance might be missed when signal is averaged with surrounding background that is included within the ROI. Moreover, the anatomical precision of this approach is illustrated in the motor and somatosensory cortices, where voxels with the most significant and greatest magnitude of cannabinoid-stimulated [^{35}S]GTPγS binding in $CB_1^{+/+}$ mice were localized in specific cortical laminae (Fig. 2.4A) in a pattern consistent with previous reports showing the highest concentration of CB_1 receptor protein in the superficial (II, III) and deep (VI) layers of cortex (Herkenham et al., 1991; Tsou et al., 1998). It is important to note that most of the significant differences between cannabinoid-stimulated [^{35}S]GTPγS binding showed bilateral symmetry. This neuroanatomical property, in addition to the known expression profile of CB_1 receptor protein, further strengthens the validity of SPM for analyzing agonist-stimulated [^{35}S]GTPγS binding autoradiographic data.

Initial studies revealed regional differences in the relative efficacies of WIN-, CP-, and M-AEA-stimulated [^{35}S]GTPγS binding. SPM comparison identified an efficacy profile of WIN > CP > M-AEA in areas including globus pallidus, hypothalamus, and periaqueductal gray. However in other brain areas including caudate-putamen, cerebellum, hippocampus, amygdala, substantia nigra and cortex, the relative efficacy for cannabinoid-stimulated G protein activity was WIN = CP > M-AEA. A different finding emerged in the thalamus, where the profile WIN = CP = M-AEA was found. A previous study using membrane preparations from cerebellum, hippocampus, and hypothalamus also reported regional differences in the relative efficacy and potency of WIN, CP, and M-AEA (Breivogel and Childers, 2000). However, the relative stimulation of receptor-activated G-proteins for these cannabinoid agonists differed somewhat from the current study. This discrepancy could be due to differences in the anatomical resolution of autoradiography versus [^{35}S]GTPγS binding in membranes prepared from grossly dissected

brain regions. While the mechanism(s) underlying regional differences in relative agonist efficacy are not known, CB_1 receptors have been shown to exhibit domain selectivity for coupling to different subtypes of $G\alpha_{i/o}$, and in various brain regions, activate different subtypes of G-proteins with varying efficacy and potency after agonist stimulation (Mukhopadhyay et al., 2000; Prather et al., 2000). Cannabinoid-selective G-protein signaling has also been demonstrated using recombinant expression of CB_1 receptors in situ with reconstitution of purified G-protein subunits (Glass and Northup, 1999). In that study, the relative efficacies of different cannabinoid agonists differed between $G\alpha_i$ versus $G\alpha_o$ activation. One can thus envision ligand- and region-specific CB_1 receptor signaling based on the stoichiometric complement of various G_α subtypes.

An alternative explanation for the higher efficacy of certain cannabinoids is the contribution of multiple receptors (e.g. CB_1 + non-CB_1 receptors) to the overall agonist-stimulated activity. To explore this question further, SPM was used to determine the extent to which WIN, CP, and M-AEA, would activate G-proteins in $CB_1^{-/-}$ mouse brains. Of these cannabinoid agonists, only the aminoalkylindole WIN significantly stimulated [^{35}S]GTPγS binding when compared to basal activity (absence of agonist). In this study, WIN stimulated [^{35}S]GTPγS binding in a subset of brain regions in $CB_1^{-/-}$ mouse brains that only partially overlapped the distribution of activity in $CB_1^{+/+}$ brains. The greatest magnitudes of WIN-stimulated G-protein activity were noted within the dorsal tegmental complex and locus coeruleus, which contain acetylcholine and norepinephrine producing neurons, respectively. Relatively high levels of G-protein activation were also found in the cerebellum, which appear to correspond to the molecular layer. Modest G-protein activation was found in the cortex, amygdala, hippocampus, and hypothalamus. Interestingly, the hypothalamus was a brain region in which SPM analysis of brains from $CB_1^{+/+}$

mice found significantly greater WIN- versus CP-stimulated [^{35}S]GTPγS binding, suggesting a possible contribution of additional non-CB_1 sites to the greater efficacy for WIN in G-protein activation. However, for other brain areas in $CB_1^{-/-}$ mice with significant WIN-stimulated [^{35}S]GTPγS binding, such as amygdala and cerebellum, there were no differences in efficacy for G-protein activation between WIN and CP in the $CB_1^{+/+}$ mice. For these brain areas, it is possible that differences in regional G-protein coupling may enhance the efficacy of CP in $CB_1^{+/+}$ mice. Interestingly, no significant WIN-stimulated [^{35}S]GTPγS binding in $CB_1^{-/-}$ mice was found in the nuclei of the basal ganglia, which normally contain the highest levels of CB_1 receptors (Herkenham et al., 1991). In contrast, the brainstem contains relatively low to moderate levels of CB_1 receptors (Herkenham et al., 1991) but the greatest magnitude of WIN-stimulated activity was detected in certain pontine nuclei. These findings are also consistent with previous reports that WIN stimulated [^{35}S]GTPγS binding, but CP had no effect, in membrane homogenates prepared from $CB_1^{-/-}$ mice (Breivogel et al., 2001). Although previous studies have also found that anandamide (AEA) stimulated G-protein activity in $CB_1^{-/-}$ mice (Breivogel et al., 2001; Di Marzo et al., 2000), the stable analog M-AEA had no effect in this study. Brain areas with significant WIN-stimulated [^{35}S]GTPγS binding compared to basal in this study (Table 2) were similar to those previously reported by Breivogel and colleagues (Breivogel et al., 2001). Both studies found WIN-stimulated G-protein activity in the brainstem, cortex, hypothalamus, and hippocampus, and no significant WIN-stimulated [^{35}S]GTPγS binding in the basal ganglia. However, no significant WIN-stimulated [^{35}S]GTPγS binding was found in the cerebellum by Breivogel and colleagues, whereas in this study significance was localized in bands that appear to correspond to the molecular layer of the cerebellum (Fig 4). The slight discrepancy in results could be due to differences in the analytical techniques, where SPM assesses changes at the

individual voxel-level in intact brain tissue sections versus the [^{35}S]GTPγS binding assay for homogenized gross brain areas.

Interestingly, non-CB_1 WIN-stimulated [^{35}S]GTPγS binding sites detected by SPM appeared to be distributed in certain functional systems. The localization of non-CB_1 sites in the locus coeruleus (LC) and its projection regions including frontal cortex, amygdala, hypothalamus, hippocampus, and cerebellum, might suggest a possible neuromodulatory role of these non-CB_1 sites within the noradrenergic system. Noradrenergic projections from the LC to forebrain regions are especially relevant to regulation of cognition, attention and anxiety (Aston-Jones et al., 1999; Bremner et al., 1996; Foote et al., 1983). Previous studies by Van Bockstaele and colleagues have shown that systemic WIN administration increased cfos expression in tyrosine hydroxalase positive LC neurons, indicating that WIN was affecting the coeruleo-cortical pathway. In addition, administration of WIN systemically (Oropeza et al., 2005) or directly into the frontal cortex (Page et al., 2008) increased norepinephrine release in an SR1-sensitive manner. Interestingly, CB_1 receptors are generally associated with presynaptic inhibition of neurotransmitter release (Schlicker and Kathmann, 2001) and inhibit NE release in the hippocampus (Schlicker et al., 1997). While it is possible that enhanced WIN-mediated NE release in the frontal cortex occurs via an indirect mechanism, it is also possible that NE release is regulated by both CB_1 and non-CB_1 receptors in this region. Approximately 30% of CB_1 receptor immunoreactive terminals in the frontal cortex also contain the catecholamine-synthesizing enzyme dopamine-β-hydroxylase (Oropeza et al., 2007), and if non-CB_1 WIN sites predominated in remaining terminals, the net result could be enhanced NE release. However, this question would need to be further examined in $CB_1^{-/-}$ mice. Thus, the anatomical profile of non-

CB_1 WIN sites found in the current study could subserve a distinct modulatory function from the endogenous cannabinoid system that has yet to be fully characterized.

Because WIN was active in $CB_1^{-/-}$ mice, pharmacological studies were conducted in $CB1^{+/+}$ mice to assess WIN-stimulated [^{35}S]GTPγS binding in the presence of the CB_1 receptor antagonist SR141716A (SR1). However, no significant G-protein activation was detected with WIN in the presence of SR1, nor did SR1 alone produce any change in [^{35}S]GTPγS binding compared to basal activity. Thus, it is possible that SR1 might bind to both CB_1 and non-CB_1/CB_2 sites. In fact, previous studies have shown that certain non-CB_1 mediated effects of WIN are inhibited by pretreatment with SR1 (Hajos et al., 2001; Hoffman et al., 2005; Pistis et al., 2004). It is further possible that multiple non-CB_1 WIN-stimulated [^{35}S]GTPγS binding sites exist, based on pharmacological and species specificity as defined in the literature (Hoffman et al 2005). Although the molecular identity of non-CB_1 WIN-binding sites in the current study is unknown, several conclusions can be reached regarding their pharmacology. WIN is an agonist of unknown efficacy, SR1 appears to be an antagonist or very low efficacy partial agonist, and CP and M-AEA are not agonists. Further, these sites are presumably coupled to inhibitory G-proteins of the $G\alpha_{i/o}$ class because agonist-stimulated [^{35}S]GTPγS autoradiography in brain does not appear to detect other classes of receptor-activated G-proteins due to the high abundance of $G\alpha_o$ in brain and the kinetics of binding under the conditions of the assay (Sim-Selley and Childers, 2002). Insensitivity to CP indicates that these sites are unlikely to be CB_2 receptors (Govaerts et al., 2004), despite previous reports that CB_2 receptors are expressed in brainstem (Van Sickle et al., 2005). These sites are also unlikely to be GPR55, which has been shown to activate G_q and G_{12} and does not respond to WIN in various *in vitro* assays (Ross, 2009). Thus, the present results provide anatomical and functional evidence supporting the existence of a

novel non-CB_1/CB_2/GRP55 WIN-stimulated [^{35}S]GTPγS binding site in defined regions of mouse brain.

In summary, Statistical Parametric Mapping (SPM) was used to assess and spatially map regional differences in cannabinoid-mediated G-protein activity in reconstructed mouse brain images derived from agonist-stimulated [^{35}S]GTPγS binding autoradiography. SPM analysis, combined with conventional ROI analysis, demonstrated regional differences in the relative efficacies of various cannabinoid agonists, and showed that certain cannabinoid agonists activate functional non-CB_1 sites, in addition to CB_1 receptors. The unique pharmacology and functional neuroanatomical distribution of non-CB_1 sites indicates that this novel system might have distinct physiological roles from the endogenous cannabinoid system that have yet to be characterized. Furthermore, the neuroanatomical distribution of these putative non-CB_1 sites suggests that this system could be exploited therapeutically. Lastly, this study demonstrates SPM as a powerful tool for the neuroanatomical analysis and functional mapping of G-protein coupled receptors in 3D reconstructed mouse brain images derived from [^{35}S]GTPγS autoradiography.

VI. Chapter 3: β-arrestin 2 regulation of the CB_1 receptor following chronic administration of THC

In the previous chapter, whole brain analysis of CB_1 receptor activity revealed region-specific differences in the relative efficacy of different classes of cannabinoid agonists. Regional differences in the relative efficacy of receptor-mediated G-protein activation suggest unique signaling properties of the CB_1 receptor that could result in differential receptor regulation by brain region. This hypothesis could have implications for the regulation of CB_1 receptor adaptation during repeated cannabinoid administration, which could affect the magnitude and/or rate of tolerance development following repeated administration of cannabinoids. Chronic administration of THC and other cannabinoid agonists generally leads to the development of tolerance to its *in vivo* effects. Tolerance has also been demonstrated to various cannabinoid-mediated effects including antinociception, hypothermia, catalepsy, spontaneous motor hypoactivity, and memory. Previous work in our laboratory demonstrated region-specific differences in the attenuation or desensitization of CB_1 receptor activity following chronic administration of THC (McKinney et al., 2008; Sim-Selley and Martin, 2002; Sim-Selley et al., 2006; Sim et al., 1996a). However, a mechanistic link between desensitization and tolerance has not been determined for cannabinoids. Studies in cell models have shown that β-arrestin 2 (βarr2) regulates CB_1 receptors *in vitro* (Jin et al., 1999; Kouznetsova et al., 2002), but evidence for involvement of βarr2 in regulation of CB_1 receptors in brain is very limited. In this chapter, we will test the hypothesis that the regulatory protein βarr2 mediates the functional adaptation of CB_1 receptors to chronic stimulation by THC in certain brain regions where the two are co-distributed. Further, we propose that βarr2-mediated regulation of CB_1 receptors contributes to the development of tolerance to THC-mediated *in vivo* effects.

3.1 β*-arrestin 2 attenuates tolerance to specific THC-mediated effects in vivo*

One study has reported the potential role of βarr2 in acute cannabinoid-mediated effects. Breivogel et al. (Breivogel et al., 2008) showed that loss of βarr2 enhanced THC-mediated antinociception and hypothermia in βarr2 knockout (KO) mice compared to wild-type (WT) mice. Similarly, Bohn et. al. reported enhanced and prolonged antinociception after morphine administration, as well as greater morphine-mediated hypothermia in mice lacking βarr2 compared with their wild-type littermates (Bohn et al., 2000; Bohn et al., 2002; Bohn et al., 1999). The role of βarr2 in cannabinoid-mediated effects following repeated cannabinoid administration has not been examined, but evidence from the μ opioid system suggests possible outcomes. In those studies, βarr2 KO mice did not develop tolerance to morphine-mediated antinociception as determined in the hot-plate test, but interestingly only delayed tolerance when assessed using the warm-water tail immersion test. These results suggest that βarr2 regulates nociceptive function through the μ opioid receptor and may have differential effects within various anatomical systems. Mu opioid receptors and CB_1 receptors both belong to the superfamily of GPCRs and interact in certain physiological responses (reviewed in (Corchero et al., 2004)). However, it is unclear whether common mechanisms regulate these receptor classes. We therefore tested the hypothesis that βarr2 is involved in producing tolerance to various THC-mediated effects.

To test this hypothesis, βarr2 KO mice and their WT littermates were treated twice daily for 6.5 days with an intraperitoneal (i.p.) administration of either vehicle (1:1:18, ethanol:cremaphor:saline) or 10 mg/kg THC. Drug dosing and *in vivo* tests were done in collaboration by Dr. Laura Bohn's laboratory (Scripps Research Institute, FL). On the morning of

the 7th day, 24 hrs following drug treatment, THC-mediated effects were assessed using a cumulative dosing paradigm (3, 7, 20, 26, 44 mg/kg for doses of 3, 10, 30, 56, 100 mg/kg i.p.) in 40 minute intervals, in which behaviors were assessed 30 minutes after each injection. The following behaviors were assessed: 1) antinociception using the tail warm-water withdrawal assay at 52°C, 2) hypothermia using rectal temperature, and 3) catalepsy using the ring immobility test. *In vivo* procedures are outlined in *Section III - Methods*.

Results revealed that abrogation of βarr2 produced effect-specific alterations in both vehicle control and THC-treated mice. Interestingly in the vehicle treated groups, βarr2 KO animals displayed a greater sensitivity to the hypothermic effect of THC compared to WTs [$F(1,84) = 7.39$, $p < 0.01$]. In contrast, mice in the vehicle treated groups, showed no difference in antinociception or immobility between genotypes. Assessment of tolerance to these effects following repeated THC treatment also showed effect-specific alterations in tolerance in βarr2 KO compared to WT mice. However in this case, only tolerance to antinociception was affected by loss of βarr2. Although both WT [$F(1,84) = 92.45$, $p < 0.0001$] and βarr2 KO [$F(1,84) = 14.72$, $p < 0.001$] animals developed tolerance to the antinociceptive effects of THC (Fig. 3.1C), tolerance to antinociception was attenuated in the THC-treated βarr2 KO group, which was significantly less than the THC-treated WT group [$F(1,84) = 13.25$, $p < 0.001$]. When tested for catalepsy, both WT [$F(1,84) = 18.13$, $p < 0.0001$] and βarr2 KO [$F(1,84) = 53.76$, $p < 0.0001$] animals developed tolerance that was of similar magnitude (Fig. 3.1B). In contrast to acute results, both WT [$F(1,84) = 51.15$, $p < 0.0001$] and βarr2 KO [$F(1,84) = 44.48$, $p < 0.0001$] animals developed tolerance to THC-mediated hypothermia following the chronic THC dosing paradigm (Fig. 3.1A) and the tolerance was similar in magnitude. These results show that βarr2 may be involved in the acute effects of THC-mediated hypothermia, whereas tolerance to

antinociception is attenuated in βarr2 KO mice. Therefore, attenuation in tolerance occurred in a behavior-specific manner, suggesting that βarr2 may regulate CB_1 receptors in a region-specific manner as well in brain.

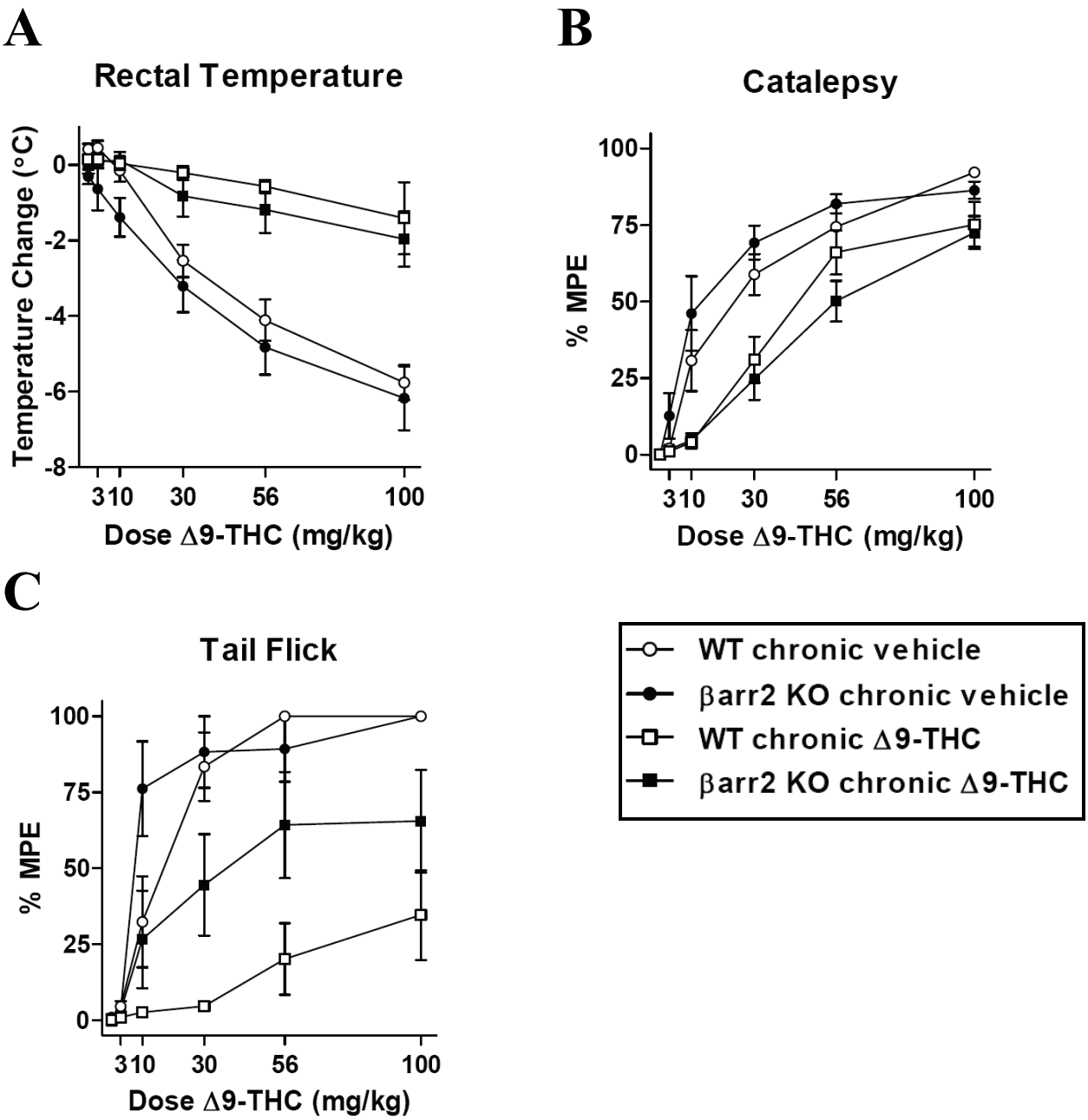

Figure 3.1. THC-mediated *in vivo* effects in βArr2 KO and WT animals following 6.5 day administration of 10 mg/kg THC or vehicle treatment (i.p.) given twice daily. THC-mediated effects including change in rectal temperature, percentage of time of ring immobility (catalepsy), and percent of maximum possible antinociceptive effect were measured. Both βArr2 KO and WT animals developed tolerance to THC-mediated hypothermia (A) and catalepsy (B). However, tolerance to THC-mediated antinociception (C) was significantly attenuated in βArr2 KO animals compared to WT. Data reflect the mean ± SEM (N = 8 per group)

3.2 β-arrestin 2 regulates CB_1 receptor desensitization in mouse spinal cord following chronic administration of THC

Persistent exposure to an agonist leads to characteristic changes at the level of the GPCR in order to dampen its signaling capacity, and thereby maintain equilibrium. The mechanisms underlying the regulation of GPCRs, specifically receptor desensitization (uncoupling of G-proteins) and downregulation (receptor degradation), have been studied extensively in cell models (Ferguson and Caron, 1998; Gainetdinov et al., 2004). In the classical sense, receptor desensitization occurs when a receptor is phosphorylated by a GPCR kinase (GRK), which leads to the binding of an arrestin protein and subsequent uncoupling of the G-protein from its cognate receptor. These same mechanisms appear to contribute to regulation of CB_1 receptors in response to persistent stimulation by an agonist. Previous work by Mackie and colleagues has shown that co-expression of both GRK3 and βarr2, using a *Xenopus Oocyte* expression system, was required for the rapid desensitization of CB_1-receptor mediated potassium currents following exposure to the full CB_1 agonist WIN55,212-2 (Jin et al., 1999). In the current study, the attenuation in tolerance to THC-mediated antinociception, as measured by tail withdrawal in βarr2 KO mice, also suggests that βarr2 regulates CB_1 receptors in anatomical circuits that may mediate this behavior. The tail withdrawal assay is largely a spinally-mediated reflex, suggesting that βarr2-mediated regulation of CB_1 receptors in the spinal cord could contribute to this observation. To test this hypothesis, whole spinal cords were collected from mice 24 hours after the behavioral tests described above. Membrane preparations from homogenized spinal cord were then used to generate concentration-effect curves of cannabinoid-stimulated [^{35}S]GTPγS binding to assess changes in CB_1 receptor-mediated G-protein activity (conducted as described in *Section III - Methods)*. No significant differences were found in basal (no agonist) [^{35}S]GTPγS binding

between genotypes or drug treatment groups, thus indicating no gross alteration in constitutive G-protein coupling (Fig 3.2). These data also indicate that residual THC did not remain in the sample because it would stimulate [^{35}S]GTPγS binding above basal levels seen in vehicle-treated mice. CP55,940 (CP)-mediated G-protein activity was first compared between vehicle-treated mice to determine whether loss of βarr2 altered baseline (e.g. no drug treatment) CB_1 receptor activity. Results showed that CP-stimulated [^{35}S]GTPγS binding did not differ between genotypes in vehicle-treated mice, with E_{max} values (expressed as %Net Stimulation, see *Methods*) of 45.04 ± 1.91% in WT and 46.41 ± 2.13% in βarr2 KO animals (Fig. 3.3A, Table 3.1). Chronic treatment with THC lead to significant desensitization of receptor-mediated G-protein activity in βarr2 WT mice, with an E_{max} value for CP-stimulated [^{35}S]GTPγS binding of 27.88 ± 3.64% in WT compared to 41.10 ± 1.80% in βarr2 KO animals, which represented an approximately 38% decrease in receptor-mediated activity (Fig. 3.3A, Table 3.1). Interestingly, CB_1 receptor desensitization was attenuated in the βarr2 KO mice, where its E_{max} value for CP-stimulated [^{35}S]GTPγS binding was reduced by approximately 11% of its respective vehicle control. Further, this E_{max} value did not significantly differ from its respective vehicle control, but did differ from THC-treated WT mice. No differences were found in the EC_{50} values for CP-stimulated [^{35}S]GTPγS binding between treatment groups (Table 3.1). This important observation indicates that there was satisfactory washout of drug prior to performing *in vitro* studies. Similar results were obtained when using the full CB_1 agonist WIN55,212-2 (WIN) to assess receptor-stimulated [^{35}S]GTPγS binding (Fig. 3.3B). Again, WIN-stimulated [^{35}S]GTPγS binding did not differ between genotypes in vehicle-treated mice, with E_{max} values of 75.46 ± 6.82% in WT and 80.87 ± 11.55% in βarr2 KO animals (Fig. 3.3B, Table 3.1). Chronic treatment also led to significant desensitization of CB_1 receptors βarr2 WT mice with an E_{max} value of

49.39 ± 4.41%, or an approximately 35% decrease in receptor-mediated G-protein activity, compared to no change in the βarr2 KO animals (E_{max} value of 72.53 ± 5.99%, or an approximately 10% decrease in receptor-mediated G-protein activity). When comparing E_{max} values between THC-treated βarr2 WT and KO mice, a close trending difference was also found ($p = 0.052$). Lastly, a significant interaction between Drug x Genotype was found [$F(1,24) = 5.68$, $p < 0.05$], suggesting that βarr2 is involved in mediating CB_1 receptor desensitization of G-protein coupling following THC treatment in spinal cord. Thus βarr2 regulation of CB_1 receptor desensitization may be one mechanism that contributes to THC-mediated antinociceptive tolerance.

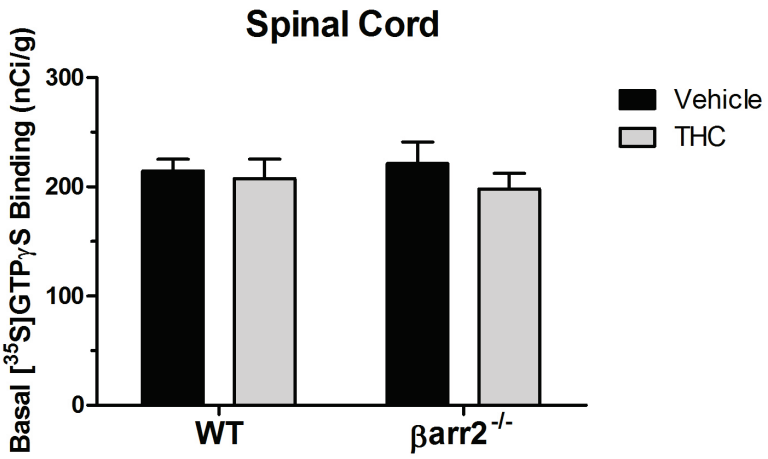

Basal [^{35}S]GTPγS Binding (nCi/g)			
WT Vehicle	**WT THC**	**βarr2$^{-/-}$ Vehicle**	**βarr2$^{-/-}$ THC**
214.7 ± 10.6	207.5 ± 17.9	221.3 ± 19.8	198 ± 14.5

Figure 3.2. Basal [^{35}S]GTPγS binding in spinal cord of βArr2 KO and WT animals following chronic THC or vehicle treatment. βArr2 KO and WT animals received 6.5 day administration of 10 mg/kg THC or vehicle treatment (i.p.) given twice daily. No differences were found in basal (no agonist) [^{35}S]GTPγS binding by genotype or drug treatment as determined by 2-way ANOVA. Binding values represent the mean ± SEM (N = 6).

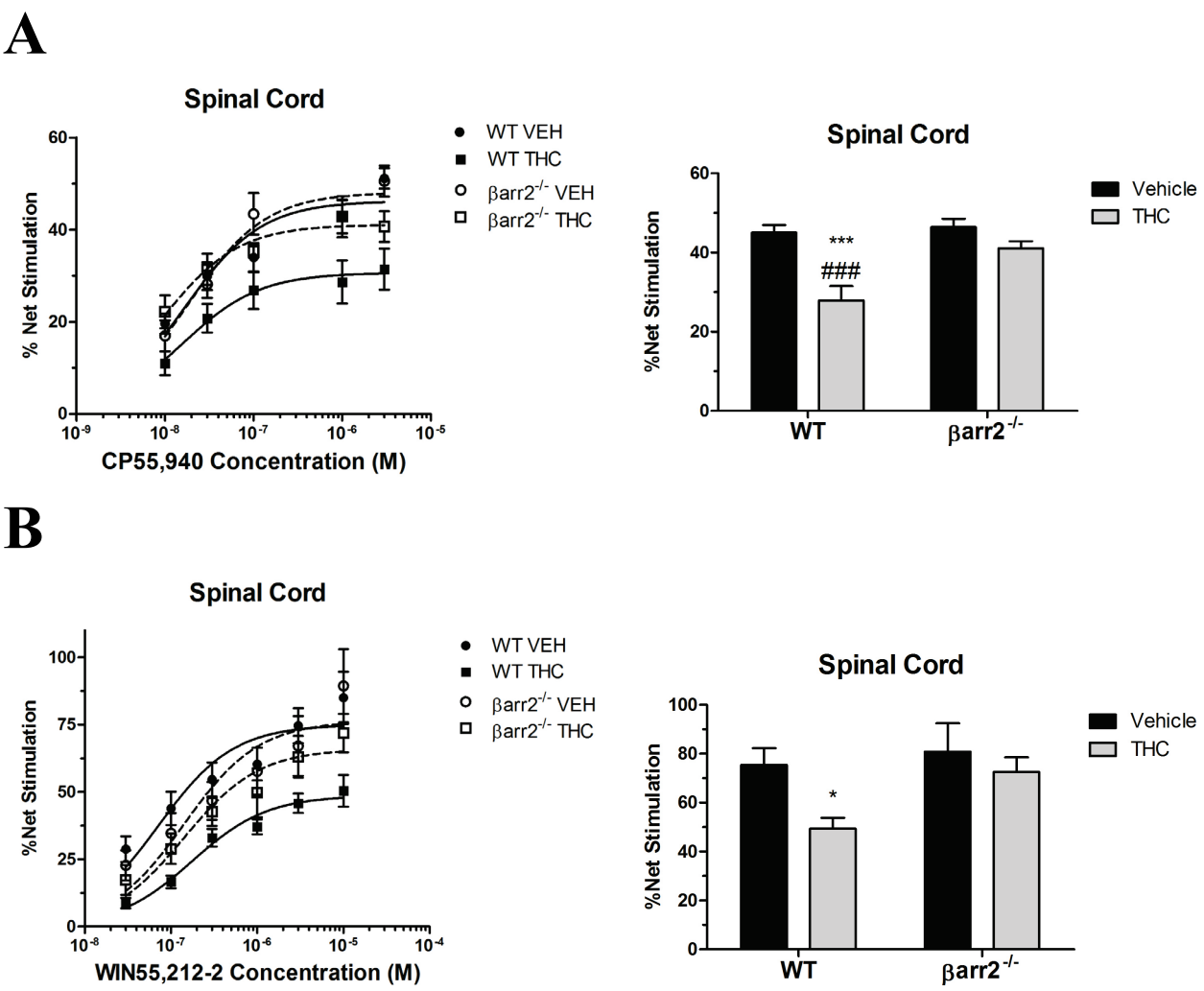

Figure 3.3. Desensitization of CB_1 receptor-mediated G-protein activation was attenuated in spinal cords of βarr2 KO animals following chronic treatment of THC. βArr2 KO and WT animals received 6.5 day administration of 10 mg/kg THC or vehicle treatment (i.p.) given twice daily. Agonist-stimulated [^{35}S]GTPγS binding curves using CP55,940 (A) or WIN55,212-2 (B) are shown and values are expressed as %Net stimulation [(agonist - basal)/basal x 100%]. Each point represents the mean ± SEM (N = 6-7 in each point) [^{35}S]GTPγS binding value. E_{max} [^{35}S]GTPγS binding values were calculated using non-linear regression analyses in Prism and are shown in the bar graphs (right). * $p < 0.05$, *** $p < 0.001$, compared to respective vehicle control; ### $p < 0.001$ versus KO THC (2-way ANOVA, Student-Newman Keuls post-hoc). Agonist-stimulated [^{35}S]GTPγS binding curves were generated as described in *Methods*.

Table 3.1. Desensitization of CB_1 receptor-mediated G-protein activation was attenuated in spinal cords of βarr2 knockout animals following chronic treatment of THC. βArr2 KO and WT animals received 6.5 day administration of 10 mg/kg THC or vehicle treatment (i.p.) given twice daily. Concentration-effect curves were constructed and analyzed for best-fit E_{max} and EC_{50} values using Prism and described in *Methods*. Values represent the mean ± SEM (N = 6-7 in each point). E_{max} [^{35}S]GTPγS binding values are expressed as %Net stimulation [(agonist - basal)/basal x 100%]. * $p < 0.05$, *** $p < 0.001$, versus respective vehicle control group; ### $p < 0.001$ versus KO THC (2-way ANOVA, bonferroni post-test).

Group	EC_{50} (μM)	E_{max} (% Net Stim.)	% Vehicle
CP55,940			
WT Vehicle	0.04 ± 0.01	45.04 ± 1.91	100 ± 4.25
WT THC	0.02 ± 0.01	27.88 ± 3.64$^{***,\#\#\#}$	61.89 ± 8.08
βarr2$^{-/-}$ Vehicle	0.02 ± 0.01	46.41 ± 2.13	100 ± 4.60
βarr2$^{-/-}$ THC	0.01 ± 0.01	41.10 ± 1.80	88.56 ± 3.88
WIN55,212-2			
WT Vehicle	0.08 ± 0.02	75.46 ± 6.82	100 ± 9.04
WT THC	0.20 ± 0.04	49.39 ± 4.41*	65.45 ± 5.84
βarr2$^{-/-}$ Vehicle	0.34 ± 0.19	80.87 ± 11.55	100 ± 14.28
βarr2$^{-/-}$ THC	0.22 ± 0.07	72.53 ± 5.99	89.67 ± 7.41

3.3 β-arrestin 2 regulates CB_1 receptor downregulation in mouse spinal cord following chronic administration of THC

βarr2 may also serve other physiological functions in the regulation of GPCR signaling. For example, βarr2 has previously been demonstrated as an adaptor protein, targeting phosphorylated β_2 adrenergic receptors towards degradation via clathrin-mediated endocytosis (Lin et al., 1997). Reduction in cell surface receptor levels, or downregulation, could therefore be another mechanism contributing to drug tolerance. We therefore evaluated the effect of βarr2 deletion on CB_1 receptor downregulation in whole spinal cord following chronic THC administration. Receptor binding saturation curves were generated using the CB_1 receptor antagonist SR141716A (SR1). No differences were found in [^{3}H]SR141716A binding between genotypes in vehicle treated mice, with B_{max} values (pmol/mg) of 0.47 ± 0.04 in WT and 0.54 ± 0.04 in βarr2 KO mice (Fig. 3.4). Chronic THC treatment resulted in significant CB_1 receptor downregulation in βarr2 WT mice (B_{max} = 59.4% of vehicle control) that was attenuated in βarr2 KO mice (B_{max} = 82.3% of vehicle control) (Fig. 3.3). Furthermore, no differences in receptor affinity were found between groups (Fig. 3.3), indicating adequate washout of drug and that downregulation was due primarily to a reduction in bound CB_1 receptor protein. It is important to note that SR1 recognizes both high and low affinity binding states of the receptor, and therefore is independent of receptor desensitization. These results thus indicate that βarr2 is also involved in regulating CB_1 receptor downregulation within the spinal cord, thus contributing to the attenuation in THC-mediated antinociceptive tolerance.

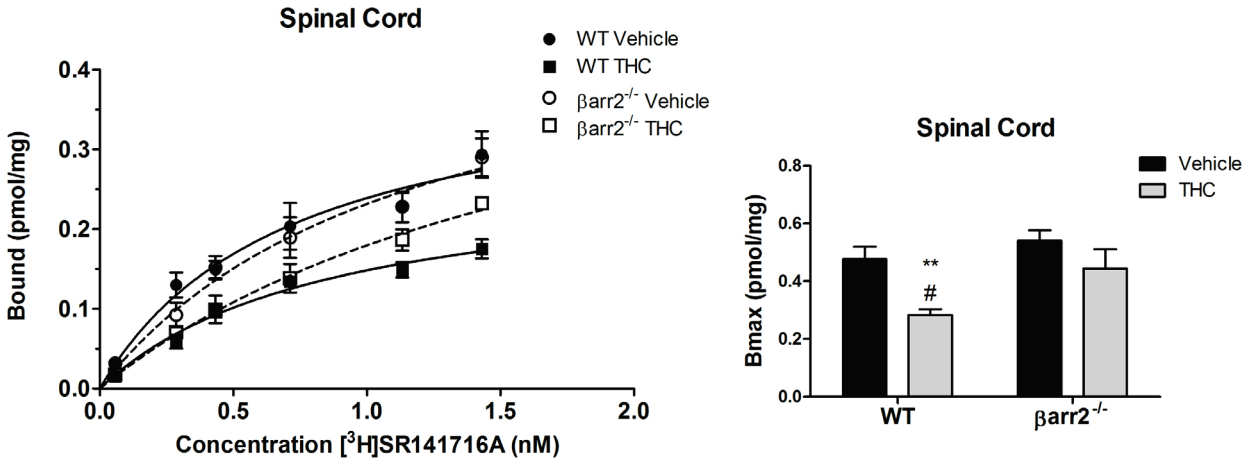

Group	K_D (nM)	B_{max} (pmol/mg)	% Vehicle
WT Vehicle	1.03 ± 0.24	0.47 ± 0.04	100 ± 9.07
WT THC	0.91 ± 0.11	0.28 ± 0.02$^{**,\#}$	59.40 ± 4.12
βarr2$^{-/-}$ Vehicle	1.43 ±0.27	0.54 ± 0.04	100 ± 6.67
βarr2$^{-/-}$ THC	1.51 ± 0.34	0.44 ± 0.07	82.30 ± 12.21

Figure 3.4. Chronic administration of THC led to downregulation of CB_1 receptors in spinal cords of WT animals, but was abolished in βarr2 KO mice. βArr2 KO and WT animals received 6.5 day administration of 10 mg/kg THC or vehicle treatment (i.p.) given twice daily. CB_1 receptor binding curves (as described in *Methods*) were generated using [^{3}H]SR141716A. B_{max} (pmol/mg) and K_D (nM) values were calculated with Prism using a one site hyperbola function and displayed as the mean ± SEM (N = 6-7 per point). ** $p < 0.01$, compared to respective vehicle control; # $p < 0.001$ versus KO THC (2-way ANOVA, Student-Newman Keuls post-hoc)

3.4 Method for 3D reconstruction of agonist-stimulated [^{35}S]GTPγS and [^{3}H]CP55,940 binding autoradiography

Results of *in vivo* studies showed that βarr2 deletion altered THC-mediated effects in a effect-specific manner. The attenuation in THC-mediated antinociceptive tolerance, but not tolerance to catalepsy or hypothermia, suggests that βarr2 may differentially regulate CB_1 receptor signaling within different neuronal populations. For example, cannabinoid-mediated antinociception is likely to be mediated by circuits that include the PAG and spinal cord (Lichtman et al., 1996). Results in membrane homogenates of spinal cord support a role for βarr2-regulated CB_1 receptor desensitization/downregulation in this region in antinociceptive tolerance. Based on *in vivo* findings, we predict that deletion of βarr2 would reduce desensitization in regions including PAG. Conversely, we do not predict that βarr2 would affect desensitization in regions such as hypothalamus and basal ganglia that contribute to hypothermia and catalepsy, respectively. To test this hypothesis, we utilized Statistical Parametric Mapping (SPM) analysis to determine whether βarr2 regulates CB_1 receptor function and levels following chronic THC treatment, using reconstructed images derived from agonist-stimulated [^{35}S]GTPγS and [^{3}H]CP55,940 binding autoradiography, respectively.

3D reconstructions of agonist-stimulated [^{35}S]GTPγS binding were conducted as outlined in Chapters 1-2. CP55,940 (CP) was used to stimulate [^{35}S]GTPγS binding, since we showed that it exhibits similar efficacy as the full CB_1 agonist WIN55,212-2 (WIN) for G-protein activation in a number of CB_1 receptor containing brain regions (see Chapter 2, Fig. 2.4) but does not activate non-CB_1/CB_2 sites as shown in mice lacking CB_1 receptors (see Chapter 2, Fig. 2.7). [^{35}S]GTPγS binding values in reconstructed images were expressed as net differences (agonist-stimulated minus basal [^{35}S]GTPγS binding). These reconstructions of net values were derived

by image subtracting basal images from their respective CP-stimulated images, both of which were spatially normalized to the same coordinate space. Estimation of spatial normalization parameters were derived from CP-stimulated images, as these provided the most contrast between anatomical structures. The image average of all CP-stimulated reconstructions from all treatment groups was used to create the template for estimation of spatial normalization of individual CP-stimulated reconstructions. These parameters were then applied to basal images that were coregistered to their respective CP-stimulated brain image. To remove artifactual binding values, such as negative numbers that result from inadequate overlap of basal and CP-stimulated images, these values were set to zero. These occurred most frequently along the contour of sections, where artifacts related to slice preparation were predominately found. Setting negative voxel values to zero thus allows the SPM program to ignore these data points and view them as background, which by default has a voxel value of zero.

To quantitate CB_1 receptor density, [^{3}H]CP55,940 (3 nM) was incubated with brain sections, in the presence (non-specific binding) or absence (total binding) of 10 μM CP55,940. Images of total binding values (specific + non-specific) were used to reconstruct images derived from [^{3}H]CP55,940 binding autoradiography. This was done because non-specific activity was low, therefore reconstructions derived from non-specific binding sections would be suboptimal given the extremely low contrast and poor structural information following image quantitation (Fig. 3.5B). Average non-specific activity ranged from 0.49% to 3.6% of total binding across all sampled brain regions of interest (see next section). This would present a technical challenge for creating image reconstructions derived from specific binding values. Reconstructions of total [^{3}H]CP55,940 binding used similar approaches as in agonist-stimulated [^{35}S]GTPγS binding images (outlined in Chapter 2).

A

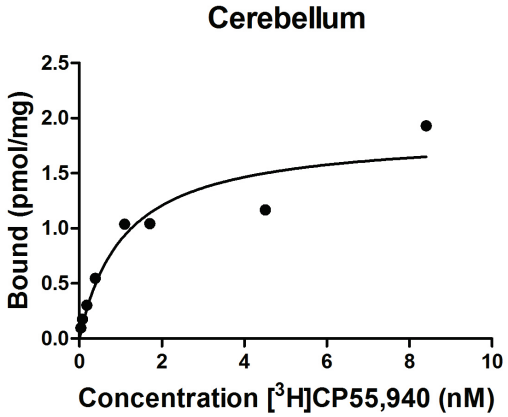

K_D (nM)	B_{max} (pmol/mg)
1.084	1.862

B

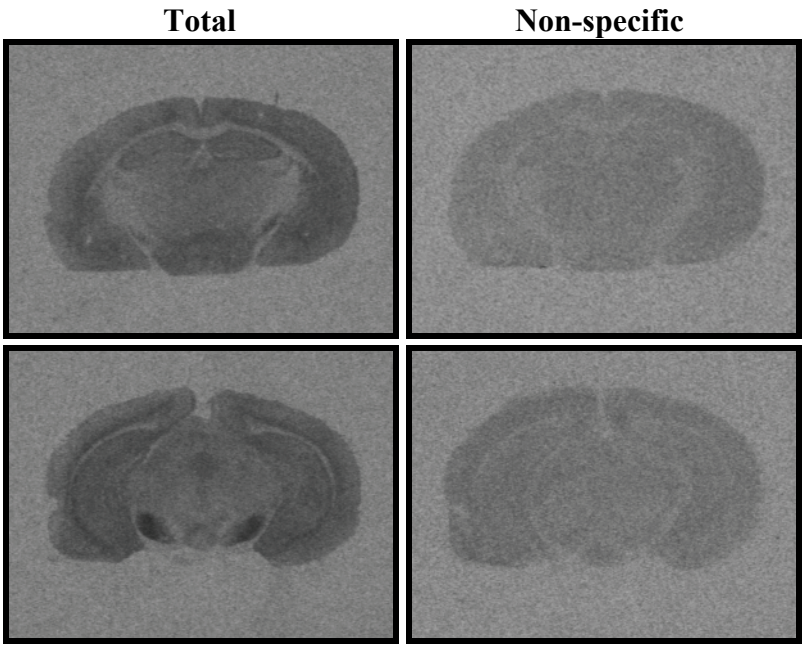

Figure 3.5. (A) CB_1 receptor B_{max} and K_D values were determined in mouse cerebellum with [^{3}H]CP55,940 using a one site hyperbola function in Prism. (B) [^{3}H]CP55,940 autoradiographic images are shown for total (left column) and non-specific (right column) binding. *[^{3}H]CP55,940 autoradiography and receptor-binding were conducted as described in Methods, Section III.*

3.5 β-arrestin 2 regulates CB_1 receptor desensitization in a region-specific manner

Previous studies from our laboratory demonstrated that CB_1 receptors undergo desensitization following chronic THC administration, with regional differences in the magnitude of reduction in CB_1 receptor-mediated G-protein activation (McKinney et al., 2008; Sim-Selley and Martin, 2002; Sim et al., 1996a). Based on *in vivo* results from this study and agonist-stimulated [^{35}S]GTPγS binding results in spinal cord, one would postulate that βarr2 could produce region-specific regulation of CB_1 receptor desensitization in the CNS. To answer this question, CB_1 receptor-mediated G-protein activity was assessed in the reconstructed mouse brain using SPM with subsequent region of interest (ROI) analyses in brains from vehicle- and THC-treated βarr2 WT and KO mice.

Under basal conditions with no agonist, there were no observed differences by genotype or drug treatment in all sampled brain areas in regards to basal [^{35}S]GTPγS binding (Fig. 3.6). Within vehicle control groups, significant differences between genotypes in CP-stimulated [^{35}S]GTPγS binding were found in certain sampled brain regions. The biggest difference was found in the piriform cortex where greater CB_1 receptor-mediated G-protein activity was found in the βarr2 KO animals (380 ± 18 nCi/g) versus WT animals (225 ± 32 nCi/g) (Fig. 3.7). In the auditory/visual (A/V) cortex, significantly greater CB_1 receptor-mediated G-protein activity was also found in the βarr2 KO animals (249 ± 26 nCi/g) versus WT animals (188 ± 20 nCi/g). Interestingly, intra-regional differences in the vehicle treated groups were found in the hippocampus, where significant differences in CB_1 receptor-mediated G-protein activity were only noted in the caudal extent. In the caudal sub-region of the hippocampus, CP-stimulated [^{35}S]GTPγS binding was 362 ± 27 nCi/g in βarr2 KO animals versus 279 ± 31 nCi/g in the WT

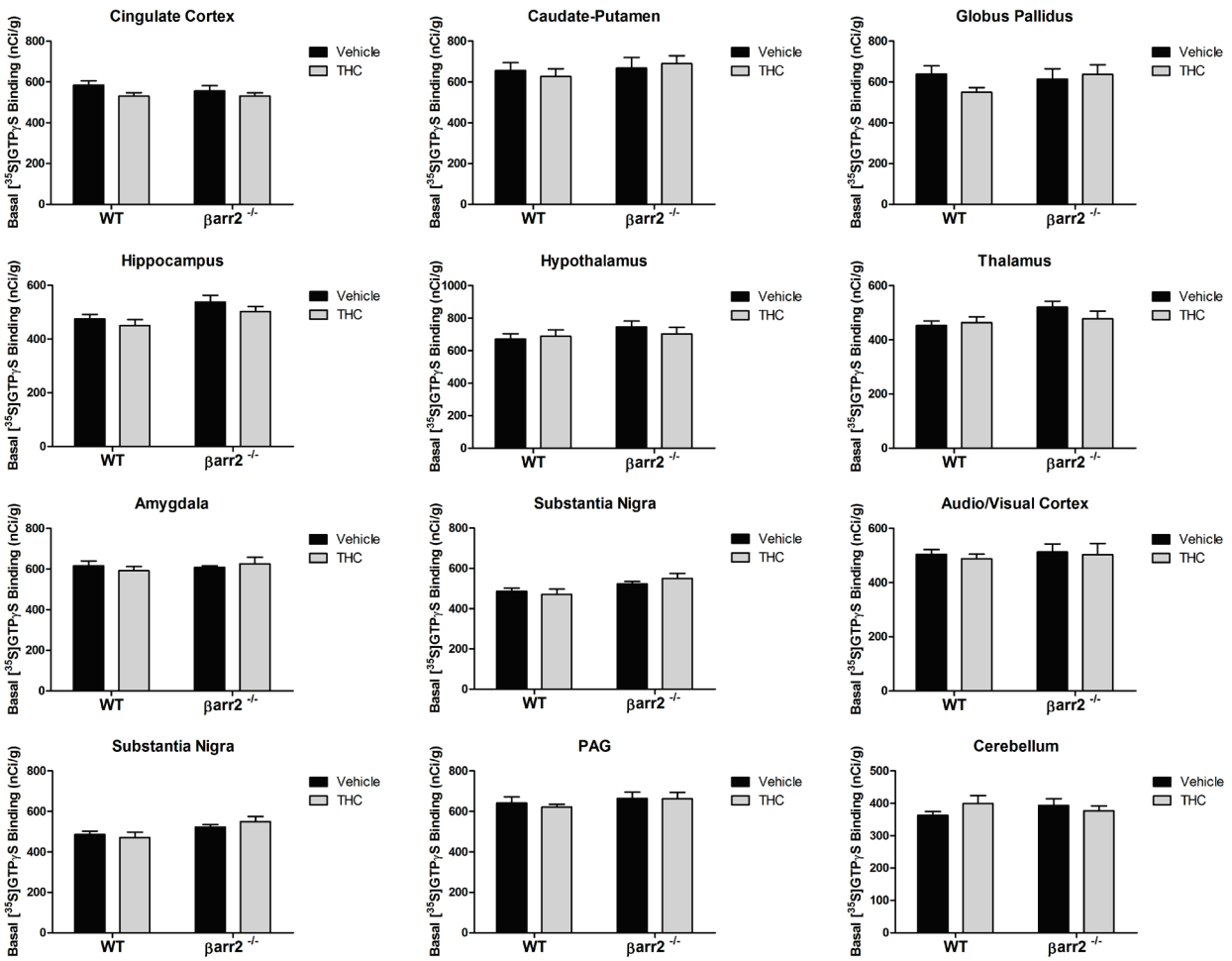

Figure 3.6. Basal [^{35}S]GTPγS binding values in βArr2 KO and WT animals following chronic administration of THC or vehicle. No differences in basal [^{35}S]GTPγS binding were found by either genotype or drug treatment in various brain regions as determined by 2-way ANOVA. Binding values represent the mean ± SEM in various sampled brain regions from βarr2 WT and KO mice following 6.5 day chronic administration of either vehicle or 10 mg/kg THC (N = 8 per group) twice daily.

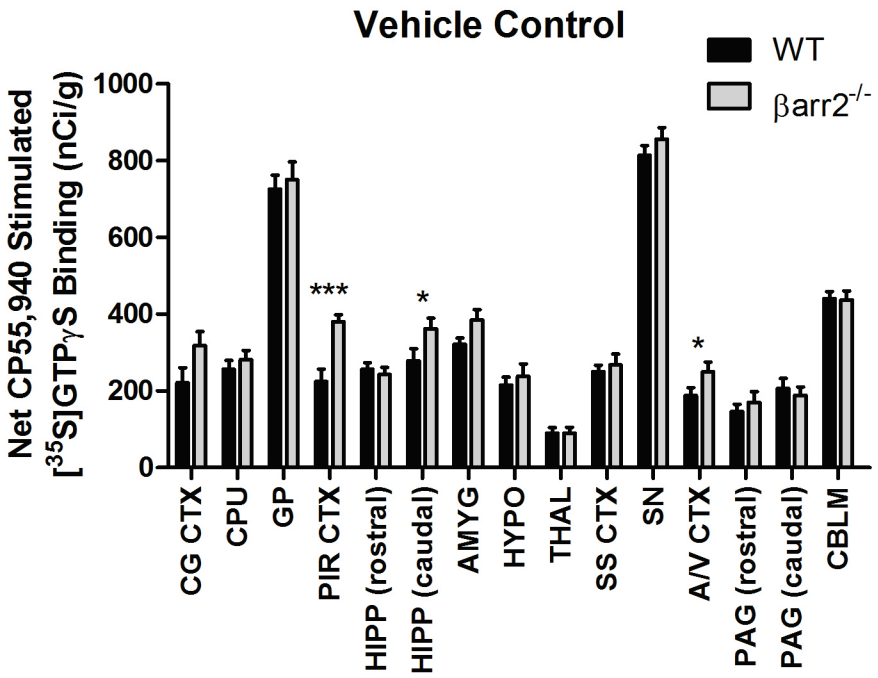

Figure 3.7. Net (agonist - basal) CP55,940-stimulated [^{35}S]GTPγS binding values (mean ± SEM) in sampled brain regions from βarr2 WT and KO mice following 6.5 day treatment with vehicle twice daily (N = 8 per group). *** $p < 0.001$, * $p < 0.05$; Two way ANOVA, Student-Newman Keuls Post-hoc. CG CTX, cingulate cortex; CPU, caudate-putamen; GP, globus pallidus; PIR CTX, piriform cortex; HIPP, hippocampus; AMYG, amygdala; HYPO, hypothalamus; THAL, thalamus; SS CTX, somatosensory cortex; SN, substantia nigra; A/V CTX, auditory/visual cortex; PAG, periaqueductal gray; *CBLM*, cerebellum

animals. Similar non-significant trends of greater CB_1 receptor-mediated G-protein activity were also noted in the cingulate cortex ($p = 0.051$), somatosensory cortex ($p = 0.078$), and amygdala ($p = 0.058$) of βarr2 KO animals versus WT (Fig. 3.7). Overall, these results showed regionally restricted differences in agonist-stimulated [^{35}S]GTPγS binding between genotypes that were generally small in magnitude.

SPM with subsequent ROI analyses was then applied to assess agonist-stimulated [^{35}S]GTPγS binding in vehicle- and THC-treated βarr2 WT and KO mice to compare the regional profile and magnitude of desensitization between genotypes. Comparing volumetric reconstructions derived from the image average of all subjects within each group, visual decreases in CB_1 receptor-stimulated [^{35}S]GTPγS binding can be appreciated in brain areas including the hippocampus, amygdala, and rostral periaqueductal gray (PAG), within both βarr2 WT and KO animals following THC treatment (Fig. 3.8-3.9). Overall, SPM analysis revealed region-specific receptor desensitization in CB_1 receptor-mediated G-protein activity (Fig. 3.10) with a similar regional relationship in magnitude of desens as previously reported: hippocampus > cerebellum > striatum/basal ganglia (McKinney et al., 2008; Sim et al., 1996a). Also, the distribution of receptor desensitization coincided with regions known to contain CB_1 receptors (Herkenham et al., 1991), as well as the anatomical distribution of CB_1 receptor activity (Chapter 2).

A subset of regions showed a similar response as seen in spinal cord and were consistent with the prediction that βarr2 regulates CB_1 receptor desensitization. The clearest example of this was in the cerebellum. SPM detected moderate desensitization in WT animals (Fig. 3.10), where

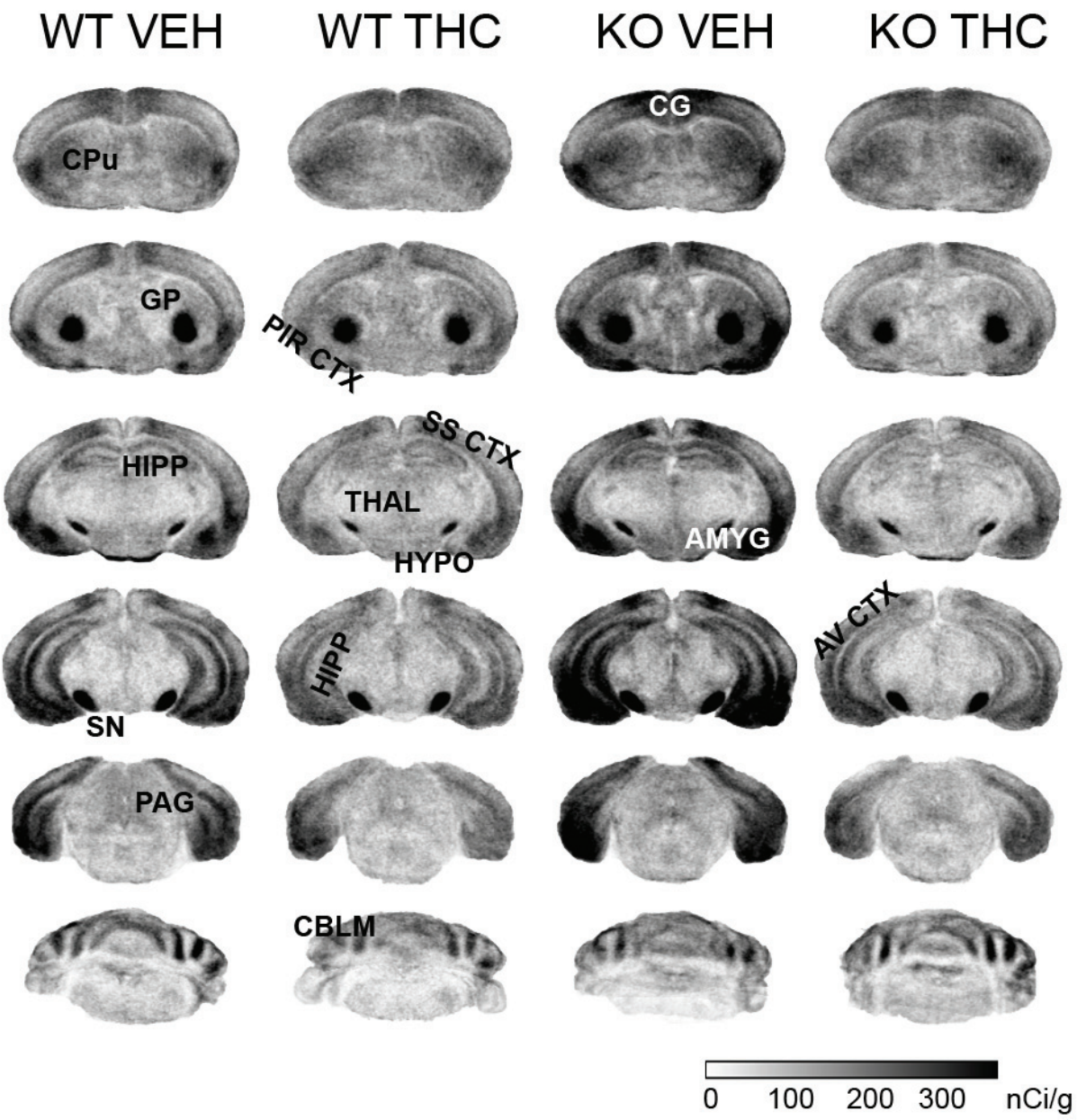

Figure 3.8. Net cannabinoid-stimulated [^{35}S]GTPγS binding reconstructions derived from the image average of all subjects within each group (N = 8). βarr2 WT and KO mice were treated for 6.5 day administration of either vehicle or 10 mg/kg THC twice daily. Original autoradiographic images are shown in grayscale and correspond to the scale (bottom right). *CG CTX*, cingulate cortex; *CPU*, caudate-putamen; *GP*, globus pallidus; *PIR CTX*, piriform cortex; *HIPP*, hippocampus; *AMYG*, amygdala; *HYPO*, hypothalamus; *THAL*, thalamus; *SS CTX*, somatosensory cortex; *SN*, substantia nigra; *A/V CTX*, auditory/visual cortex; *PAG*, periaqueductal gray; *CBLM*, cerebellum.

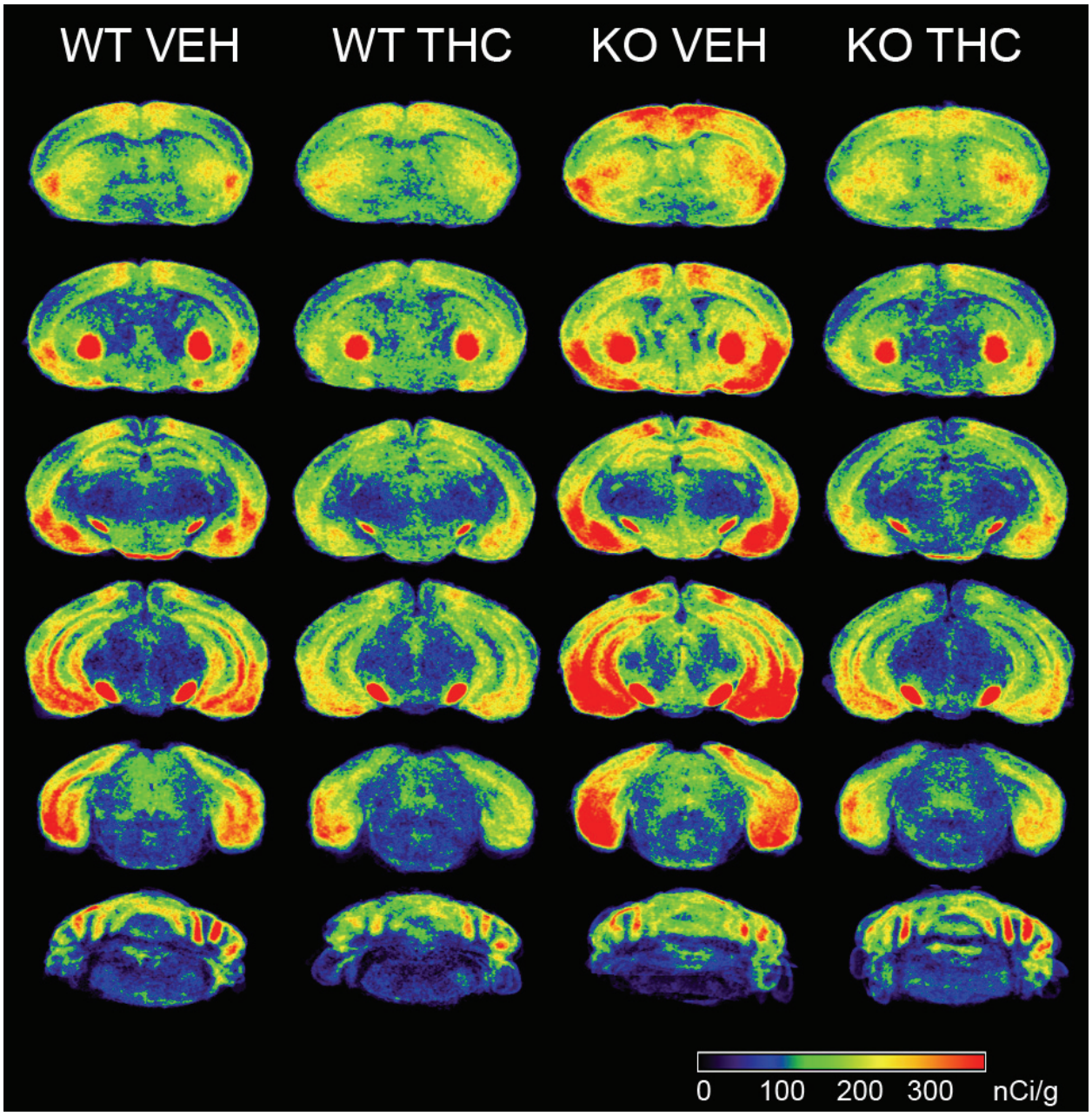

Figure 3.9. Net cannabinoid-stimulated [^{35}S]GTPγS binding reconstructions derived from the image average of all subjects within each group (N = 8). βarr2 WT and KO mice were treated for 6.5 day administration of either vehicle or 10 mg/kg THC twice daily. Images are shown in pseudocolor and correspond to the color scale (bottom right). Anatomical reference labels are shown in Fig. 3.8.

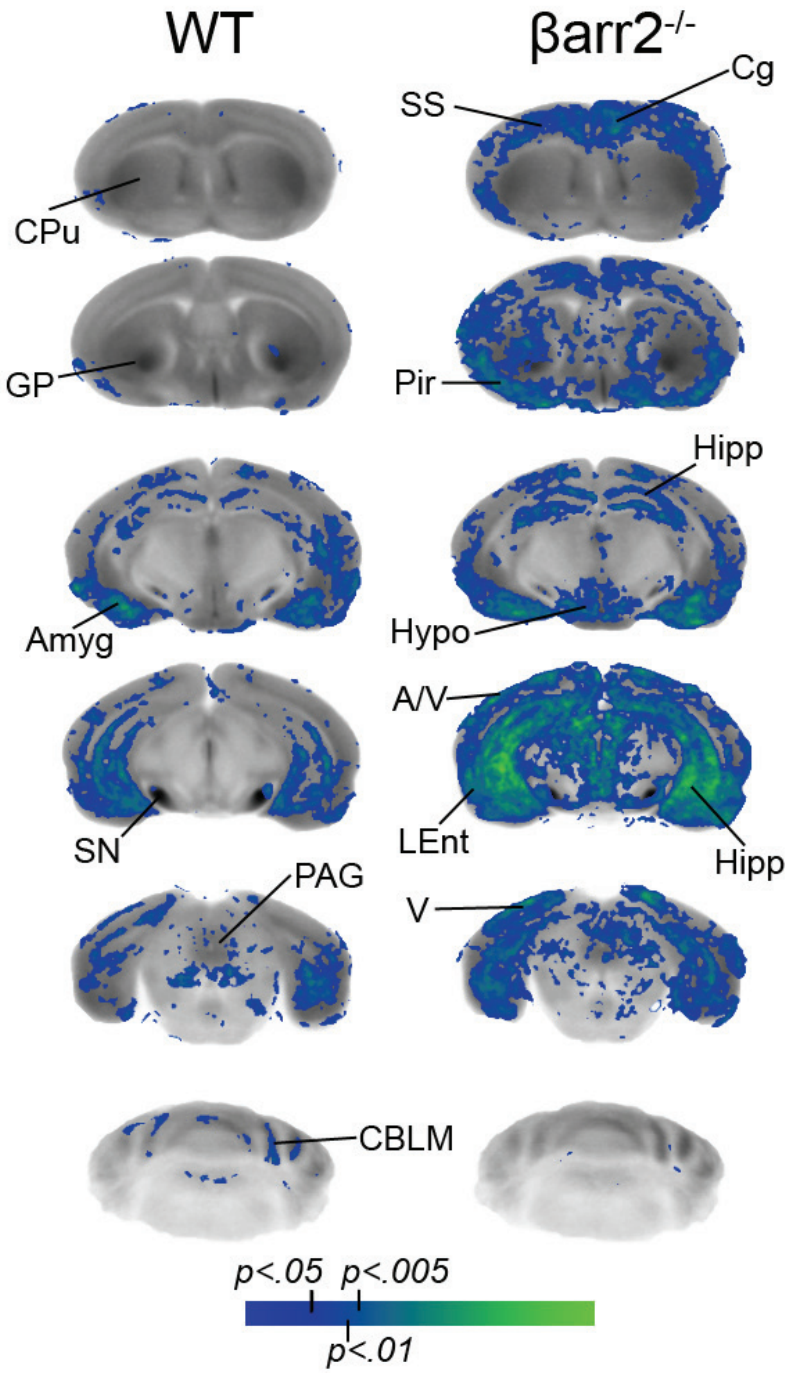

Figure 3.10. SPM analysis revealed both region- and genotypic-specific differences in desensitization of CB_1 receptor-mediated G-protein activation in the reconstructed mouse brain of βarr2 WT and KO mice following 6.5 day chronic administration of either vehicle or 10 mg/kg THC (N = 8 per group) twice daily. Brain regions within each genotype demonstrating significant desensitization ($p < 0.05$, 2-way ANOVA, N = 8) are colored in blue/green and correspond to the significance scale (bottom). *AMYG*, amygdala; *A/V CTX*, auditory/visual cortex; *CBLM*, cerebellum; *CG*, cingulate cortex; *CPU*, caudate-putamen; *GP*, globus pallidus; *HIPP*, hippocampus; *HYPO*, hypothalamus; *PAG*, periaqueductal gray; *PIR*, piriform cortex; *SN*, substantia nigra; *SS*, somatosensory cortex; *THAL*, thalamus; *V,* visual cortex;.

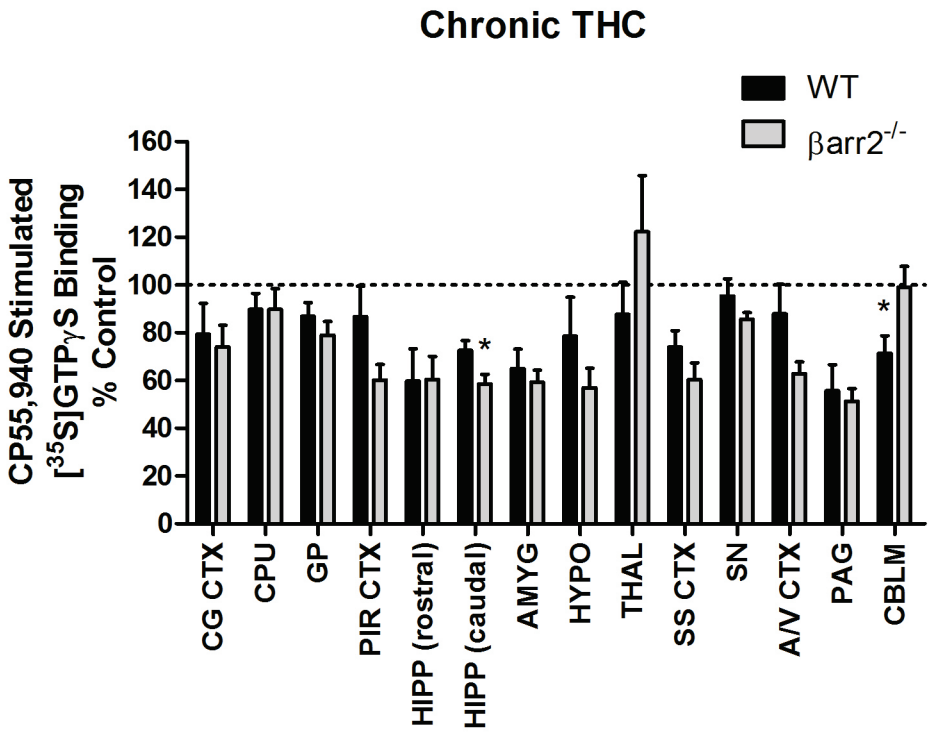

Figure 3.11. Region- and genotypic-specific differences were found in the magnitude of CB_1 receptor desensitization following chronic 6.5 day THC treatment twice daily in both βarr2 WT and KO mice (N = 8 per group). CP55,940-stimulated [^{35}S]GTPγS binding values are shown normalized to vehicle and represent the mean ± SEM (N = 8). * $p < 0.05$, Student's two-sample *t*-test. *CG CTX*, cingulate cortex; *CPU*, caudate-putamen; *GP*, globus pallidus; *PIR CTX*, piriform cortex; *HIPP*, hippocampus; *AMYG*, amygdala; *HYPO*, hypothalamus; *THAL*, thalamus; *SS CTX*, somatosensory cortex; *SN*, substantia nigra; *A/V CTX*, auditory/visual cortex; *PAG*, periaqueductal gray; *CBLM*, cerebellum.

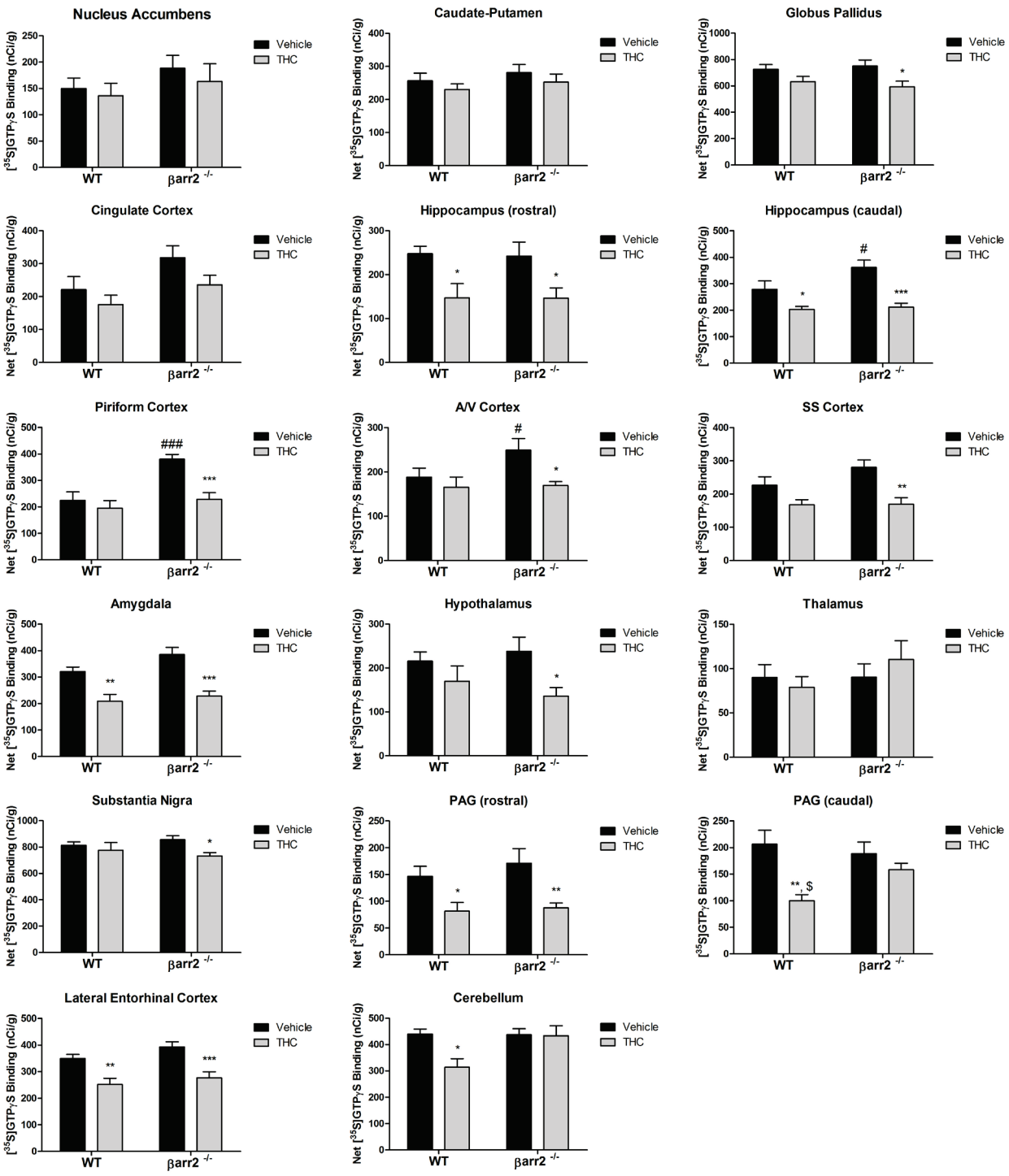

Figure 3.12. Net CP55,940-stimulated [35S]GTPγS binding values (mean ± SEM) in sampled brain regions (N = 8 per group) of βarr2 WT and KO mice following 6.5 day chronic administration of either vehicle or 10 mg/kg THC twice daily. *** $p < 0.001$, ** $p < 0.01$, * $p < 0.05$ versus respective vehicle; ### $p < 0.001$, # $p < 0.05$ versus WT vehicle; $ versus KO THC (Two way ANOVA, Student-Newman Keuls Post-hoc). A/V, auditory/visual; SS, somatosensory

Table 3.2
Net CP55,940-stimulated [^{35}S]GTPγS binding values in brain tissue sections from βarr2 WT and KO mice following 6.5 day chronic administration of either vehicle or 10 mg/kg THC (N = 8 per group) twice daily

Brain sections were incubated with 0.04 nM [^{35}S]GTPγS, 3 μM CP55,940, and 2 mM GDP as described under *III. Methods*. [^{35}S]GTPγS binding values represent the mean ± SEM.). *** $p < 0.001$, ** $p < 0.01$, * $p < 0.05$ versus respective vehicle; ### $p < 0.001$, # $p < 0.05$ versus WT vehicle; $ versus KO THC (N = 8 per group, two way ANOVA, Student-Newman Keuls Post-hoc)

	Vehicle		THC	
Region	**WT**	**βarr2$^{-/-}$**	**WT**	**βarr2$^{-/-}$**
NAc	150 ± 20	189 ± 24	136 ± 24	163 ± 33
CPu	256 ± 23	282 ± 24	230 ± 17	252 ± 25
GP	726 ± 36	751 ± 47	631 ± 41	593 ± 43*
CG CTX	221 ± 39	318 ± 36	176 ± 29	235 ± 29
HIPP (rostral)	248 ± 17	242 ± 32	147 ± 32*	146 ± 23*
HIPP (caudal)	279 ± 31	362 ± 27$^{\#}$	203 ± 12*	212 ± 14***
PIR CTX	225 ± 32	380 ± 18$^{\#\#\#}$	195 ± 29	229 ± 25***
A/V CTX	188 ± 21	249 ± 26	165 ± 23$^{\#}$	169 ± 9*
SS CTX	226 ± 25	281 ± 22	168 ± 15	169 ± 20**
AMYG	321 ± 17	385 ± 27	209 ± 26**	228 ± 19***
HYPO	216 ± 21	238 ± 32	169 ± 35	136 ± 20*
THAL	90 ± 15	90 ± 15	79 ± 12	110 ± 21
SN	814 ± 26	856 ± 30	776 ± 58	733 ± 24*
PAG (rostral)	146 ± 19	171 ± 28	81 ± 16*	88 ± 9**
PAG (caudal)	207 ± 26	189 ± 22	100 ± 12$^{**,\$}$	158 ± 12
LEnt CTX	350 ± 16	393 ± 19	252 ± 23**	277 ± 23***
CBLM	440 ± 19	437 ± 23	314 ± 32*	434 ± 38

ROI analysis showed that CB_1 receptor-mediated G-protein activity in THC-treated WT mice was 71 ± 7% of vehicle levels. In contrast, CB_1 receptor desensitization was nearly abolished in βarr2 KO mice following chronic treatment with THC, and CB_1 receptor-mediated G-protein activity was comparable in βarr2 KO and WT mice. A significant interaction of Drug treatment X Genotype was also found [$F(1,28) = 4.51$, $p < 0.05$], suggesting that βarr2 is involved in mediating CB_1 receptor desensitization within the cerebellum following this treatment paradigm. Interestingly, intra-regional differences in the magnitude of CB_1 receptor desensitization were revealed by SPM analysis, which underscores an advantage of using a whole-brain approach to assess the regulatory role of βarr2 in mediating CB_1 receptor desensitization in highly different neuroanatomical systems and brain regions. In these regions, βarr2 attenuated desensitization in certain aspects of the nucleus, whereas desensitization was similar between genotypes in other subregions. For example, initial ROI examination of the caudal sub-region of the PAG showed that chronic THC lead to a greater reduction in CB_1 receptor-mediated activity in the WT animals (48 ± 5% of respective vehicle) versus βarr2 KO animals (84 ± 6% of respective vehicle) (Fig. 3.8). However, in more rostral portions of the PAG, SPM analysis revealed significant desensitization within the βarr2 KO animals (51 ± 5% of respective vehicle). Subsequent ROI analysis substantiated these findings, demonstrating significant desensitization within both βarr2 WT and KO mice (Fig. 3.12, Table 3.2).

Other regions showed no difference between βarr2 KO and WT mice either because both genotypes exhibited desensitization (i.e. amygdala) or neither genotype exhibited desensitization (i.e. striatum). Consistent with previous reports using similar dosing paradigms (McKinney et al., 2008; Sim-Selley and Martin, 2002; Sim et al., 1996a), there were no differences in CB_1 receptor-mediated G-protein activity in the caudate-putamen and nucleus accumbens within

either genotype, as determined by both SPM and ROI analyses. Interestingly, different results were found in the striatal/basal ganglia output nuclei, as discussed below. In the thalamus, a brain area with relatively sparse concentrations of CB_1 receptors (Herkenham et al., 1991), there were also no differences in CP-stimulated [^{35}S]GTPγS binding following THC treatment in either genotype. Similar magnitudes of desensitization were found in the amygdala region within both genotypes, where there was slightly greater desensitization in βarr2 KO (59 ± 5% of respective control) versus WT animals (65 ± 8% of respective control). Among all sampled cortical regions in this study, including cingulate, somatosensory, piriform, and auditory/visual cortex, CB_1 receptor G-protein activity in the WT mice was apparently reduced following THC treatment, ranging between 74-87%, but did not differ from vehicle-treated mice. Significant desensitization however was found in the lateral entorhinal cortex within WT THC-treated animals. Interestingly, there was a trend towards greater desensitization in the βarr2 KO mice, particularly in the piriform (60 ± 6% of vehicle) and auditory/visual cortex (68 ± 3% of vehicle), as demonstrated by SPM analysis and subsequently confirmed by an independent ROI analysis (Fig. 3.10, Fig. 3.11). This appeared to result from the slightly higher, but insignificant difference from WT level of CP-stimulated [^{35}S]GTPγS binding in vehicle-treated βarr2 KO mice. As noted above, the piriform cortex was also a brain region where CP-stimulated [^{35}S]GTPγS binding in the vehicle treated groups was greater in the βarr2 KO versus WT mice (Fig. 3.7).

Unexpectedly, SPM analysis identified enhanced desensitization in certain regions of βarr2 KO mice. SPM showed significant desensitization of CB_1 receptor-mediated G-protein activation in the hypothalamus of βarr2 KO animals (57 ± 8% of vehicle), but not in WT mice (79 ± 16% of vehicle) This was subsequently confirmed by ROI analysis, which showed no

difference in CP-stimulated [^{35}S]GTPγS binding between vehicle- and THC-treated WT animals. The basal ganglia output nuclei, including the substantia nigra and globus pallidus, contain the highest concentrations of CB_1 receptors (Herkenham et al., 1991) and are relatively insensitive to changes in CB_1 receptor activity following THC treatment. Although WT animals exhibited no changes in CB_1 receptor-mediated G-protein activity after THC treatment, βarr2 KO animals interestingly displayed a significant reduction in the substantia nigra (85 ± 3% of respective vehicle) and a trend in the globus pallidus (79 ± 6%, p = 0.053). Subregional differences in desensitization were also found in the hipocampus. In this region, desensitization was more robust in the caudal extent of βarr2 KO mice (Fig. 3.10). This was confirmed by a subsequent ROI analysis, which showed significantly greater desensitization in the caudal aspects of the hippocampus in βarr2 KO mice (58.6 ± 4% of vehicle), compared to WT mice (72.6 ± 4% of vehicle). Significant reductions in CP-stimulated [^{35}S]GTPγS binding were also found in the rostral hippocampus of βarr2 KO and WT animals, where both exhibited about a 40% reduction following chronic THC treatment.

Increases in the apparent efficacy of CP-stimulated [^{35}S]GTPγS binding in various brain regions in βarr2 KO mice appeared to be associated with the enhancement or unmasking of CB_1 receptor desensitization in the these same brain regions following chronic administration of THC. Interestingly, the relative magnitude of desensitization of βarr2 KO when normalized to WT animals was positively correlated with the relative efficacy of CP-stimulated [^{35}S]GTPγS binding in βarr2 KO mice when normalized to WT animals (p = 0.0101, R^2 = 0.5; Fig. 3.13). For example, a 1.5 fold increase in the relative efficacy of CP-stimulated [^{35}S]GTPγS binding in βarr2 KO mice was equal to about a 2 fold increase in the relative magnitude of desensitization in βarr2 KO mice. This suggests that increases in the apparent efficacy of cannabinoid agonists

in βarr2 KO mice may enhance other regulatory pathways thus producing greater CB_1 receptor desensitization.

Together, these results suggest a regional-specificity in the regulation of CB_1 receptors by βarr2 at the level of G-protein coupling. However, it is unclear whether βarr2 may regulate other mechanisms of CB_1 receptor adaptation, such as receptor downregulation or degradation of proteins.

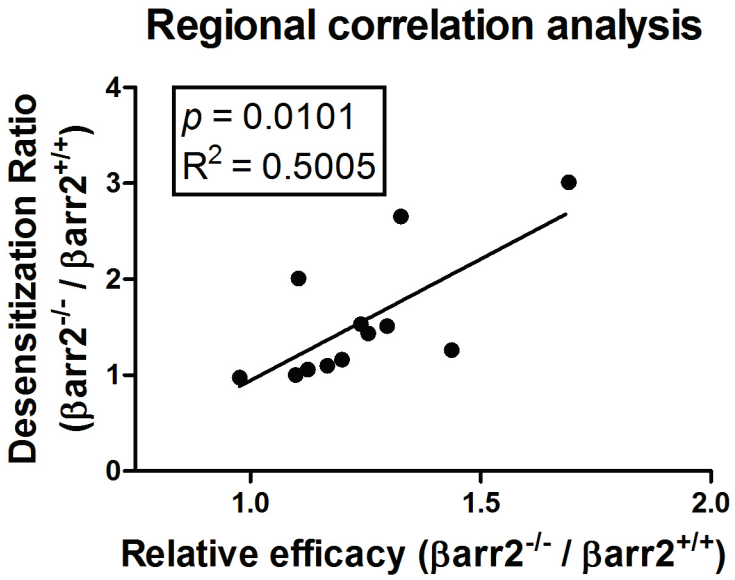

Brain Region	Desensitization Ratio	Relative efficacy
Cingulate cortex	1.44 ± 0.16	1.26 ± 0.44
Somatosensory cortex	1.24 ± 0.10	1.53 ± 0.27
Auditory-Visual cortex	1.33 ± 0.14	2.65 ± 0.30
Piriform cortex	1.69 ± 0.08	3.01 ± 0.49
Lateral Enthorhinal cortex	1.12 ± 0.05	1.06 ± 0.21
Amygdala	1.20 ± 0.08	1.16 ± 0.14
Hippocampus (rostral)	0.98 ± 0.13	0.97 ± 0.24
Hippocampus (caudal)	1.30 ± 0.10	1.51 ± 0.14
Periaqueductal gray (rostral)	1.17 ± 0.19	1.10 ± 0.12
Caudate Putamen	1.10 ± 0.09	1.00 ± 0.85
Hypothalamus	1.10 ± 0.15	2.01 ± 0.38
Nucleus Accumbens	1.26 ± 0.16	1.44 ± 1.91

Figure 3.13. Relative efficacy of CP-stimulated [^{35}S]GTPγS binding is positively correlated with the relative magnitude of CB_1 receptor desensitization in βarr2 KO mice following chronic THC administration (top graph). βArr2 KO and WT animals received 6.5 day administration of 10 mg/kg THC or vehicle treatment (i.p.) given twice daily. Each point in the graph represents a brain area (listed in the table above) corresponding to its mean Desensitization Ratio and mean Relative efficacy. The Desensitization Ratio was calculated by normalizing the magnitudes of desensitization in βarr2 KO mice to the mean magnitude of desensitization in βarr2 WT mice. The Relative efficacy was calculated by normalizing the magnitudes of CP-stimulated [^{35}S]GTPγS binding in vehicle treated βarr2 KO mice by the mean magnitude of CP-stimulated [^{35}S]GTPγS binding in vehicle treated βarr2 WT mice. Calculated ratios in the table represent the mean ± SEM (N = 8). Linear regression analysis was performed in Graphpad Prism 5.

3.6 β-arrestin 2 is involved in CB_1 receptor downregulation in the cerebellum

βarr2 targeting of GPCRs towards internalization and subsequent degradation represents another mechanism by which GPCRs respond to persistent stimulation by agonists. To investigate whether there were changes in CB_1 receptor levels within the brain following THC treatment, SPM and ROI analyses of [^{3}H]CP55,940 binding were performed. Results in sampled brain regions showed that [^{3}H]CP55,940 binding did not differ between genotypes in vehicle-treated mice (Fig. 3.14). Comparing volumetric reconstructions derived from the image average of all subjects within each group, visual decreases in [^{3}H]CP55,940 binding can be seen in the cortex, hippocampus, and PAG (Figs. 3.15-3.16). Again, striatal regions including the caudate-putamen and basal ganglia output nuclei (globus pallidus, substantia nigra), demonstrated minimal changes in [^{3}H]CP55,940 binding.

In the cerebellum, CB_1 receptors were significantly downregulated (55 ± 10% of vehicle) and this response was virtually abolished in βarr2 KO mice. In addition, a significant interaction of Drug treatment X Genotype was found in the cerebellum [$F(1,28) = 4.277$, $p < 0.05$], suggesting that βarr2 is involved in mediating CB_1 receptor downregulation in this particular brain area (Fig 3.18, Table 3.3).

In general, there were no significant differences in CB_1 receptor levels according to SPM analysis (data not shown) and in all sampled brain regions using ROI, within βarr2 KO mice following chronic THC treatment. Within WT mice, only an insignificant trend towards decreased receptor levels were found following THC treatment in the hypothalamus (71 ± 20% of respective vehicle), hippocampus (75 ± 17% of respective vehicle), and PAG (68 ± 15% of respective vehicle) (Fig. 3.17). Collectively, these results suggest that βarr2 may be involved in mediating receptor downregulation in the cerebellum.

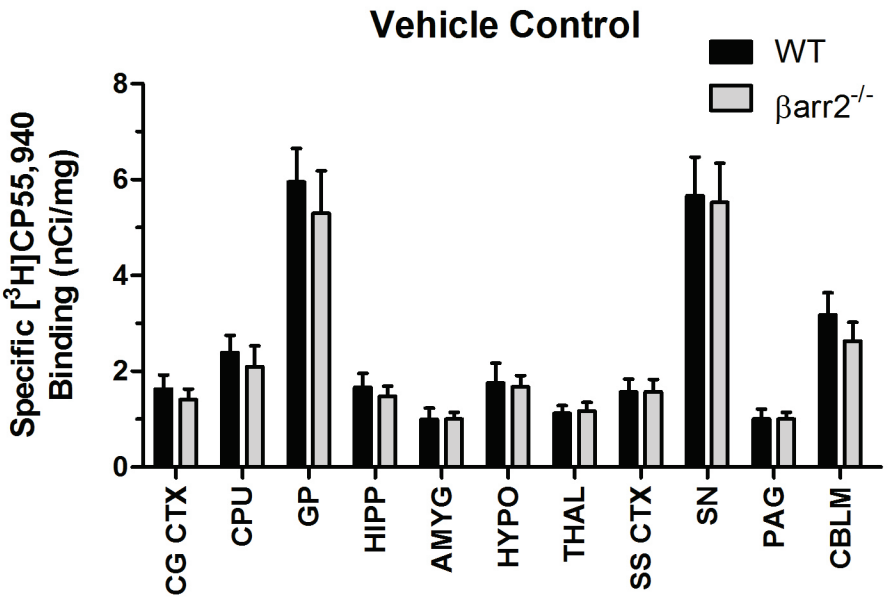

Figure 3.14. [^{3}H]CP55,940 binding values (mean ± SEM) in sampled brain regions from βarr2 WT and KO mice following 6.5 day chronic administration of either vehicle or 10 mg/kg THC twice daily (N = 8 per group). *CG CTX*, cingulate cortex; *CPU*, caudate-putamen; *GP*, globus pallidus; *HIPP*, hippocampus; *AMYG*, amygdala; *HYPO*, hypothalamus; *THAL*, thalamus; *SS CTX*, somatosensory cortex; *SN*, substantia nigra; *PAG*, periaqueductal gray; *CBLM*, cerebellum. [^{3}H]CP55,940 autoradiography was performed as described in *Methods*

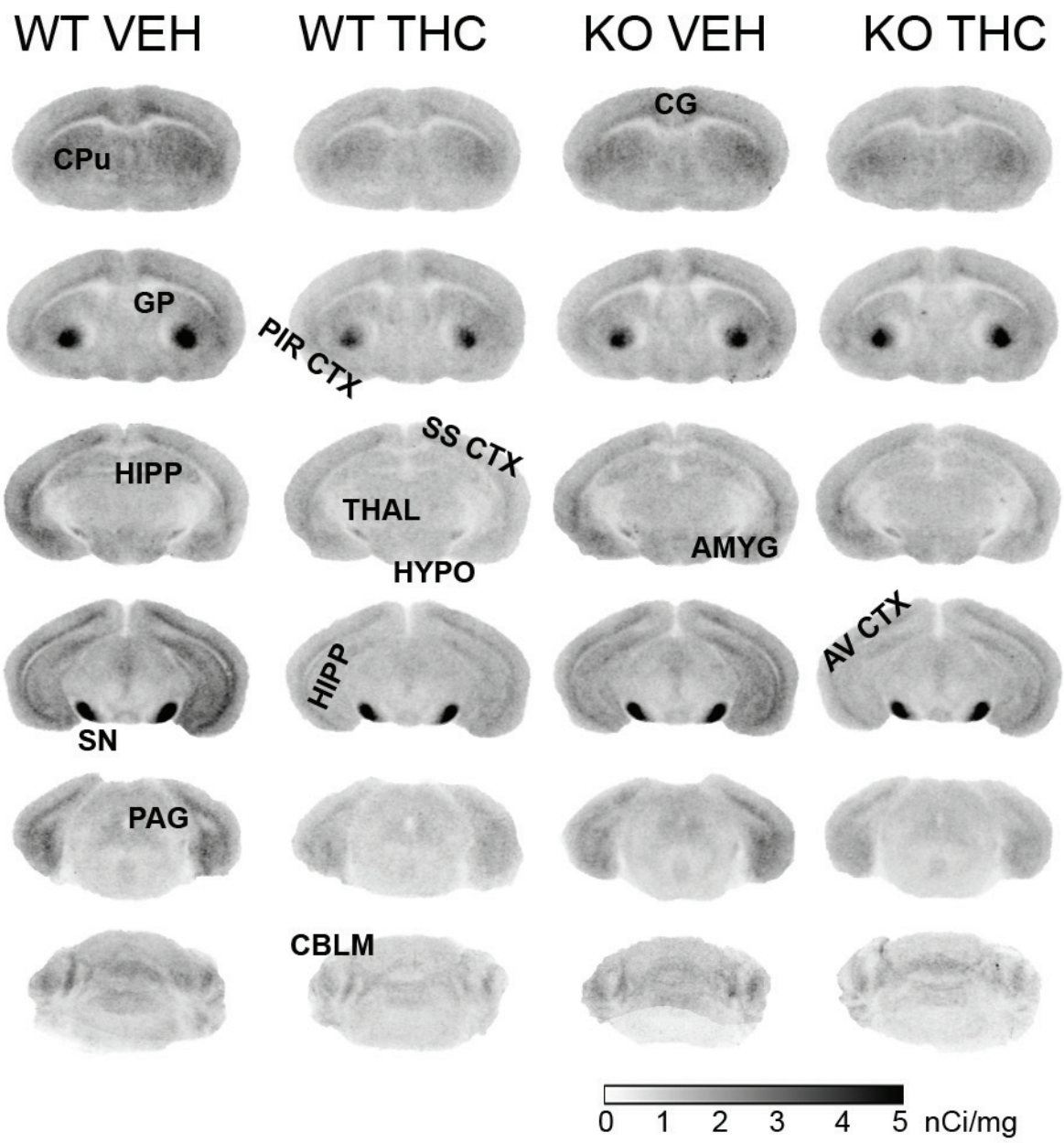

Figure 3.15. [^{3}H]CP55,940 receptor binding reconstructions derived from the image average of all subjects within each group (N = 8 per group). βarr2 WT and KO mice were treated 6.5 day with either vehicle or 10 mg/kg THC twice daily. Original autoradiographic images are shown in grayscale and correspond to the scale of binding values (bottom right). *CG CTX*, cingulate cortex; *CPU*, caudate-putamen; *GP*, globus pallidus; *PIR CTX*, piriform cortex; *HIPP*, hippocampus; *AMYG*, amygdala; *HYPO*, hypothalamus; *THAL*, thalamus; *SS CTX*, somatosensory cortex; *SN*, substantia nigra; *A/V CTX*, auditory/visual cortex; *PAG*, periaqueductal gray; *CBLM*, cerebellum. [^{3}H]CP55,940 autoradiography was performed as described in *Methods*

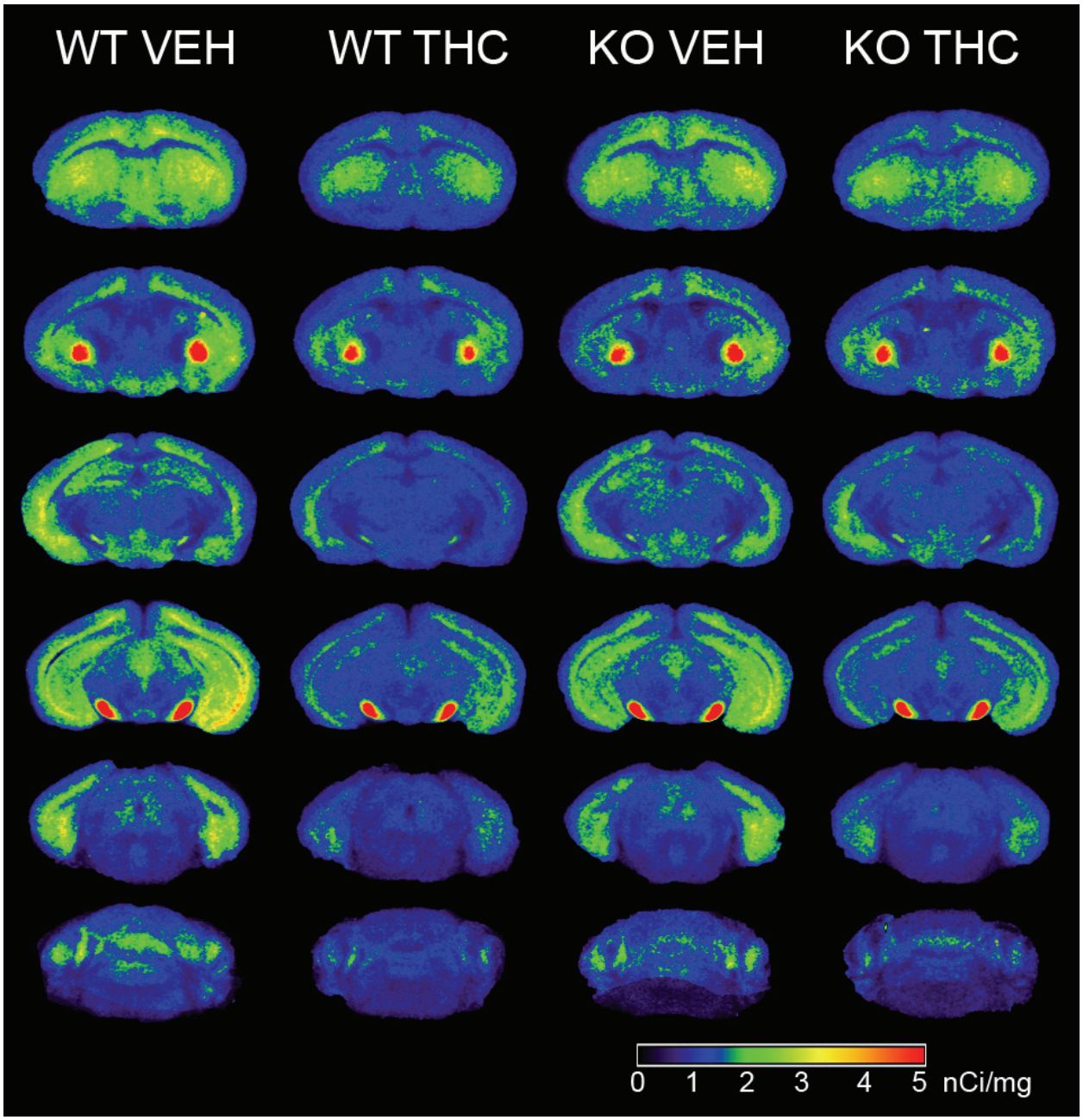

Figure 3.16. [^{3}H]CP55,940 receptor binding reconstructions derived from the image average of all subjects within each group (N = 8 per group). βarr2 WT and KO mice were treated 6.5 day with either vehicle or 10 mg/kg THC twice daily. Images are shown in pseudocolor and correspond to the color scale of binding values (bottom right). Anatomical reference labels are shown in Fig. 3.15. [^{3}H]CP55,940 autoradiography was performed as described in *Methods*

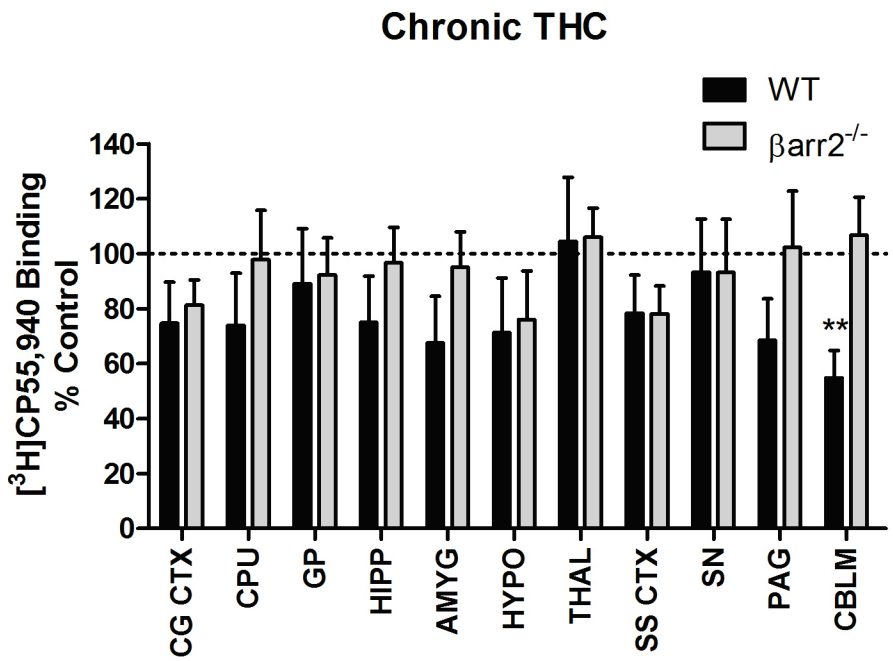

Figure 3.17. [^{3}H]CP55,940 binding values normalized to vehicle (mean ± SEM) in sampled brain regions from βarr2 WT and KO mice following 6.5 day chronic administration of either vehicle or 10 mg/kg THC twice daily (N = 8 per group). ** $p < 0.05$, Student's two-sample *t*-test. *CG CTX*, cingulate cortex; *CPU*, caudate-putamen; *GP*, globus pallidus; *PIR CTX*, piriform cortex; *HIPP*, hippocampus; *AMYG*, amygdala; *HYPO*, hypothalamus; *THAL*, thalamus; *SS CTX*, somatosensory cortex; *SN*, substantia nigra; *PAG*, periaqueductal gray; *CBLM*, cerebellum. [^{3}H]CP55,940 autoradiography was performed as described in *Methods*

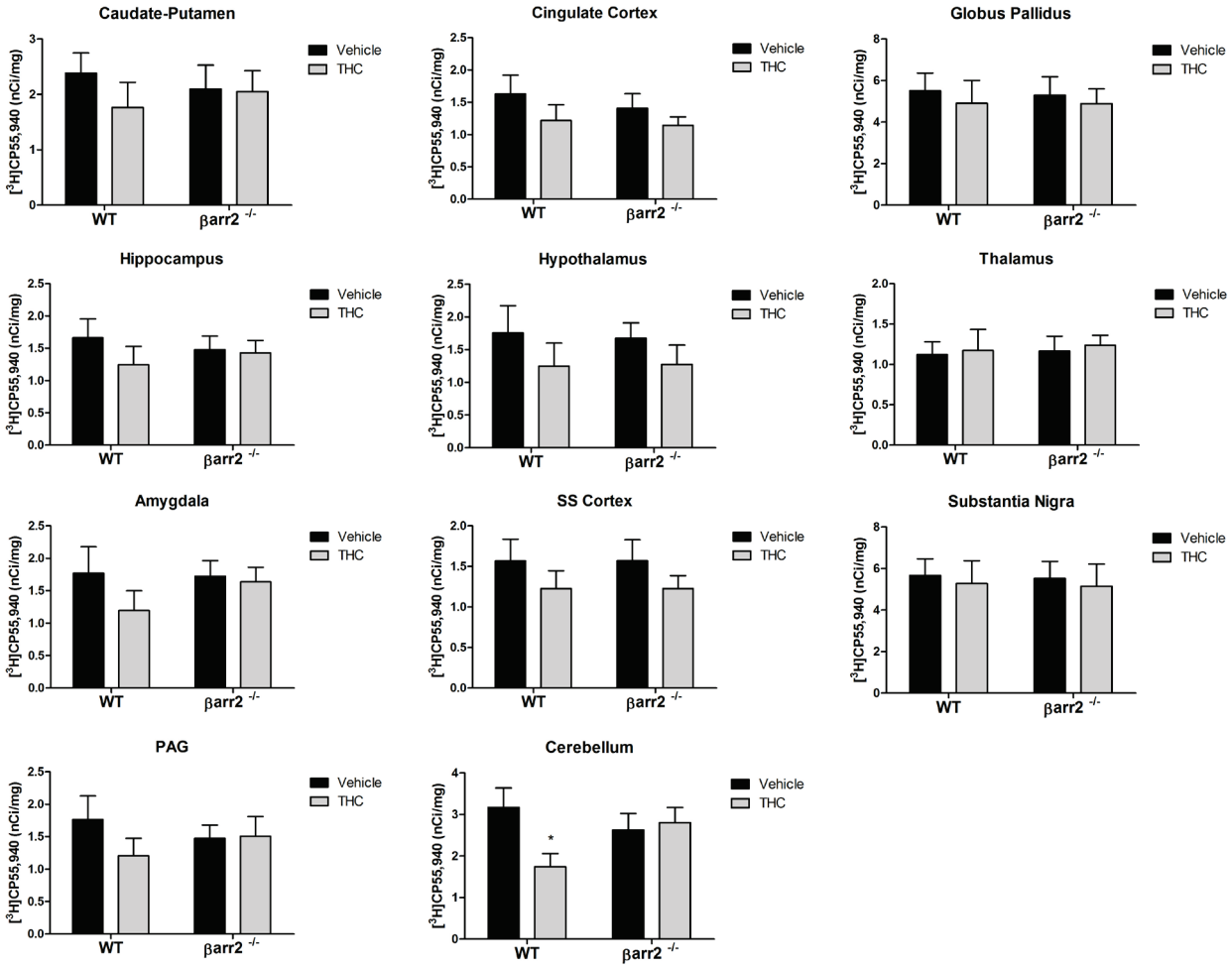

Figure 3.18. [^{3}H]CP55,940 binding values (mean ± SEM) in sampled brain regions (N = 8 per group) from βarr2 WT and KO mice treated 6.5 day with either vehicle or 10 mg/kg THC twice daily.. * $p < 0.05$ versus respective vehicle (Two way ANOVA, Student-Newman Keuls Post-hoc). *SS*, somatosensory. [^{3}H]CP55,940 autoradiography was performed as described in *Methods*

Table 3.3
[^{3}H]CP55,940 binding values in brain tissue sections from βarr2 WT and KO mice treated 6.5 day with either vehicle or 10 mg/kg THC twice daily (N = 8 per group).

Brain sections were incubated with 3 nM [^{3}H]CP55,940 as described under *Methods*. [^{3}H]CP55,940 binding values represent the mean ± SEM. $p < 0.05$ versus respective vehicle (Two way ANOVA, Student-Newman Keuls Post-hoc). *CG CTX*, cingulate cortex; *CPU*, caudate-putamen; *GP*, globus pallidus; *PIR CTX*, piriform cortex; *HIPP*, hippocampus; *AMYG*, amygdala; *HYPO*, hypothalamus; *THAL*, thalamus; *SS CTX*, somatosensory cortex; *SN*, substantia nigra; *PAG*, periaqueductal gray; *CBLM*, cerebellum.

	Vehicle		THC	
Region	**WT**	**βarr2$^{-/-}$**	**WT**	**βarr2$^{-/-}$**
CPU	2.39 ± 0.36	2.10 ± 0.43	1.76 ± 0.46	2.05 ± 0.38
CG CTX	1.63 ± 0.29	1.41 ± 0.22	1.22 ± 0.24	1.14 ± 0.13
GP	5.51 ± 0.86	5.29 ± 0.89	4.90 ± 1.11	4.88 ± 0.72
HIPP	1.66 ± 0.29	1.48 ± 0.21	1.24 ± 0.28	1.43 ± 0.19
HYPO	1.75 ± 0.42	1.67 ± 0.23	1.25 ± 0.35	1.27 ± 0.29
THAL	1.12 ± 0.16	1.17 ± 0.18	1.17 ± 0.26	1.24 ± 0.12
AMYG	1.77 ± 0.40	1.72 ± 0.24	1.20 ± 0.30	1.64 ± 0.22
SS CTX	1.57 ± 0.27	1.57 ± 0.25	1.23 ± 0.22	1.23 ± 0.16
SN	5.66 ± 0.80	5.52 ± 0.82	5.28 ± 1.09	5.15 ± 1.07
PAG	1.76 ± 0.37	1.47 ± 0.21	1.21 ± 0.27	1.51 ± 0.30
CBLM	3.18 ± 0.46	2.63 ± 0.40	1.74 ± 0.32*	2.80 ± 0.36

3.7 Discussion

The overall finding of this study is that βarr2-mediated CB_1 receptor adaptation following chronic THC treatment occurs in a region-specific manner, which was also reflected in differential effects on tolerance. Deletion of βarr2 resulted in the loss of desensitization in the cerebellum, rostral PAG, and spinal cord. In addition, CB_1 receptor downregulation occurred in only the spinal cord and cerebellum, and was attenuated in βarr2 KO animals following chronic THC treatment. Whole-brain analysis using SPM revealed that other brain regions retained the ability to desensitize in βarr2 KO animals following chronic THC treatment, suggesting other potential regulatory mechanisms either compensating for the absence of βarr2 or serving as the primary mediator of desensitization in these specific populations of neurons. For example, the hippocampus, amygdala, and rostral PAG retained the ability to desensitize to chronic THC treatment despite the absence of βarr2. Interestingly, desensitization was found in the hypothalamus and almost all examined cortical regions of βarr2 KO, but not WT animals. Further, a greater magnitude of desensitization was noted in the caudal hippocampus and amygdala of βarr2 KO animals. Regional differences in βarr2-mediated CB_1R adaptation were associated with differential effects on tolerance, where THC-mediated antinociception, but not catalepsy or hypothermia, was attenuated in βarr2 KO mice. These results demonstrate not only inter-regional, but intra-regional differences in the involvement of βarr2-mediated regulation of CB_1 receptor signaling.

Deletion of βarr2 resulted in a region-specific loss in desensitization of CB_1 receptor-mediated G-protein activity after chronic administration of THC. This occurred in the cerebellum, caudal aspects of the PAG, and spinal cord of βarr2 KO animals. This is consistent with previous reports in cell models demonstrating that desensitization of CB_1 receptor-mediated

activation of $K_{ir}3$ channels is dependent on both G-protein receptor kinase 3 (GRK3) and βarr2 (Jin et al., 1999). In addition, other reports have shown decreases in the rate and extent of desensitization of various GPCRs in cells with reduced concentrations of β-arrestin (Mundell and Benovic, 2000; Mundell et al., 1999), and conversely augmentation of desensitization following overexpression of β-arrestin (Pippig et al., 1993). Results from studies in cell models thus demonstrate that when in proximity with other important components of the desensitization machinery (i.e. GRKs), βarr2 plays an important regulatory role in the desensitization of receptors following persistent stimulation with an agonist. Mechanistically, this may also have important implications regarding the development of tolerance. In this study, βarr2 KO mice exhibited an attenuation in tolerance to THC-mediated antinociception, which is related to the loss in CB_1 receptor desensitization in the spinal cord and caudal PAG and loss of downregulation in the spinal cord. These are two brain areas that serve important functions in modulating the perception of pain (Lichtman et al., 1996).

The hippocampus, amygdala, rostral PAG, and lateral entorhinal cortex, were brain areas where desensitization occurred in both genotypes following chronic THC treatment. The finding that desensitization of CB_1 receptor-mediated G-protein can still occur despite deletion of βarr2, suggests that other mechanisms may be present. One possibility is the involvement of the other non-visual arrestin isoform, βarr1, which shares structural similarity (78% amino acid homology) and has a very similar anatomical distribution as βarr2 (Attramadal et al., 1992; Gurevich et al., 2002). In addition, the expression of βarr1 exceeds βarr2 by two to three fold in the CNS (Gurevich et al., 2002). Knockout of either βarr1 or βarr2 results in a viable phenotype, whereas the deletion of both isoforms is embryonic lethal (Kohout et al., 2001). This suggests that either isoform can substitute for the other, however emerging data (reviewed in (DeWire et al., 2007))

and results in this study indicate that they may not completely substitute, since CB_1 receptor desensitization was not present in all examined brain regions.

Unexpectedly, CB_1 receptor-mediated G-protein activity was desensitized in the hypothalamus and cortical regions, including the cingulate, piriform, auditory/visual, and somatosensory cortex, of βarr2 KO animals but not WT animals. In some instances, desensitization was greater in magnitude in particular brain regions in βarr2 KO compared to WT, such as the caudal extent of the hippocampus and amygdala. Thus it appears that deletion of βarr2 enhanced CB_1 receptor desensitization in these particular brain areas. It's interesting to note that the relative abundance of βarr2 is highest and overlaps the expression profile of CB_1 receptors in areas such as the hypothalamus, amygdala, and cortex (Gurevich et al., 2002), suggesting a potential association between deletion of βarr2 and the observed enhancement of desensitization. One possible explanation is that under normal conditions, βarr2 may shift the population of CB_1 receptors toward an inactive state, such that in its absence, the available pool of functional CB_1 receptors are increased. In fact, studies in HEK-293 cells showed that constitutively active CB_1 receptors undergo constitutive endocytosis and recycling to the membrane, with a substantial proportion of CB_1 receptors localized in intracellular vesicles (Leterrier et al., 2004). A subsequent report later showed that this constitutive endocytosis was required for the proper axonal targeting of CB_1 receptors in hippocampal neurons (Leterrier et al., 2006), indicating an important functional role for the constitutive endocytosis and recycling of CB_1 receptors. In other GPCRs, constitutively active mutant isoforms of the $5HT_{2C}$ serotonin receptor also displayed constitutive endocytosis that was βarr2 dependent (Marion et al., 2004).

If deletion of βarr2 results in an overall increase in the population of functional CB_1 receptors, this may possibly increase the apparent efficacy of an agonist. Potential increases in

the apparent efficacy of cannabinoids in βarr2 KO animals suggest an involvement of βarr2 in the acute regulation of CB_1 receptor signaling. Such increases in the apparent efficacy of an agonist may result in an increase in the magnitude of desensitization. Interestingly, Breivogel et. al. found that acute treatment with THC produced greater decreases in body temperature and antinociception in βarr2 KO versus WT mice (Breivogel et al., 2008). This enhancement in the sensitivity of THC was not replicated by other structurally different classes of cannabinoids, including the bicyclic analogue CP55,940, metabolically stable synthetic endocannabinoid derivatives methanandamide and O-1812, and the aminoalkylindole JWH-073. This suggests a possible ligand-specific sensitivity to some cannabinoid *in vivo* effects. Similarily, previous reports utilizing βarr2 KO mice showed greater morphine-mediated hypothermia and enhanced analgesia, with associated increases in μ-opioid receptor-mediated G-protein activation produced by the selective μ-opioid receptor agonist [D-Ala^2, $MePhe^4$, Gly^5-*ol*]enkephalin (DAMGO) (Bohn et al., 1999). Follow up studies also found ligand-specific prolonged and enhanced antinociceptive responses in βarr2 KO mice upon administration with equipotent doses of morphine and the structurally similar agonist heroin, but not upon administration with etorphine, fentanyl, or methadone (Bohn et al., 2004). Paradoxically, the lower efficacy μ-opioid receptor agonists morphine and heroin generally do not promote receptor internalization yet produces rapid development of tolerance (Finn and Whistler, 2001; Zhang et al., 1998). Similarily, low efficacy cannabinoid agonists such as anandamide and THC induce little internalization compared to higher efficacy cannabinoid agonists such as WIN, CP, HU210, and 2-AG, which promote more rapid and greater internalization (Hsieh et al., 1999; Wu et al., 2008). In the current study, although both genotypes displayed relatively equal degrees of tolerance to THC-mediated hypothermia, significant differences between the genotypes were found within the

vehicle treated groups. Specifically, vehicle treated βarr2 KO animals produced a greater decrease in body temperature compared to WT animals when tested with THC, consistent with results by Breivogel and colleagues (Breivogel et al., 2008). This may also be related to the observation of desensitization in βarr2 KO but not WT animals in the hypothalamus, which is a brain area that likely mediates the hypothermia effects of THC. One possibility is that the increase in apparent efficacy of cannabinoid agonists within the hypothalamus of βarr2 KO mice may unmask desensitization in this brain region, whereas in the wild-type animals reduction in stimulated G-protein activity was only moderate following the current treatment paradigm. Vehicle treated βarr2 KO animals also had greater CP-stimulated G-protein activity compared to WT animals in other brain regions including the hippocampus and cortex, indicating that deletion of βarr2 had enhanced the apparent efficacy of CP in stimulating G-protein activity in these particular brain areas.

Other mechanisms involving second-messenger dependent kinases may also mediate CB_1 receptor desensitization and contribute towards the development of tolerance. In one study, inhibiting cAMP-dependent kinase (PKA) or Src family tyrosine kinase inhibitor reversed THC-induced antinociceptive tolerance (Lee et al., 2003). Further, no effects were seen when inhibiting other kinases, including protein kinase C (PKC), cGMP-dependent protein kinase (PKG), GRK inhibitor, and phosphatidylinositol-3 kinase (PI3-K), indicating involvement of specific kinases in the development of THC-mediated antinociception. The involvement of PKA in mediating antinociceptive tolerance is supported by the fact that there is an enhanced activation of the cAMP pathway in brain regions of animals tolerant to the analgesic effect of THC (Rubino et al., 2000). In a related study, inhibition of PKA reversed tolerance to THC-induced antinociception, catalepsy, and hypoactivity, but not hypothermia (Bass et al., 2004).

The differential effects on cannabinoid tolerance from PKA inhibition suggests involvement of distinct signaling pathways in different neuronal populations. Interestingly, reversal of tolerance to hypoactivity occurred as early as after 1.5 day treatment with THC, whereas for antinociceptive tolerance reversal was apparent after the 6.5 day treatment time point (Bass et al., 2004). The differences in the time course of these two behavioral measures indicate that the relative contribution of PKA in mediating tolerance may vary among different neuronal populations. For example, brain regions involved in pain sensation may predominately involve PKA at a later time point compared to regions subserving motor function in the development of tolerance. Other studies have noted increased basal levels of cAMP and PKA activity in membrane homogenates of striatum, cortex, and cerebellum following chronic administration of THC (Rubino et al., 2000), further suggesting an involvement of PKA during the development of cannabinoid tolerance.

Emerging evidence suggests that phosphorylation-independent mechanisms may also contribute to the regulation of GPCR function (reviewed in (Ferguson, 2007)). In a recent report, GRK2-mediated desensitization and internalization of mGluR5 in striatal neurons occurred independently of receptor phosphorylation, and rather via GRK2 RH domain interactions with $G\alpha_{q/11}$ binding (Ribeiro et al., 2009). GRK2 is highly abundant throughout the CNS and is the ost highly expressed GRK isoform in the brain (Arriza et al., 1992). The anatomical co-distribution of CB_1 receptors and GRK2, as well as the subcellular localization of GRK2 in the cytoplasm and presynaptic axon terminals (Arriza et al., 1992), suggest that these two proteins may colocalize and that GRK2 may serve a function in the regulation of CB_1 receptor signaling. This is supported by evidence demonstrating that presynaptic expression of a dominant negative GRK2 reduced desensitization of WIN55,212-2-induced presynaptic inhibition of glutamatergic

neurotransmission in rat hippocampal neurons (Kouznetsova et al., 2002). Further, GRK2 expression is particularly high in regions such as the hippocampus (Murga et al., 1998), which in the current study was a brain region that demonstrated desensitization of CB_1 receptor-mediated G-protein activity (particularly pronounced in the more caudal extent) despite the absence of βarr2. In addition, GRK2 is also abundant throughout the cortex (Arriza et al., 1992). Although the THC treatment paradigm used in this study did not produce desensitization in almost all cortical regions examined (except lateral entorhinal cortex) in WT animals, desensitization was apparent in βarr2 KO animals. It is possible that GRK2-dependent regulatory mechanisms become more prominent following THC treatment in the absence of βarr2.

In this study we have demonstrated region-specific differences in the involvement of βarr2 in the regulation of CB_1 receptor adaptations following chronic administration of THC. In the absence of βarr2, CB_1 receptors in βarr2 KO animals still retained the ability to desensitize and downregulate in specific brain areas, suggesting that additional signaling pathways may also contribute towards its regulation. Moreover, deletion of βarr2 did not attenuate any acute effects of THC, suggesting that it does not mediate THC-induced effects including antinociception, hypothermia, and catalepsy. Involvement of multiple regulatory pathways in different neuronal populations illustrates the complexity and fine tuning of CB_1 receptor signaling. Diverse regulation of CB_1 receptor signaling among highly distinct anatomical brain regions, further support the importance of performing an anatomically inclusive analysis of CB_1 receptor signaling and the power of utilizing a whole-brain unbiased analytical approach. Investigating the complete regulation of CB_1 receptor signaling within various anatomical contexts will further facilitate our understanding of the neuromodulatory role of CB_1 receptors as well as provide

exciting therapeutic avenues in the design of drugs for the selective enhancement and/or attenuation of tolerance development of specific cannabinoid-mediated effects.

VII. Conclusion and Perspectives

In the preceding studies we proposed that regional-differences in the acute and chronic signaling of CB_1 receptors reflect differences in its regional regulation, and that this specificity would be revealed using a novel whole-brain unbiased approach. This was successfully accomplished by adapting Statistical Parametric Mapping (SPM) to study CB_1 receptors in reconstructed mouse brain images derived from autoradiographic data, which previously has not been described. Using this approach to investigate the acute signaling properties of CB_1 receptors, regional differences in the relative efficacy of cannabinoid agonists were demonstrated. In addition, the aminoalkylindole WIN55,212-2 (WIN), activated G-protein coupled non-$CB_{1/2/GPR55}$ sites in specific brain regions that partially overlapped with CB_1 receptor containing regions. Moreover, the presence of these putative novel sites in brainstem nuclei, including the lateral dorsal tegmental nuclei and locus coeruleus, suggest a possible role in regulating the release of neurotransmitters such as acetylcholine and norepinephrine, respectively. Regional differences in the relative efficacy of cannabinoid agonists to produce CB_1 receptor-mediated G-protein activation suggests unique signaling properties of the CB_1 receptor within various brain areas. This may have important implications regarding the chronic regulation of CB_1 receptors, as well as the development of cannabinoid tolerance, particularly if the contribution of different regulatory mechanisms has regional-specificity. Another possible explanation for regional differences in CB_1 receptor regulation is the co-localization of CB_1 receptors with specific signaling or regulatory proteins. This question was investigated by examining the role of β-arrestin-2 (βarr2) on CB_1 receptor adaptation using a βarr2 knockout (KO) mouse model. Interestingly, studies using βarr2 KO animals showed that involvement of

βarr2 in the regulation of CB_1 receptor adaptations, including desensitization of receptor-mediated G-protein activity and downregulation of CB_1 receptors, have regional-specificity as well. Deletion of βarr2 resulted in a loss of desensitization in the cerebellum, caudal PAG, and spinal cord, with a corresponding attenuation in THC-mediated antinociception. However in regions such as the amygdala and rostral hippocampus, desensitization was found in both genotypes and did not differ in magnitude. Unexpectedly, in regions such as the hypothalamus, caudal hippocampus, and cortex, desensitization appeared to be enhanced in βarr2 KO mice. CB_1 receptor downregulation was found only in the cerebellum and spinal cord of wild-type mice after chronic treatment with THC, and this was lost in βarr2 KO mice. Tolerance to THC-mediated catalepsy and hypothermia were further unaffected in the absence of βarr2.. Collectively, these results in βarr2 KO mice suggest that βarr2 may play a role in the regulation of CB_1 receptor signaling in specific brain areas, whereas in other brain regions different mechanisms of regulation may exist with anatomical and perhaps temporal specificity.

Regional differences in the signaling and regulation of CB_1 receptors is not perhaps surprising, given the highly diverse cellular architecture, and its co-localization and interaction with various signaling components. From a biological and signaling perspective, this might be expected for a highly abundant GPCR in the CNS that has an important neuromodulatory function in the fine tuning and physiological action of other receptor systems. Due to the high degree of interaction of CB_1 receptors with other functionally distinct receptor systems, complex and overlapping pathways likely exist to regulate and fine-tune cannabinoid-mediated signaling.

Studies in CB_1 KO mice demonstrated that non-$CB_{1/2/GPR55}$ sites exhibited a unique pharmacology and neuroanatomical localization. One important question is the functional relevance of non-CB_1 sites. For example, given the anatomical localization and systems

connectivity of non-$CB_{1/2/GPR55}$ sites in the cortex and its afferent projections from the locus coeruleus and amygdala, one hypothesis is that these putative novel cannabinoid sites may modulate behaviors such as attention or emotional learning. Another unanswered question is the potency and efficacy of WIN at non-$CB_{1/2/GPR55}$ sites revealed by SPM analysis. Thus, full concentration-effect curves using WIN or structurally similar agonists in these specific regions is needed. Perhaps most important would be the molecular identification and cloning of this putative novel cannabinoid receptor, which might be assisted by results in this dissertation mapping the functional distribution of non-$CB_{1/2/GPR55}$ sites. Identification of "WIN-binding" sites, which is probably one of several apparently distinct novel cannabinoid sites, may reveal unique physiological roles of the endocannabinoid system and its therapeutic exploitation.

SPM analysis revealed a number of interesting observations from chronic THC studies using βarr2 KO mice, and results have generated multiple questions regarding the regulation of CB_1 receptor signaling. For example, to what extent is βarr1 involved in mediating CB_1 receptor adaptations to chronic THC treatment? Do second-messenger dependent kinases contribute to the development of tolerance of some THC-mediated effects, and if so can it be reversed in βarr2 KO mice if we disrupted these kinase-dependent pathways? What is the time course of action for adaptation through other putative regulatory mechanisms in βarr2 KO mice and how does it vary by brain region? Interestingly, deletion of βarr2 resulted in an enhancement of desensitization in areas such as the hippocampus. What role does βarr2 play in learning and memory? These are a few important and exciting questions that will further our understanding of the regulation of CB_1 receptor signaling.

Whole-brain based analytical approaches are not only important to the study of CB_1 receptor signaling, but other receptor systems as well. Voxel-based analyses provide an

unprecedented level of anatomical precision, which is highly suitable for answering questions and investigating the nature of receptor signaling among various distinct populations of neurons. Doing so may potentially give important insight as to the physiological function and role of receptors and/or their signaling proteins. This is particularly advantageous for the cannabinoid system due to its neuromodulatory role and widespread abundance throughout the CNS. In addition, this paradigm allows an important translation of knowledge gained from mechanistic studies in well defined cellular systems into different anatomical contexts within the brain. Such an approach can be termed "Functional Anatomics", inspiring the next step in the study of biological systems. Fundamentally speaking, this concept is similar to other large-scale data mining paradigms including proteomics, functional genomics, lipidomics, bioinformatics, etc. One interesting idea would be the integration of gene expression databases, such as the Allen Brain Atlas, to identify potential interactions or involvement of specific proteins, for example based on their overlapping subcellular localization in different brain regions.

Understanding the relationship between structure and function within the human brain as well as the integration of distinct neuronal populations has historically been a challenging effort. Yet, accumulating evidence of receptor functional selectivity further points to the importance of understanding the regulation of signal transduction within various anatomical contexts. Studies in this dissertation demonstrated regional specificity in the acute and chronic signaling and regulation of CB_1 receptors in the reconstructed mouse brain. These results not only highlight the importance of performing an anatomically inclusive analysis, but suggest that mechanisms of CB_1 receptor signaling and regulation are diverse among different neuronal populations. This has extremely important implications in regard to understanding the cannabinoid system in relevance to human health and disease, as well as the potential design of cannabinoid-based therapeutics to

maximize clinical efficacy and minimize their side effects. It is important to note that repeated use of cannabinoids for management of chronic clinical conditions, such as multiple sclerosis, pain, etc., is susceptible to the development of tolerance, and possibly dependence and addiction. Because of diverse CB_1 receptor regulatory mechanisms among various brain regions, tolerance is likely to develop differentially for various cannabinoid-mediated effects with respect to relative magnitude, and to its onset and duration following cessation of cannabinoid administration. Lastly, understanding the regional regulation of CB_1 receptor signaling may allow better insight into the possibility of thwarting tolerance to the desired therapeutic effects of cannabinoids.

VIII. Appendix

This section contains supplementary thesis data from various collaborative studies. The reader is referred to the primary reference of each study for further details when appropriate. Supporting information for thesis chapters are also included.

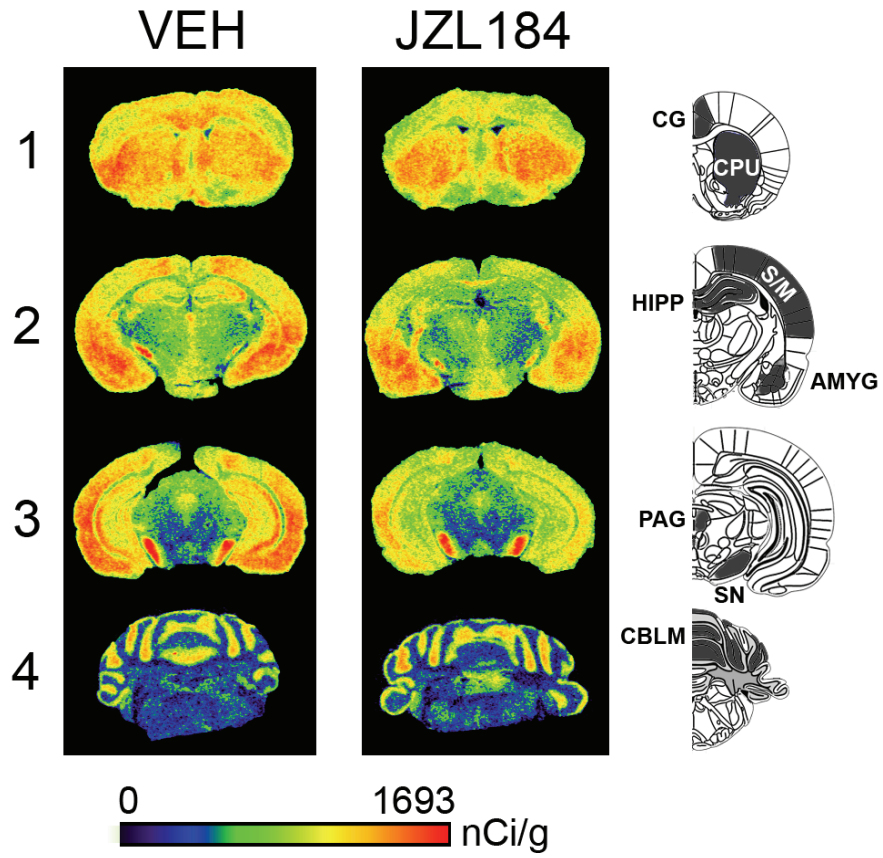

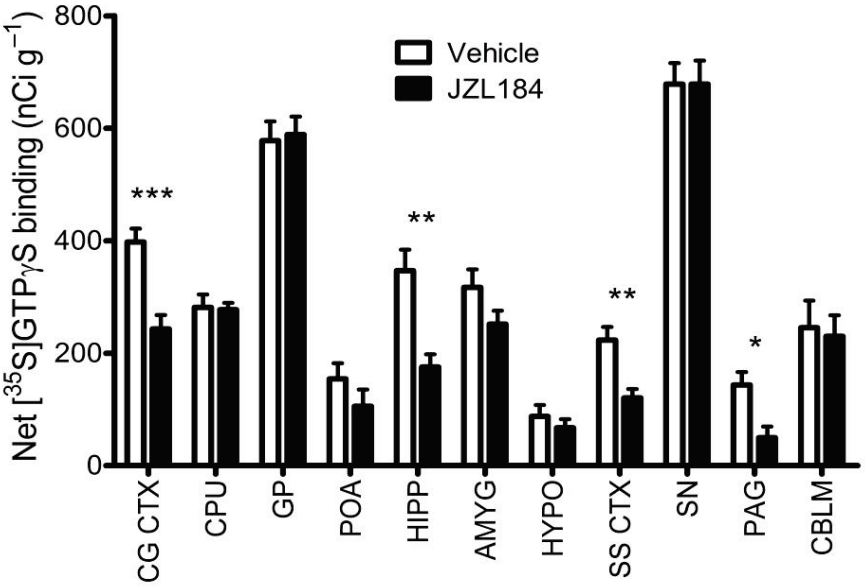

Figure A1. Regional changes in cannabinoid agonist-stimulated [^{35}S]GTPγS binding following chronic disruption of MAGL by the MAGL inhibitor JZL 184. (Top) Representative autoradiograms showing CP55,940-stimulated [^{35}S]GTPγS binding in coronal brain sections following either chronic vehicle (left column) or JZL 184 (right column) treatment. Pseudocolor images indicate levels of receptor-mediated G-protein activity and highlight significant decreases in CB_1 receptor activation in the cingulate cortex (CG CTX, row 1), hippocampus (HIPP, row 2) and periaqueductal gray (PAG, row 3), while no differences are apparent in the caudate-putamen (CPU, row 1) or cerebellum (CBLM, row 4). Colors correspond to a quantitative scale depicting [^{35}S]GTPγS binding values (nCi/g). Line cartoons in the rightmost column are shown for anatomical reference and areas shaded in gray are sampled regions of interest (Bottom) Densitometric analysis of CP55,940-stimulated [^{35}S]GTPγS binding in selected brain regions, including: cingulate cortex (CG CTX), caudate putamen (CPU), globus pallidus (GP), preoptic area of the hypothalamus (POA), hippocampus (HIPP), amygdala (AMYG), hypothalamus (HYPO), somatosensory cortex (SS CTX), substantia nigra (SN), periaqueductal gray (PAG), & cerebellum (CBLM). Data are presented as means ± SEM (N = 8 per group, sampled in triplicate slices for each targeted region). * $p < 0.05$, ** $p < 0.01$, *** $p < 0.001$ versus vehicle treatment for specific region (Student's t-test).

Work in collaboration with Dr. Liu's laboratory (Medical College of Wisconson), Dr. Lichtman's laboratory (Virginia Commonwealth University), and Dr. Cravatt's laboratory (Scripps Research Institute).

Source: Chronic monoacylglycerol lipase blockade causes functional antagonism of the endocannabinoid system. J.E. Schlosburg, J.L. Blankman, J.Z. Long, D.K. Nomura, B. Pan, S.G. Kinsey, P.T. Nguyen, D. Ramesh, L. Booker, J.J. Burston, E.A. Thomas, D.E. Selley, L.J. Sim-Selley, Q. Liu, A.H. Lichtman, B.F. Cravatt. 2010. *In press, Nature Neuroscience.*

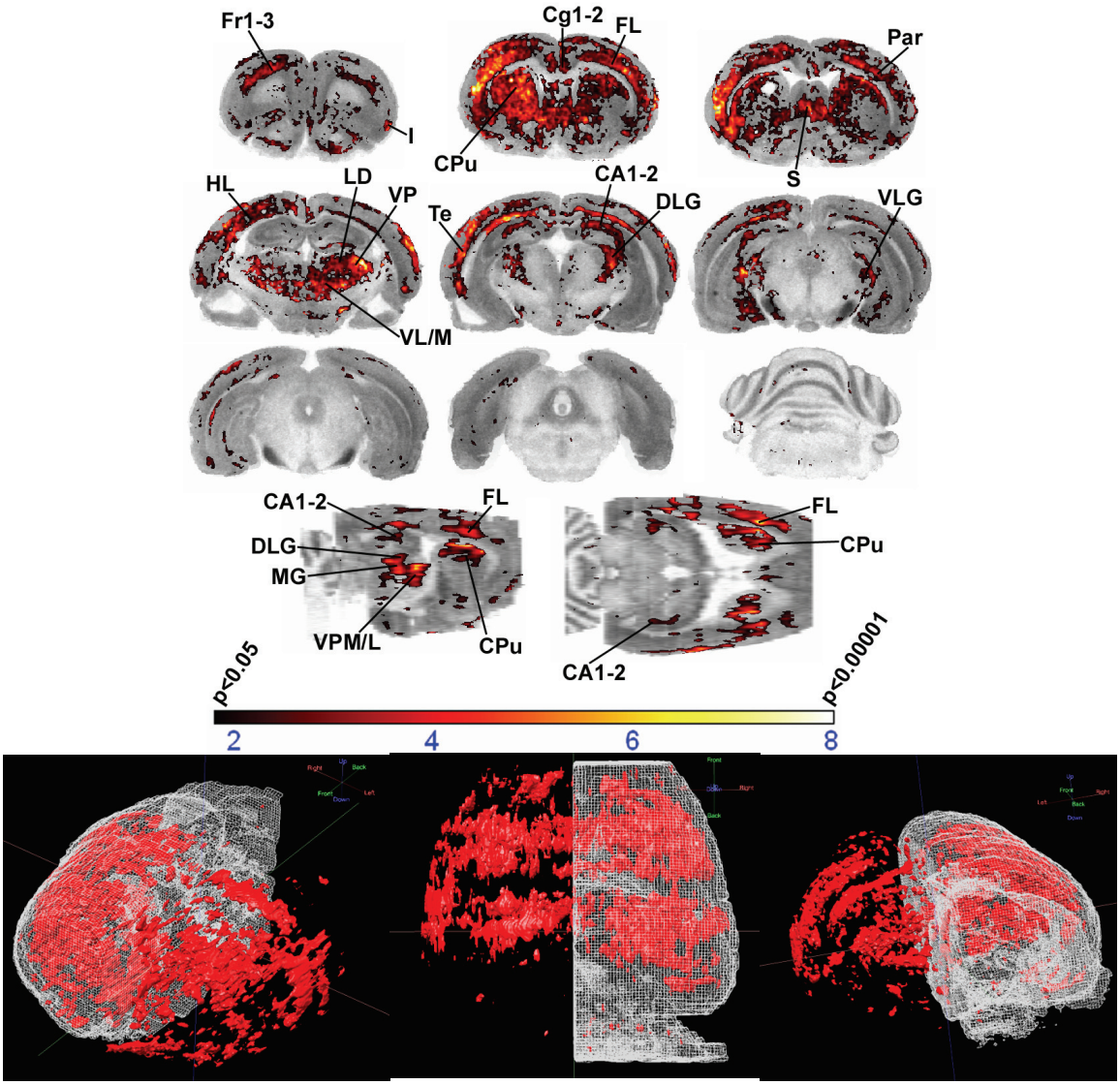

Figure A2. Statistical Parametric Mapping (SPM) reveals greater CB_1 receptor-mediated activity in epileptic animals versus controls in discrete forebrain regions. SPM analysis illustrates regions with significantly greater net WIN55,212-2-stimulated [^{35}S]GTPγS binding in epileptic rats when compared to control. Representative coronal sections (top panel) and volumetric rendered images (bottom panel) illustrate the spatial extent of differences in magnitude of G-protein activation shown as colored overlays (red to yellow) that correspond to significance level. Fr1-3 (frontal cortex, areas 1-3), I (insular cortex), Cg1-2 (cingulate gyrus, areas 1-2), CPu (caudate putamen), FL (forelimb cortex), S (septum), Par (parietal cortex), HL (hindlimb cortex), LD (laterodorsal thalamic nucleus), VL/M (ventrolateral/medial thalamic nuclei), Te (temporal cortex), hippocampal area CA3, DLG (dorsal lateral geniculate nucleus), VLG (ventral lateral geniculate nucleus), MG (medial geniculate nucleus), VPM/L (ventral posterolateral/medial thalamic nuclei).

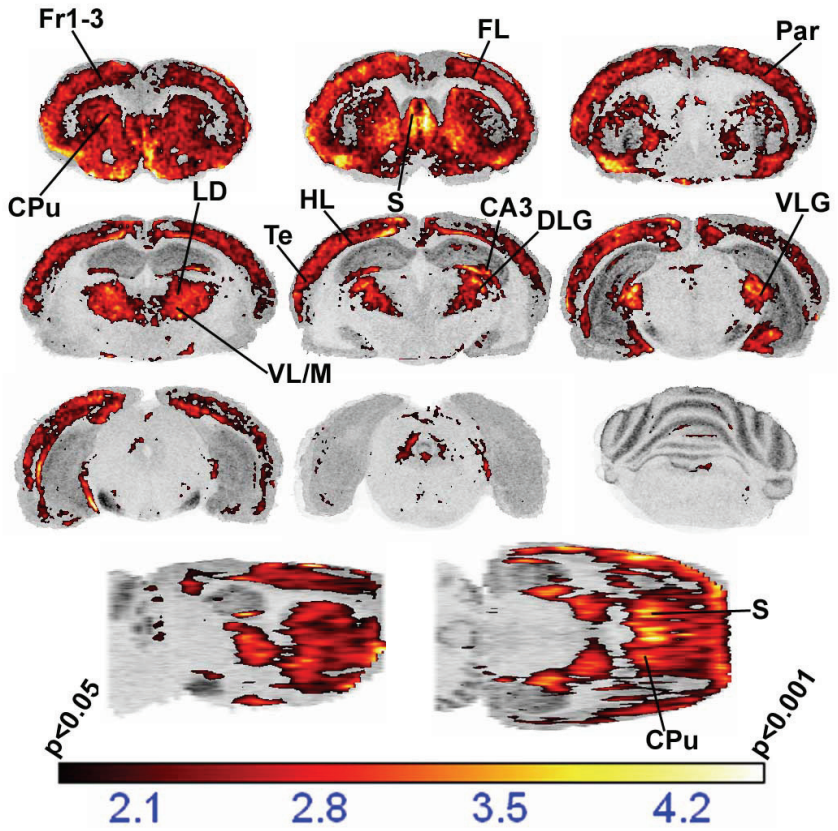

Figure A3. Statistical Parametric Mapping (SPM) reveals increases in CB_1 receptors in discrete forebrain regions of epileptic animals versus controls. SPM analysis illustrates regions with greater total [^{3}H]WIN55,212 binding in epileptic rats when compared to control. Representative coronal sections and volumetric rendered saggital and transverse images illustrate the spatial extent of differences in magnitude of CB_1 receptor binding shown as colored overlays (red to yellow) that correspond to significance level. Fr1-3 (frontal cortex, areas 1-3), I (insular cortex), Cg1-2 (cingulate gyrus, areas 1-2), CPu (caudate putamen), FL (forelimb cortex), S (septum), Par (parietal cortex), HL (hindlimb cortex), LD (laterodorsal thalamic nucleus), VL/M (ventrolateral/medial thalamic nuclei), Te (temporal cortex), hippocampal area CA3, DLG (dorsal lateral geniculate nucleus), VLG (ventral lateral geniculate nucleus), MG (medial geniculate nucleus), VPM/L (ventral posterolateral/medial thalamic nuclei).

Table A1. Region of interest (ROI) analysis reveals increases in specific [^{3}H]WIN55,212 binding and net WIN55,212-stimulated [^{35}S]GTPγS binding in forebrain regions of epileptic animals. ROI analysis was conducted and compared to SPM to evaluate increases in [^{35}S]GTPγS binding observed in epileptic animals. Overall, several regions were confirmed using ROI analysis, such as the stratum radiatum of the hippocampus, whole thalamus, and caudate putamen. * $p < 0.05$, Student's two-sample *t*-test.

	[^{3}H]WIN binding (nCi/mg)		**Net [^{35}S]GTPγS binding (nCi/g)**	
Region	Control	Epileptic	Control	Epileptic
Whole Hippocampus	2.10 ± 0.35	2.80 ± 0.23	290 ± 39	370 ± 26
Stratum Radiatum	1.92 ± 0.32	3.33 ± 0.35*	366 ± 38	513 ± 28*
Whole Thalamus	0.50 ± 0.15	1.04 ± 0.18*	130 ± 21	239 ± 28*
Cerebellum Mol Layer	4.30 ± 0.72	4.38 ± 0.42	409 ± 43	436 ± 24
Substantia Nigra	5.20 ± 1.00	5.04 ± 0.67	789 ± 43	754 ± 50
Caudate Putamen	1.37 ± 0.20	2.40 ± 0.32*	293 ± 46	436 ± 19*
Globus Pallidus	4.39 ± 0.84	5.70 ± 0.87	969 ± 55	736 ± 51*
Cingulate Cortex	1.52 ± 0.23	2.33 ± 0.27*	354 ± 44	236 ± 53
Periaqueductal Gray	0.62 ± 0.15	0.80 ± 0.11	173 ± 31	58 ± 15*
Deep (HL) Cortex	1.30 ± 0.29	3.55 ± 0.28*	396 ± 45	506 ± 42
Entorhinal Cortex	0.86 ± 0.10	1.53 ± 0.21*	464 ± 72	329 ± 51

Data presented in Figures A2 and A3, and Table A1 were done in collaboration with Dr. Falenski in Dr. DeLorenzo's laboratory (Virginia Commonwealth University).

Source: Statistical Parametric Mapping of the Regional Alterations in Cannabinoid CB_1 Receptor Expression, Binding, and G-Protein Activation in the 3D Epileptic Rat Brain. Falenski KW, Nguyen PT, Sim-Selley LJ, DeLorenzo RJ. 2010. *Manuscript in preparation*.

Table A2. Internet links to downloadable analytical software and resources on brain imaging

Software	
ImageJ	http://rsbweb.nih.gov/ij/ ImageJ is a multi-operating system (MAC, PC, Linux) image analysis suite with an online library of plugins that are created and updated by an extensive user base.
MRIcro/MRIcron	http://www.cabiatl.com/mricro/ MRIcron (MRIcro is the original older name) is a free brain imaging viewer that has 3D rendering capabilities, region/volume of interest creation, and image header viewing/editing functions. MRIcron can also overlay results from SPM analyses (i.e. SPM statistical maps) onto reference brain images
Spamalize	http://brainimaging.waisman.wisc.edu/~oakes/spam/spam_frames.htm Image viewer that has 3D volumetric rendering capabilities. Requires the program IDL
SPM	http://www.fil.ion.ucl.ac.uk/spm/ Statistical Parametric Mapping (SPM) homepage also includes documentation, bibliography, and links to download the free software (requires the program Matlab).
Documentation	
Brain imaging wikis	http://imaging.mrc-cbu.cam.ac.uk/imaging/CbuImaging Wiki on image preprocessing, SPM beginner tutorials and documentation http://en.wikibooks.org/wiki/SPM Another SPM wiki
SPM Forum	https://www.jiscmail.ac.uk/cgi-bin/webadmin?A0=spm SPM community forums

List of References

Arriza, J.L., Dawson, T.M., Simerly, R.B., Martin, L.J., Caron, M.G., Snyder, S.H., Lefkowitz, R.J., 1992. The G-protein-coupled receptor kinases beta ARK1 and beta ARK2 are widely distributed at synapses in rat brain. J Neurosci 12, 4045-4055.

Ashburner J., K.J.F., 1999. Nonlinear spatial normalization using basis functions. Human Brain Mapping 7, 254-266.

Aston-Jones, G., Rajkowski, J., Cohen, J., 1999. Role of locus coeruleus in attention and behavioral flexibility. Biol Psychiatry 46, 1309-1320.

Attramadal, H., Arriza, J.L., Aoki, C., Dawson, T.M., Codina, J., Kwatra, M.M., Snyder, S.H., Caron, M.G., Lefkowitz, R.J., 1992. Beta-arrestin2, a novel member of the arrestin/beta-arrestin gene family. J Biol Chem 267, 17882-17890.

Barna, I., Soproni, K., Arszovszki, A., Csabai, K., Haller, J., 2007. WIN-55,212-2 chronically implanted into the CA3 region of the dorsal hippocampus impairs learning: a novel method for studying chronic, brain-area-specific effects of cannabinoids. Behav Pharmacol 18, 515-520.

Bass, C.E., Welch, S.P., Martin, B.R., 2004. Reversal of delta 9-tetrahydrocannabinol-induced tolerance by specific kinase inhibitors. Eur J Pharmacol 496, 99-108.

Benowitz, N.L., Jones, R.T., 1975. Cardiovascular effects of prolonged delta-9-tetrahydrocannabinol ingestion. Clin Pharmacol Ther 18, 287-297.

Bisogno, T., Howell, F., Williams, G., Minassi, A., Cascio, M.G., Ligresti, A., Matias, I., Schiano-Moriello, A., Paul, P., Williams, E.J., Gangadharan, U., Hobbs, C., Di Marzo, V., Doherty, P., 2003. Cloning of the first sn1-DAG lipases points to the spatial and temporal regulation of endocannabinoid signaling in the brain. J Cell Biol 163, 463-468.

Block, R.I., O'Leary, D.S., Ehrhardt, J.C., Augustinack, J.C., Ghoneim, M.M., Arndt, S., Hall, J.A., 2000. Effects of frequent marijuana use on brain tissue volume and composition. Neuroreport 11, 491-496.

Bohn, L.M., Dykstra, L.A., Lefkowitz, R.J., Caron, M.G., Barak, L.S., 2004. Relative opioid efficacy is determined by the complements of the G protein-coupled receptor desensitization machinery. Mol Pharmacol 66, 106-112.

Bohn, L.M., Gainetdinov, R.R., Lin, F.T., Lefkowitz, R.J., Caron, M.G., 2000. Mu-opioid receptor desensitization by beta-arrestin-2 determines morphine tolerance but not dependence. Nature 408, 720-723.

Bohn, L.M., Lefkowitz, R.J., Caron, M.G., 2002. Differential mechanisms of morphine antinociceptive tolerance revealed in (beta)arrestin-2 knock-out mice. J Neurosci 22, 10494-10500.

Bohn, L.M., Lefkowitz, R.J., Gainetdinov, R.R., Peppel, K., Caron, M.G., Lin, F.T., 1999. Enhanced morphine analgesia in mice lacking beta-arrestin 2. Science 286, 2495-2498.

Bouaboula, M., Perrachon, S., Milligan, L., Canat, X., Rinaldi-Carmona, M., Portier, M., Barth, F., Calandra, B., Pecceu, F., Lupker, J., Maffrand, J.P., Le Fur, G., Casellas, P., 1997. A selective inverse agonist for central cannabinoid receptor inhibits mitogen-activated protein kinase activation stimulated by insulin or insulin-like growth factor 1. Evidence for a new model of receptor/ligand interactions. J Biol Chem 272, 22330-22339.

Boucher, A.A., Vivier, L., Metna-Laurent, M., Brayda-Bruno, L., Mons, N., Arnold, J.C., Micheau, J., 2009. Chronic treatment with Delta(9)-tetrahydrocannabinol impairs spatial memory and reduces zif268 expression in the mouse forebrain. Behav Pharmacol 20, 45-55.

Bradford, M.M., 1976. A rapid and sensitive method for the quantitation of microgram quantities of protein utilizing the principle of protein-dye binding. Anal Biochem 72, 248-254.

Breivogel, C.S., Childers, S.R., 2000. Cannabinoid agonist signal transduction in rat brain: comparison of cannabinoid agonists in receptor binding, G-protein activation, and adenylyl cyclase inhibition. J Pharmacol Exp Ther 295, 328-336.

Breivogel, C.S., Childers, S.R., Deadwyler, S.A., Hampson, R.E., Vogt, L.J., Sim-Selley, L.J., 1999. Chronic delta9-tetrahydrocannabinol treatment produces a time-dependent loss of cannabinoid receptors and cannabinoid receptor-activated G proteins in rat brain. J Neurochem 73, 2447-2459.

Breivogel, C.S., Griffin, G., Di Marzo, V., Martin, B.R., 2001. Evidence for a new G protein-coupled cannabinoid receptor in mouse brain. Mol Pharmacol 60, 155-163.

Breivogel, C.S., Lambert, J.M., Gerfin, S., Huffman, J.W., Razdan, R.K., 2008. Sensitivity to delta9-tetrahydrocannabinol is selectively enhanced in beta-arrestin2 -/- mice. Behav Pharmacol 19, 298-307.

Breivogel, C.S., Sim, L.J., Childers, S.R., 1997. Regional differences in cannabinoid receptor/G-protein coupling in rat brain. J Pharmacol Exp Ther 282, 1632-1642.

Bremner, J.D., Krystal, J.H., Southwick, S.M., Charney, D.S., 1996. Noradrenergic mechanisms in stress and anxiety: I. Preclinical studies. Synapse 23, 28-38.

Carlini, E.A., 1968. Tolerance to chronic administration of Cannabis sativa (marihuana) in rats. Pharmacology 1, 135-142.

Cherry, S.R., 2006. The 2006 Henry N. Wagner Lecture: Of mice and men (and positrons)--advances in PET imaging technology. J Nucl Med 47, 1735-1745.

Claing, A., Laporte, S.A., Caron, M.G., Lefkowitz, R.J., 2002. Endocytosis of G protein-coupled receptors: roles of G protein-coupled receptor kinases and beta-arrestin proteins. Prog Neurobiol 66, 61-79.

Compton, D.R., Rice, K.C., De Costa, B.R., Razdan, R.K., Melvin, L.S., Johnson, M.R., Martin, B.R., 1993. Cannabinoid structure-activity relationships: correlation of receptor binding and in vivo activities. J Pharmacol Exp Ther 265, 218-226.

Corchero, J., Manzanares, J., Fuentes, J.A., 2004. Cannabinoid/opioid crosstalk in the central nervous system. Crit Rev Neurobiol 16, 159-172.

Cravatt, B.F., Giang, D.K., Mayfield, S.P., Boger, D.L., Lerner, R.A., Gilula, N.B., 1996. Molecular characterization of an enzyme that degrades neuromodulatory fatty-acid amides. Nature 384, 83-87.

D'Souza, D.C., Ranganathan, M., Braley, G., Gueorguieva, R., Zimolo, Z., Cooper, T., Perry, E., Krystal, J., 2008. Blunted psychotomimetic and amnestic effects of delta-9-tetrahydrocannabinol in frequent users of cannabis. Neuropsychopharmacology 33, 2505-2516.

Devane, W.A., Dysarz, F.A., 3rd, Johnson, M.R., Melvin, L.S., Howlett, A.C., 1988. Determination and characterization of a cannabinoid receptor in rat brain. Mol Pharmacol 34, 605-613.

Devane, W.A., Hanus, L., Breuer, A., Pertwee, R.G., Stevenson, L.A., Griffin, G., Gibson, D., Mandelbaum, A., Etinger, A., Mechoulam, R., 1992. Isolation and structure of a brain constituent that binds to the cannabinoid receptor. Science 258, 1946-1949.

Dewey, W.L., 1986. Cannabinoid pharmacology. Pharmacol Rev 38, 151-178.

Dewey, W.L., McMillan, D.E., Harris, L.S., Turk, R.F., 1973. Distribution of radioactivity in brain of tolerant and nontolerant pigeons treated with 3 H- 9 -tetrahydrocannabinol. Biochem Pharmacol 22, 399-405.

DeWire, S.M., Ahn, S., Lefkowitz, R.J., Shenoy, S.K., 2007. Beta-arrestins and cell signaling. Annu Rev Physiol 69, 483-510.

Di Marzo, V., Bisogno, T., De Petrocellis, L., Brandi, I., Jefferson, R.G., Winckler, R.L., Davis, J.B., Dasse, O., Mahadevan, A., Razdan, R.K., Martin, B.R., 2001. Highly selective CB(1) cannabinoid receptor ligands and novel CB(1)/VR(1) vanilloid receptor "hybrid" ligands. Biochem Biophys Res Commun 281, 444-451.

Di Marzo, V., Breivogel, C.S., Tao, Q., Bridgen, D.T., Razdan, R.K., Zimmer, A.M., Zimmer, A., Martin, B.R., 2000. Levels, metabolism, and pharmacological activity of anandamide in CB(1) cannabinoid receptor knockout mice: evidence for non-CB(1), non-CB(2) receptor-mediated actions of anandamide in mouse brain. J Neurochem 75, 2434-2444.

Dinh, T.P., Carpenter, D., Leslie, F.M., Freund, T.F., Katona, I., Sensi, S.L., Kathuria, S., Piomelli, D., 2002. Brain monoglyceride lipase participating in endocannabinoid inactivation. Proc Natl Acad Sci U S A 99, 10819-10824.

Dubois, A., Herard, A.S., Flandin, G., Duchesnay, E., Besret, L., Frouin, V., Hantraye, P., Bonvento, G., Delzescaux, T., 2008. Quantitative validation of voxel-wise statistical analyses of autoradiographic rat brain volumes: application to unilateral visual stimulation. Neuroimage 40, 482-494.

Elsohly, M.A., Slade, D., 2005. Chemical constituents of marijuana: the complex mixture of natural cannabinoids. Life Sci 78, 539-548.

Falenski, K.W., Thorpe, A.J., Schlosburg, J.E., Cravatt, B.F., Abdullah, R.A., Smith, T.H., Selley, D.E., Lichtman, A.H., Sim-Selley, L.J., 2010. FAAH-/- mice display differential tolerance, dependence, and cannabinoid receptor adaptation after delta 9-tetrahydrocannabinol and anandamide administration. Neuropsychopharmacology 35, 1775-1787.

Fan, F., Tao, Q., Abood, M., Martin, B.R., 1996. Cannabinoid receptor down-regulation without alteration of the inhibitory effect of CP 55,940 on adenylyl cyclase in the cerebellum of CP 55,940-tolerant mice. Brain Res 706, 13-20.

Ferguson, S.S., 2007. Phosphorylation-independent attenuation of GPCR signalling. Trends Pharmacol Sci 28, 173-179.

Ferguson, S.S., Caron, M.G., 1998. G protein-coupled receptor adaptation mechanisms. Semin Cell Dev Biol 9, 119-127.

Ferrari, F., Ottani, A., Vivoli, R., Giuliani, D., 1999. Learning impairment produced in rats by the cannabinoid agonist HU 210 in a water-maze task. Pharmacol Biochem Behav 64, 555-561.

Ferraro, D.P., Grilly, D.M., 1973. Lack of tolerance to 9 -tetrahydrocannabinol in chimpanzees. Science 179, 490-492.

Finn, A.K., Whistler, J.L., 2001. Endocytosis of the mu opioid receptor reduces tolerance and a cellular hallmark of opiate withdrawal. Neuron 32, 829-839.

Foote, S.L., Bloom, F.E., Aston-Jones, G., 1983. Nucleus locus ceruleus: new evidence of anatomical and physiological specificity. Physiol Rev 63, 844-914.

Franklin, K., Paxinos, G., 2008. The Mouse Brain in Stereotaxic Coordinates, 3rd ed. Elsevier, New York, NY.

Freedland, C.S., Whitlow, C.T., Miller, M.D., Porrino, L.J., 2002. Dose-dependent effects of Delta9-tetrahydrocannabinol on rates of local cerebral glucose utilization in rat. Synapse 45, 134-142.

Friston, K.J., Ashburner, J., Kiebel, S., Nichols, T., Penny, W.D., 2007. Statistical Parametric Mapping: the analysis of functional brain images, 1st ed. Academic Press, San Diego.

Friston, K.J., Ashburner, J., Poline, J.B., Frith, C.D., Heather, J.D., Frackowiak, R.S., 1995a. Spatial registration and normalization of images. Human Brain Mapping 2, 165-168.

Friston, K.J., Frith, C.D., Liddle, P.F., Frackowiak, R.S., 1991. Comparing functional (PET) images: the assessment of significant change. J Cereb Blood Flow Metab 11, 690-699.

Friston, K.J., Holmes, A., Poline, J.B., Price, C.J., Frith, C.D., 1996. Detecting activations in PET and fMRI: levels of inference and power. Neuroimage 4, 223-235.

Friston, K.J., Holmes, A., Worsley, K.J., Poline, J.B., Frith, C.D., Frackowiak, R.S., 1995b. Statistical parametric maps in functional imaging: A general linear approach. Human Brain Mapping 2, 189-210.

Friston, K.J., Worsley, K.J., Frackowiak, R.S., Mazziotta, J.C., Evans, A.C., 1994. Asessing the significance of focal activations using their spatial extent. Human Brain Mapping 1, 214-220.

Gainetdinov, R.R., Premont, R.T., Bohn, L.M., Lefkowitz, R.J., Caron, M.G., 2004. Desensitization of G protein-coupled receptors and neuronal functions. Annu Rev Neurosci 27, 107-144.

Gao, Y., Vasilyev, D.V., Goncalves, M.B., Howell, F.V., Hobbs, C., Reisenberg, M., Shen, R., Zhang, M.Y., Strassle, B.W., Lu, P., Mark, L., Piesla, M.J., Deng, K., Kouranova, E.V., Ring, R.H., Whiteside, G.T., Bates, B., Walsh, F.S., Williams, G., Pangalos, M.N., Samad, T.A., Doherty, P., 2010. Loss of retrograde endocannabinoid signaling and reduced adult neurogenesis in diacylglycerol lipase knock-out mice. J Neurosci 30, 2017-2024.

Gaoni, Y., Mechoulam, R., 1964. Isolation, structure and partial synthesis of an active constituent of Hashish. J Am Chem Soc 86, 1646-1647.

Gierschik, P., Moghtader, R., Straub, C., Dieterich, K., Jakobs, K.H., 1991. Signal amplification in HL-60 granulocytes. Evidence that the chemotactic peptide receptor catalytically activates guanine-nucleotide-binding regulatory proteins in native plasma membranes. Eur J Biochem 197, 725-732.

Gifford, A.N., Makriyannis, A., Volkow, N.D., Gatley, S.J., 2002. In vivo imaging of the brain cannabinoid receptor. Chem Phys Lipids 121, 65-72.

Glass, M., Northup, J.K., 1999. Agonist selective regulation of G proteins by cannabinoid CB(1) and CB(2) receptors. Mol Pharmacol 56, 1362-1369.

Gonzalez, S., Cebeira, M., Fernandez-Ruiz, J., 2005. Cannabinoid tolerance and dependence: a review of studies in laboratory animals. Pharmacol Biochem Behav 81, 300-318.

Govaerts, S.J., Hermans, E., Lambert, D.M., 2004. Comparison of cannabinoid ligands affinities and efficacies in murine tissues and in transfected cells expressing human recombinant cannabinoid receptors. Eur J Pharm Sci 23, 233-243.

Gulyas, A.I., Cravatt, B.F., Bracey, M.H., Dinh, T.P., Piomelli, D., Boscia, F., Freund, T.F., 2004. Segregation of two endocannabinoid-hydrolyzing enzymes into pre- and postsynaptic compartments in the rat hippocampus, cerebellum and amygdala. Eur J Neurosci 20, 441-458.

Guo, J., Ikeda, S.R., 2004. Endocannabinoids modulate N-type calcium channels and G-protein-coupled inwardly rectifying potassium channels via CB1 cannabinoid receptors heterologously expressed in mammalian neurons. Mol Pharmacol 65, 665-674.

Gurevich, E.V., Benovic, J.L., Gurevich, V.V., 2002. Arrestin2 and arrestin3 are differentially expressed in the rat brain during postnatal development. Neuroscience 109, 421-436.

Hajos, N., Katona, I., Naiem, S.S., MacKie, K., Ledent, C., Mody, I., Freund, T.F., 2000. Cannabinoids inhibit hippocampal GABAergic transmission and network oscillations. Eur J Neurosci 12, 3239-3249.

Hajos, N., Ledent, C., Freund, T.F., 2001. Novel cannabinoid-sensitive receptor mediates inhibition of glutamatergic synaptic transmission in the hippocampus. Neuroscience 106, 1-4.

Hall, R.A., Premont, R.T., Lefkowitz, R.J., 1999. Heptahelical receptor signaling: beyond the G protein paradigm. J Cell Biol 145, 927-932.

Herer, J., 2000. The Emperor Wears No Clothes: The Authoritative Historical Record of Cannabis and the Conspiracy Against Marijuana 11th ed. Quick American Archives.

Herkenham, M., Lynn, A.B., Johnson, M.R., Melvin, L.S., de Costa, B.R., Rice, K.C., 1991. Characterization and localization of cannabinoid receptors in rat brain: a quantitative in vitro autoradiographic study. J Neurosci 11, 563-583.

Hess, A., Lohmann, K., Gundelfinger, E.D., Scheich, H., 1998. A new method for reliable and efficient reconstruction of 3-dimensional images from autoradiographs of brain sections. J Neurosci Methods 84, 77-86.

Hoffman, A.F., Macgill, A.M., Smith, D., Oz, M., Lupica, C.R., 2005. Species and strain differences in the expression of a novel glutamate-modulating cannabinoid receptor in the rodent hippocampus. Eur J Neurosci 22, 2387-2391.

Hollister, L.E., 1998. Health aspects of cannabis: revisited. Int J Neuropsychopharmcol 1, 71-80.

Holschneider, D.P., Yang, J., Sadler, T.R., Nguyen, P.T., Givrad, T.K., Maarek, J.M., 2006. Mapping cerebral blood flow changes during auditory-cued conditioned fear in the nontethered, nonrestrained rat. Neuroimage 29, 1344-1358.

Horti, A.G., Van Laere, K., 2008. Development of radioligands for in vivo imaging of type 1 cannabinoid receptors (CB1) in human brain. Curr Pharm Des 14, 3363-3383.

Howlett, A.C., Barth, F., Bonner, T.I., Cabral, G., Casellas, P., Devane, W.A., Felder, C.C., Herkenham, M., Mackie, K., Martin, B.R., Mechoulam, R., Pertwee, R.G., 2002. International Union of Pharmacology. XXVII. Classification of cannabinoid receptors. Pharmacol Rev 54, 161-202.

Howlett, A.C., Fleming, R.M., 1984. Cannabinoid inhibition of adenylate cyclase. Pharmacology of the response in neuroblastoma cell membranes. Mol Pharmacol 26, 532-538.

Howlett, A.C., Qualy, J.M., Khachatrian, L.L., 1986. Involvement of Gi in the inhibition of adenylate cyclase by cannabimimetic drugs. Mol Pharmacol 29, 307-313.

Hsieh, C., Brown, S., Derleth, C., Mackie, K., 1999. Internalization and recycling of the CB1 cannabinoid receptor. J Neurochem 73, 493-501.

Ishac, E.J., Jiang, L., Lake, K.D., Varga, K., Abood, M.E., Kunos, G., 1996. Inhibition of exocytotic noradrenaline release by presynaptic cannabinoid CB1 receptors on peripheral sympathetic nerves. Br J Pharmacol 118, 2023-2028.

Jansen, E.M., Haycock, D.A., Ward, S.J., Seybold, V.S., 1992. Distribution of cannabinoid receptors in rat brain determined with aminoalkylindoles. Brain Res 575, 93-102.

Jin, W., Brown, S., Roche, J.P., Hsieh, C., Celver, J.P., Kovoor, A., Chavkin, C., Mackie, K., 1999. Distinct domains of the CB1 cannabinoid receptor mediate desensitization and internalization. J Neurosci 19, 3773-3780.

Kathmann, M., Bauer, U., Schlicker, E., Gothert, M., 1999. Cannabinoid CB1 receptor-mediated inhibition of NMDA- and kainate-stimulated noradrenaline and dopamine release in the brain. Naunyn Schmiedebergs Arch Pharmacol 359, 466-470.

Katona, I., Rancz, E.A., Acsady, L., Ledent, C., Mackie, K., Hajos, N., Freund, T.F., 2001. Distribution of CB1 cannabinoid receptors in the amygdala and their role in the control of GABAergic transmission. J Neurosci 21, 9506-9518.

Kohout, T.A., Lin, F.S., Perry, S.J., Conner, D.A., Lefkowitz, R.J., 2001. beta-Arrestin 1 and 2 differentially regulate heptahelical receptor signaling and trafficking. Proc Natl Acad Sci U S A 98, 1601-1606.

Kouznetsova, M., Kelley, B., Shen, M., Thayer, S.A., 2002. Desensitization of cannabinoid-mediated presynaptic inhibition of neurotransmission between rat hippocampal neurons in culture. Mol Pharmacol 61, 477-485.

Kreitzer, A.C., Carter, A.G., Regehr, W.G., 2002. Inhibition of interneuron firing extends the spread of endocannabinoid signaling in the cerebellum. Neuron 34, 787-796.

Landsman, R.S., Burkey, T.H., Consroe, P., Roeske, W.R., Yamamura, H.I., 1997. SR141716A is an inverse agonist at the human cannabinoid CB1 receptor. Eur J Pharmacol 334, R1-2.

Lee, M.C., Smith, F.L., Stevens, D.L., Welch, S.P., 2003. The role of several kinases in mice tolerant to delta 9-tetrahydrocannabinol. J Pharmacol Exp Ther 305, 593-599.

Lefkowitz, R.J., 1993. G protein-coupled receptor kinases. Cell 74, 409-412.

Lefkowitz, R.J., 1998. G protein-coupled receptors. III. New roles for receptor kinases and beta-arrestins in receptor signaling and desensitization. J Biol Chem 273, 18677-18680.

Lefkowitz, R.J., Hausdorff, W.P., Caron, M.G., 1990. Role of phosphorylation in desensitization of the beta-adrenoceptor. Trends Pharmacol Sci 11, 190-194.

Leterrier, C., Bonnard, D., Carrel, D., Rossier, J., Lenkei, Z., 2004. Constitutive endocytic cycle of the CB1 cannabinoid receptor. J Biol Chem 279, 36013-36021.

Leterrier, C., Laine, J., Darmon, M., Boudin, H., Rossier, J., Lenkei, Z., 2006. Constitutive activation drives compartment-selective endocytosis and axonal targeting of type 1 cannabinoid receptors. J Neurosci 26, 3141-3153.

Leung, D., Saghatelian, A., Simon, G.M., Cravatt, B.F., 2006. Inactivation of N-acyl phosphatidylethanolamine phospholipase D reveals multiple mechanisms for the biosynthesis of endocannabinoids. Biochemistry 45, 4720-4726.

Lichtman, A.H., Cook, S.A., Martin, B.R., 1996. Investigation of brain sites mediating cannabinoid-induced antinociception in rats: evidence supporting periaqueductal gray involvement. J Pharmacol Exp Ther 276, 585-593.

Lin, F.T., Krueger, K.M., Kendall, H.E., Daaka, Y., Fredericks, Z.L., Pitcher, J.A., Lefkowitz, R.J., 1997. Clathrin-mediated endocytosis of the beta-adrenergic receptor is regulated by phosphorylation/dephosphorylation of beta-arrestin1. J Biol Chem 272, 31051-31057.

Lin, S., Khanolkar, A.D., Fan, P., Goutopoulos, A., Qin, C., Papahadjis, D., Makriyannis, A., 1998. Novel analogues of arachidonylethanolamide (anandamide): affinities for the CB1 and CB2 cannabinoid receptors and metabolic stability. J Med Chem 41, 5353-5361.

Liu, J., Wang, L., Harvey-White, J., Osei-Hyiaman, D., Razdan, R., Gong, Q., Chan, A.C., Zhou, Z., Huang, B.X., Kim, H.Y., Kunos, G., 2006. A biosynthetic pathway for anandamide. Proc Natl Acad Sci U S A 103, 13345-13350.

Llano, I., Leresche, N., Marty, A., 1991. Calcium entry increases the sensitivity of cerebellar Purkinje cells to applied GABA and decreases inhibitory synaptic currents. Neuron 6, 565-574.

Long, J.Z., Li, W., Booker, L., Burston, J.J., Kinsey, S.G., Schlosburg, J.E., Pavon, F.J., Serrano, A.M., Selley, D.E., Parsons, L.H., Lichtman, A.H., Cravatt, B.F., 2009. Selective blockade of 2-arachidonoylglycerol hydrolysis produces cannabinoid behavioral effects. Nat Chem Biol 5, 37-44.

Mackie, K., 2008. Signaling via CNS cannabinoid receptors. Mol Cell Endocrinol 286, S60-65.

Marion, S., Weiner, D.M., Caron, M.G., 2004. RNA editing induces variation in desensitization and trafficking of 5-hydroxytryptamine 2c receptor isoforms. J Biol Chem 279, 2945-2954.

Marsicano, G., Wotjak, C.T., Azad, S.C., Bisogno, T., Rammes, G., Cascio, M.G., Hermann, H., Tang, J., Hofmann, C., Zieglgansberger, W., Di Marzo, V., Lutz, B., 2002. The endogenous cannabinoid system controls extinction of aversive memories. Nature 418, 530-534.

Martin, B.R., Dewey, W.L., Harris, L.S., Beckner, J.S., 1976. 3H-delta9-tetrahydrocannabinol tissue and subcellular distribution in the central nervous system and tissue distribution in peripheral organs of tolerant and nontolerant dogs. J Pharmacol Exp Ther 196, 128-144.

Martini, L., Thompson, D., Kharazia, V., Whistler, J.L., 2010. Differential regulation of behavioral tolerance to WIN55,212-2 by GASP1. Neuropsychopharmacology 35, 1363-1373.

Matsuda, L.A., Lolait, S.J., Brownstein, M.J., Young, A.C., Bonner, T.I., 1990. Structure of a cannabinoid receptor and functional expression of the cloned cDNA. Nature 346, 561-564.

McKinney, D.L., Cassidy, M.P., Collier, L.M., Martin, B.R., Wiley, J.L., Selley, D.E., Sim-Selley, L.J., 2008. Dose-related differences in the regional pattern of cannabinoid receptor adaptation and in vivo tolerance development to delta9-tetrahydrocannabinol. J Pharmacol Exp Ther 324, 664-673.

McLaughlin, P.J., Winston, K., Swezey, L., Wisniecki, A., Aberman, J., Tardif, D.J., Betz, A.J., Ishiwari, K., Makriyannis, A., Salamone, J.D., 2003. The cannabinoid CB1 antagonists SR 141716A and AM 251 suppress food intake and food-reinforced behavior in a variety of tasks in rats. Behav Pharmacol 14, 583-588.

Mechoulam, R., Ben-Shabat, S., Hanus, L., Ligumsky, M., Kaminski, N.E., Schatz, A.R., Gopher, A., Almog, S., Martin, B.R., Compton, D.R., et al., 1995. Identification of an endogenous 2-monoglyceride, present in canine gut, that binds to cannabinoid receptors. Biochem Pharmacol 50, 83-90.

Melvin, L.S., Johnson, M.R., 1987. Structure-activity relationships of tricyclic and nonclassical bicyclic cannabinoids. NIDA Res Monogr 79, 31-47.

Misner, D.L., Sullivan, J.M., 1999. Mechanism of cannabinoid effects on long-term potentiation and depression in hippocampal CA1 neurons. J Neurosci 19, 6795-6805.

Moise, A.M., Eisenstein, S.A., Astarita, G., Piomelli, D., Hohmann, A.G., 2008. An endocannabinoid signaling system modulates anxiety-like behavior in male Syrian hamsters. Psychopharmacology (Berl) 200, 333-346.

Moore, C.A., Milano, S.K., Benovic, J.L., 2007. Regulation of receptor trafficking by GRKs and arrestins. Annu Rev Physiol 69, 451-482.

Mukhopadhyay, S., McIntosh, H.H., Houston, D.B., Howlett, A.C., 2000. The CB(1) cannabinoid receptor juxtamembrane C-terminal peptide confers activation to specific G proteins in brain. Mol Pharmacol 57, 162-170.

Mundell, S.J., Benovic, J.L., 2000. Selective regulation of endogenous G protein-coupled receptors by arrestins in HEK293 cells. J Biol Chem 275, 12900-12908.

Mundell, S.J., Loudon, R.P., Benovic, J.L., 1999. Characterization of G protein-coupled receptor regulation in antisense mRNA-expressing cells with reduced arrestin levels. Biochemistry 38, 8723-8732.

Munro, S., Thomas, K.L., Abu-Shaar, M., 1993. Molecular characterization of a peripheral receptor for cannabinoids. Nature 365, 61-65.

Murga, C., Penela, P., Zafra, F., Mayor, F., Jr., 1998. The subcellular and cellular distribution of G protein-coupled receptor kinase 2 in rat brain. Neuroscience 87, 631-637.

Nakazi, M., Bauer, U., Nickel, T., Kathmann, M., Schlicker, E., 2000. Inhibition of serotonin release in the mouse brain via presynaptic cannabinoid CB1 receptors. Naunyn Schmiedebergs Arch Pharmacol 361, 19-24.

National Research Council, 1996. Guide for the care and use of laboratory animals. National Academy Press, Washington, D.C.

Nguyen, P.T., Holschneider, D.P., Maarek, J.M., Yang, J., Mandelkern, M.A., 2004. Statistical parametric mapping applied to an autoradiographic study of cerebral activation during treadmill walking in rats. Neuroimage 23, 252-259.

Nguyen, P.T., Selley, D.E., Sim-Selley, L.J., 2010. Statistical Parametric Mapping reveals ligand and region-specific activation of G-proteins by CB1 receptors and non-CB1 sites in the 3D reconstructed mouse brain. Neuroimage 52, 1243-1251.

Nowicky, A.V., Teyler, T.J., Vardaris, R.M., 1987. The modulation of long-term potentiation by delta-9-tetrahydrocannabinol in the rat hippocampus, in vitro. Brain Res Bull 19, 663-672.

Ohno-Shosaku, T., Matsui, M., Fukudome, Y., Shosaku, J., Tsubokawa, H., Taketo, M.M., Manabe, T., Kano, M., 2003. Postsynaptic M1 and M3 receptors are responsible for the muscarinic enhancement of retrograde endocannabinoid signalling in the hippocampus. Eur J Neurosci 18, 109-116.

Onaivi, E.S., Ishiguro, H., Gong, J.P., Patel, S., Perchuk, A., Meozzi, P.A., Myers, L., Mora, Z., Tagliaferro, P., Gardner, E., Brusco, A., Akinshola, B.E., Liu, Q.R., Hope, B., Iwasaki, S., Arinami, T., Teasenfitz, L., Uhl, G.R., 2006. Discovery of the presence and functional expression of cannabinoid CB2 receptors in brain. Ann N Y Acad Sci 1074, 514-536.

Oropeza, V.C., Mackie, K., Van Bockstaele, E.J., 2007. Cannabinoid receptors are localized to noradrenergic axon terminals in the rat frontal cortex. Brain Res 1127, 36-44.

Oropeza, V.C., Page, M.E., Van Bockstaele, E.J., 2005. Systemic administration of WIN 55,212-2 increases norepinephrine release in the rat frontal cortex. Brain Res 1046, 45-54.

Oviedo, A., Glowa, J., Herkenham, M., 1993. Chronic cannabinoid administration alters cannabinoid receptor binding in rat brain: a quantitative autoradiographic study. Brain Res 616, 293-302.

Pacheco, M., Childers, S.R., Arnold, R., Casiano, F., Ward, S.J., 1991. Aminoalkylindoles: actions on specific G-protein-linked receptors. J Pharmacol Exp Ther 257, 170-183.

Page, M.E., Oropeza, V.C., Van Bockstaele, E.J., 2008. Local administration of a cannabinoid agonist alters norepinephrine efflux in the rat frontal cortex. Neurosci Lett 431, 1-5.

Pertwee, R.G., 2005a. Inverse agonism and neutral antagonism at cannabinoid CB1 receptors. Life Sci 76, 1307-1324.

Pertwee, R.G., 2005b. Pharmacological actions of cannabinoids. Handb Exp Pharmacol, 1-51.

Pertwee, R.G., Stevenson, L.A., Griffin, G., 1993. Cross-tolerance between delta-9-tetrahydrocannabinol and the cannabimimetic agents, CP 55,940, WIN 55,212-2 and anandamide. Br J Pharmacol 110, 1483-1490.

Pippig, S., Andexinger, S., Daniel, K., Puzicha, M., Caron, M.G., Lefkowitz, R.J., Lohse, M.J., 1993. Overexpression of beta-arrestin and beta-adrenergic receptor kinase augment desensitization of beta 2-adrenergic receptors. J Biol Chem 268, 3201-3208.

Pistis, M., Perra, S., Pillolla, G., Melis, M., Gessa, G.L., Muntoni, A.L., 2004. Cannabinoids modulate neuronal firing in the rat basolateral amygdala: evidence for CB1- and non-CB1-mediated actions. Neuropharmacology 46, 115-125.

Prather, P.L., Martin, N.A., Breivogel, C.S., Childers, S.R., 2000. Activation of cannabinoid receptors in rat brain by WIN 55212-2 produces coupling to multiple G protein alpha-subunits with different potencies. Mol Pharmacol 57, 1000-1010.

Reyes, B.A., Rosario, J.C., Piana, P.M., Van Bockstaele, E.J., 2009. Cannabinoid modulation of cortical adrenergic receptors and transporters. J Neurosci Res.

Ribeiro, F.M., Ferreira, L.T., Paquet, M., Cregan, T., Ding, Q., Gros, R., Ferguson, S.S., 2009. Phosphorylation-independent regulation of metabotropic glutamate receptor 5 desensitization and internalization by G protein-coupled receptor kinase 2 in neurons. J Biol Chem 284, 23444-23453.

Rinaldi-Carmona, M., Barth, F., Heaulme, M., Shire, D., Calandra, B., Congy, C., Martinez, S., Maruani, J., Neliat, G., Caput, D., et al., 1994. SR141716A, a potent and selective antagonist of the brain cannabinoid receptor. FEBS Lett 350, 240-244.

Ross, R.A., 2009. The enigmatic pharmacology of GPR55. Trends Pharmacol Sci 30, 156-163.

Rubino, T., Patrini, G., Parenti, M., Massi, P., Parolaro, D., 1997. Chronic treatment with a synthetic cannabinoid CP-55,940 alters G-protein expression in the rat central nervous system. Brain Res Mol Brain Res 44, 191-197.

Rubino, T., Vigano, D., Massi, P., Spinello, M., Zagato, E., Giagnoni, G., Parolaro, D., 2000. Chronic delta-9-tetrahydrocannabinol treatment increases cAMP levels and cAMP-dependent protein kinase activity in some rat brain regions. Neuropharmacology 39, 1331-1336.

Rubino, T., Vigano, D., Premoli, F., Castiglioni, C., Bianchessi, S., Zippel, R., Parolaro, D., 2006. Changes in the expression of G protein-coupled receptor kinases and beta-arrestins in mouse brain during cannabinoid tolerance: a role for RAS-ERK cascade. Mol Neurobiol 33, 199-213.

Schlicker, E., Kathmann, M., 2001. Modulation of transmitter release via presynaptic cannabinoid receptors. Trends Pharmacol Sci 22, 565-572.

Schlicker, E., Timm, J., Zentner, J., Gothert, M., 1997. Cannabinoid CB1 receptor-mediated inhibition of noradrenaline release in the human and guinea-pig hippocampus. Naunyn Schmiedebergs Arch Pharmacol 356, 583-589.

Schmid, H.H., Schmid, P.C., Natarajan, V., 1990. N-acylated glycerophospholipids and their derivatives. Prog Lipid Res 29, 1-43.

Selley, D.E., Rorrer, W.K., Breivogel, C.S., Zimmer, A.M., Zimmer, A., Martin, B.R., Sim-Selley, L.J., 2001. Agonist efficacy and receptor efficiency in heterozygous CB1 knockout mice: relationship of reduced CB1 receptor density to G-protein activation. J Neurochem 77, 1048-1057.

Selley, D.E., Stark, S., Sim, L.J., Childers, S.R., 1996. Cannabinoid receptor stimulation of guanosine-5'-O-(3-[35S]thio)triphosphate binding in rat brain membranes. Life Sci 59, 659-668.

Shen, M., Piser, T.M., Seybold, V.S., Thayer, S.A., 1996. Cannabinoid receptor agonists inhibit glutamatergic synaptic transmission in rat hippocampal cultures. J Neurosci 16, 4322-4334.

Sim-Selley, L.J., 2003. Regulation of cannabinoid CB1 receptors in the central nervous system by chronic cannabinoids. Crit Rev Neurobiol 15, 91-119.

Sim-Selley, L.J., Brunk, L.K., Selley, D.E., 2001. Inhibitory effects of SR141716A on G-protein activation in rat brain. Eur J Pharmacol 414, 135-143.

Sim-Selley, L.J., Childers, S.R., 2002. Neuroanatomical localization of receptor-activated G proteins in brain. Methods Enzymol 344, 42-58.

Sim-Selley, L.J., Martin, B.R., 2002. Effect of chronic administration of R-(+)-[2,3-Dihydro-5-methyl-3-[(morpholinyl)methyl]pyrrolo[1,2,3-de]-1,4-b enzoxazinyl]-(1-naphthalenyl)methanone mesylate (WIN55,212-2) or delta(9)-tetrahydrocannabinol on cannabinoid receptor adaptation in mice. J Pharmacol Exp Ther 303, 36-44.

Sim-Selley, L.J., Schechter, N.S., Rorrer, W.K., Dalton, G.D., Hernandez, J., Martin, B.R., Selley, D.E., 2006. Prolonged recovery rate of CB1 receptor adaptation after cessation of long-term cannabinoid administration. Mol Pharmacol 70, 986-996.

Sim, L.J., Hampson, R.E., Deadwyler, S.A., Childers, S.R., 1996a. Effects of chronic treatment with delta9-tetrahydrocannabinol on cannabinoid-stimulated [35S]GTPgammaS autoradiography in rat brain. J Neurosci 16, 8057-8066.

Sim, L.J., Selley, D.E., Childers, S.R., 1995. In vitro autoradiography of receptor-activated G proteins in rat brain by agonist-stimulated guanylyl 5'-[gamma-[35S]thio]-triphosphate binding. Proc Natl Acad Sci U S A 92, 7242-7246.

Sim, L.J., Selley, D.E., Dworkin, S.I., Childers, S.R., 1996b. Effects of chronic morphine administration on mu opioid receptor-stimulated [35S]GTPgammaS autoradiography in rat brain. J Neurosci 16, 2684-2692.

Sim, L.J., Selley, D.E., Xiao, R., Childers, S.R., 1996c. Differences in G-protein activation by mu- and delta-opioid, and cannabinoid, receptors in rat striatum. Eur J Pharmacol 307, 97-105.

Simon, G.M., Cravatt, B.F., 2006. Endocannabinoid biosynthesis proceeding through glycerophospho-N-acyl ethanolamine and a role for alpha/beta-hydrolase 4 in this pathway. J Biol Chem 281, 26465-26472.

Simon, G.M., Cravatt, B.F., 2010. Characterization of mice lacking candidate N-acyl ethanolamine biosynthetic enzymes provides evidence for multiple pathways that contribute to endocannabinoid production in vivo. Mol Biosyst 6, 1411-1418.

Soto-Montenegro, M.L., Vaquero, J.J., Pascau, J., Gispert, J.D., Garcia-Barreno, P., Desco, M., 2008. Detection of Visual Activation in the Rat Brain Using 2-deoxy-2-[(18)F]fluoro-D: -glucose and Statistical Parametric Mapping (SPM). Mol Imaging Biol.

Sugiura, T., Kondo, S., Sukagawa, A., Nakane, S., Shinoda, A., Itoh, K., Yamashita, A., Waku, K., 1995. 2-Arachidonoylglycerol: a possible endogenous cannabinoid receptor ligand in brain. Biochem Biophys Res Commun 215, 89-97.

Szabo, B., Muller, T., Koch, H., 1999. Effects of cannabinoids on dopamine release in the corpus striatum and the nucleus accumbens in vitro. J Neurochem 73, 1084-1089.

Tanimura, A., Yamazaki, M., Hashimotodani, Y., Uchigashima, M., Kawata, S., Abe, M., Kita, Y., Hashimoto, K., Shimizu, T., Watanabe, M., Sakimura, K., Kano, M., 2010. The endocannabinoid 2-arachidonoylglycerol produced by diacylglycerol lipase alpha mediates retrograde suppression of synaptic transmission. Neuron 65, 320-327.

Tappe-Theodor, A., Agarwal, N., Katona, I., Rubino, T., Martini, L., Swiercz, J., Mackie, K., Monyer, H., Parolaro, D., Whistler, J., Kuner, T., Kuner, R., 2007. A molecular basis of analgesic tolerance to cannabinoids. J Neurosci 27, 4165-4177.

Thévenaz, P., Ruttimann, U.E., Unser, M., 1998. A Pyramid Approach to Subpixel Registration Based on Intensity. IEEE Trans Image Proc 7, 27-41.

Thomas, E.A., Cravatt, B.F., Danielson, P.E., Gilula, N.B., Sutcliffe, J.G., 1997. Fatty acid amide hydrolase, the degradative enzyme for anandamide and oleamide, has selective distribution in neurons within the rat central nervous system. J Neurosci Res 50, 1047-1052.

Tsou, K., Brown, S., Sanudo-Pena, M.C., Mackie, K., Walker, J.M., 1998. Immunohistochemical distribution of cannabinoid CB1 receptors in the rat central nervous system. Neuroscience 83, 393-411.

Tsou, K., Mackie, K., Sanudo-Pena, M.C., Walker, J.M., 1999. Cannabinoid CB1 receptors are localized primarily on cholecystokinin-containing GABAergic interneurons in the rat hippocampal formation. Neuroscience 93, 969-975.

Valverde, O., Karsak, M., Zimmer, A., 2005. Analysis of the endocannabinoid system by using CB1 cannabinoid receptor knockout mice. Handb Exp Pharmacol, 117-145.

Van Sickle, M.D., Duncan, M., Kingsley, P.J., Mouihate, A., Urbani, P., Mackie, K., Stella, N., Makriyannis, A., Piomelli, D., Davison, J.S., Marnett, L.J., Di Marzo, V., Pittman, Q.J., Patel, K.D., Sharkey, K.A., 2005. Identification and functional characterization of brainstem cannabinoid CB2 receptors. Science 310, 329-332.

Varma, N., Carlson, G.C., Ledent, C., Alger, B.E., 2001. Metabotropic glutamate receptors drive the endocannabinoid system in hippocampus. J Neurosci 21, RC188.

Varvel, S.A., Hamm, R.J., Martin, B.R., Lichtman, A.H., 2001. Differential effects of delta 9-THC on spatial reference and working memory in mice. Psychopharmacology (Berl) 157, 142-150.

Westlake, T.M., Howlett, A.C., Ali, S.F., Paule, M.G., Scallet, A.C., Slikker, W., Jr., 1991. Chronic exposure to delta 9-tetrahydrocannabinol fails to irreversibly alter brain cannabinoid receptors. Brain Res 544, 145-149.

Wickman, K., Clapham, D.E., 1995. Ion channel regulation by G proteins. Physiol Rev 75, 865-885.

Williams, C.M., Rogers, P.J., Kirkham, T.C., 1998. Hyperphagia in pre-fed rats following oral delta9-THC. Physiol Behav 65, 343-346.

Wilson, R.I., Kunos, G., Nicoll, R.A., 2001. Presynaptic specificity of endocannabinoid signaling in the hippocampus. Neuron 31, 453-462.

Wilson, R.I., Nicoll, R.A., 2001. Endogenous cannabinoids mediate retrograde signalling at hippocampal synapses. Nature 410, 588-592.

Wilson, R.I., Nicoll, R.A., 2002. Endocannabinoid signaling in the brain. Science 296, 678-682.

Worsley, K.J., Evans, A.C., Marrett, S., Neelin, P., 1992. A three-dimensional statistical analysis for CBF activation studies in human brain. J Cereb Blood Flow Metab 12, 900-918.

Wu, D.F., Yang, L.Q., Goschke, A., Stumm, R., Brandenburg, L.O., Liang, Y.J., Hollt, V., Koch, T., 2008. Role of receptor internalization in the agonist-induced desensitization of cannabinoid type 1 receptors. J Neurochem 104, 1132-1143.

www.justice.gov, 2010. U.S. Drug Enforcement Administration: Drug Scheduling.

www.ProCon.org, 2010. 14 Legal Medical Marijuana States: Laws, Fees, and Possession Limits.

Yang, J., Sadler, T.R., Givrad, T.K., Maarek, J.M., Holschneider, D.P., 2007. Changes in brain functional activation during resting and locomotor states after unilateral nigrostriatal damage in rats. Neuroimage 36, 755-773.

Zhang, J., Ferguson, S.S., Barak, L.S., Bodduluri, S.R., Laporte, S.A., Law, P.Y., Caron, M.G., 1998. Role for G protein-coupled receptor kinase in agonist-specific regulation of mu-opioid receptor responsiveness. Proc Natl Acad Sci U S A 95, 7157-7162.

Zimmer, A., Zimmer, A.M., Hohmann, A.G., Herkenham, M., Bonner, T.I., 1999. Increased mortality, hypoactivity, and hypoalgesia in cannabinoid CB1 receptor knockout mice. Proc Natl Acad Sci U S A 96, 5780-5785.

Vita

Peter Tiendung Nguyen was born on September 22, 1980, in San Gabriel Valley, California. Peter graduated from Nogales High School, La Puente, California, in 1998. He then attended the University of California Irvine, Irvine, California, and graduated in 2003 as a double major in Chemistry and Biological Sciences. In 2004, Peter began his physician-scientist M.D./Ph.D. training at the Medical College of Virginia (MCV) Campus, Virginia Commonwealth University (VCU) School of Medicine, Richmond, Virginia. He entered the Neuroscience Graduate Program in 2006 through the Department of Pharmacology and Toxicology and began his dissertation work on cannabinoid receptors in the laboratory of Dr. Laura Sim-Selley. Peter will defend his dissertation and begin the clinical year of his medical training in August of 2010.

Peter has presented abstracts at several national and international scientific conferences, including the International Cannabinoid Research Society, Society for Neuroscience, Experimental Biology (The American Society for Pharmacology and Experimental Therapeutics), American Physician Scientists Association, and the Association of University Professors of Neurology. He was on the MCV Campus X-Ray yearbook staff from 2005-2008, where he served as Editor-in-Chief during the last two years and established the first web-based yearbook production platform at MCV in collaboration with Jostens publishing. He was also an executive board member of the MCV Campus Student Government Association from 2006-2008 and participated in committees including the establishment of student services in the new Hunton Student Center and newly renovated Larrick Student Center. In 2007, he created the official Neuroscience Graduate Program website and has served as webmaster. Peter has received awards and recognition, including multiple student travel awards and honors at scientific conferences, recognition at VCU Watts Day and at the Central VA Society for Neuroscience symposium, VCU University Service Award, induction into Phi Kappa Phi honor society, and the Anthony Ambrose and Lauren A. Woods awards for the top 3rd year and graduating Ph.D. student in the Department of Pharmacology and Toxicology, respectively. His first publication at VCU, based on initial work with Statistical Parametric Mapping and CB_1 receptors, made the journal cover in the October 2010 issue of NeuroImage. He also received a Ruth L. Kirschstein National Research Service Award Predoctoral Fellowship (National Institute of Drug Abuse F30DA023758: 5/08-5/12) entitled “Cannabinoid Regulation of CB_1 Receptor Function".

Research Papers

Nguyen PT, Schmid C, Raehal K, Selley DE, Bohn L, Sim-Selley LJ. 2010. Beta-arrestin 2 regulates CB1 receptor desensitization and downregulation and THC-mediated antinociceptive tolerance. *Manuscript in preparation*.

Falenski K, **Nguyen PT**, Sim-Selley LJ, DeLorenzo R. 2010. Statistical Parametric Mapping of the Regional Alterations in Cannabinoid CB_1 Receptor Expression, Binding, and G-Protein Activation in the 3D Epileptic Rat Brain. *Manuscript in preparation.*

Sadler TR, **Nguyen PT**, Yang J, Givrad TK, Mayer EA, Maarek JM, Hinton DR, and Holschneider DP. 2010. Antenatal Maternal Stress Alters Functional Brain Responses and Neuronal Survival During Fear Conditioning in Adult Offspring. *Submitted to Biological Psychiatry.*

Schlosburg JE, Blankman JL, Long JZ, Nomura DK, Pan B, Kinsey SG, **Nguyen PT**, Ramesh D, Booker L, Burston JJ, Thomas EA, Selley DE, Sim-Selley LJ, Liu QS, Lichtman AH, Cravatt BF. 2010. Chronic monoacylglycerol lipase blockade causes functional antagonism of the endocannabinoid system. *In Press, Nature Neuroscience*.

Nguyen PT, Selley DE, Sim-Selley LJ. 2010. Statistical Parametric Mapping reveals ligand and region specific G-protein activation by CB1 receptors and non-CB1 sites in the 3D reconstructed mouse brain. NeuroImage 52(4), 1243-1251.

Hashimoto H, Monserratt L, **Nguyen P**, Feil D, Harwood D, Mandelkern M, Sultzer DL. 2006. Anxiety and regional cortical glucose metabolism in patients with Alzheimer's disease. J Neuropsychiatry Clin Neurosci. 18(4): 521-8.

Holschneider, DP, Yang, J, Sadler, TR, **Nguyen, PT**, Givrad, TK, and Maarek, JM. 2006. Mapping cerebral blood flow changes during auditory-cued conditioned fear in the nontethered, nonrestrained rat. NeuroImage 29(4), 1344-1358.

Nguyen, PT, Holschneider, DP, Maarek, JM, Yang, J, and Mandelkern, MA. 2004. Statistical parametric mapping applied to an autoradiographic study of cerebral activation during treadmill walking in rats. NeuroImage 23(1), 252-259.

Abstracts and Presentations

Sadler TR, Yang, J, Givrad T, **Nguyen PT**, Maarek J-MI, Holschneider DP. 2004. Functional brain mapping in rats during conditioned fear memory. Society for Neuroscience, Program # 206.12.

Nguyen PT, Holschneider DP, Maarek J-MI, Yang, J, Mandelkern MA. 2004. Statistical parametric mapping applied to an autoradiographic study of cerebral activation during treadmill walking in rats. 2004. Society for Neuroscience, Program # 922.19.

Sulzter DL, Feil D, Harwood D, Monserratt L, Freedman E, **Nguyen PT**, Mandelkern MA. "PET Imaging Correlates of Donepezil Treatment Response in Alzheimer's Disease". 2004. From the Department of Psychiatry and Biobehavioral Sciences, David Geffen School of Medicine at UCLA, and the VA Greater Los Angeles Healthcare System. *Annual Meeting of the American Association for Geriatric Psychiatry*.

Hashimoto H, Monserratt L, **Nguyen P**, Feil D, Harwood D, Mandelkern M, Sultzer D. Anxiety and regional cortical metabolism in patients with Alzheimer's disease. J Neuropsychiatry Clin Neurosci 17:2, Spring 2005.

Nguyen PT, Falenski KW, Selley DE, Sim-Selley LJ. 2007. Mapping Cannabinoid-Mediated G-Protein Activity in the 3D Reconstructed Mouse Brain. International Cannabinoid Research Society 17th Meeting.

Nguyen PT, Selley DE, Sim-Selley LJ. 2008. Functional Imaging of Cannabinoid-Mediated G-Protein Activity in the 3D Reconstructed Mouse Brain. Experimental Biology 2008 Meeting (American Society for Pharmacology and Experimental Therapeutics). Program # 711.2

Nguyen PT, Selley DE, Sim-Selley LJ. 2008. Ligand and region specific activation of G-proteins by CB1 receptors and non-CB1 sites in the 3D reconstructed mouse brain. International Cannabinoid Research Society 18th Meeting.

Falenski KW, **Nguyen PT**, Deshpande LS, Blair RE, Sim-Selley LJ, and DeLorenzo RJ. 2008. Long-term regional differences in CB1 receptor-mediated G-protein activity following pilocarpine-induced status epilepticus. Society for Neuroscience.

Nguyen PT, Selley DE, Sim-Selley LJ. 2008. Statistical Parametric Mapping reveals ligand and region specific G-protein activation by CB1 receptors and non-CB1 sites in the 3D reconstructed mouse brain. Society for Neuroscience. Presentation #321.3

Falenski KW, **Nguyen PT**, Blair RE, Sim-Selley LJ, and DeLorenzo RJ. 2008. Pilocarpine-Induced Status Epilepticus Causes Long-Term Regional Differences in Brain Cannabinoid Type-1 Receptor Expression, Receptor Binding, and G-Protein Activation. American Epilepsy Society.

Nguyen PT, Schmid C, Raehal K, Selley DE, Bohn L, Sim-Selley LJ, 2009. Beta-arrestin 2 regulates CB1 receptor desensitization and THC-mediated antinociceptive tolerance. International Cannabinoid Research Society 19th Meeting. *Oral Presentation*.